

CONTENTS

CONTENTS	i
EDITORIAL BOARD	iii
PREFACE	iv
Comparison the mass composition of coconut shell in TiO₂ towards its characterization for supercapacitor applications <i>Sinta Marito Siagian, Samaria Chrisna H. S, Ferdinan Rinaldo Tampubolon, Palma Juanta</i>	1–12
Comparison the adsorption of Pb with ecofriendly bio-adsorbent from rice husk ash and boiler fly ash <i>Enda Rasilta Tarigan, Anna Angela Sitinjak, Meriahni Silalahi, Switamy Angnitha Purba, Yenny Sitanggang, Darry Purba</i>	13–24
Smart control and monitoring system for closed poultry house based on IoT <i>Surateno, Syamsiar Kautsar, Risse Entikaria Rachmanita, Aan Anwaludin, M. Adhiyatma, Rosa Tri Hertawamati, Budi Hariono, Fendik Eko Purnomo, Sryang Tera Sarena</i>	25–40
Misconceptions about acceleration among prospective physics teacher: the importance of discussion of acceleration as a vector quantity <i>Tarsisius Sarkim</i>	41–52
Expected value of the occupation times of brownian motion <i>Herry Pribawanto Suryawan</i>	53–62
Mobile forensic investigation on iOS & Android smartphones: case study investigation on WhatsApp <i>Shadi Khaled Zakarneh</i>	63–98
Design of maximum torque per ampere control method in squirrel cage three-phase induction motor <i>Regina Chelinia Erianda Putri, Feri Yusivar</i>	99–112
Evaluation of impact of biofertilizer and mulch types on growth and production of tomato cultivar gustavi F1 in lowland areas <i>Raida Kartina, Ratih Rahhutami, Wika Anrya Darma, Sekar Utami Putri, Dede Tiara, Rianida Taisa, Fahri Ali</i>	113-124

Response of shoots from porang leaf bulbs to cytokinins and IAA in shoot multiplication in vitro	125–136
<i>Lisa Erfa, Desi Maulida, Rahmadyah Hamiranti, Ferziana, Yuriansyah, Betari Safitri, Yeni</i>	
Implementation of scrum in the manufacture of non-invasive blood sugar detection devices using photoplethysmography signals	137-160
<i>Rafly Arief Kanza, Erita Cicilia Febrianti, Izza Nur Afifah, Rifqi Affan, Arna Fariza, Hestiasari Rante</i>	
Characteristics of straight trapezoidal cross-sectional fins under unsteady conditions	161-168
<i>Michael Seen, Doddy Purwadianto, Gilang Argya Dyaksa, Heryoga Winarbawa, Rines, Stefan Mardikus, Wibowo Kusbandono, Y. B. Lukiyanto</i>	
Clustering and trend analysis of priority commodities in the archipelago capital region (IKN) using a data mining approach	169-182
<i>Pandu Pangestu, Syamsul Maarip, Yuldan Nur Addinsyah, Vega Purwayoga</i>	
Sentiment analysis on tweets about waste problem in Yogyakarta using SVM	183-196
<i>Robertus Adi Nugroho, Sri Hartati Wijono, Kartono Pinaryanto, Ridowati Gunawan, F.X. Sinungharjo</i>	
Image detection analysis for javanese character using YOLOv9 models	197-208
<i>Hari Suparwito</i>	
AUTHOR GUIDELINES	209-210

EDITORIAL BOARD

Editor in Chief

Dr. I Made Wicaksana Ekaputra (*Sanata Dharma University, Yogyakarta, Indonesia*)
Email: made@usd.ac.id

Associate Editor

Dr. Pham Nhu Viet Ha (*Vietnam Atomic Energy Institute, Hanoi, Vietnam*)
Dr. Hendra Gunawan Harno (*Gyeongsang National University, Jinju, The Republic of Korea*)
Dr. Mukesh Jewariya (*National Physical Laboratory, New Delhi, India*)
Dr. Mongkolserj Lin (*Institute of Technology of Cambodia, Phnom Penh, Cambodia*)
Dr. Yohanes Baptista Lukiyanto (*Sanata Dharma University, Yogyakarta, Indonesia*)
Dr. Apichate Maneewong (*Thailand Institute of Nuclear Technology, Bangkok, Thailand*)
Prof. Dr. Sudi Mungkasi (*Sanata Dharma University, Yogyakarta, Indonesia*)
Dr. Pranowo (*Universitas Atma Jaya Yogyakarta, Yogyakarta, Indonesia*)
Dr. Monica Cahyaning Ratri (*Sanata Dharma University, Yogyakarta, Indonesia*)
Dr. Mahardhika Pratama (*Nanyang Technological University, Singapore*)
Prof. Dr. Leo Hari Wiryanto (*Bandung Institute of Technology, Bandung, Indonesia*)
Dr. Ranggo Tungga Dewa (*Universitas Pertahanan, Bogor, Indonesia*)

Editorial Assistant

Rosalia Arum Kumalasanti, M.T. (*Sanata Dharma University, Yogyakarta, Indonesia*)
Vittalis Ayu, M.Cs. (*Sanata Dharma University, Yogyakarta, Indonesia*)

Contact us

International Journal of Applied Sciences and Smart Technologies
Faculty of Science and Technology
Universitas Sanata Dharma
Kampus III Paingan, Maguwoharjo, Depok, Sleman
Yogyakarta, 55282
Phone : +62 274883037 ext. 523110, 52320
Fax : +62 272886529
Email : editorial.ijasst@usd.ac.id
Website : <http://e-journal.usd.ac.id/index.php/IJASST>

IJASST is an open-access peer-reviewed journal that mediates the dissemination of research and studies conducted by academicians, researchers, and practitioners in science, engineering, and technology.

PREFACE

Dear readers, we are delighted to serve you Volume 6, Issue 1 of *International Journal of Applied Sciences and Smart Technologies* (IJASST), which is managed and published by the Faculty of Science and Technology, Universitas Sanata Dharma. IJASST is an open-access peer-reviewed journal that mediates the dissemination of research and studies conducted by academicians, researchers, and practitioners in science, engineering, and technology. Its scope also includes basic sciences which relate to technology, such as applied mathematics, physics, and chemistry.

In this edition, we have fourteen papers authored by researchers from Indonesia, United Kingdom, and Palestine. Submitted papers are reviewed fairly using the open journal system (OJS) of IJASST. After the review process, accepted papers of the journal are publicly available for free at the website of IJASST. For future issues, we are looking forward to your contributions to IJASST.

Dr. I Made Wicaksana Ekaputra
Editor in Chief
IJASST

Comparison Mass Composition of Coconut Shell in TiO₂ towards its Characterization for Supercapacitor Applications

Sinta Marito Siagian^{1*}, Samaria Chrisna HS²,
Ferdinan Rinaldo Tampubolon², Palma Juanta³

¹*Teknik Listrik, Politeknik Negeri Medan, Indonesia*

²*Teknik Elektronika, Politeknik Negeri Medan, Indonesia*

³*Universitas Prima Indonesia, Indonesia*

*Corresponding Author: sintasiagian@polmed.ac.id

(Received 27-10-2023; Revised 03-11-2023; Accepted 05-11-2023)

Abstract

This study aims to evaluate the effect of the mass ratio on the capacitance of electrodes made from TiO₂-based composites. The composites were synthesized using a wet chemical method and applied using the doctor blade technique, incorporating TiO₂ and rGO derived from coconut shell activated carbon. Our findings reveal that at a 1:1 mass ratio, the atomic composition of Ti and O was non-uniform, although there was evident adherence of TiO₂ elements to the sample surface. In contrast, at mass ratios of 1:3 and 1:5, a decrease in the concentration of Ti atoms and an increase in O atoms were observed, indicating a reduction in Ti oxidation. SEM analysis further revealed that particle size significantly impacts capacitance: smaller particle sizes yielded higher capacitance. In the 1:1 mass variation, the discharge process was protracted, taking up to 29.3 minutes and generating an electrical energy of 0.000413 joules with a capacitance of 489 μF. These insights are pivotal for optimizing the composition and mass ratio, fostering the development of electrode materials characterized by enhanced capacitance and energy efficiency. Such advancements hold promising potential for a range of applications in the energy storage sector.

Keywords: Activated carbon, Capacitance, Supercapacitor

1 Introduction

Supercapacitors are currently gaining attention as a future energy storage system due to their superior performance in terms of capacitance compared to conventional capacitors. However, supercapacitors have drawbacks, including lower energy density compared to batteries and unstable voltage output. Consequently, many researchers are investigating solutions to these issues for a wide range of applications, from small to large



scale [1]. The supercapacitor fabrication process is efficient, easy and environmentally friendly because it does not produce any pollution. Therefore, the use of supercapacitors is a step that can overcome global issues regarding warming and environmental damage [2]. In principle, capacitors have two types of capacitors based on their storage media ELDC capacitors are capacitors with a type of physical storage by accumulating charge between two electrodes which are separated by a thin electrical double layer and there is an interaction between positive and negative charges which causes the energy storage process to occur. Pseudocapacitors use transition metal oxides as electrode materials. Some transition metal oxides commonly used in pseudocapacitors include ZnO [3], TiO₂ [4], CuO [5], Mn₂O₃ [6], and metal oxides with three metal components [7]. Meanwhile, another type of capacitor is a pseudocapacitor which carries out energy storage by chemical means involving Faradaic redox where electrons are transferred to ions at an electrode. Basically, this type stores more energy than ELDC, but the rate of charging and discharging is too fast due to the influence of chemical properties [8]. Although pseudocapacitors have high capacitance, several material limitations make them not optimal for large-scale applications. Meanwhile, EDLC, which uses carbon materials, offers stability and abundance that makes it a more practical and economical choice for various applications [9]. Basically, TiO₂ material has stable chemical properties at low cost, is abundant in nature and can improve the electrochemical performance of the electrode material. This shows that TiO₂ is considered a potential candidate to increase the efficiency and effectiveness of supercapacitors [10]. Therefore, it is the focus of research in developing electrode materials for supercapacitors. Currently, a new design has been carried out on a composite of activated carbon, conductive carbon, and TiO₂. The material composition has been optimized to obtain electrode performance with high capacitance and longer service life [11]. Carbon material is generally the choice that is often used as an electrode in making supercapacitors because it is easy to find, can be renewed and has high performance in energy storage so that it can be a sustainable energy solution [12]. When compared with commercial carbon-based materials, activated carbon derived from biomass is cheaper, environmentally friendly, and rich in surface functional groups. Therefore, many biomasses have been sought for use as raw materials or precursors in the manufacture of activated carbon, such as durian peel [13], Cassava peel

[14], mangosten peel [15] and cocnut shell [12]. In the research carried out the analysis made was EDX [16]. EDX or Energy Dispersive X-ray Spectroscopy is a method used to evaluate the composition of chemical elements in a sample. This technique can be used to analyze the materials used in supercapacitors, which generally consist of materials such as activated carbon, electrolytes and electrodes.

2 Material and Methods

This research activity was carried out by mixing coconut shell activated carbon that had been synthesized initially with TiO_2 material. TiO_2 : Coconut Shell then put into a glass beaker and mix with 1-Butanol. Next, homogenize the ingredients using a magnetic stirrer for 3 hours and dry in the oven. The dried material is called the TiO_2/rGO composite [17]. The variations used by researchers in the mixing process are 1:1, 1:3 and 1:5. Next, add 50 ml of H_2SO_4 to the TiO_2/rGO composite while stirring for 1 hour, then slowly add 2 g of KmnO_4 and stir again for 1 hour. Then add 100 ml of distilled water. then add 5 ml of H_2O_2 to remove the potassium permanganate level and dry using an oven [18]. Before coating the aluminum plate, there are several things that must be done, namely mixing poly urethane in the TiO_2/rGO composite and then stirring until evenly distributed. Next, apply the material to the aluminum plate and leave it for 2 hours so that the material sticks well to the aluminum. The next step is to drip phosphoric acid on tissue paper which functions as a separator between the anode and cathode as a polarity bridge. Stick the tissue paper on the aluminum filled with graphene. The next stage is to insert the supercapacitor plate into vacuum plastic so that it does not become contaminated with air because this will interfere with the capacitance value [19]. This research is designed to make a supercapacitor material by applying TiO_2/rGO composite material to an aluminum plate as shown in the following figure. Fig. 1 is a supercapacitor design that has a cable attached to one end and is then ready to be connected to a power supply for charging and discharging measurements as shown in Fig. 2.



Figure 1. Composite of TiO₂: Coconut Shell that has been bonded to an Aluminum Plate

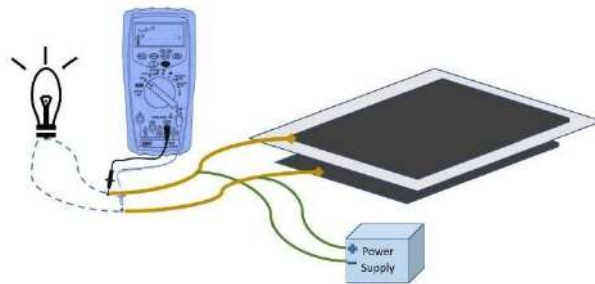


Figure 2. Approximate scheme of charging and discharging

3 Results and Discussions

1. Energy Dispersive X-Ray Analysis

The analysis carried out was TiO₂/Carbon with mass ratios of 1:1, 1:3 and 1:5 respectively. The morphology at a mass ratio of 1:1 can be seen in Fig. 3. Based on Fig. 3, it can be explained that the morphology of the 1:1 mass ratio is known to be not uniform, but the Ti element has adhered to the surface of the sample as indicated by the percentage of Ti atoms of 45.17% and the O atom content of 37.7%, while the P atoms are 1.12% and the K atoms are 2.03%. This compound was formed because during the sample making process using Phosphoric Acid and Potassium Permanganate. However, the content is very small, namely approx.

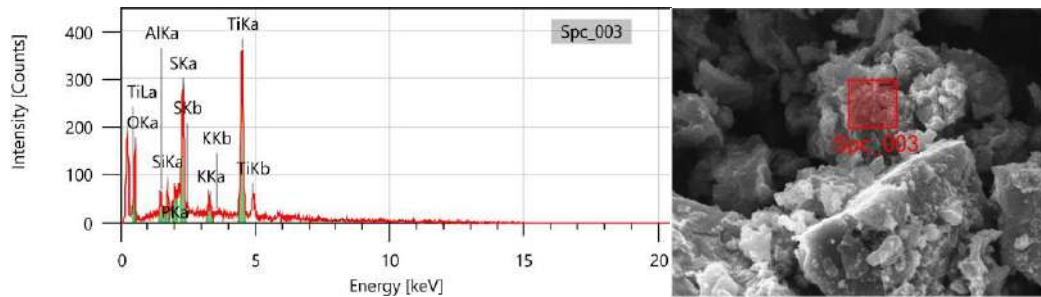


Figure 3. SEM-EDX Comparison 1:1 with magnification 2500x

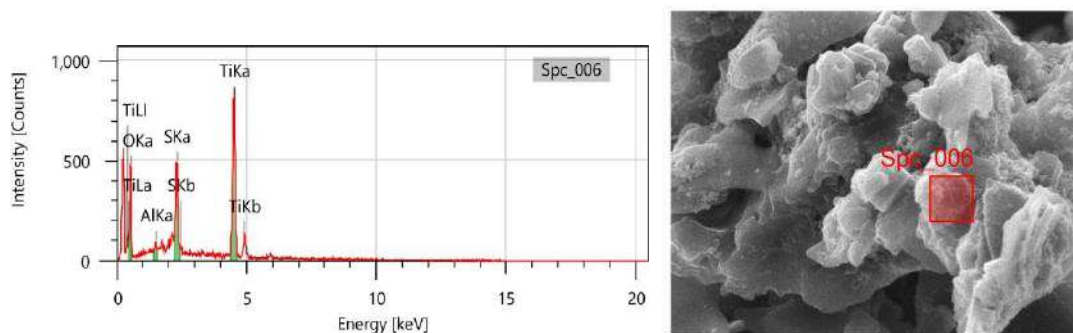


Figure 4. SEM-EDX Comparison 1:3 with magnification 2500x

In Fig. 4 it is known that the morphology looks uniform and the TiO_2 semiconductor is also attached, it is known that Ti atoms are 20% and O atoms are 67%. It can be seen that there is a decrease in the mass of the Ti atom and an increase in the mass of the O atom. In the graph the ratio 1:3 is found to be smoothly coated on the aluminum surface. This happens because contamination from equipment can occur when equipment used in experiments, such as containers, grinders, or other laboratory equipment, accidentally contaminates samples during the preparation or analysis process. In some cases, particles or residues of other metals thrown off or remaining on the equipment can enter the sample and then be detected in the EDX analysis. In this research, the author produced sample preparation results when heating aluminum foil. This can make it a contaminant at a mass ratio of 1:3. The 1:5 comparison of morphological analysis can be seen in Fig. 5.

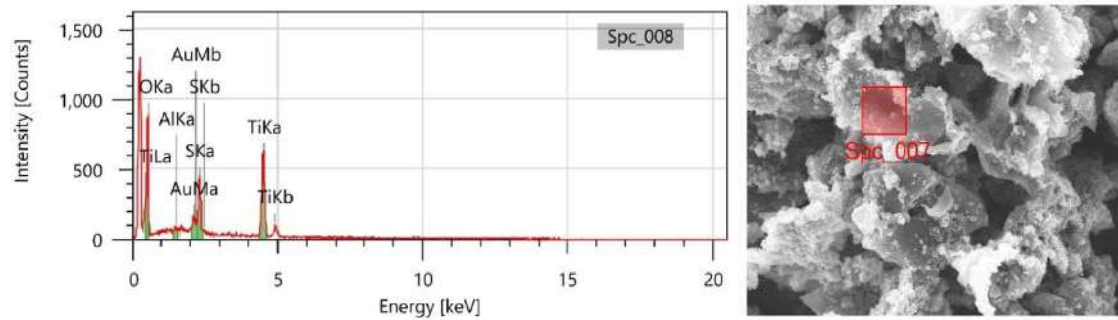


Figure 5. SEM-EDX Comparison 1:5 with magnification 2500x

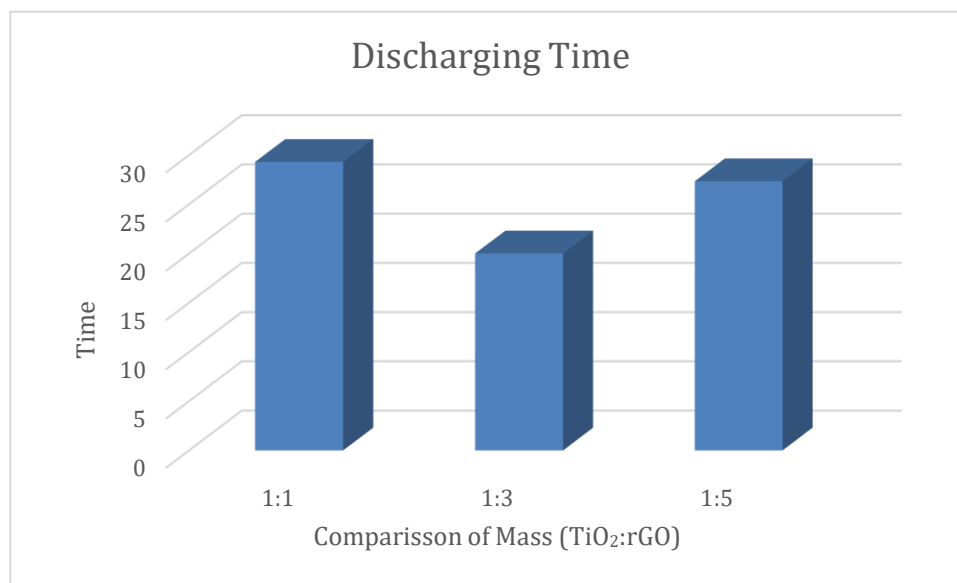


Figure 6. Diagram of Discharging Capacitors

In Fig. 5, the morphology formed based on the measurement results is uniform and semiconductive TiO₂ formed on the attached surface with the respective compositions of Ti and O being 27.01% and 48.28%. This percentage indicates that the Ti element also experiences a decrease in oxidation. This happens because the oxide value is higher compared to the 1:3 composition. The particle size obtained in this study was that at a mass ratio of 1:1 the size was 6.5 μm, while at a mass ratio of 1:3 it was 8.9 μm and the third ratio was 7.7 μm. From the results found, it is known that the smallest particle size is found in a ratio of 1:1. The difference in particle size in the material has an influence on capacitance, this happens because when particles come into contact with electrolyte ions, they can facilitate charge which of course has a role in charging and discharging supercapacitors [20]. An increase in particle size can also occur due to agglomeration,

causing an increase in intraparticle porosity. When smaller particles collect around larger particles, they create gaps or pores in the larger particles [21].

2. Charging and discharging analysis of supercapacitors

Based on Table 1, it can be seen that with a constant variable charging time of around 8 minutes, the emptying time varies. At a mass ratio of 1:1 the time required to empty is 29.3 minutes, while at a mass ratio of 1:3 the emptying is 20 minutes. There was a decrease in emptying time by around 9 minutes. This is because the mass of carbon produced is less than the mass of 1:1, apart from that, based on FTIR analysis, O-H bonds or carboxyl acids are formed which have an impact on supercapacitor applications. At a mass ratio of 1:5, the emptying time is 27.33 higher than 1:3. This happens because the composition of oxide and carbon is higher than 1:3 but lower than 1:1. Based on the Table 1, the mass ratio of 1:1 takes longer to empty compared to the others. This happens because more carbon elements are formed in this composition. The longest emptying time is at a mass ratio of 1:1, which is in line with the smallest particle size in that ratio. From the results of this research, it was found that particle size influences the discharge of supercapacitors.

3. Electrical Energy Analysis

In this research, electrical energy values were also calculated which can be seen in Table 2. The varying capacitance values are due to a decrease in specific capacitance and rapid mechanical degradation due to swelling, shrinkage and cracking during the doping/dedoping process. In this context, the doping/dedoping process refers to the entry and exit of ions or molecules into/from the electrode structure, which is part of the operational mechanism of energy storage and release [22]. Apart from that, the decrease

Table 1. Charging and discharging times

TiO ₂ : rGO	Charging (Minute)	Discharging (Minute)
1:1	8	29.3
1:3	8	20
1:5	8	27.33

Table 2. Electrical Energy

Mass Comparison	Kapasitance (μf)	V Saving (Volt)	Electrical Energy (Joule)
1:1	489	1.3	0.000413
1:3	58	1.1	0.000035
1:4	211	0.9	0.000085

also occurs because the morphological structure is not uniform, resulting in differences in surface area as a load storage. Based on Table 2, it can be seen that the greatest electrical energy is found at a mass ratio of 1:1, namely 0.000413 joules, and the lowest energy is at a mass ratio of 1:3, namely 0.000035 joules. The greater the capacitance value, the greater the electrical energy and vice versa, if the capacitance value is low, the electrical energy is also low. It was also reported that the activation method, type of activator, pyrolysis conditions provide different surface areas for the activated carbon produced, and this will have an influence on the capacitance values obtained [23]. Apart from that, differences in capacitance values can also occur due to inhomogeneous grains on a sample surface [24]. This is in accordance and store with $E = \frac{1}{2} CV^2$ where the E value is directly proportional to the capacitance and stored voltage obtained in each sample that has been made.

4 Conclusions

In research related to the addition of activated carbon mass in supercapacitor applications, it can be concluded that:

1. The more coconut shell mass mixed with activated carbon, the Ti value in the EDX results decreases. The highest Ti mass value is at a mass ratio of 1:1.
2. The fastest emptying time is in the ratio 1:3 and the longest emptying time is in the ratio 1:1 up to 29.3 minutes.
3. The largest capacitance value is at a mass ratio of 1:1 and this also results in an increase in the value of the electrical energy produced.

Acknowledgements

The author would like to thank the Medan State Polytechnic for the funding provided through Contract: B/471/PL5/PT.01.05/2023 which comes from DIPA POLMED funds in 2023.

References

- [1] R. Lakra, R. Kumar, D. Thatoi, and A. Soam, "Synthesis of TiO₂ nanoparticles as electrodes for supercapacitor," *Materials Today: Proceedings*, vol. 74, pp. 863-866, 2023.
- [2] S. Sawadsitang, T. Duangchuen, A. Karaphun, T. Putjuso, P. Kumnorkaew, and E. Swatsitang, "Synthesis, characterization and electrochemical properties of activated coconut fiber carbon (ACFC) and CuO/ACFC nanocomposites for applying as electrodes of supercapacitor devices," *Surfaces and Interfaces*, vol. 25, p. 101174, 2021.
- [3] J. Jayachandiran *et al.*, "Synthesis and electrochemical studies of rGO/ZnO nanocomposite for supercapacitor application," *Journal of Inorganic and Organometallic Polymers and Materials*, vol. 28, pp. 2046-2055, 2018.
- [4] P. Nagaraju, A. Alsalme, A. Alswieleh, and R. Jayavel, "Facile in-situ microwave irradiation synthesis of TiO₂/graphene nanocomposite for high-performance supercapacitor applications," *Journal of Electroanalytical Chemistry*, vol. 808, pp. 90-100, 2018.
- [5] S. Yousaf *et al.*, "Hierarchically porous CuO microspheres and their r-GO based nanohybrids for electrochemical supercapacitors applications," *Journal of Materials Research and Technology*, vol. 9, no. 6, pp. 14158-14167, 2020.
- [6] Y.-H. Son, P. T. Bui, H.-R. Lee, M. S. Akhtar, D. K. Shah, and O.-B. Yang, "A rapid synthesis of mesoporous Mn₂O₃ nanoparticles for supercapacitor applications," *Coatings*, vol. 9, no. 10, p. 631, 2019.
- [7] S. Saini, P. Chand, and A. Joshi, "Biomass derived carbon for supercapacitor applications," *Journal of Energy Storage*, vol. 39, p. 102646, 2021.

-
- [8] X. Xu, J. Gao, Q. Tian, X. Zhai, and Y. Liu, "Walnut shell derived porous carbon for a symmetric all-solid-state supercapacitor," *Applied Surface Science*, vol. 411, pp. 170-176, 2017.
- [9] K. Chopngam, M. Luengchavanon, M. Khangkhamano, K. Chetpattananondh, and W. Limbut, "Coating activated carbon from coconut shells with $\text{Co}_3\text{O}_4/\text{CeO}_2$ for high-performance supercapacitor applications: an experimental study," *BioResources*, vol. 16, no. 4, p. 8022, 2021.
- [10] C. Zhang *et al.*, "A Facile Synthesis of $\text{TiO}_2\text{-NiCo}_2\text{S}_4\text{-Ti}_3\text{C}_2$ Electrode material by Hydrothermal Method and its electrochemical performance for Supercapacitor Application," *International Journal of Electrochemical Science*, vol. 17, no. 9, p. 220925, 2022.
- [11] M. Diantoro, I. Luthfiyah, H. Wisodo, J. Utomo, and W. Meevasana, "Electrochemical Performance of Symmetric Supercapacitor Based on Activated Carbon Biomass TiO_2 Nanocomposites," in *Journal of Physics: Conference Series*, 2022, vol. 2243, no. 1, p. 012077: IOP Publishing.
- [12] S. R. A. Sasono, M. F. Rois, W. Widiyastuti, T. Nurtono, and H. Setyawan, "Nanofiber-enrich dispersed activated carbon derived from coconut shell for supercapacitor material," *Results in Engineering*, vol. 18, p. 101070, 2023.
- [13] J. Y. Chua, K. M. Pen, J. V. Poi, K. M. Ooi, and K. F. Yee, "Upcycling of biomass waste from durian industry for green and sustainable applications: An analysis review in the Malaysia context," *Energy Nexus*, p. 100203, 2023.
- [14] T. Amakoromo, O. Abumere, J. Amusan, V. Anye, and A. Bello, "Porous carbon from *Manihot Esculenta* (cassava) peels waste for charge storage applications," *Current Research in Green and Sustainable Chemistry*, vol. 4, p. 100098, 2021.
- [15] J. Khajonrit *et al.*, "Mangosteen peel-derived activated carbon for supercapacitors," *Progress in Natural Science: Materials International*, vol. 32, no. 5, pp. 570-578, 2022.
- [16] A. Murugan, V. Siva, A. Shameem, S. A. Bahadur, S. Sasikumar, and N. Nallamuthu, "Structural and charge density distribution studies on Tin Oxide nanoparticles for Supercapacitor application," *Journal of Energy Storage*, vol. 28, p. 101194, 2020.

-
- [17] A. B. Aritonang, P. Parwaty, M. A. Wibowo, P. Ardiningsih, and A. Adhitiyawarman, "Sintesis TiO₂-rGO Dengan Pereduksi Alumunium untuk Fotokatalisis Degradasi Metilen Biru dibawah Irradiasi Sinar Tampak," *Equilibrium Journal of Chemical Engineering*, vol. 6, no. 2, pp. 150-156, 2023.
- [18] A. D. Setyoputra, H. Ruffa, H. Sutanto, and A. Subagio, "The Characterisation of MWCNT-rGO-TiO₂ Nanocomposite as Potential Electrode Material for Hybrid Supercapacitor," *International Journal of Electrochemical Science*, vol. 17, no. 5, p. 22053, 2022.
- [19] F. I. Pasaribu, "Superkapasitor Sebagai Penyimpan Energi Menggunakan Bahan Graphene," *RELE (Rekayasa Elektrikal dan Energi): Jurnal Teknik Elektro*, vol. 2, no. 2, pp. 65-72, 2020.
- [20] A. Toghan, M. Khairy, E. Kamar, and M. Mousa, "Effect of particle size and morphological structure on the physical properties of NiFe₂O₄ for supercapacitor application," *journal of materials research and technology*, vol. 19, pp. 3521-3535, 2022.
- [21] A. Macías-García, D. Torrejón-Martín, M. Á. Díaz-Díez, and J. P. Carrasco-Amador, "Study of the influence of particle size of activate carbon for the manufacture of electrodes for supercapacitors," *Journal of Energy Storage*, vol. 25, p. 100829, 2019.
- [22] O. Yoruk, Y. Bayrak, and M. Ates, "Design and assembly of supercapacitor based on reduced graphene oxide/TiO₂/polyaniline ternary nanocomposite and its application in electrical circuit," *Polymer Bulletin*, vol. 79, no. 5, pp. 2969-2993, 2022.
- [23] O. N. Tetra, "Superkapasitor berbahan dasar karbon aktif dan larutan ionik sebagai elektrolit," *Jurnal Zarah*, vol. 6, no. 1, pp. 39-46, 2018.
- [24] D. N. Rositawati, "Influences of Annealing on the Electrical Properties of BaO, 5SrO, 5TiO₃," *International Journal of Applied Sciences and Smart Technologies*, vol. 1, no. 1, pp. 23-32, 2019.

This page intentionally left blank

Comparison the Adsorption of Pb with Ecofriendly Bio-Adsorbent from Rice Husk Ash and Boiler Fly Ash

Enda Rasilta Tarigan¹, Anna Angela Sitinjak^{1*},
Meriahni Silalahi¹, Switamy Angnitha Purba¹,
Yenny Sitanggang, Darry Purba¹

¹Politeknik Teknologi Kimia Industri Medan, Medan, 20228 Indonesia

*Corresponding Author: annaangelasitinjak@yahoo.co.id

(Received 10-09-2023; Revised 16-11-2023; Accepted 29-11-2023)

Abstract

The amount of environmental pollution is in line with the increasing of industry. Industry can generate waste in the form of solid, liquid or gas. Utilization of waste as an adsorbent is a solution that can be done in dealing with waste such as metal waste contained in water. Therefore, this research aims to make a bio-adsorbent in the form of silica from rice husk ash and boiler fly ash and know the comparison of the Pb absorbed. The research method used is an experimental method by synthesizing the manufacture of silica. Then testing of Pb based on contact time was 30 minutes, 60 minutes, 90 minutes and 120 minutes. The results showed that the two silica-based bio-adsorbents could adsorb Pb. Bio-adsorbent from rice husk ash absorbed 56.51% of Pb in 30 minutes, 52.93% in 60 minutes, 48.65% in 90 minutes and 43.55% in 120 minutes. The bio-adsorbent from the fly ash boiler absorbed 50.15% of Pb in 30 minutes, 44.28% in 60 minutes, 38.48% in 90 minutes and 36.45% in 120 minutes. Bio-adsorbent from rice husk ash absorbs more Pb ions than from boiler fly ash. Because the silica in the rice husk ash forms a collection in the pores, whereas in the fly ash boiler there is silica that is spread out.

Keywords: Bio-adsorbent, Fly ash boiler, Rice husk ash, Waste

1 Introduction

The increased industrial development actually causes high waste or environmental pollution problems [1]. The boiler combustion process from the palm oil processing industry produces various waste products, one of which is fly ash [2-4]. Fly ash is a large amount of solid waste and is simply thrown away or piled up in industrial areas. Likewise with the waste from the rice milling industry, in the form of rice husk ash. Boiler fly ash

and rice husk ash can cause problems for the environment [5], such as by accumulation and when it rains it can be carried into waters so that the water is polluted and the quality of the ecosystem decreases, and disrupts breathing [6,7].

Apart from air and solid waste, environmental pollution also occurs from liquid waste. Water is more often polluted by inorganic components. Initially, liquid waste started from household waste, then developed from industrial activity sources. It is because the industry does not process waste optimally. The content of these metals can be toxic to living things. Because the life cycle of living creatures is very dependent on water, indirectly, living creatures may consume polluted water [8]. The importance of water for the survival of living things is our main task in maintaining water quality.

The utilizing waste into a product is one way to deal with the waste produced, one of which is by turning it into an adsorbent [9]. Adsorbents are solid substances that can absorb certain components in a solution. Adsorbents usually use materials that have pores or at certain locations within the particle. In general, these pores are small so that their surface area becomes larger than the outer surface. Separation occurs due to differences in molecular weight or differences in polarity, which cause some molecules to stick more tightly to the surface than other molecules. In the adsorption process, many factors can influence the rate of the adsorption process and the amount of adsorbate that can be absorbed. The factors that influence the adsorption process [10] are agitation, adsorbent characteristics, adsorbent pore size and contact time. The activating materials used in activating the adsorbent are like NaOH and HCl. Activating ingredients function to degrade or hydrate organic molecules during the process, limiting tar formation and assisting the decomposition of organic compounds during subsequent activation.

Various research has been carried out in dealing with waste. Tandung, Nur and Mardiah [11] researched the effect of boiler ash as an absorption agent and used as an air cathode by analyzing it mathematically (multiple linear regression model). Nurhasni [12] found that the absorption of Cd and Cr metal ions in wastewater can be using rice husks. From the results of previous studies were stated that boiler fly ash and rice husk ash could be modified and useful in absorbing liquid waste.

Boiler fly ash and rice husk ash have similarities in terms of the main compounds in the cell walls, namely polysaccharides (coarse fibre or cellulose, lignin and

hemicellulose) which have hydroxyl groups that can play a role in the adsorption process, so in this study used oil palm boiler fly ash and rice husk ash as an active metal bio-adsorbent in liquid waste as an effort to tackle wastewater pollution and in which the differences between the two will be seen in terms of their ability to absorb Pb based on contact time.

2 Material and Methods

Materials

The materials used in this research are NaOH NaOH for analysis Merck, HCl 37 % Merck, DI water, double distilled water, Pb(NO₃) for analysis Merck, boiler fly ash, rice husk ash.

Instrumentation

Rice husk ash and boiler fly ash were characterized by SEM-EDX JEOL JSM-6510LA, FTIR Perkin-Elmer UATR Spectrum Two, AAS.

Methods

Synthesis SiO₂ from Palm Oil Boiler Fly Ash.

Fly ash from palm oil mill waste is calcined at a temperature of 500 °C for 5 hours, Fly Ash is mixed with 5M HCl with a ratio of 1:4, stirred and heated at a temperature of 70 °C for 4 hours using a magnetic stirrer with a rotation speed of 300 rpm, then the solution was filtered to obtain the precipitate. The fly ash precipitate formed was added with NaOH in a ratio of 1:4 for 4 hours at a temperature of 70°C and stirred with a magnetic stirrer at a rotation speed of 300 rpm for 8 hours and silica powder was formed. Next, washed with distilled water until the pH was neutral and dried in an oven at 105 for 2 hours. Hydrothermal for 8 hours at 180⁰C. Furthermore, silica powder was tested by SEM/EDX to determine surface morphology. Next, the silica powder was interacted with Pb ions with a mass of 1 gram of silica powder and varied the contact time of the adsorbent with Pb and tested with AAS.

Synthesis SiO₂ from Rice Husk Ash

Rice husk ash from palm oil mill waste is calcined at a temperature of 500 °C for 5 hours, rice husk ash is mixed with 5M HCl at a ratio of 1:4, stirred and heated at a

temperature of 70 °C for 4 hours using a magnetic stirrer with a rotation speed of 300 rpm , then the solution was filtered to obtain a precipitate. The rice husk ash precipitate that was formed was added with NaOH at a ratio of 1:4 for 4 hours at a temperature of 70°C and stirred with a magnetic stirrer at a rotation speed of 300 rpm for 8 hours and silica powder was formed. Furthermore, it was washed with distilled water until the pH was neutral and dried in an oven at 105 for 2 hours. Hydrothermal for 8 hours at 180 °C. Furthermore, silica powder was tested by SEM/EDX to determine surface morphology. Next, the silica powder was interacted with Pb ions with a mass of 1 gram of silica powder and varied the contact time of the adsorbent with Pb and tested with AAS.

Testing of Bio-Adsorbent on Pb Metal

A concentration of 1000ppm of Pb metal was prepared by dissolving 1.56gr of PbNO₃ in 1000mL of DI water. Rice husk bio-adsorbent was weighed as much as 1 gr and put into 100 mL of PbNO₃ solution and stirred at 300rpm with variations in contact time of 10 minutes, 20 minutes, 30 minutes, 60 minutes and 120 minutes. Doing the same thing to the bio-adsorbent made from fly ash boiler.

3 Results and Discussions

The initial concentration of Pb metal was 1000 mg/L. Table 1 below shows the concentration of Pb metal left in the solution after contact with samples of rice husk ash and fly ash with a sample mass of 1 gram.

Table 1. The Remaining Pb Metal Concentration in Solution

No	Contact Time (Minute)	Concentration of Pb metal remaining after contact with the rice husk ash sample which was activated physically and chemically (mg/L)	Concentration of Pb metal remaining after contact using fly ash which is activated physically and chemically (mg/L)
1	30	434,9190	498,4790
2	60	470,7070	557,1720
3	90	513,4530	615,1210
4	120	564,4800	635,5050

From the research results it was found that after being contacted for 30 minutes, 60 minutes, 90 minutes and 120 minutes, absorption of Pb metal occurred in both bio-adsorbents. This means that rice husk ash silica and boiler fly ash can absorb Pb metal in water and can be used as an adsorbent that is environmentally friendly because it does not dissolve easily in water [13-15].

FTIR characterization in this study was only carried out on rice husk ash which had absorbed Pb, to determine the main functional groups. The FTIR results of rice husk ash silica are shown in the Fig. 1.

The results of the Fourier Transform Infra-Red (FTIR) Spectrum show that the O-H (Stretching) functional group has an absorption band of around 3325.04 [16] and O-H bending around 1637.64 [17]. In the figure above, the silica functional group is no longer visible. In the adsorption of Pb, ion exchange occurs where silica containing silanol (Si-OH) and Siloxane (Si-O-Si) functional groups are bonded with certain metal ions, in this case Pb ions [18]), so that level of Pb in water decrease.

The comparison of absorption results between bio-adsorbent from rice husk ash and boiler fly ash, it can be seen that the optimum contact time for the absorption of Pb is around 30 minutes, after which there is a decrease in the absorption of both bio-adsorbents. Because the longer the two bio-adsorbents are in contact with Pb, the bonding between the H^+ ions in the solution and the hydroxyl groups in cellulose to form OH_2^+

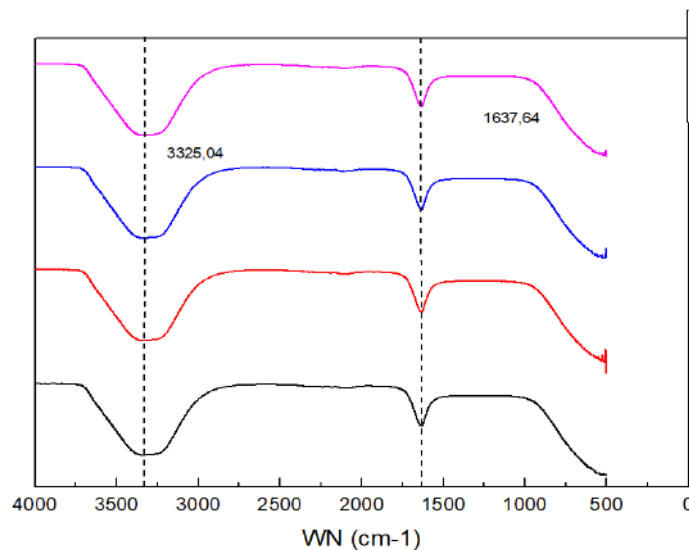


Figure 1. Test Result of FTIR

increases, resulting in rejection of the metal ions so that the pores of the bio-adsorbent become saturated and absorption decreases. This is in line with the research of Mujiyanti, Nurmasari and Nurhikmah [19] which states that the optimum time of absorption for Pb is about 30 minutes. From the graph it is also found that the highest absorption of Pb is bio-adsorbent from rice husk ash at 43% to 57%, while in boiler fly ash it is between 36% to 50%.

Table 2. Physically activated rice husk composition (Test results with EDX)

ZAF Method Standardless Quantitative Analysis (Oxide)							
Fitting Coefficient : 0.0382							
Total Oxide : 24.0							
Element	(keV)	Mass%	Sigma	Mol%	Compound	Mass%	Cation
K							
C K	0.277	11.04	0.33	39.02	C	11.04	0.00
2.9069							
O		45.24					
Mg K	1.253	0.44	0.05	0.78	MgO	0.74	0.16
0.7126							
Si K	1.739	37.68	0.46	56.94	SiO ₂	80.62	11.39
84.5326							
P K	2.013	0.76	0.10	0.52	P ₂ O ₅	1.74	0.21
1.1617							
K K	3.312	4.31	0.10	2.34	K ₂ O	5.20	0.94
9.5541							
Mn K	5.894	0.51	0.07	0.40	MnO	0.66	0.08
1.1320							
Total		100.00		100.00		100.00	12.77

Table 3. Physically activated Fly ash composition (Test results with EDX)

ZAF Method Standardless Quantitative Analysis (Oxide)							
Fitting Coefficient : 0.0326							
Total Oxide : 24.0							
Element	(keV)	Mass%	Sigma	Mol%	Compound	Mass%	Cation
K							
C K	0.277	14.41	0.34	45.73	C	14.41	0.00
4.0288							
O		39.63					
Na K	1.041	7.72	0.16	6.40	Na ₂ O	10.41	3.25
14.6926							
Mg K	1.253	0.37	0.05	0.59	MgO	0.62	0.15
0.5482							
Al K	1.486	1.19	0.08	0.84	Al ₂ O ₃	2.25	0.43
2.1237							
Si K	1.739	29.86	0.40	40.53	SiO ₂	63.88	10.30
62.8020							
Cl K	2.621	1.89	0.05	2.04	Cl	1.89	0.00
4.3513							
K K	3.312	1.75	0.06	0.85	K ₂ O	2.11	0.43
3.9540							
Ca K	3.690	3.17	0.10	3.02	CaO	4.44	0.77
7.4994							
Total		100.00		100.00		100.00	15.33

From Table 2 and 3 regarding to the EDX test results, it is found that the SiO₂ content in rice husk ash is 80.62% and in boiler fly ash is 63.88%. From the table it also appears that the presence of carbon is 11.04% in rice husk ash and 14.41% in boiler fly ash. Then chemical treatment was added and the EDX results were obtained as listed in Tables 4 and 5.

From Table 4 and 5, it was found that silica in rice husk ash after physical and chemical activation was 79.53% and carbon 17.94%. Silica in the fly ash boiler after physical and chemical activation was 80.35% and carbon 17.02%. From result experimental, only given physical treatment (before chemical treatment) silica in rice husk ash was higher than boiler fly ash but carbon in rice husk ash was lower than boiler

Table 4. Physically and chemically activated rice husk composition

ZAF Method Standardless Quantitative Analysis (Oxide)							
Fitting Coefficient : 0.0371							
Total Oxide : 24.0							
Element	(keV)	Mass%	Sigma	Mol%	Compound	Mass%	Cation
C K	0.277	17.94	0.39	52.36	C	17.94	0.00
5.2345							
O		42.93					
Mg K	1.253	0.30	0.04	0.44	MgO	0.50	0.11
0.5259							
Si K	1.739	37.18	0.43	46.39	SiO ₂	79.53	11.84
90.3234							
K K	3.312	0.89	0.05	0.40	K ₂ O	1.07	0.20
2.1286							
Cu K	8.040	0.76	0.10	0.42	CuO	0.95	0.11
1.7876							
Total		100.00		100.00		100.00	12.26

Table 5. Summary of Physically and chemically activated rice husk composition

No	Sample	Parameter	Unit	Value of Analysis Result	Test Method
1	SP 23-1088-06-01-1 (Ash Akt)	C	%	17.02	SEM/Jeol Jsm 6510 La
		Na ₂ O		0.67	
		SiO ₂		80.35	
		K ₂ O		0.59	
		CaO		0.45	
		CuO		0.91	

fly ash. After physical and chemical treatment, there was a decrease in silica in rice husk ash but the carbon content increased and was the highest compared to carbon fly ash, although there was an increase in silica and carbon content. The bio-adsorbent that is connected with Pb metal in water is a bio-adsorbent that has received physical and chemical treatment. This means that through the addition of chemical activation, it causes an increase in the carbon content, in which carbon helps or facilitates silica in the uptake of Pb metal. This is because physical and chemical activation forms pores so that they can effectively absorb various kinds of heavy metals. From this research, knowledge was obtained that if the adsorbent contains silica and carbon, the metal absorption can be higher. This is in line with previous research [20] that silica-activated carbon composites can be formed and have a greater adsorption capacity for heavy metals compared to silica and activated carbon itself.

From the SEM test above to see the morphology or topography of the AKF ash samples from the Fig. 2(a) and 3(a). Fly Ash it shows that the morphology of the two samples is not homogeneous or has an uneven size distribution and agglomeration is formed. By using the image J and Origin applications, pore diameters were obtained in both samples, namely around 3.43 nm (Fig. 2(b) for fly ash and 3.58 nm for rice husk Fig.3(b). The particle size of the active ash sample is larger than rice husk, indicating that the absorption capacity of rice husk is higher in adsorbing the active metal Pb which has an atomic radius of around 30 -300 pm.

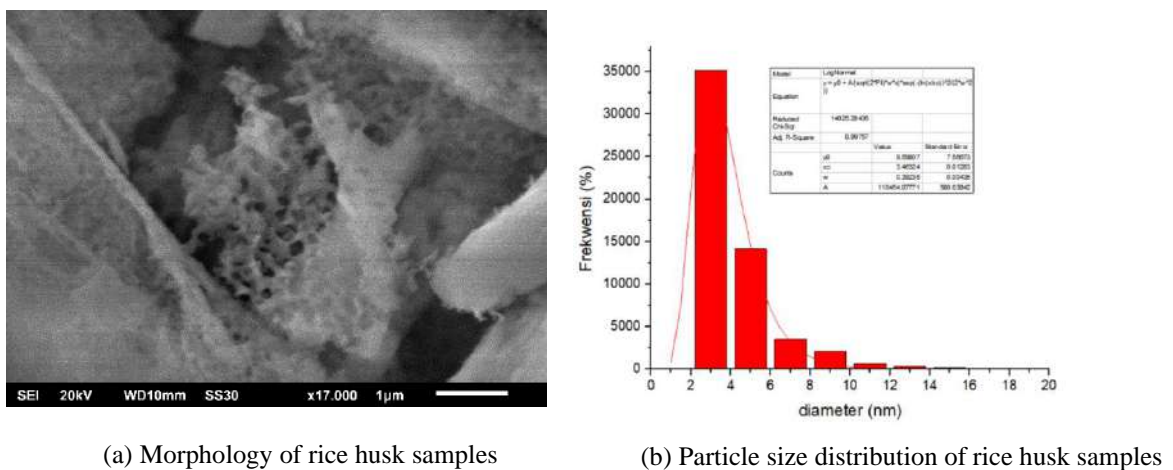
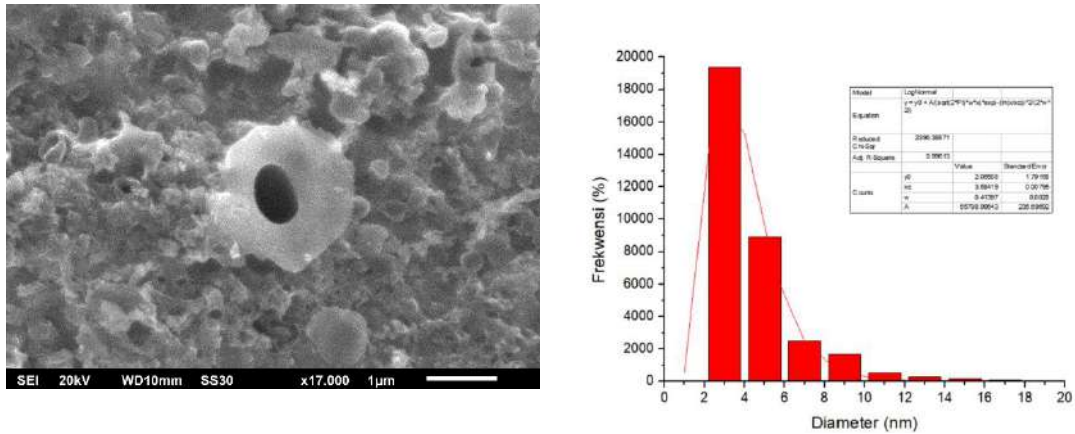


Figure 2. Characterization results of rice husk samples that were physically and chemically activated using SEM



(a). Morphology of the physically and chemically activated boiler fly ash sample

(b). Particle size distribution of fly ash

Figure 3. Characterization results of fly ash sample that were physically and chemically activated using SEM

The particle size distribution of the sample can be seen in the Fig. 2(a) rice husk and Fig. 3(b) is the fly ash. This particle size distribution can also show the absorption capacity of the active ash and active husk samples against the contact time, where as the contact time increases the adsorption of the metal Pb decreased, this was because the diameter of the sample particles, both active ash and active husk, was greater than the atomic radius of Pb.

4 Conclusions

Waste can be processed into products that can overcome the waste problem. Utilizing rice husk ash and boiler fly ash waste into bio-adsorbent in the form of silica can be done, especially since the price of these two bio-adsorbents is relatively cheap and does not dissolve easily in water. From the research it was found that both bio-adsorbents from rice husk ash and boiler fly ash can absorb Pb. Then, after physical and chemical activation, porous silica is formed and there is an increase in carbon. The silica in rice husk ash forms clusters that are visible from the morphology so that it binds Pb ions more strongly, whereas in boiler fly ash the silica is dispersed, plus the carbon content in rice

husk ash is higher than boiler fly ash. For this reason, the ability to absorb Pb by bio-adsorbents from rice husk ash is higher than boiler fly ash.

Acknowledgements

The researcher would like to thank PTKI Medan through the UPPM unit for the financial assistance provided so that this research could be carried out well.

References

- [1] A. F. Dashti, M. O. Fatehah, M. A. Zahed, "Waste management of the palm oil industry: present status and future perspective," *Journal of Environmental Engineering and Science*, vol. 17, no. 2, pp. 75-88, 2022.
- [2] J. J. P. Telaumbanau, "Using Fly Ash and Bottom Ash Boiler of Palm Oil Factories as Adsorbents for Adsorption of Color in Artificial Liquid Waste," *Jurnal Mekintek*, vol. 11, no. 2, pp. 59-67, 2020.
- [3] R.Y. Farandia, M. Olivia, L. Darmayanti, "Kinerja Beton High Volume POFA," *Jurnal Online Mahasiswa (JOM) Bidang Teknik dan Sains*, vol. 1, no. 1, 2015.
- [4] M. Liu, C. P. Chua, U. J. Alengaram, and M. Z. Jumaat, "Utilization of Palm Oil Fluel Ash as Binder in Lightweight Oil Palm Shell Geopolymer Concrete," *Hindawi Publishing Corporation Advances Amterial Science and Engineering*, vol. 12, 2014.
- [5] S.K.S. Hossain, L.Mathur & P.K. Roy, "Rice Husk ash as an alternative source of silica in ceramics: a review," *Journal of Assian Ceramic Societies*, vol. 6, no. 4, pp. 299-313, 2018.
- [6] PTPN., *Material Balance Pengolahan Kelapa Sawit*. Pekanbaru, 2011.
- [7] M. Riyadi, "Pemanfaatn Abu Sekam Padi sebagai Substitusi Sebagian Semen pada Mortar Semen Pasir," *Politeknologi*, vol. 12, no. 5, pp. 39-46, 2013.
- [8] R. Pratiwi, D.P.S. Prinajati, "Adsorption for lead removal by chitosan from shrimp shells," *Indonesian Journal of Urban and Environmental Technology*, vol. 2, no. 1, pp. 35-46, 2018.

- [9] S. Arita, D. Kristianti, L. N. Komariah, "Effectiveness of Biomass-Based Fly Ash in Pulp and Paper Liquid Waste Treatment," *South African Journal of Chemical Engineering*, vol. 41, pp. 79-84, 2022.
- [10] I. Syauqiah, M. Amalia, H. A. Kartini, "Analisis Variasi Waktu dan Kecepatan Pengaduk pada Proses Adsorpsi Limbah Logam berat dengan Arang Aktif," *Info Teknik*, vol. 12, no. 1, pp. 11-20, 2011.
- [11] M.R. Tandung, S. Nur, Mardiah, "Utilization of Palm Boiler Ash as Air Catode Material in Air Aluminium Battery," *Jurnal Chemurgy*, vol. 4, no. 2, pp. 38-44, 2020.
- [12] Nurhasni, *Penyerapan Ion Logam Cd dan Cr dalam Air Limbah Mneggunakan Sekam Padi*, Tesis Universitas UIN Syarif Hidayatullah: Jakarta, 2014.
- [13] H. K., Okoro, S. M. Alao, S. Pandey, S. Jimoh, K. A. Basheeru, Z. Caliphs, J.C. Ngila, "Recent Potential Application of Rice Husk as an Eco-friendly adsorbent for removal of heavy metals," *Springer Applied Water Science*, vol. 12, no. 259, 2022.
- [14] P.S. Utama, R. Yamsaengsung, C. Sangwichien, "Silica Gel Derived from Palm Oil Fly Ash," *Songklanakarin J.Sci. Technol.*, vol. 40, no. 1, pp. 121-126, 2018.
- [15] Y. Poo-arporn, et al., "The Investigation of SiO₂ structure obtained from the combustion of rice husk", *International Conference on Engineering and Industrial Technology-IOP Publishing*, 2020,
- [16] N. P. S. N. Utari, I W. Sudiarta, dan P. Suarya, "Sintesis Dan Karakterisasi Silika Gel Dari Abu Vulkanik Gunung Agung Melalui Teknik Sol-Gel," *Jurnal Kimia (Journal of Chemistry)*, vol. 14, no. 1, pp. 30-36, 2020.
- [17] F. Huang, H. Hao, W. Sheng, X. Lang, "Dye-TiO₂/SiO₂ assembly photocatalysis for blue light-initiated selective aerobic oxidation of organic sulphides," *Chemical Engineering Journal*, vol. 423, 2021.
- [18] I. S. Hardyanti, et al., "Pemanfaatan Silika (SiO₂) dan Bentonit sebagai Adsorben Logam Berat Fe pada Limbah Batik," *Jurnal Sains Terapan*, vol. 3, no. 2, pp. 37-41, 2017.
- [19] D. R. Mujiyanti, R. Nurmasari, Nurhikmah, "Adsorption Pb(II) on Silica Gel from Rice Husk Ash," *Sains dan Terapan Kimia*, vol. 10, no. 1, 33-38, 2016.

- [20] M. H. Givianrad, M. Rabani, M. Saber-Tehrani, P. Aberoomand-Azar, M. Hosseini Sabzevari, "Preparation and characterization of nanocomposite, silica aerogel, activated carbon and its adsorption properties for Cd (II) ions from aqueous solution," *Journal of Saudi Chemical Society*, vol. 17, pp. 329-335, 2013.

Smart Control and Monitoring System for Closed Poultry House based on IoT

Surateno¹, Syamsiar Kautsar^{2*}, Risse Entikaria Rachmanita², Aan Anwaludin³, M. Adhiyatma³, Rosa Tri Hertawamati³, Budi Hariono⁴, Fendik Eko Purnomo², and Sryang Tera Sarena⁵

¹*Department of Information Technology,
Politeknik Negeri Jember, Jember 164, Indonesia*

²*Department of Engineering,
Politeknik Negeri Jember, Jember 164, Indonesia*

³*Department of Animal Science,
Politeknik Negeri Jember, Jember 164, Indonesia*

⁴*Department of Agricultural Technology,
Politeknik Negeri Jember, Jember 164, Indonesia*

⁵*Department of Electrical and Electronic Engineering,
University of Nottingham, United Kingdom*

**Corresponding Author: syamsiar_kautsar@polije.ac.id*

(Received 23-08-2023; Revised 07-12-2023; Accepted 18-03-2024)

Abstract

The application of technology in the livestock sector has been carried out to increase the productivity of the livestock business. Closed chicken coops are one of the applications of technology in the livestock sector by utilizing a microcontroller that can control the temperature and ammonia levels in the coop under optimal conditions for fattening chickens. When the temperature rises (hot), the system set on the microcontroller will make the fan turn on automatically. This study aims to improve the offline and semi-manual fan control system in closed chicken coops to become automatic. By utilizing Internet of Things (IoT)-based technology, monitoring the condition of the chicken coop can be more easily accessed remotely. The method uses the if-then rule to regulate fan performance based on variable temperature and ammonia levels. The fan work set-point value can be set through the Android application online. Based on test results, the use of the IoT system can work well with an average delay of around 3,3 seconds. A consumer satisfaction survey was conducted on breeders with satisfactory results to ensure its suitability as a commercial product with a satisfaction level of 87.55 (very good).

Keywords: broiler, closed-house, IoT, microcontroller,



1 Introduction

The application of technology to increase the productivity of a business has been widely carried out. It has become a mandatory thing that must be done in modern times like today, including the application of technology in animal husbandry. One application of technology in animal husbandry is the application of technology that can intervene in the environment in the cage to be suitable for optimizing livestock growth. Technological interventions to make the environment in the cage suitable for these needs are often called microclimates.

The technology to create a microclimate in this cage by utilizing a temperature and humidity sensor connected to a microcontroller makes it possible to automatically adjust the temperature and humidity in the cage according to the needs [1, 2]. One example of a tool used in the field is the Temptron which is the primary tool for controlling temperature and humidity in closed-house chicken coops. Temptron has a microcontroller connected to the temperature and humidity sensor in the enclosure so that the microcontroller will turn on the fan when the temperature increases from the expected standard.

Temptron as a microclimate controller in closed-house chicken coops, is still offline, which means that temperature and humidity data can only be accessed on Temptron, with the coops looking directly at the data presented on Temptron. This can be done routinely by cage children in charge of raising livestock daily. However, of course, it is impossible to be done by supervisors responsible for several cages with cage locations that may be far apart or even in different areas.

This research was conducted to design and prototype a tool or platform that allows Temptron to be accessed online using the Internet of Things (IoT) [3, 4]. This will benefit the cage supervisor to monitor and evaluate the microclimate of several closed-house chicken coops without always having to come directly to the cage.

The cage is one of the most critical factors in the maintenance of chickens because the comfort of the cage dramatically affects the productivity that will be produced. The cage system for raising chickens is divided into two: the open-house system and the closed-house system. Open-house cages have microclimate characteristics depending on the climatic conditions of the surrounding environment. In contrast, closed-house cages

have microclimate characteristics that can be adjusted with a tool according to the required conditions [5]. Environmental factors influence productivity in chicken rearing during maintenance, including the internal environment in the cage. Farmers need help regulating the temperature and humidity in the open house system, so it does not have an optimal effect on achieving chicken productivity. The cage has another function as a place for chickens to move in addition to protection, so a comfortable cage is needed during maintenance [6].

A closed house is a cage design with a closed system so that environmental conditions can be adjusted according to needs. A system is also designed to remove excess heat and gases (such as CO₂) and ammonia. This closed system cage is a solution for raising chickens susceptible to heat stress [7]. Chickens quickly experience heat stress at high environmental temperatures because chickens belong to warm-blooded animals (homeothermic), which have skin without sweat glands, and most of their bodies are covered with feathers. This causes chickens to have difficulty dissipating excess heat in the body.

Meanwhile, if there is a decrease in environmental temperature, the chicken tries to produce heat by moving and eating less, which will interfere with chicken productivity [8]. The closed cage has two working systems, a tunnel and an evaporative cooling system (ECS), controlled by a microcontroller chip. These systems utilize wind flow to remove residual gas, heat, and water vapor and provide oxygen to the cage. Especially the ECS system for controlling air circulation in the cage is also accompanied by flowing water in the fibrous field [9].

The industrial revolution 4.0 "forces" and provides space for every field of business to improve quality in facing global challenges, including the livestock sector. One of the current applications of industrial technology is the development of systems that assist humans in controlling an electronic system with an Internet of Things (IoT)-based program. The development of technology in the field of animal husbandry by utilizing the IoT system is expected to be able to help increase livestock productivity [10]. IoT is a computing and communication technology that adds sensors, microcontrollers, and media for sending information on an object to be accepted and even controlled by a particular application/platform by utilizing the internet network. The system can be used

in everyday life with unique markers of objects with a platform to send and receive data over a network without direct human intervention [11].

2 Material and Methods

The IoT-based control system in the Closed House consists of 3 panels: the sensor panel, the main panel, and the contactor panel. The sensor panel is mounted in the center of the cage. This panel contains an integrated sensor to read the condition of the Closed house and send the data to the controller on the main panel serially. The sensor and main panels are connected via a 25-meter DB9 serial cable. The central panel consists of a controller, LCD, AC load driver, and wifi devices to send data to the cloud database via the Internet. The contactor panel consists of a 3-phase contactor, a thermal overload relay, and an MCB as a 'bridge' to control the 3-phase exhausting fan in the Closed House.

Integrated sensor [12] consists of ammonia, temperature, and humidity sensors. The Ammonia sensor used is the MQ137 type. In comparison, the humidity and temperature sensors use the AM2315 sensor. The MQ137 sensor outputs analog data, which is then read by the ADC pin on the microcontroller. In contrast, the AM2315 sensor uses I2C data communication. ATmega328 microcontroller is used as a controller on the integrated sensor. Fig. 1 is a picture of the installation and block diagram of the integrated sensor system installed in the closed house.



Figure 1. System block diagram of sensor unit

The central panel is located outside the cage, next to the entrance. This facilitates offline data monitoring by the operator without entering the cage. The controller on the main panel uses an ATmega2560 + ESP8266 microcontroller. The ATmega2560 microcontroller is tasked with reading serial data from the sensor panel and processing the data to control the Exhaust Fan. The ATmega2560 also forwards serial data received from the sensor panel to the ESP8266. When connected to the internet, the ESP8266 will send temperature, humidity, and ammonia data to the cloud database [4, 13]. Fig. 2 is an installation photo and a system block diagram of the main panel.

The contactor panel is located inside the enclosure, near the exhaust fan. Exhaust fans used in closed houses use 3-phase electricity. For this reason, the contactor panel is equipped with a 3-phase 18A contactor plus a thermal overload relay. The coil to activate the contactor is connected to the Solid-State Relay on the main panel. Solid-state relays are electronic components that control AC loads with a 5-volt DC trigger input. When the microcontroller provides logic 1 (5volt), the SSR is active, so the 3-phase contactor is also active. When the 3phase contactor is active, the exhaust fan will turn on. Fig. 3 is a photo of the installation of the contactor panel circuit.

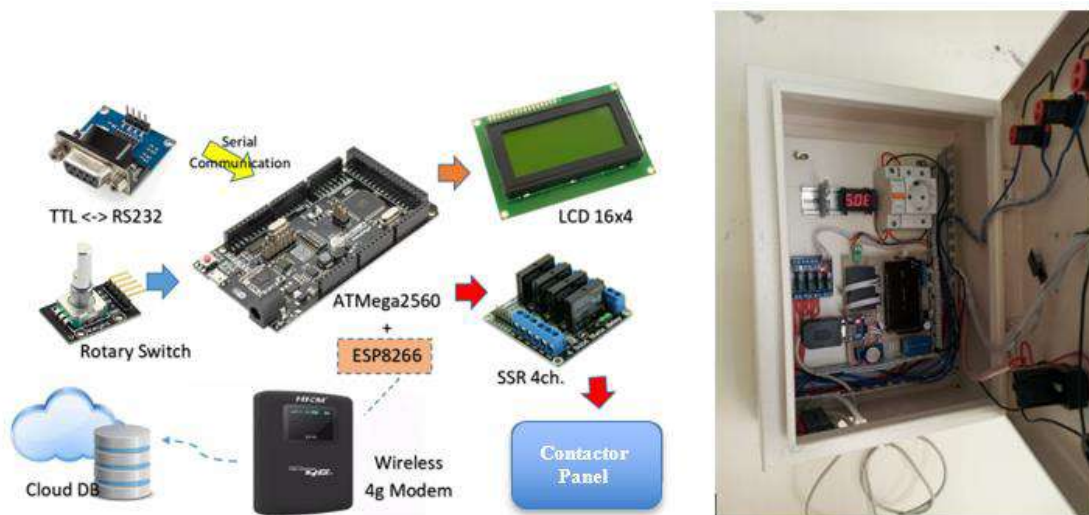


Figure 2. System block diagram of controller unit



Figure 3. Contactor panel unit.

ATMega328 microcontroller will read sensor data MQ137 and AM2315. The data is combined into 1 data protocol with the format shown in Fig. 4. The data is sent to the ATMega2560 microcontroller via a serial cable. The TTL to serial RS232 serial converter module is used to send data using a long cable. RS232 serial communication allows data cables with a maximum length of 100 meters. Where 'xxx' is the temperature value, 'yyy' is the humidity value, and 'zzz' is the value of NH₃ content.

The central panel has an ESP8266, which reads and sends data to the cloud database. The data sent to the cloud is on temperature, humidity, and ammonia gas levels. While the data read from the cloud is data set point temperature, humidity and ammonia gas levels, and manual fan setting data. These data can also be accessed through the Android application on a smartphone. Fig. 5 illustrates data communication between the ATMega328, ATMega2560, and ESP8266 Microcontrollers.

$$\boxed{\text{xxx}+\text{A}+\text{yyy}+\text{B}+\text{zzz}}$$

Figure 4. Protocol data format.

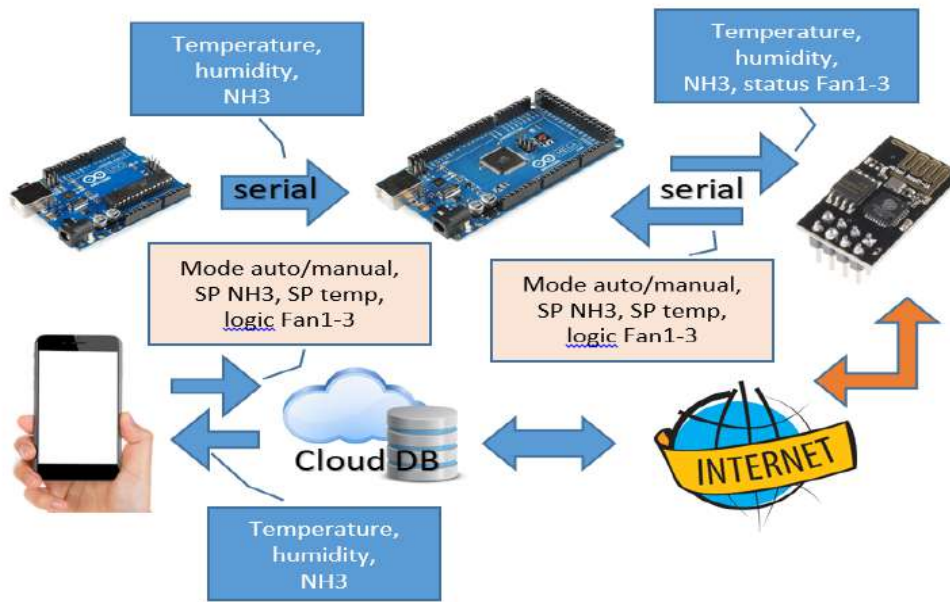


Figure 5. Data communication process.

On the central controller, there are two modes: automatic mode and manual mode [1, 14]. The exhaust fan can be activated via a smartphone by entering manual mode. The three exhaust fans will be activated by entering automatic mode based on the parameters stored in the cloud database. There are 12 parameters for the activation of the three fans. Fan1 NH₃ low level, Fan1 NH₃ High level, Fan2 NH₃ low level, Fan2 NH₃ high level, Fan3 NH₃ low level, Fan3 NH₃ High level, Fan1 temperature low level, Fan1 temperature high level, Fan2 temperature low level, Fan2 temperature high level, Fan3 temperature low level, and Fan3 temperature high level. The ATMega2560 controller for the exhaust fan control system works like the flowchart in Fig. 6. Humidity is limited to monitoring in this system. In the cage for this study, a humidifier was not used to regulate the humidity of the cage. When the fan is active when the temperature or ammonia is at a certain level, the humidity will also naturally adjust to the outside environment of the cage.

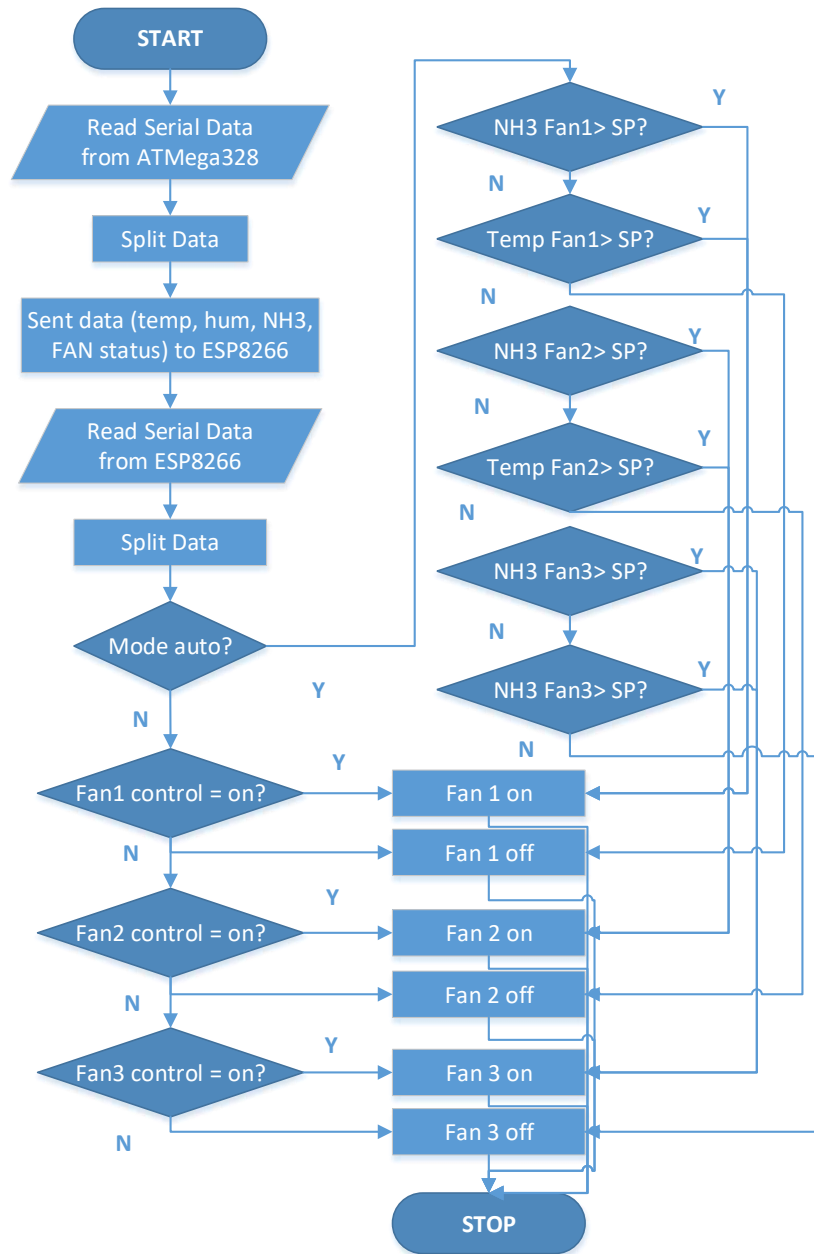


Figure 6. Flowchart system.

3 Results and Discussions

The exhaust fan can be activated via a smartphone by entering manual mode. At this stage, the overall features of the Smart Closed House system are tested. The first step is to validate the sensor used. This is to find out whether the data read by the sensor is following the actual conditions. The MQ137 sensor was validated using an Ammonia Gas

Detector Smart Sensor type AR8500, while the AM2315 sensor was validated using a UT333 Digital Temperature & Humidity Meter. Data is taken as much as five every minute at the exact location. Table 1 is sensor validation data with digital measuring instruments. From the measurement results, the sensor measurement results are obtained, which are not much different from the manufacturer's measuring instrument values.

The next test is to check the data communication between the sensor and the control panel. Checked the data accessed from the sensor and displayed it on the LCD on the main panel. Table 2 is the result of testing data communication between the ATmega328 microcontroller and the ATmega2560. A sampling of data was carried out every 10 minute 10 times a day. Based on the test results, the data can be sent 100%.

Next, check the data from ATmega2560 with the data displayed on the smartphone. As discussed in the previous subchapter, data sampling was done every 10 minutes a day. The delay in sending data to the cloud database is also measured. Based on the test results, data can be sent 100% with an average IoT-based data communication time of 3,3 seconds (Table 3). Fig. 7 is an example of data displayed on a smartphone with internet speed, as listed. Information on the application is made in Bahasa, to make it easier for users to use.

Table 1. Sensor validation

	Minutes	Sensor	Digital	Δ
NH ₃ PPM	1	7,1	7,2	0,1
	2	7,1	7,2	0,1
	3	7,1	7,3	0,2
	4	7,2	7,3	0,1
	5	7,2	7,3	0,1
			<i>average</i>	<i>0,12</i>
Temperature °C	1	32	32,4	0,4
	2	32	32,4	0,4
	3	32	32,4	0,4
	4	32	32,4	0,4
	5	32	32,4	0,4
			<i>average</i>	<i>0,4</i>
Humidity (%)	1	74	74,2	0,2
	2	74	74,2	0,2
	3	74	74,2	0,2
	4	74	74,2	0,2
	5	74	74,2	0,2
			<i>average</i>	<i>0,2</i>

Table 2. Serial communication data test

Data	Sensor (NH ₃ , temperature, Humidity) ATmega328	Sensor (NH ₃ , temperature, humidity) ATmega2560	Error
1	0, 30, 82	0, 30, 82	0%
2	0, 31, 82	0, 31, 82	0%
3	0, 30, 85	0, 30, 85	0%
4	0, 30, 82	0, 30, 82	0%
5	0, 30, 82	0, 30, 82	0%
6	0, 31, 82	0, 31, 82	0%
7	0, 31, 85	0, 31, 85	0%
8	0, 30, 82	0, 30, 82	0%
9	0, 30, 85	0, 30, 85	0%
10	0, 30, 82	0, 30, 82	0%

Table 3. On-line Communication Data Test.

Data	Sensor (NH ₃ , temperature, Humidity) ATmega2560	Sensor (NH ₃ , temperature, Humidity) Smartphone	Error	Delay (second)
1	0, 27, 87	0, 27, 87	0%	3
2	0, 27, 87	0, 27, 87	0%	2
3	0, 27, 87	0, 27, 87	0%	3
4	0, 28, 87	0, 28, 87	0%	4
5	0, 28, 83	0, 28, 83	0%	3
6	0, 29, 83	0, 29, 83	0%	3
7	0, 29, 85	0, 29, 85	0%	4
8	0, 29, 83	0, 29, 83	0%	5
9	0, 28, 85	0, 28, 85	0%	3
10	0, 29, 85	0, 29, 85	0%	3

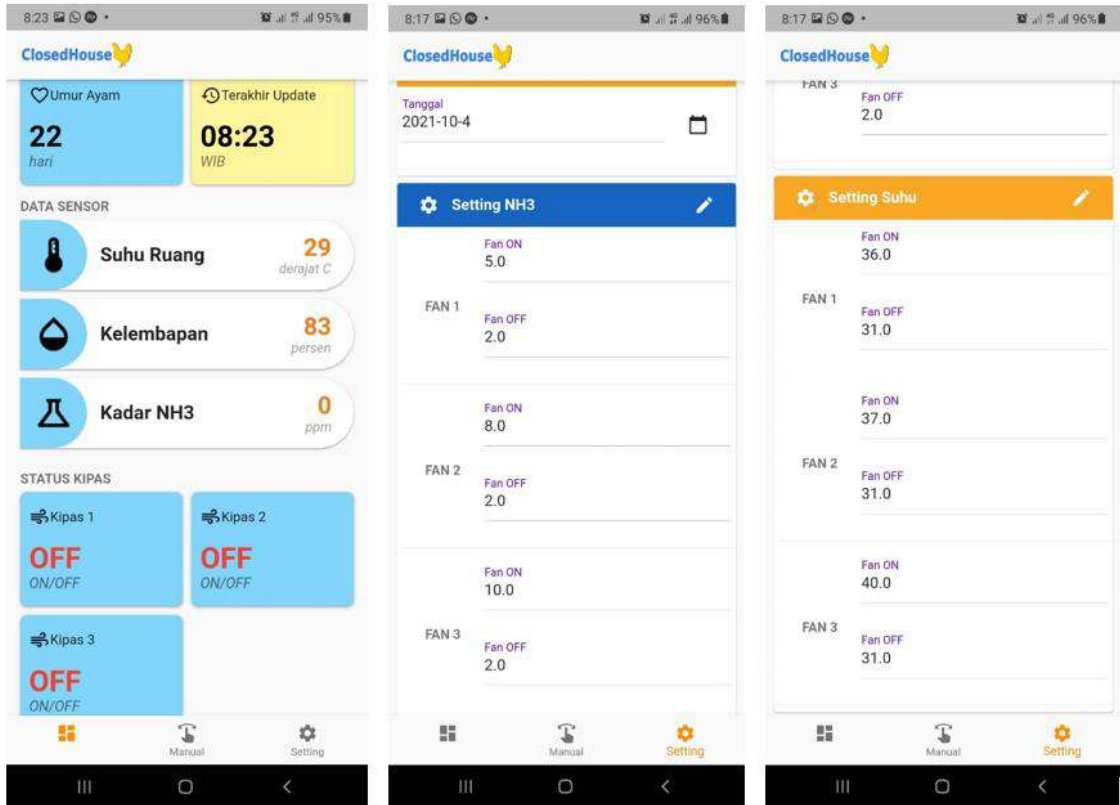


Figure 7. Application display.

In the next stage, a manual control trial was conducted using the Android application. Testing is done by setting the on-off fan through the application. The system response delay was also measured using a stopwatch. Table 4 is the result of testing the conditions of the three exhaust fans in the closed house. At the same time, Fig. 3 is an example of the condition of the application settings and fan response.

Table 4. Actuator Response Test.

Data ke-	Data Fan (1, 2, 3) Mobile App.	Data fan (1, 2, 3) Closed House	Error	Delay
1	off, off, off	Off, off, off	0%	3
2	on, off, off	on, off, off	0%	2
3	off, on, off	Off, on, off	0%	3
4	off, off, on	Off, off, on	0%	4
5	on, on, off	on, on, off	0%	3
6	off, on, on	Off, on, on	0%	3
7	on, on, on	On, on, on	0%	4

Finally, the automatic mode test was carried out. For the controller's performance testing, the sensor is conditioned to meet the work criteria in the flowchart in Fig. 6. For the AM2315 sensor; a heater is used to increase the temperature read by the sensor. For the MQ137 sensor, liquid ammonia is used, which is brought closer to the AM2315 sensor. Table 3 is the result of testing the automatic mode on the Smart Closed House system. The test with the sensor set point value is shown in Fig. 7.

Satisfaction of application users or customers as end users is another important factor that needs to be considered in application development. Application development will be built by looking at the assessment of customers (application users). If there are deficiencies or customer input, it will help improve an application. Customer satisfaction is a condition and post-purchase reaction, or after using a product (service), related to the buyer's negative or positive emotions [15]. The assessment of the sampling of application users is needed to see the reactions of application users to assess an application that is built will certainly provide benefits for evaluating an application or getting an overview of the use value obtained by users with the application. The method used is a poll (survey), which is information collected from respondents through a questionnaire whose questionnaire contains the parameters of customer satisfaction, including the ease of use of the application, the completeness of the application features, the effectiveness of the application's usefulness, and the quality of application design. A survey is one of the research methods to collect data by taking samples from a population and using a questionnaire to collect data [16]. The sample data taken involved 100 respondents who were involved in animal husbandry, including students and breeders. The assessment of each parameter is 1 - 100, with a score range of 0 – 20 is very poor; 21 – 40 is poor; 41 – 60 is sufficient; 61 – 80 is good; and 81 – 100 is very good. The results of the survey (questionnaire) obtained on the parameters of the ease of use of the application obtained an average value of 87.55 or very good, the parameter of completeness of the application features obtained an average value of 83.20 or very good, the parameter of the effectiveness of the usefulness of the application obtained an average value of 90, 87 or very good, and the application design quality parameters obtained an average value of 89.28 or very good.

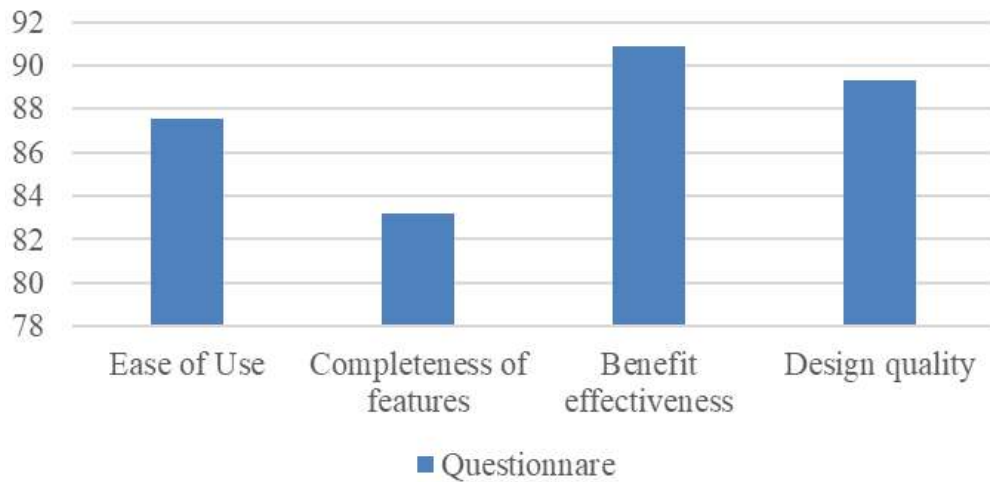


Figure 8. Application user satisfaction survey results.

The survey value of respondents on the parameters of the ease of use of the application obtained an average value of 87.55 (very good). This application is designed with simple principles and optimal function, so users are expected to understand and operate efficiently. The ease of use offered in an application will make it easier for an application product to be accepted by the user community, who is the target of building an application in this case. These people are engaged in livestock, especially Closed Houses. There are four indicators of convenience: ease of identification, ease of navigation, ease of gathering information, and ease of purchase [17] as shown in Fig. 8.

4 Conclusions

The Smart Closed House system can work well based on the test results. Serial communication between microcontrollers can work entirely with a transmission distance of 25 meters. HTTP requests for reading and sending data to and from cloud computing also work well. Data reading speed depends on internet speed. Based on the trial in the first month, the consumption of the data package needed for the IoT system is not more than 2GB. The Smart Closed House system can also use energy efficiency for closed houses. If the closed house is activated using a timer, the fan will still work according to the specified time without considering environmental conditions. System settings can also be done online to provide more flexibility to Closed House operators. The survey results from respondents on the parameters of the effectiveness of the application's usefulness

obtained an average value of 87.55 or very good. From these results, it can be described that the respondents assessed that the built Closed house application provided additional benefits to them in managing a Closed House enclosure.

References

- [1] I. Lahlouh, A. Elakkary and N. Sefiani, "State Feedback controller in a closed poultry house system," *2018 24th International Conference on Automation and Computing (ICAC)*, pp. 1-6, 2018.
- [2] A. Laknizi, A. ElMaakoul, A. Ben Abdellah, M. Bouya, S. Dhimdi and S. Said, "Evaluation of earth-air heat exchanger for cooling and heating a poultry house: Case study in Morocco," *2015 3rd International Renewable and Sustainable Energy Conference (IRSEC)*, pp. 1-5, 2015.
- [3] M. H. Lashari, A. A. Memon, S. A. A. Shah, K. Nenwani and F. Shafqat, "IoT Based Poultry Environment Monitoring System," *2018 IEEE International Conference on Internet of Things and Intelligence System (IOTAIS)*, pp. 1-5, 2018.
- [4] N. Manshor, A. R. Abdul Rahiman and M. K. Yazed, "IoT Based Poultry House Monitoring," *2019 2nd International Conference on Communication Engineering and Technology (ICCET)*, pp. 72-75, 2019.
- [5] N. S. N. Abd Aziz, S. Mohd Daud, R. A. Dziauddin, M. Z. Adam and A. Azizan, "A Review on Computer Vision Technology for Monitoring Poultry Farm— Application, Hardware, and Software," in *IEEE Access*, vol. 9, pp. 12431-12445, 2021.
- [6] Muharlién et al, "Microclimate Analysis of Opened House and Closed House in Broiler Rearing", *IOP Conf. Ser.: Earth Environ. Sci.* pp. 478 012078, 2020.
- [7] B. Song, et al, "Comparison and Correlation Analysis of Immune Function and Gut Microbiota of Broiler Chickens Raised in Double-Layer Cages and Litter Floor Pens", *ASM Journals.* vol. 10, pp. e0004522, 2022.
- [8] A. Nawaz, "Poultry Response to Heat Stress: Its Physiological, Metabolic, and Genetic Implications on Meat Production and Quality Including Strategies to Improve Broiler Production in a Warming World," *Frontiers in Veterinary Science.*, vol. 8, no. 2, pp. 1 – 16, 2021.

-
- [9] L. Ilyas, E. Ahmed and S. Nacer, "PID Controller of a MIMO system using Ant Colony Algorithm and its application to a poultry house system," *5th International Conference on Optimization and Applications (ICOA)*, pp. 1-7, 2019.
- [10] S. V. Johansen, M. R. Jensen, B. Chu, J. D. Bendtsen, J. Mogensen and E. Rogers, "Broiler FCR Optimization Using Norm Optimal Terminal Iterative Learning Control," in *IEEE Transactions on Control Systems Technology*, vol. 29, no. 2, pp. 580-592, March 2021.
- [11] T. Cao-Hoang, C.N. Duy, "Environment monitoring system for agricultural application based on wireless sensor network," In *7th International Conference on Information Science and Technology*, pp. 99 – 102, 2017.
- [12] S. A. J. Singh, P. Raviram and K. ShanthoshKumar, "Embedded based Green House Monitoring system using PIC microcontroller," *2014 International Conference on Green Computing Communication and Electrical Engineering (ICGCCEE)*, pp. 1-4, 2014.
- [13] M. R. Bhuiyan and P. Wree, "Animal Behavior for Chicken Identification and Monitoring the Health Condition Using Computer Vision: A Systematic Review," in *IEEE Access*, vol. 11, pp. 126601-126610, 2023.
- [14] X. Hu, L. Gao, L. Huo, L. Li and M. Er, "Optimal Placement of Laying Hen House Temperature Sensors Based on Genetic Algorithm," in *IEEE Access*, vol. 10, pp. 7234-7244, 2022.
- [15] Aladwani, "The development of two tools for measuring the easiness and Usefulness of transactional web sites," *Eur J Inf Syst.*, vol. 11, p. 223 – 234, 2002.
- [16] A. A. Hamiyanti, et al, "Production Performance of the Broiler Under Open, Semi-closed, and Closed House Systems During Rainy Season," *3rd International Conference on Environmentally Sustainable Animal Industry*, p. 411 – 419, 2023.
- [17] "User Acceptance Testing," in *ITNOW*, vol. 55, no. 4, pp. 62-62, Dec. 2013.

This page intentionally left blank

Misconceptions about Acceleration among Prospective Physics Teacher: The Importance of Discussion of Acceleration as a Vector Quantity

Tarsisius Sarkim^{1*}

¹*Faculty of Teacher Training and Education/Sanata Dharma University,
Jl. Affandi, Mrican, Yogyakarta, 55281*

**Corresponding Author: tsarkim@usd.ac.id*

(Received 20-02-2024; Revised 23-02-2024; Accepted 25-02-2024)

Abstract

Acceleration is a fundamental concept in mechanics. Understanding this concept influences understanding of other concepts in physics. The author's experience of teaching mechanics to prospective teacher students found that many students experienced misconceptions. Literature shows that the problem of misconceptions about acceleration is not unique to researchers. The researcher was curious about what caused this misconception. Researchers suspect that students' misconceptions about acceleration occur because the concept of acceleration is not fully understood as a vector quantity and understanding acceleration is independent of understanding the influence of force on acceleration. This research aims to describe the problem of misconceptions experienced by prospective physics teacher students regarding acceleration and its possible causes. Data was collected over four years, namely from 114 prospective physics teacher students in the first semester of the physics education study program until 2022. They were high school graduates majoring in science where physics, which includes mechanics, is one of the compulsory subjects. Data was collected through multiple choice tests and descriptions. The research results show that the misconceptions experienced by students are: 1) Acceleration is not fully understood as a vector quantity; 2) Students have difficulty explaining the relationship between acceleration and the force that causes it.

Keywords: Acceleration, Misconception, Vector,

1 Introduction

Acceleration is a fundamental concept in Physics. The concept of acceleration is identified as the basic building blocks of scientific theories that are highly successful in explaining and predicting observable phenomena. The ability to this concept correctly is an essential prerequisite for any scientific work. Even though it is important, the concept of acceleration is difficult for students to understand. Many first-year students have

misconceptions about acceleration even though this concept has been studied in high school.

Allen [1] defined misconceptions as preconceived notions, non-scientific beliefs, conceptual misunderstandings, vernacular misconceptions, and factual misconceptions. Misconceptions occur when students consider physical phenomena using their minds and confidence of being able to explain them with the correct knowledge. Meanwhile, Kuzmann formulated misconceptions as beliefs which contradict accepted scientific theories [2]. Kuzmann further explained that Misconceptions in physics give seemingly true explanations for correlations and phenomena, but they are not consistent with the experiment. They are based on superficial, commonplace considerations.

Suprpto [3] identified five types of misconceptions, namely: are five kinds of misconceptions, namely: (a) preconceived notions; (b) non-scientific beliefs; (c) conceptual misunderstandings; (d) misconceptions of local languages (vernacular misconceptions); and (e) factual misconceptions. The source of misconception could be the result of teaching materials, daily experience or teaching and learning process [4].

The problem of misconceptions about acceleration is not unique to researchers but is also found in various places. Number of studies show that this concept is difficult for students to understand, and many students understand it incorrectly or even have misconceptions [5-8].

This research aims to uncover the problem of misconceptions about acceleration faced by prospective physics teacher students who are in their first semester at Sanata Dharma University, as well as the possible causes. The results of this research are useful for reducing the level of misconceptions about acceleration which can be applied not only to physics learning at the university level but also at the high school level.

2 Material and Methods

The respondents of this research were 114 people consisting of four generations of students. Participants in the research were all students who took Kinematics courses in

2019, 2020, 2021 and 2022. The number of students taking Kinematics courses in four years is presented in Table 1.

Data was collected using multiple choice tests and essay questions. Data were analyzed descriptively. Based on experience teaching mechanics, researchers suspect that the misconceptions about acceleration experienced by students are related to students' understanding of acceleration as a vector. Based on this suspicion, the researcher designed questions specifically intended to reveal it. Data was collected through closed-answer questions and descriptive questions. In descriptive questions, students are given the freedom to express their opinions regarding a particular concept.

3 Results and Discussions

Question A.

If the acceleration of an object is negative, then the object's motion is slowed down, and if the acceleration is positive then the object's motion is accelerated. True/False.

This statement is wrong because negative or positive indicates direction, while accelerated or slowed down is the value of acceleration. If the object is moving to the left and the acceleration is also to the left, the object will speed up or accelerate.

Student answers are presented in Fig. 1a is the student answer per student year group and Fig. 1b is the total answer from the four groups. The students' answer to question A revealed that 89.47% of students believed that if the object's acceleration was negative then the object's motion was slowed down and if the object's acceleration was positive then the object's motion was accelerated.

Table 1. Participants of the research.

Year	Number of students
2029	35
2020	32
2021	20
2022	27
Total	114

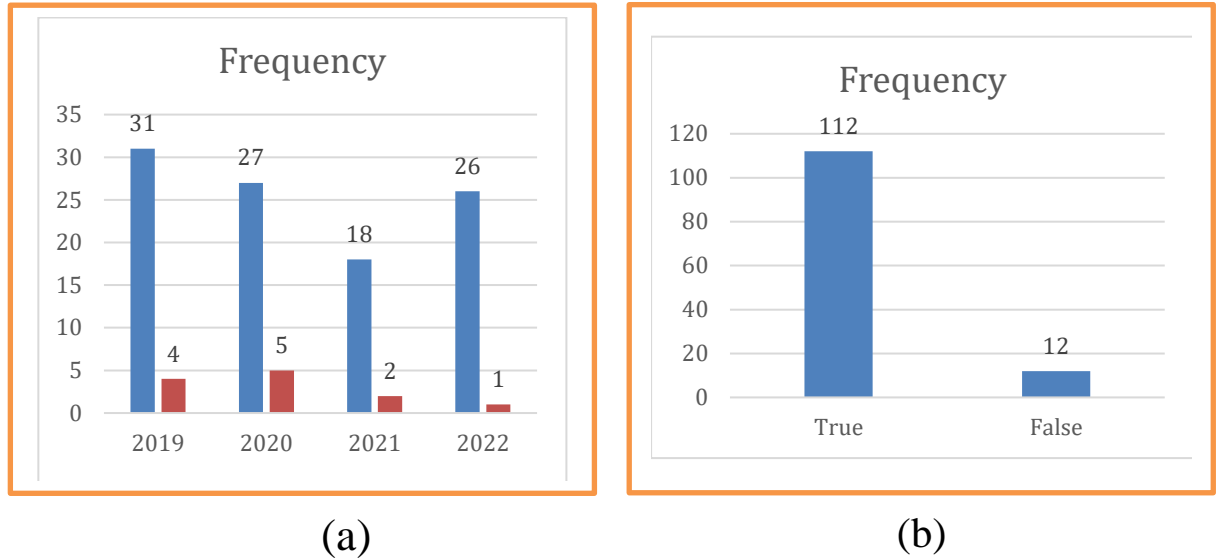


Figure 1. Students' answer to Question A: (a) per year group students; b (total).

The students' beliefs were confirmed through their answers when they agreed to the statement that the acceleration of an object thrown vertically upwards is negative and the acceleration of an object experiencing free fall is positive.

Difficulty understanding the positive sign (+) and negative sign (-) in acceleration was also revealed in research conducted by Shodiqin and Taqwa [9] with student respondents who were prospective physics teachers. Students' understanding that when an object's acceleration is negative, the object experiences deceleration shows that students' understanding is influenced by intuitive understanding in everyday life regarding acceleration and deceleration [10-11].

Students understand that acceleration is a change in speed per unit of time. In everyday life, positive changes have the meaning of increase and negative changes have the meaning of reduction. Using this intuitive understanding, positive acceleration is interpreted as an increase in speed or acceleration and negative acceleration is interpreted as a reduction in speed or deceleration. This is confirmed through the following statement from one of the students:

"... positive acceleration means the change is positive, yes it means the speed gets bigger and bigger... the object's motion accelerates, and if the acceleration is negative, it means the speed decreases.... Mmm things are getting slower." (student 1)

Providing this explanation, students do not consider that acceleration is a vector quantity. This shows that students do not fully understand that the concept of acceleration involves physical concepts and vectors to represent it. Such difficulties were also found in research conducted by Pedrill [12].

Question B.

This question was intended to confirm the answer to question A. In everyday life, it is known that if an object is thrown vertically upwards, the object will slow down and then fall again. When it falls, the object's motion gets faster and faster. Students are given the following statement. Students are asked to assess whether the statement is true or false.

A ball is thrown vertically upwards and then falls back down. When it is moving up, the ball experiences negative acceleration and when it goes down the ball experiences positive acceleration.

This statement is wrong. Whether the object is moving up or down, the object's acceleration remains negative, the direction is downwards. The acceleration experienced by an object is the gravitational acceleration that arises because of the Earth's gravitational force, the direction of gravitational force is always towards the center of the Earth. Student answers are presented in Figs.F 2a and 2b, 2a is the student answer per student year group and 2b is the total answer from the four groups.

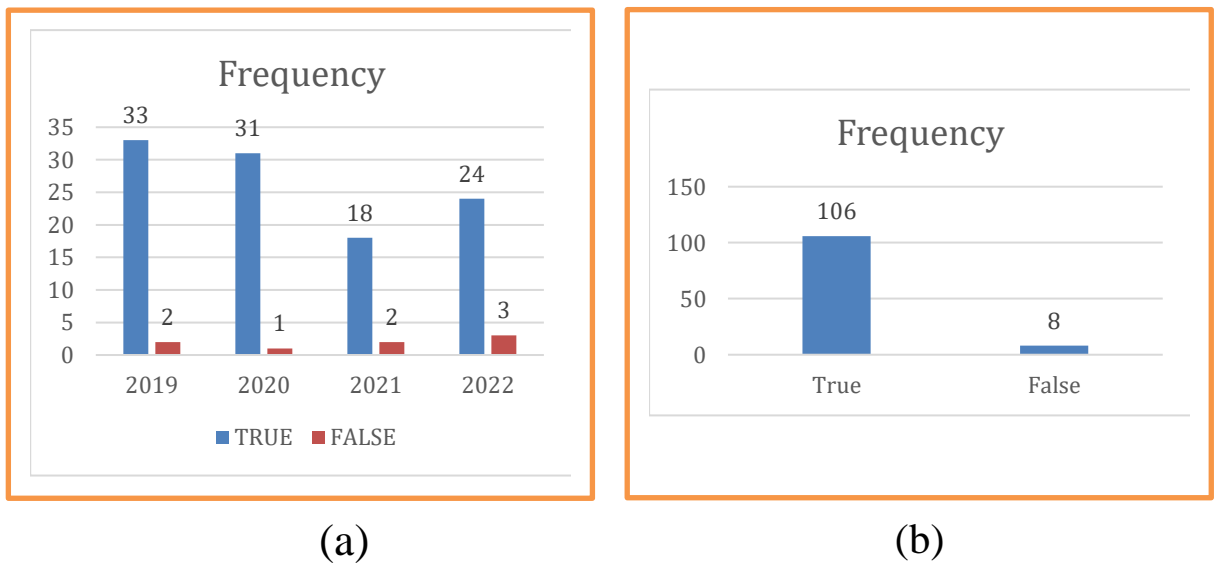


Figure 2. Students' answer to Question B: (a) per year group students; b (total)

The student's answer to question B confirms the student's intuitive understanding. When an object is thrown upwards, the object's motion slows down, students understand that the object's acceleration is negative. On the other hand, when an object is falling, the object accelerates, students understand that the object's acceleration is positive.

Based on students' answers to questions A and question B, it seems quite convincing to state that students' understanding of acceleration is greatly influenced by the intuitive understanding in everyday life that positive has the meaning of increasing and negative has the meaning of decreasing. By using this understanding, students understand that positive acceleration causes objects to speed up and negative acceleration causes objects to slow down.

Question C.

Through questions A and B, it was revealed that students had misconceptions about acceleration. Students cannot understand acceleration as a vector quantity where the positive and negative signs are not related to accelerated or slowed motion. Understanding accelerated or slowed motion requires simultaneously paying attention to the direction of motion and the direction of acceleration.

Next, the researcher asked questions accompanied by pictures to help students understand the problem visually. Given an object is moving to the left and the object experiences acceleration in the direction to the left. Students are given several statements that must be judged as true or false. The statements that must be judged true or false are: 1. The speed of the object is negative; 2. The acceleration of the object is negative; and 3. The movement of objects gets faster and faster. The answers to these statements are: 1. Correct, the speed of the object is negative; 2. Correct, the acceleration of the object is negative; and 3. True, the movement of objects gets faster and faster.

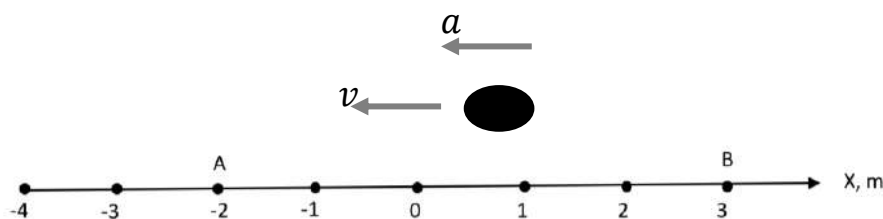


Figure 3. Object moving across horizontal line.

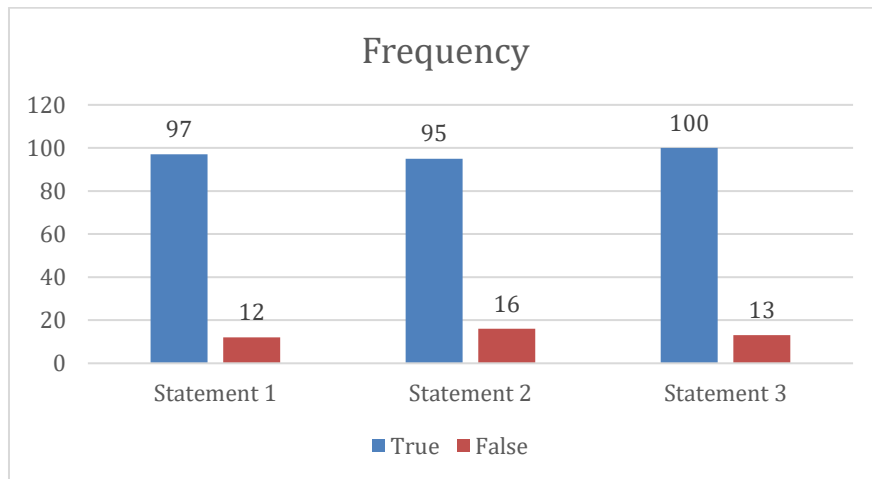


Figure 4. Students' answer to question C.

Students' answer to question C reveal something different from the answer to Question A and B. The student's answer to question C shows that the student understands that speed and acceleration are quantities that have value and direction, namely vector quantities, as expressed by student 5.

"If you are moving to the left and experiencing acceleration to the left then the object is getting faster, because the object seems to be being pushed, conversely if the object is moving to the left but the acceleration is to the right... the object seems to be held... the object is slowed down."

Based on students' answers to question C, it can be concluded that when students are reminded about the direction of speed and acceleration, students can provide correct answers and explanations.

This fact strengthens the researchers' suspicion that students' misconceptions occur because the discussion they receive in secondary school does not emphasize discussion of speed and acceleration as vector quantities. Apart from that, the physics textbooks they use may also contain misconceptions as stated in one of the following books published by the Ministry of Education and Culture [13]. On page 26 of the book, it is explained that the equation of motion for an object thrown vertically upwards is:

$$\begin{aligned}
 v_t &= v_0 - g \cdot t \\
 h &= v_0 \cdot t - \frac{1}{2} g t^2 \\
 v_t^2 &= v_0^2 - 2 g h
 \end{aligned}$$

v = velocity; h : height; g : gravitational acceleration, t : time;

v_0 : Initial velocity; v_t : velocity on t

Figure 5. Equation for vertical moving object in high school physics textbook.

Meanwhile, the equation of motion for an object in free fall, namely when the object experiences no force other than the force of gravity, is stated on page 29 as seen in Fig. 6.

Based on the explanation in the high school physics textbook as described above, it can be assumed that the misconceptions held by students originate from studying physics in high school. Considering that the book was published by the Ministry of Education and Culture, it can be assumed that the book is used in various regions of Indonesia. Hopefully this explains why some students who have just graduated from high school have the misconceptions as described above.

Question D.

This question was intended to reveal the extent to which students understood the concept of acceleration which was studied in the discussion about rectilinear motion and acceleration because of force.

$$\begin{aligned}
 v_t &= v_0 + g \cdot t \\
 h &= v_0 \cdot t + \frac{1}{2} g t^2 \\
 v_t^2 &= v_0^2 + 2 g h
 \end{aligned}$$

Figure 6. Equation for free fall object in high school physics textbook.

The question or in fact the assignment was given to the students draw an object that was thrown vertically upwards and then the object came back down. Students were asked to describe the motion of objects along with the velocity vector, acceleration vector and gravitational force vector as shown in Fig. 7.

When trying to draw, almost none of the students drew correctly on the first drawing they made. Some are not even able to represent the velocity vector, acceleration vector and force vector correctly. After going through discussions and explanations, finally several students were able to draw correctly. The following are two examples of drawings made by students.

This phenomenon provides information to researchers that students have not been able to relate their understanding of the three concepts of speed, acceleration, and force as a whole in one single event. Based on the data revealed from this research, the author suspects that the stages of discussing rectilinear motion and Newton's laws of motion in secondary schools play a role in the emergence of student misconceptions. In high school physics lessons, discussions of rectilinear motion are not linked to discussions of force.

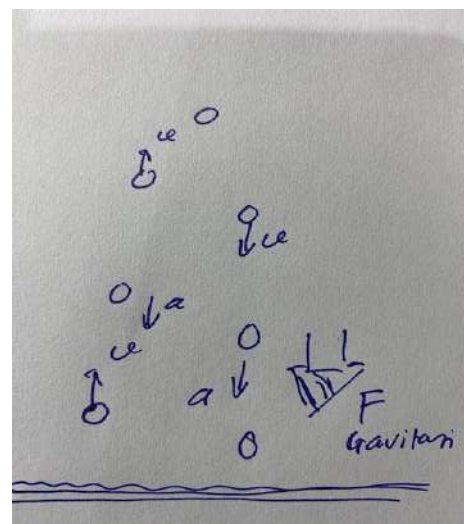
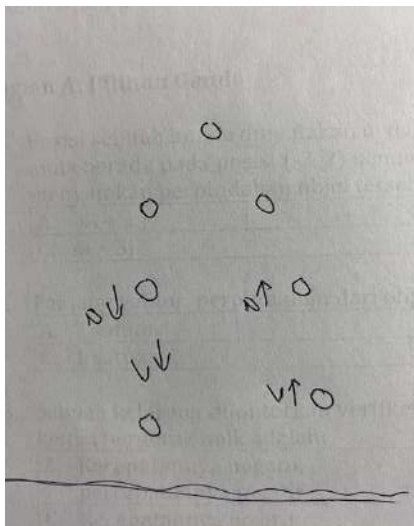


Figure 7. Students' illustration about vertical moving object with velocity, acceleration, and force vectors.

The answers that reveal students' misconceptions about acceleration show that acceleration is indeed a complex concept. This concept, as mentioned in the literature mentioned above, involves aspects of mathematics, vectors and physics. Judging from its relationship to other concepts in physics, the concept of acceleration is directly related to the concept of motion and the concept of force.

Fig. 8 shows the relationship between the concept of acceleration in rectilinear motion and the concept of acceleration because of force. In the context of motion, the concept of acceleration is discussed after first discussing the concepts of position, displacement, and speed. To provide a correct understanding of the concept of acceleration, then since the discussion regarding position and displacement it must be consistently discussed that position and displacement are vector quantities. Likewise, when discussing speed, speed must be discussed consistently as a vector quantity. With the consistency of position, displacement and speed discussed as vector quantities, acceleration is also discussed as a vector quantity.

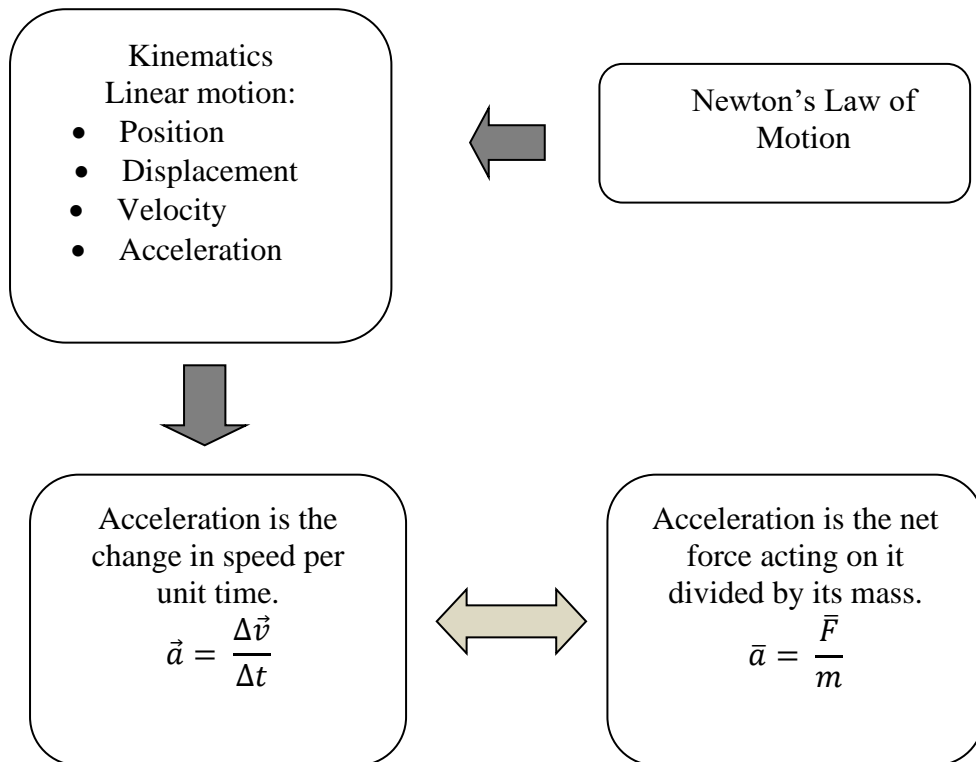


Figure 8. Relationship between concept of acceleration in Linear motion and Force

The second thing that can be learned from Fig. 8 is acceleration as a result of a force. By looking at diagram in Fig. 8 it seems clear that the discussion regarding acceleration should be carried out in its entirety, both acceleration as an entity in the movement and acceleration as a result of force. Teachers need to help students understand the concept of acceleration as a movement entity and because of a force as a whole and not fragmented.

Learning from the diagram above, it is hoped that when teaching about acceleration, teachers not only discuss acceleration as a change in speed in the context of straight motion but also need to discuss acceleration because of a force whose value is influenced by the magnitude of the force and the mass of the object and whose direction is the same as the direction.

4 Conclusions

Students' misconceptions about acceleration are influenced by intuitive knowledge from everyday life which is not in line with the laws of physics. From this research it is also revealed that misconceptions about acceleration arise due to a lack of attention to acceleration as a vector quantity. Other information revealed from this research is that students' understanding of acceleration is not fully integrated with their understanding of the causes of acceleration. Based on the findings above, researchers recommend that learning about rectilinear motion be consistently discussed using vector quantities to avoid misconceptions. Second, the discussion about acceleration is discussed in its entirety, including force as the cause of acceleration.

References

- [1] M. Allen, *Misconceptions in Primary Science* 2nd Edition, Open University Press, 2014.
- [2] I. Kuczmann, "The Structure of Knowledge and Students' Misconceptions in Physics," *AIP Conf. Proc.*, vol. 1916, pp. 050001, 2017.

- [3] N. Suprpto, "Do We Experience Misconceptions? An Ontological Review of Misconceptions in Science," *Studies in Philosophy of Science and Education (SiPoSE)*, vol.1, no.2, pp. 50-55, 2020.
- [4] P. Molefe, & M.N. Kwanda, "Activities to enhance students' understanding of acceleration: Part B," *International Conference on Physics Education (ICPE)*, 2018.
- [5] Arons, A. A., *Teaching Introductory Physics*, John Wiley, New York, 1997.
- [6] L.C. McDermott, "Guest comment: how we teach and how students learn – a mismatch?," *Am. J. Phys.*, vol. 61, pp. 295-298, 1993.
- [7] J.J. Piaget, *The Child's Conception of Movement and Speed*, Basic Books, New York, 1970.
- [8] D.E. Trowbridge, and L.C. McDermott, "Investigation of student understanding of the conception of the acceleration in one dimension," *Am. J. Phys.*, vol. 49, pp. 242, 1981
- [9] M.I. Shodiqin, & M.R.A. Taqwa, "Identification of student difficulties in understanding kinematics: focus of study on the topic of acceleration," *Journal of Physics: Conference Series*, vol. 1918, pp. 022016, 2020.
- [10] L.M. Buteler, & E.A. Coleoni, "Exploring the Relation Between Intuitive Physics Knowledge and Equations During," *Electronic Journal of Science Education*, vol. 18, no. 2. 2014.
- [11] M. McCloskey, Intuitive Physics, *Scientific American*, Pp: 122-131, 1983.
- [12] A.M. Pedrill, "Understanding acceleration: An interplay between different mathematics and physics representations," *Journal of Physics: Conf. Series*, vol. 1286, pp. 012070, 2019.
- [13] N.E. Josephine, *Gerak Lurus Fisika Kelas X*. Direktorat SMA, Direktorat Jenderal PAUD, DIKDAS dan DIKMEN. Kementrian Pendidikan, Kebudayaan, Riset dan Teknologi. 2020

Expected Value of the Occupation Times of Brownian Motion

Herry Pribawanto Suryawan

*Department of Mathematics, Faculty of Science and Technology
Sanata Dharma University, Yogyakarta, Indonesia
herrypribs@usd.ac.id*

(Received 20-10-2023; Revised 20-02-2024; Accepted 25-04-2024)

Abstract

The duration spent by a stochastic process within a specific spatial range over a given finite time period is referred to as the occupation times of the process. In the nonwoven production industry, this phenomenon manifests itself during the fiber lay-down process. The occupation time can be understood as the mass of fiber material accumulated within a specific area. It is crucial to have knowledge of the average mass per unit area of the final fleece from an application standpoint. In this paper derive an expression for the expected value of the occupation times in terms of Gaussian error functions.

Keywords: occupation times, Brownian motion, expected value

1 Introduction

Technical textiles have garnered significant interest across various industries in recent decades because of their cost-effective production methods. Random fiber webs are created by overlapping numerous individual slender fibers, resulting in nonwoven materials that are utilized in various industries such as textile, construction, and hygiene. These materials serve as essential components in products like baby diapers, clothing textiles, filters, and medical devices, among others. Endless fibers are manufactured through

melt-spinning processes, where numerous individual fibers are created by continuously extruding molten polymer through closely spaced narrow nozzles arranged in a row on a spinning beam. The viscous or viscoelastic fibers undergo stretching and spinning processes until they solidify as a result of exposure to cooling air currents. Prior to being placed on a moving conveyor belt to create a web, the elastic fibers tangle and form loops because of the turbulent air flows. The homogeneity and load capacity of the fiber web are crucial textile characteristics when evaluating the quality of industrial nonwoven fabrics. The modeling and simulation of fiber dynamics and lay-down are essential for optimizing and controlling fleece quality. The fleece's mass per unit area is typically the available data used to assess its quality, particularly when evaluating it on an industrial scale.

Due to its complexity it is not possible to study the whole process using mathematical means at a stroke. In recent years, research has led to the development of a series of models that effectively capture specific elements of the process chain. The papers [4, 6, 9] presented and examined a probabilistic model concerning the fiber deposition process in nonwoven manufacturing. The model relies on stochastic differential equations to depict the final position of the fiber on the conveyor belt, taking into account the impact of turbulent air currents. In [1] the estimation of the Ornstein-Uhlenbeck process's parameter from the available data on mass per unit area, the occupation time in mathematical terms, was done.

Definition 1.1. Let $[a, b] \subset \mathbb{R}$ be a compact interval in \mathbb{R} and let $X = (X_t)_{t \in [0, T]}$, $0 < T < \infty$, be a stochastic process. The occupation time $M_{T, [a, b]}(X)$ is defined as

$$M_{T, [a, b]}(X) := \int_0^T \mathbf{1}_{[a, b]}(X_t) dt = \int_0^T \int_a^b \delta_0(X_t - x) dx dt,$$

where δ_0 and $\mathbf{1}_{[a, b]}$ is the Dirac-delta function and the indicator function of the interval $[a, b]$, respectively.

Occupation times formally represent the duration that a stochastic process occupies the spatial interval $[a, b]$ within the time interval $[0, T]$. In terms of our physical framework for the manufacturing of nonwoven materials, the occupation time can be understood as the quantity of fiber material accumulated within the range $[a, b]$, specifically the mass per unit area of the resulting fleece.

In this research, we investigate the occupation time of one-dimensional Brownian motion based on our previous work [18]. In that paper we show that occupation times of

one-dimensional Brownian motion is a Hida distribution. The present paper derives the explicit form of the expectation of the occupation times in terms of the Gaussian error function. In subsequent investigations, we employ a white noise approach to extend the concept to higher dimensions, despite the availability of classical probabilistic methods for studying the problem. In Section 2, we present essential background information on the theory of white noise. The main result, along with its proof, is presented in Section 3.

2 White Noise Analysis

This section provides essential background information on the theory of white noise. For a more thorough examination of white noise theory we refer to [8, 11] and references therein. We start with the Gelfand triple

$$\mathcal{S}(\mathbb{R}) \hookrightarrow L^2(\mathbb{R}) \hookrightarrow \mathcal{S}'(\mathbb{R}),$$

where $L^2(\mathbb{R})$ is the real Hilbert space of all real-valued Lebesgue square-integrable functions, $\mathcal{S}(\mathbb{R})$ is the space of real-valued Schwartz test function, and $\mathcal{S}'(\mathbb{R})$ is the space of real-valued tempered distributions. We construct a probability space $(\mathcal{S}'(\mathbb{R}), \mathcal{C}, \mu)$ where \mathcal{C} is the Borel σ -algebra on $\mathcal{S}'(\mathbb{R})$ generated by cylinder sets. The Bochner-Minlos theorem guarantees the unique determination of the probability measure μ by specifying the characteristic function

$$C(f) := \int_{\mathcal{S}'(\mathbb{R})} \exp(i\langle \omega, f \rangle) d\mu(\omega) = \exp\left(-\frac{1}{2}|f|_0^2\right)$$

for all $f \in \mathcal{S}(\mathbb{R})$. The standard norm in the space $L^2(\mathbb{R})$ is denoted by $|\cdot|_0$, while the dual pairing between the spaces $\mathcal{S}'(\mathbb{R})$ and $\mathcal{S}(\mathbb{R})$ is denoted by $\langle \cdot, \cdot \rangle$. The dual pairing is regarded as the extension of the inner product on $L^2(\mathbb{R})$, i.e.

$$\langle g, f \rangle = \int_{\mathbb{R}} g(x)f(x) dx,$$

for all $g \in L^2(\mathbb{R})$ and $f \in \mathcal{S}(\mathbb{R})$. The real-valued white noise space is identified by this probability space as it encompasses the paths of the one-dimensional Gaussian white noise. In this framework a one-dimensional Brownian motion can be defined by a continuous modification of the process $B = (B_t)_{t \geq 0}$ with

$$B(t) := \langle \cdot, \mathbf{1}_{[0,t]} \rangle,$$

where $\mathbf{1}$ denotes the indicator function.

In the sequel, we shall employ the the Gel'fand triple

$$(\mathcal{S}) \hookrightarrow L^2(\mu) := L^2(\mathcal{S}'(\mathbb{R}), \mathcal{C}, \mu) \hookrightarrow (\mathcal{S})^*$$

where (\mathcal{S}) is the space of white noise test functions and $(\mathcal{S})^*$ is the topological dual space of (\mathcal{S}) . The terms *Hida test functions* and *Hida distributions* refer to the components of (\mathcal{S}) and $(\mathcal{S})^*$, respectively. In this setting, white noise can be precisely characterized as the temporal rate of change of Brownian motion with respect to the topology of $(\mathcal{S})^*$. The S-transform, a crucial tool in the white noise analysis, is defined for any $\Phi \in (\mathcal{S})^*$ as

$$(S\Phi)(\varphi) := \langle \langle \Phi, : \exp(\langle \cdot, \varphi \rangle) : \rangle \rangle, \quad \varphi \in \mathcal{S}(\mathbb{R}).$$

Here,

$$: \exp(\langle \cdot, \varphi \rangle) ::= C(\varphi) \exp(\langle \cdot, \varphi \rangle),$$

is the so-called Wick exponential and $\langle \langle \cdot, \cdot \rangle \rangle$ denotes the topological dual pairing between $(\mathcal{S})^*$ and (\mathcal{S}) . The S-transform may be considered as the analog of the Laplace transform in an infinite dimensional space with respect to the Gaussian measure. The S-transform offers a convenient method for identifying a Hida distribution $\Phi \in (\mathcal{S})^*$, especially in cases where finding the explicit form of the Wiener-Itô chaos decomposition of Φ proves to be challenging..

Theorem 2.1. [11] *The S-transform is injective, i.e. if $S\Phi(\varphi) = S\Psi(\varphi)$ for all $\varphi \in \mathcal{S}(\mathbb{R})$, then $\Phi = \Psi$.*

In the subsequent discussion, we present a condition that is sufficient for the Bochner integrability of a collection of Hida distributions that are contingent upon an additional parameter.

Theorem 2.2. [10] *Let $(\Omega, \mathcal{A}, \nu)$ be a measure space and $\lambda \mapsto \Phi_\lambda$ be a function from Ω to $(\mathcal{S})^*$. If*

- (1) *the function $\lambda \mapsto S(\Phi_\lambda)(\varphi)$ is measurable for all $\varphi \in \mathcal{S}(\mathbb{R})$, and*
- (2) *there are $C_1(\lambda) \in L^1(\Omega, \mathcal{A}, \nu)$, $C_2(\lambda) \in L^\infty(\Omega, \mathcal{A}, \nu)$ and a continuous seminorm $\|\cdot\|$ on $\mathcal{S}(\mathbb{R})$ such that for all $z \in \mathbb{C}$, $\varphi \in \mathcal{S}(\mathbb{R})$*

$$|S(\Phi_\lambda)(z\varphi)| \leq C_1(\lambda) \exp(C_2(\lambda)|z|^2 \|\varphi\|^2),$$

then Φ_λ is Bochner integrable in $(\mathcal{S})^*$. It follows that $\int_\Omega \Phi_\lambda d\nu(\lambda) \in (\mathcal{S})^*$. Moreover,

$$S\left(\int_\Omega \Phi_\lambda d\nu(\lambda)\right) = \int_\Omega S(\Phi_\lambda) d\nu(\lambda).$$

We define Donsker's delta distribution by

$$\delta_0(B_t - x) = \delta_0(\langle \cdot, \mathbf{1}_{[0,t]} \rangle - x) := \frac{1}{2\pi} \int_{\mathbb{R}} \exp(i\lambda(\langle \cdot, \mathbf{1}_{[0,t]} \rangle - x)) d\lambda.$$

It has been demonstrated that $\delta_0(B_t - x) \in (\mathcal{S})^*$. Moreover, the S-transform of the aforementioned is expressed as

$$S\delta_0(B_t - x)(\varphi) = \frac{1}{\sqrt{2\pi t}} \exp\left(-\frac{1}{2t}(\langle \varphi, \mathbf{1}_{[0,t]} \rangle - x)^2\right),$$

for any $\varphi \in \mathcal{S}(\mathbb{R})$. For further information and evidence, refer to the sources such as [8, 11]. The Donsker delta distribution holds significant importance as a subject of study in the realm of Gaussian analysis. For instance, it can be employed to examine local times, self-intersection local times, stochastic current, and Feynman integrals, see e.g. [2, 3, 7, 13, 14, 17]. The derivatives of Donsker's delta distribution has been also investigated in previous research such as [15]. In the context of stochastic processes with memory, the analysis of Donsker's delta distribution is presented in [16].

3 Main Result

In [18] the following results have been proved.

Theorem 3.1. 1. Let $B = (B_t)_{t \in [0, T]}$ be a one-dimensional standard Brownian motion and let $[a, b] \subset \mathbb{R}$ be a compact interval. The occupation time

$$M_{T, [a, b]}(B) := \int_0^T \int_a^b \delta_0(B_t - x) dx dt$$

is a Hida distribution.

2. The expression for the S-transform of the occupation times of Brownian motion, for any $\varphi \in \mathcal{S}(\mathbb{R})$, is provided by

$$SM_{T, [a, b]}(B)(\varphi) = \int_0^T \frac{1}{\sqrt{2\pi t}} \int_a^b \exp\left(-\frac{1}{2t} \left(\int_0^t \varphi(s) ds - x\right)^2\right) dx dt.$$

In this paper we improve the above result by deriving an explicit form for the expected value of the occupation times of Brownian motion in terms of the Gaussian error function:

$$\operatorname{erf}(x) := \frac{2}{\sqrt{\pi}} \int_0^x e^{-y^2} dy, \quad x > 0.$$

The following integration formula are required for this purpose.

Lemma 3.2 ([12], formula 14). *For any $n \geq 2$*

$$\int \operatorname{erf}(az)z^{-n} dz = -\frac{\operatorname{erf}(az)}{(n-1)z^{n-1}} + \frac{2a}{(n-1)\sqrt{\pi}} \int \frac{1}{z^{n-1}} e^{-a^2 z^2} dz.$$

Lemma 3.3 ([5], formula 3.461(5)). *For any $u > 0$ and $|\arg \mu| < \frac{\pi}{2}$*

$$\int_u^\infty \frac{e^{-\mu x^2}}{x^2} dx = \frac{1}{u} e^{\mu x^2} - \sqrt{\mu\pi} (1 - \operatorname{erf}(u\sqrt{\mu})).$$

Now, we are ready to prove our main result.

Theorem 3.4. *The expectation of the occupation times $M_{T,[a,b]}(B)$ of one-dimensional standard Brownian motion $B = (B_t)_{t \in [0,T]}$ is given by*

$$\begin{aligned} & \mathbb{E}_\mu (M_{T,[a,b]}(B)) \\ &= \sqrt{\frac{T}{2\pi}} \left(b e^{-\frac{b^2}{2T}} - a e^{-\frac{a^2}{2T}} \right) - \frac{b^2 - a^2}{2} + \frac{T + b^2}{2} \operatorname{erf} \left(\frac{b}{\sqrt{2T}} \right) - \frac{T + a^2}{2} \operatorname{erf} \left(\frac{a}{\sqrt{2T}} \right). \end{aligned}$$

Proof: Since $M_{T,[a,b]}(B) = \int_0^T \int_a^b \delta_0(B_t - x) dx dt \in (\mathcal{S})^*$, then, using Theorem 2.2, we have

$$\begin{aligned} \mathbb{E}_\mu (M_{T,[a,b]}(B)) &= S M_{T,[a,b]}(B)(0) \\ &= S \left(\int_0^T \int_a^b \delta_0(B_t - x) dx dt \right) (0) \\ &= \int_0^T \int_a^b S \delta_0(B_t - x)(0) dx dt \\ &= \int_0^T \int_a^b \frac{1}{\sqrt{2\pi t}} e^{-\frac{1}{2t} (\langle 0, \mathbf{1}_{[0,t]} \rangle - x)^2} dx dt \\ &= \int_0^T \int_a^b \frac{1}{\sqrt{2\pi t}} e^{-\frac{x^2}{2t}} dx dt \\ &= \int_0^T \frac{1}{\sqrt{2\pi t}} \int_a^b e^{-\frac{x^2}{2t}} dx dt \\ &= \int_0^T \frac{1}{\sqrt{2\pi t}} \int_{a/\sqrt{2t}}^{b/\sqrt{2t}} \sqrt{2t} e^{-y^2} dy dt \end{aligned}$$

$$\begin{aligned}
&= \frac{1}{\sqrt{\pi}} \int_0^T \left(\int_0^{b/\sqrt{2t}} \sqrt{2t} e^{-y^2} dy - \int_0^{a/\sqrt{2t}} \sqrt{2t} e^{-y^2} dy \right) dt \\
&= \frac{1}{2} \int_0^T \left(\operatorname{erf} \left(\frac{b}{\sqrt{2t}} \right) - \operatorname{erf} \left(\frac{a}{\sqrt{2t}} \right) \right) dt.
\end{aligned}$$

Let us now compute $\int_0^T \operatorname{erf} \left(\frac{b}{\sqrt{2t}} \right) dt$. Using substitution $r = \frac{b}{\sqrt{2t}}$ we get

$$\int_0^T \operatorname{erf} \left(\frac{b}{\sqrt{2t}} \right) dt = b^2 \int_{b/\sqrt{2T}}^{\infty} \frac{\operatorname{erf}(r)}{r^3} dr.$$

An application of Lemma 3.2 yields

$$\int \frac{\operatorname{erf}(r)}{r^3} dr = -\frac{\operatorname{erf}(r)}{2r^2} + \frac{1}{\sqrt{\pi}} \int \frac{1}{r^2} e^{-r^2} dr.$$

Hence,

$$\begin{aligned}
\int_{b/\sqrt{2T}}^{\infty} \frac{\operatorname{erf}(r)}{r^3} dr &= \lim_{s \rightarrow \infty} \left[-\frac{\operatorname{erf}(r)}{2r^2} \right]_{b/\sqrt{2T}}^s + \frac{1}{\sqrt{\pi}} \int \frac{1}{r^2} e^{-r^2} dr \\
&= \frac{T \operatorname{erf} \left(\frac{b}{\sqrt{2T}} \right)}{b^2} + \frac{1}{\sqrt{\pi}} \int_{b/\sqrt{2T}}^{\infty} \frac{1}{r^2} e^{-r^2} dr.
\end{aligned}$$

Since $\frac{b}{\sqrt{2T}} > 0$ and $|\arg 1| < \frac{\pi}{2}$, then, by using Lemma 3.3, we obtain

$$\int_{b/\sqrt{2T}}^{\infty} \frac{1}{r^2} e^{-r^2} dr = \frac{\sqrt{2T}}{b} e^{-\frac{b^2}{2T}} - \sqrt{\pi} \left(1 - \operatorname{erf} \left(\frac{b}{\sqrt{2T}} \right) \right).$$

Therefore,

$$\int_{b/\sqrt{2T}}^{\infty} \frac{\operatorname{erf}(r)}{r^3} dr = \frac{T \operatorname{erf} \left(\frac{b}{\sqrt{2T}} \right)}{b^2} + \frac{1}{b} \sqrt{\frac{2T}{\pi}} e^{-\frac{b^2}{2T}} - \left(1 - \operatorname{erf} \left(\frac{b}{\sqrt{2T}} \right) \right)$$

and

$$\begin{aligned}
\int_0^T \operatorname{erf} \left(\frac{b}{\sqrt{2t}} \right) dt &= b^2 \int_{b/\sqrt{2T}}^{\infty} \frac{\operatorname{erf}(r)}{r^3} dr \\
&= b^2 \left(\frac{T \operatorname{erf} \left(\frac{b}{\sqrt{2T}} \right)}{b^2} + \frac{1}{b} \sqrt{\frac{2T}{\pi}} e^{-\frac{b^2}{2T}} - \left(1 - \operatorname{erf} \left(\frac{b}{\sqrt{2T}} \right) \right) \right) \\
&= (T + b^2) \operatorname{erf} \left(\frac{b}{\sqrt{2T}} \right) + \sqrt{\frac{2T}{\pi}} b e^{-\frac{b^2}{2T}} - b^2.
\end{aligned}$$

Similarly,

$$\int_0^T \operatorname{erf} \left(\frac{a}{\sqrt{2t}} \right) dt = (T + a^2) \operatorname{erf} \left(\frac{a}{\sqrt{2T}} \right) + \sqrt{\frac{2T}{\pi}} a e^{-\frac{a^2}{2T}} - a^2.$$

Finally, we have

$$\begin{aligned}
& \mathbb{E}_\mu (M_{T,[a,b]}(B)) \\
&= \frac{1}{2} \int_0^T \left(\operatorname{erf} \left(\frac{b}{\sqrt{2t}} \right) - \operatorname{erf} \left(\frac{a}{\sqrt{2t}} \right) \right) dt \\
&= \frac{1}{2} \left((T + b^2) \operatorname{erf} \left(\frac{b}{\sqrt{2T}} \right) + \sqrt{\frac{2T}{\pi}} b e^{-\frac{b^2}{2T}} - b^2 - (T + a^2) \operatorname{erf} \left(\frac{a}{\sqrt{2T}} \right) \right. \\
&\quad \left. - \sqrt{\frac{2T}{\pi}} a e^{-\frac{a^2}{2T}} + a^2 \right) \\
&= \sqrt{\frac{T}{2\pi}} \left(b e^{-\frac{b^2}{2T}} - a e^{-\frac{a^2}{2T}} \right) - \frac{b^2 - a^2}{2} + \frac{T + b^2}{2} \operatorname{erf} \left(\frac{b}{\sqrt{2T}} \right) - \frac{T + a^2}{2} \operatorname{erf} \left(\frac{a}{\sqrt{2T}} \right).
\end{aligned}$$

The proof is finished. ■

4 Conclusions

In this paper we derive an explicit expression for the expected value of the occupation times of a standard one-dimensional Brownian motion in terms of Gaussian error function. This explicit form is preferred from an application standpoint as it offers greater utility for computational tasks. Our current findings are constrained to a one-dimensional setting. As a further research plan, we will generalize the present result to higher spatial dimensions.

Acknowledgements

We express our sincere gratitude for the financial assistance provided by the Institute for Research and Community Service (LPPM) of Universitas Sanata Dharma through research grant No. 012/Penel./LPPM-USD/II/2023.

References

- [1] W. Bock et al., "Parameter estimation from occupation times—a white noise approach," *Communications on Stochastic Analysis*, **26**(3), 29-40, 2014.

-
- [2] W. Bock, J. L. da Silva, and H. P. Suryawan, "Local times for multifractional Brownian motion in higher dimensions: A white noise approach," *Infinite Dimensional Analysis, Quantum Probability and Related Topics*, **19**(4), id. 1650026, 16 pp, 2016.
- [3] W. Bock, J. L. da Silva, and H. P. Suryawan, "Self-intersection local times for multifractional Brownian motion in higher dimensions: A white noise approach," *Infinite Dimensional Analysis, Quantum Probability and Related Topics*, **23**(1), id. 2050007, 18 pp, 2020.
- [4] T. Götz et al, "A stochastic model and associated Fokker-Planck equation for the fiber lay-down process in nonwoven production processes," *SIAM Journal of Applied Mathematics*, **67**(6), 1704-1717, 2007.
- [5] I. S. Gradshteyn and I. M. Ryzhik, "Table of Integrals, Series, and Products, seventh edition" *Academic Press, Amsterdam*, 2007.
- [6] M. Grothaus et al, "Application of a three-dimensional fiber lay-down model to nonwoven production processes," *Journal of Mathematics in Industry*, **4**(4), 1-19, 2014.
- [7] M. Grothaus, F. Riemann, and H. P. Suryawan, "A White Noise approach to the Feynman integrand for electrons in random media," *Journal of Mathematical Physics*, **55**(1), id. 013507, 16 pp, 2014.
- [8] T. Hida et al, "White Noise. An Infinite Dimensional Calculus," *Kluwer Academic Publisher, Dordrecht*, 1993.
- [9] A. Klar, J. Maringer, and R. Wegener, "A 3D model for fiber lay-down nonwoven production processes," *Mathematical Models and Methods in Applied Sciences*, **22**(9), 1-18, 2012.
- [10] Y. Kondratiev et al, "Generalized functionals in Gaussian spaces: The characterization theorem revisited," *Journal of Functional Analysis*, **141** article number 0130, 301-318, 1996.
- [11] H.H. Kuo, "White Noise Distribution Theory," *CRC Press, Boca Raton*, 1996.

- [12] E. W. Ng and M. Geller, "A table of integrals of the error function," *Journal of Research of the National Bureau of Standards, Section B: Mathematical Sciences*, **73B**(1), 1-20, 1969.
- [13] H.P. Suryawan, "A white noise approach to the self intersection local times of a Gaussian process," *Journal of Indonesian Mathematical Society*, **20**(2), 111-124, 2014.
- [14] H.P. Suryawan, "Weighted local times of a sub-fractional Brownian motion as Hida distributions," *Jurnal Matematika Integratif*, **15**(2), 81-87, 2019.
- [15] H.P. Suryawan, "Derivative of the Donsker delta functionals," *Mathematica Bohemica*, **144**(2), 161-176, 2019.
- [16] H.P. Suryawan, "Donsker's delta functional of stochastic processes with memory," *Journal of Mathematical and Fundamental Sciences*, **51**(3), 265-277, 2019.
- [17] H.P. Suryawan, "Pendekatan analisis derau putih untuk arus stokastik dari gerak Brown subfraksional," *Limits: Journal of Mathematics and Its Applications*, **19**(1), 15-25, 2022.
- [18] H.P. Suryawan, "A white noise approach to occupation times of Brownian motion," *International Journal of Applied Sciences and Smart Technologies*, **4**(2), 131-140, 2022.

Mobile Forensic Investigation on iOS & Android Smartphones: Case Study Investigation on WhatsApp

Shadi K. A. Zakarneh^{1*}

¹*M.Sc. Student, Palestine Technical University- Kadoorei, Tulkarem, Palestine,
zakarnehshadi@gmail.com*

(Received 03-07-2023; Revised 01-04-2024; Accepted 25-04-2024)

Abstract:

Following the exponential growth of information and communication technologies, the smartphone market, as well as advances in wireless data networks (3G and 4G), has accelerated. Mobile apps for social networking and instant messaging have been created by these firms. Other instant messaging (IM) smartphone programs like WhatsApp (WA), Viber, and IMO have also been created. WA is the most widely used instant messaging program. With WA, you can send and receive messages in a variety of formats, including text, voice, video, and documents. Various cybercrime incidents were committed through WA's. WA use leaves several artifacts that may be examined to detect the digital evidence. In addition, iOS and Android are two of the most popular smartphone operating systems. Because of this, the inquiry will involve the use of forensic investigative techniques and methodologies. Forensics on both iOS and Android cellphones were utilized to investigate a digital crime that was believed to have been perpetrated in WA. To conclude the investigation, we analyzed chat logs, phone records, and other media to gather proof. Legal framework and established processes were used to guarantee that evidence was preserved from change or destruction and that the witness's account was acceptable in court throughout the investigative process. It was finally stated that the inquiry and evidence had been presented. As a result, WA forensic artifacts might be evaluated and found effectively utilizing the mobile forensic procedure.

Keywords: WhatsApp; Forensic; iOS; Smartphone; Seizure; Acquisition; Analysis; Investigation.

1 Introduction

Many virtual communication apps have emerged as a consequence of the quick and huge expansion of communications and the Internet, such as social networks and IM programs such as Facebook, Twitter, Snapchat, Skype, and WhatsApp (WA). These



innovations have made communication between individuals easier, faster, and free, as well as removed geographical barriers [1].

As a consequence of the advancement of technology and communication, cellphones have supplanted PCs in many applications because of their portability, affordability, and low energy consumption; this trend is expected to continue [2]. Also, Some fundamental mobile phone services, such as SMS, have been superseded by IM programs [2].

Among the many IM applications on smartphones, WA is the most widely used IM service [3]. According to a Statista report from October 2020, the most popular and widely used IM app based on the number of monthly active users would be WA [4], WA is the most used by 2 billion active users, followed by Facebook Messenger 1.3 billion, WeChat 1.206 billion, QQ 648 million, Snapchat 433 million, and the Telegram has 400 million active users, as shown in Fig. 1.

For illegal reasons, the widespread usage of WA, as well as the vast range of material that may be shared over it (text messages; photos; videos; audio files; etc.), makes it hard to prohibit WA from being used [2]. Several artifacts occur from WA calls and messages. A forensic examination is carried out on these artifacts to get evidential information [3]. Although cybercrime is on the rise and may be used for a wide range of bad intentions, it is more common to do it for personal gain, business gain, intellectual property theft, personal theft, bullying, harassment, and even terrorism. Law enforcement must be involved in the investigation and prosecution of cybercrimes at all times [5]. As well, cybercrime, its tools, categories, and criminals must be defined under particular legislation. As a result, specialist law enforcement entities must be established to investigate and deliver this information to the courts. In addition, it is necessary to update the criminal code to reflect this new category of offense [6].

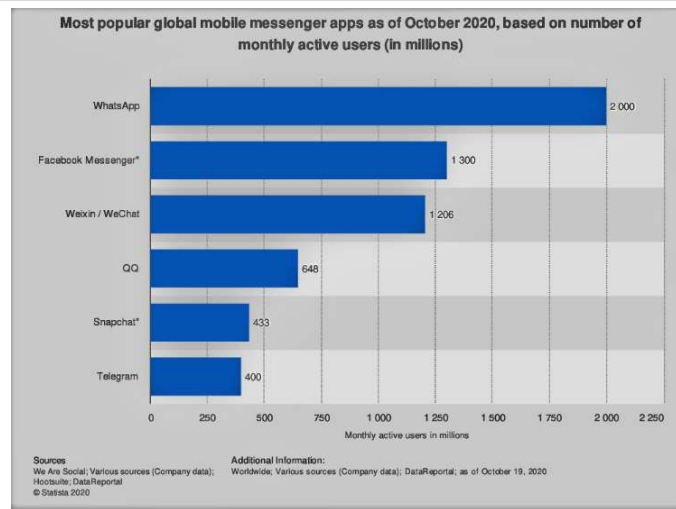


Figure. 1. Mobile instant messaging applications statistic [4]

Most countries around the world are issuing cybercrime laws. Specialized law-enforcement agencies are also founded to investigate this type of crime [7]. The state of Palestine and many other countries issued a cybercrime law by Decree No. 10 of 2018. This law defines activities, tools, and terminology related to cybercrime, and determined the law enforcement agencies that are responsible for the investigation and prosecution of cybercrime and the penalties for these crimes [8].

This research aims to explore the artifacts in WA on iOS and android platforms and the use of tools related to the digital investigation to access digital evidence in WA by extracting messages and calls, analyzing them, and linking them in a chronological sequence to reach the digital evidence of the case.

2 Literature Review

WA is independent on smartphone platforms, as it works on different platforms such as iOS, Android, Windows Phone, and Symbian. In addition to that WA is a free charge application for most platforms, and it is charge-free in sending text, voice, images, and video messages [9].

2.1 iOS Operating System

The iOS operating system developed by Apple, iOS constitutes the primary platform for Apple mobile devices [10]. This system controls all services and parts of Apple

devices. the iOS operating system was launched for the first time in the year 2007 with the launch of the first iPhone device, where the name of the operating system was OS X, after that the name was changed in 2010 to iOS [11]. The iOS operating system architecture has four layers which are the core OS, core services, media, and Cocoa Touch layer [12].

The iOS operating system acts as an intermediary between the applications running on the screen and the hardware components of the device. iPhone has two partitions, the iOS system partition and the iOS data partition [13]. The contents of the iOS system partition maybe not be evidentiary which is used for the operating system and read-only for the user, but it may be necessary to examine it [13]. The iOS data partition is used as a read/write for the user and the applications so the evidence can be acquired from this partition [13]. iOS performs its roles through four layers [11], as shown in Fig. 2.

The top layer of the iOS architecture, This layer consists of a set of basic frameworks for developing the visual interface and providing the basic infrastructure for applications on the iOS system such as touch, multi-touch, input services and processes, and high-level tasks [11]. This application consists of basic multimedia frameworks such as audio, video, and graphics. This layer provides an aided environment for programmers to create

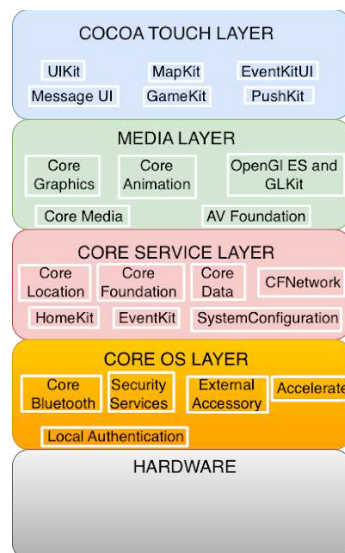


Figure. 2. iOS layered Architecture [14]

applications with a distinctive graphic appearance [11]. This layer works to provide the basic services required for applications on the system, such as location services, communication services, and iCloud services [14]. This layer is located directly above the device's hardware, and it deals with basic, low-level functions in the device, such as memory management, file system, communication, and networking [11].

2.2 Android Operating System

Android is an operating system for mobile devices developed by Android Inc., then Google bought it, and it was bought finally by the Open Handset Alliance. Android is based on the Linux kernel. Android Platform can be used on different hardware with different mobile phone manufacturers. Because android integrates seamlessly and robustly with Google products and strongly supports cloud computing, making it the best operating system for mobile devices [9].

Android OS is an open system architecture using a hierarchical structure. As shown in Fig. 3 android structure is divided into five layers [9]. Linux 2.6 kernel is the android OS base layer, as this layer is responsible for the basic functions of the system such as memory management, process management, device management, and power management. Linux kernel provides better interaction with the peripheral devices in the smartphone [16].

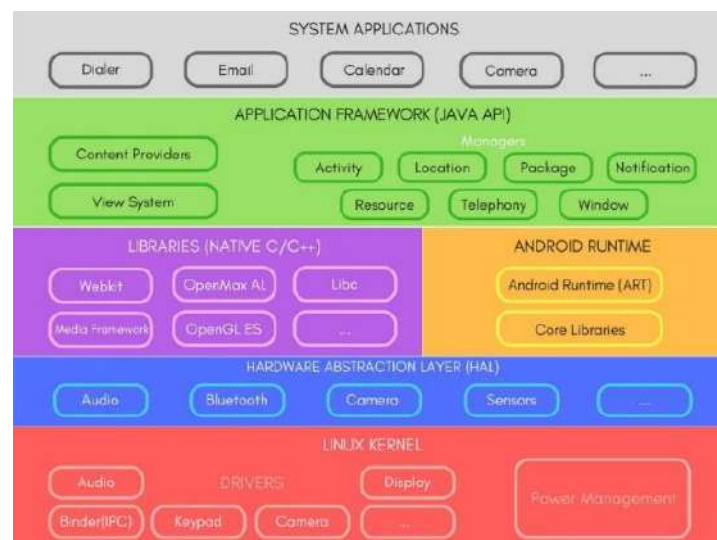


Figure. 3. Android Architecture [15]

The hardware Abstraction (HAL) layer is above the Linux kernel layer. This layer provides an interface between system services and device drivers for those services. It makes Android neutral concerning low-level drivers [17]. The Android system includes a set of main basic libraries that are exposed to developers through the Android application framework; these libraries are SQLite, FreeType, Webkit, OpenGL ES, and Media Framework. These libraries are written in C ++, and they enable the device to deal with different types of data [17].

The basic functions of the device are managed by the application layer. This layer provides user applications with application programming interfaces (APIs) that are used by applications for several purposes including getting notifications, accessing the telephony system, and sharing data. The application framework consists of an activity manager that works to manage application activity, content providers responsible for managing data sharing between applications, a location manager that works to manage locations through GPS, a telephony manager responsible for managing voice calls in applications, and managing the various resources used In applications by the resource manager [16].

The Applications layer is the top layer in android architecture, it includes the basic applications such as the contacts manager application, the SMS application, the dialer application, and the web browser application. This layer also includes applications that are developed by third parties. Since third-party developers have access to this layer, they can re-develop some basic features and applications such as the user interface and other applications to replace the basic applications of the system, this is a strong feature of the open-source Android system. Applications are written by developers in java. The developed applications are interpreted by the Dalvik virtual machine, which is replaced by Android Runtime (ART) [16].

Android OS uses a file system to organize the data on storage; the efficiency of the file system depends on the speed of storing, reading, and retrieving data. The file allocation system 32 (FAT32), yet another flash file system 2 (YAFFS2), and extended file system (EXT) file systems are used in the Android platform. These systems are used to operate the device, boot, store, and retrieve data. Also, These systems are used to organize data and files on SD memory. On flash memory, the YAFFS2 file system is used [17].

2.4 WhatsApp (WA)

WA is a popular IM application on smartphones. WA allows users to exchange text messages, images, video files, audio files, and many other types of files such as document files, pdf files, and others. WA allows users to create user groups to send messages and files to all group members. WA also allows the user to control personal profile information such as name, profile photo, and information about the user [18]. WA messaging is done in end-to-end encryption, and therefore no man-in-the-middle can read messages between two WA users [19]. WA stores its data in the mobile phone's internal memory. WA automatically connects to the phone contacts database, detects the contacts that use the WA application, and adds them to its database. WA application also includes a procedure named "com.whatsapp", which is a procedure for operating the external media management service and the messaging service that runs in the background, as this procedure works when turning on the smartphone [20]. WA used the SQLite database "ChatStorage.sqlit" to save messages that were exchanged between users and other information from the user activities on WA [10].

Old versions of WA used the SQLite database "msgstore.db" to save messages that were exchanged between users, this database was unencrypted. Because unencrypting the database, led to easy access to the details of the messages stored in it, to bypass this problem and achieve better protection for users' privacy, an encryption mechanism was developed for the WA database on the Android platform using Advanced Encryption Algorithm (AES) with an encryption key 192-bit length. As a result, the database name has changed to msgstore.db.crypt, msgstore.db.crypt5, msgstore.db.crypt7, and msgstore.db.crypt8. In recent versions of WA, the AES algorithm was used with a 256-bit key and the database became msgstore.db.crypt12 [20].

Research studies mostly deal with forensic methodologies on various mobile applications, such as forensic analysis of contact lists, SMS messages, and social media. Some researchers have compared several analysis tools by applying them to the analysis of processes for obtaining WA messages and files on android platforms. Other researchers determined different artifacts on android platforms generated by WA such as contacts database, messages database, and the database encryption key. (Shidek, Cahyani, and Wardana, 2020). Another study focused on the decryption of WA encrypted

databases, in this study, the researcher used five different tools to achieve his goals; these tools are WA key/db extractor, WA viewer, WA extract, SQLite spy, and android backup extractor. Some of these tools are written in python code, so a python compiler is also needed in their experiment [21]. A comparison study between two forensic tools for examining iPhone devices [13]. The study showed a comparison between Elcomsoft iOS Forensic Toolkit and Oxygen 2012 in terms of the ability of these tools to examine non-jailbreak and jailbreak iPhones [13]. This study focused on mobile forensic investigation in WA on iOS and Android platforms using a variety of digital forensic tools.

3 Research Method

This study's goal is to undertake a forensic assessment of Android and iOS cellphones. To perform the mobile forensic steps and evaluate the evidence gathered from WA, a hypothetical scenario will be utilized to simulate the case. This concludes the mobile forensics investigation report writing process.

The scenario illustrates the perpetrator using phone calls and text messages sent through WA to exert blackmail pressure on the victim. When dealing with evidence, the investigator has to follow the mobile forensic procedure to grab it, make sure it's safe, and keep it from being altered in any way. After that, the data from the evidence image is recovered so that investigators may investigate the discussions, phone calls, and photographs that took place between the perpetrator and the victim when they were communicating through WA. In this circumstance, the smartphone is in a capable position to be switched on since it is already operating.

Fig. 4 shows the mobile forensic method that was employed in the simulation. To deliver a witness report to the court, all necessary efforts were done to acquire legitimate and acceptable evidence.



Figure. 4. Mobile Forensic Process

For the seizing step, a legal body such as the Public Prosecution must issue a reasoned and specified search warrant. Defining digital evidence in a search warrant is essential. Digital evidence seizures are conducted by professional law enforcement officers or digital investigation specialists accompanied by court authorities to guarantee that digital evidence is safe and secure. This is also a time to make sure that all the protocols used in the seizure process are followed, as well as the laws governing personal privacy and individual rights. As part of their duties, judicial seizure officers are responsible for securing and documenting the crime scene. There are further documents that are included with a seizure report that include a list of confiscated devices and their owner's identity. Remaining in their original state is the goal of the preservation effort. Disconnecting the devices' wireless networks and any communication signals is also necessary to avoid any alteration or destruction of the digital evidence.

Forensic tools are then used to analyze and verify the evidence on the smartphone's backup and image data. The data imaging procedure was carried out with the help of the Final Mobile Forensic tool in this investigation. During the acquisition step, this procedure is carried out.

Data acquisition from a confiscated mobile phone was done using a logical acquisition, whereby the internal memory was backed up, the backup image was put in a storage medium to safeguard it, and the analysis procedure was performed afterward. Finally, the information gleaned from this procedure will be recorded and documented in a report. This information contains the name of the file, its size, and the MD5 hash value of the file, as well as the time and date of the image acquisition.

Using the previous stage's photograph, the investigator was able to do further investigation into the crime. Using the WA database, you may search for and view the evidence. The investigator checks the integrity of the evidence picture by recalculating the image hash value (MD5) and comparing it to a hash value obtained during the acquisition procedure.

A report will be issued when each step of the inquiry has been completed. There is information on the investigator and an introduction to the crime in this section of the file. Documentation of all evidence gathered, including a timeline of events, is

included in the report's findings. For the report to be acceptable in court, all operations must be conducted following the law and recognized procedures.

4 Experiment

Based on the Anti-Corruption Commission's legal competence to accept and examine allegations of corruption, based on the legislation enacted by decree No. 7 of 2010 to fight corruption. Seizure and investigation methods, in addition to the measures that have already been established. The following are the first steps taken in the envisioned scenario:

- 1- Following a claim by a victim of corruption, an investigative department issued a search warrant for a suspect based on anti-corruption and cybercrime laws, according to a statement from the Palestinian Anticorruption Commission.
- 2- A digital evidence seizure procedure based on Decree No. 10 of 2018 on cybercrime has been sought by the investigation department's judicial officials, who have asked for the aid of digital investigation specialists.

4.1. Seizure Stage

Based on an anticorruption prosecutor's search order granted under article 32 (paragraphs 1 and 2) of the legislation on cybercrime, this step was carried out. A seizure report based on Articles 32 and 33 was used to capture the following facts throughout the seizure process:

1. The Reporting agency: Anticorruption commission/ Digital Forensic Department.

2. Case Identifier:

Investigative Case No: 20/2021. (Assumption)

Digital Forensic Case No.: 7/2021. (Assumption)

3. Forensic Investigator:

Job ID NO.: 00046.

Name: Shadi K. Zakarneh.

I am a computer systems engineer. I have experience in digital forensics and information security. I am a general director of the information technology directorate in the Palestinian Anti-corruption commission. I am now a master's degree student in

Science in Cybercrimes & Digital Evidence Analysis program at Palestine technical university – Kadoorie.

4. **Identity of the submitter:** Anticorruption commission/ Investigation Department.
5. **Date of the evidence receipt:** 20/04/2021.
6. **Details of the seized devices:** are shown in Tables 1 and 2.

Table 1. the iPhone Seized device details

Device category	Smartphone
The Owner	The mobile is owned individually by XXXXX
Make	Apple iPhone 11
Model No.	MWM42HB/A
Serial No.	F4GZW027N73H
IMEI	356562105937766
MEID	35656210593776
ICCID	899702812233269067083
iOS Version	14.4.2
Internal Storage	128 GB
External Storage	No
SIM carrier	Jawwal
Passcode	The mobile passcode is: 989429 “Provided by the suspect”
Front Color	Black
Back Color	Yellow
Power state	Power ON
Battery Charge Percentage	79%
Mobile external case	No Damages, No Scratches
Device Photographs	proposed

Table 2. The Android Seized device details

Device category	Smartphone
The Owner	The mobile is owned individually by YYYY
Make	Samsung
Model No.	Galaxy J6 SM-J600F
Serial No.	RF8KA38324A
IMEI	356423092355498
Android Version	Android 10 with Knox version 3.5
Internal Storage	32 GB
External Storage	No
SIM carrier	Jawwal
Passcode	12345 provided by the suspect
Front Color	Black
Back Color	Black
Power state	Power ON
Battery Charge Percentage	95%
Mobile external case	No Damages, No Scratches
Device Photographs	proposed

Suspected gadgets were turned on and remained on throughout the seizure procedure. In addition, airplane mode was selected on the devices. Wireless connectivity was cut off. To confirm that all radio signals have been removed, a Faraday bag is utilized. Deed 10 of 2018 on cybercrime mandated certain steps to safeguard digital evidence under article no. 33 (paragraph 5).

7. Tools used in the seizure process

The documentation of the process: handwriting documentation.

Photography: Digital Camera used.

To ensure signals are disconnected: a Faraday bag is used.

8. Chain of Custody documentation

Documentation of the confiscated device was completed at the same time. The owner's name, investigation case number, digital forensic case number, and receipt date are all printed on the device. Next, it's stored in a secure location until the next step in testing. The name of the digital forensic examiner is also included in the record of this information.

4.2. Acquisition Stage

Following Article 32 (paragraph 4) of the Decree No. 10 of 2018 on Cybercrime, the anti-corruption prosecutor issued a direct access warrant for this stage. The ADB backup command-line tools, the Belkadoft forensic tool, the mobileedit tool, and the final mobile forensic tool will all be utilized to collect data from the confiscated device. To connect the mobile device, we will utilize a Samsung small USB cable. Storage media will also be employed to store the obtained evidence picture. The purpose of the investigation and the facts necessary for the inquiry must be established before the investigation can begin.

The documentation information of this stage includes the following:

- 1- The examiner's name and information.
- 2- The suspect device details
- 3- The tools used in the process.
- 4- Date and time of the process.
- 5- The duration of the process.
- 6- The name of the image file.
- 7- Size of the image file.
- 8- The hash value of the generated image.

A warrant granted by the prosecutor's office allowed me to see it. As mandated by Article 32 (paragraph 4) in the Decree issued on December 10, 2018, the purchase was carried out. The logical acquisition was utilized when the device was unlocked.

4.2.1: iOS Acquisition

This step was carried out with the use of a variety of forensic instruments. Once iTunes was installed, more programs were employed to extract evidence from the device's backups.

For the Acquisition phase many software can be used to conduct this phase, The iTunes software is used to take a backup for the iPhone device. Also, Enigma Recovery Software can be used for iOS acquisition. In addition to DB Browser for SQLite that can be used to explore SQLite databases that are recovered from mobile devices. Moreover, the iBackup Viewer Pro tool can be used to explore iTunes local backup and explore and view the backup data.

One of the more popular mobile forensic software used is the Belkasoft Evidence Center, this software was used in the experiment to acquire the iOS evidence.

iOS acquisition using Belkasoft Evidence Center

Forensic investigators may access a smartphone's backup directly using this forensic tool, which allows them to do the logical or physical acquisition. An iTunes-created mobile picture was opened on the local computer and used to get this information.

1- Fig. 5 shows how the new case was produced in the Belkssoft evidence center. Fig. 6 shows how the iTunes backup folder was loaded using a mobile image. Fig. 7 depicts the selection of relevant data and apps for the search. As may be seen in Figs. 8 and 9, the results of interpreting and obtaining the picture are rather impressive.

Case name:	New case (08/05/2021 4:51:43 PM)
Root folder:	D:\Master\cases\iphone 11-Belkasoft-06-05-2021
Case folder:	D:\Master\cases\iphone 11-Belkasoft-06-05-2021\New case (08_05_2021 4_51_43 PM)
Investigator:	zakar
Time zone:	(UTC+02:00) Jerusalem
Description:	

Figure. 5. Belkasoft Create a new case

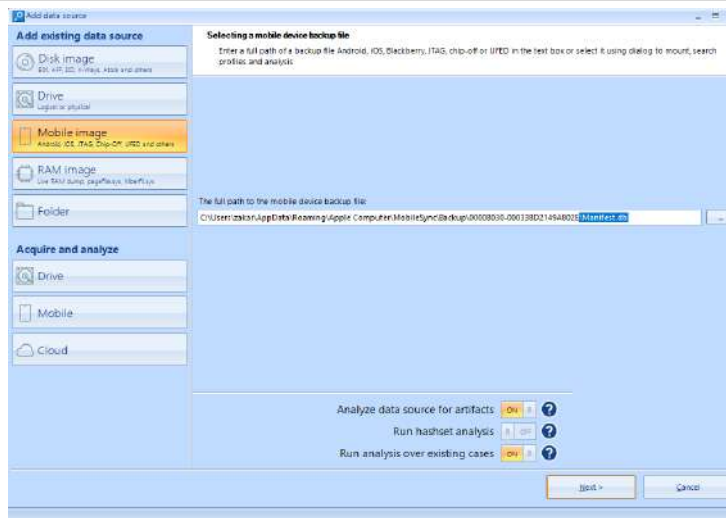


Figure. 6. Balkasoft determining data source

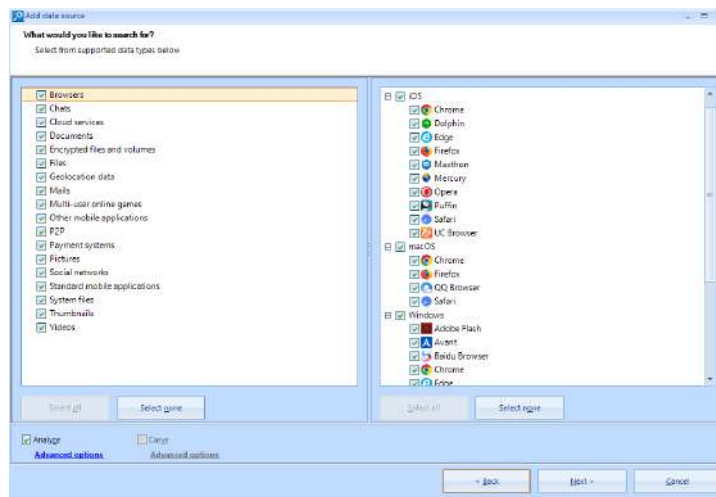


Figure. 7. Balkasoft determining what would you like to search.



Figure. 8. Balkasoft backup reading and acquiring results



Figure. 9: Balkasoft: device information acquired from iTunes backup

4.2.2 Android Acquisition

Different tools can be used for android acquisition such as ADB command line tools, Before the logical acquisition, the developer options and USB debugging were enabled, Belkasoft evidence center forensic software, final mobile forensic software, and MOBILedit forensic software.

4.2.2.1 Android acquisition using ADB command-line tools

The result of the acquisition stage is documented as shown in Table 3:

Table 3. Documented information from the acquisition stage using ADB command-line tool

No.	Examiner Name	Shadi Zakarneh
-	Suspect device details	As it is documented in the seizure stage and the acquisition tool record this information
-	Acquisition tools	ADB command-line tools
-	Date and time of the process	2021-07-07 14:19:09 ~ 2021-07-07 14:24:36
-	Process duration	5 minutes and 27 seconds
-	Acquired Folder name	J607072021
-	Image file size	12.6 MB
-	The hash value of the generated image	57B48282FC97403F827A0A173A0C12F2

ADB command-line tools were used to restore the mobile's backup before the purchase began. Open the backup files using the Belksoft evidence center and Final mobile forensics, and then extract the data. The purchase procedure will be described in depth in the following phases:

- 1- After identifying the suspect's device, the examiner compared the information to seizure information.
- 2- Fig. 10 shows the command-line tool ADB used to back up the device.
- 3- When the backup is finished, you'll get a backup of your data. An archived copy of an original file. Fig. 11 shows a tar file that may be utilized with forensic software tools.

4.2.2.2 Android acquisition using belkasoft evidence center forensic software

The result of the acquisition stage is documented as shown in Table 4.

```
C:\platform-tools>adb.exe devices
List of devices attached
52002fbe4a4995e1    device

C:\platform-tools>adb backup -shared -all
WARNING: adb backup is deprecated and may be removed in a future release
Now unlock your device and confirm the backup operation...
```

Figure. 10. ADB command lines to backup android devices

```
C:\platform-tools>java -jar abe.jar unpack backup.ab backup.tar
C:\platform-tools>
```

Figure. 11. Convert backup.ab file to backup.tar file

Table 4. Documented information from the acquisition stage using belkasoft evidence center

No.	Examiner Name	Shadi Zakarneh
1-	Suspect device details	As it is documented in the seizure stage and the acquisition tool record this information
2-	Acquisition tools	Belkasoft evidence center
3-	Date and time of the process	2021-07-07 18:11:17 ~ 2021-07-07 18:19:36
4-	Process duration	8 minutes and 19 seconds
5-	Acquired Folder name	Android\belka
6-	Image file size	14.9 MB
7-	The hash value of the generated image	AECCCE50E9338B1CD4167B522DB6E5B 4

This procedure began with the creation of a case in the belkasoft evidence center and a backup of a mobile device. The purchase procedure will be described in depth in the following phases:

- 1- Fig. 12 shows how the data source was added to the constructed case by choosing the mobile data source and mobile type.
- 2- Belkasoft then established a connection with the device and displayed information such as the make, model, and type (see Fig. 13).
- 3- ADB backup creation began shown in Fig. 14.
- 4- According to Fig. 15, a backup operation was performed and the data written for analysis was picked.
- 5- Now the acquired data is ready for the analysis stage.



Figure. 12. Select data source in Belkasoft evidence center

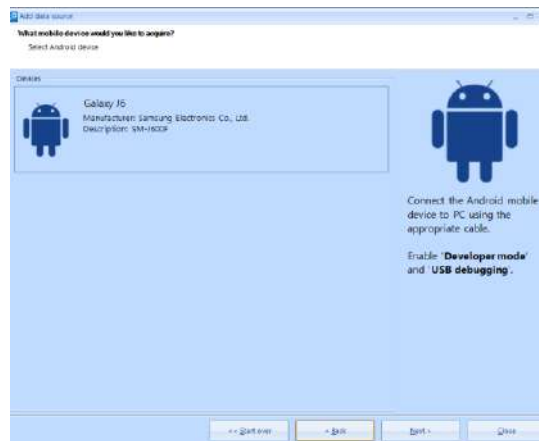


Figure. 13. Belkasoft evidence center connected with the device

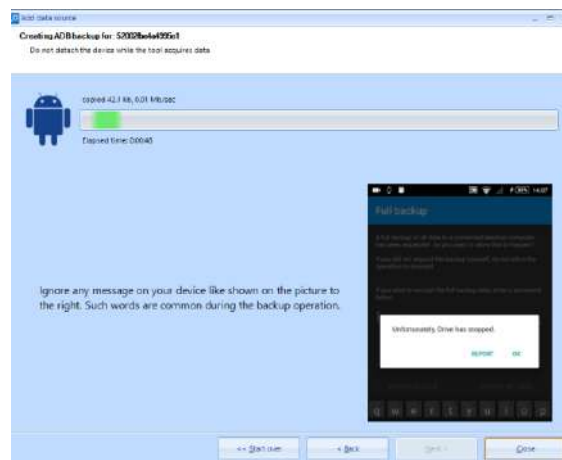


Figure. 14. Belkasoft creating ADB backup process

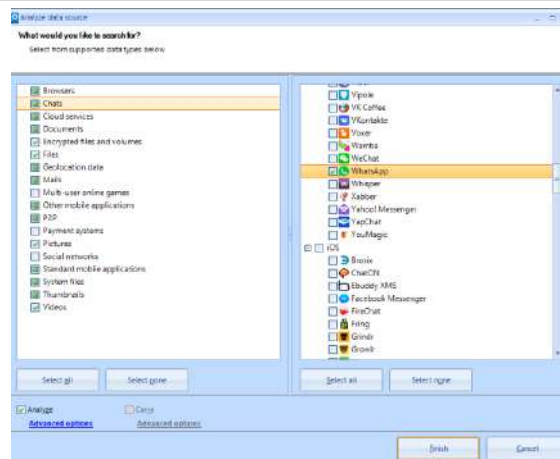


Figure. 15. Selecting the data types needed for the analysis stage

4.3. Analysis Stage

The analysis process succeeded as the evidence was found by reviewing WA chats and calls, as well as reviewing audio files, video files and photos exchanged through the WA application.

4.3.1 iOS Analysis

Using the iBackup viewer, the applications list in the manifest.plist files explored. By this tool, the WA version was determined and it was 2.21.72.1 as shown in Fig. 16.

iOS analysis using Magnet AXIOM Examine

Fig. 17 shows the dashboard information regarding the obtained case in Magnet Axiom Examine. The Magnet AXIOM Examine was able to categorize all items as illustrated in Fig. 18 by investigating them.

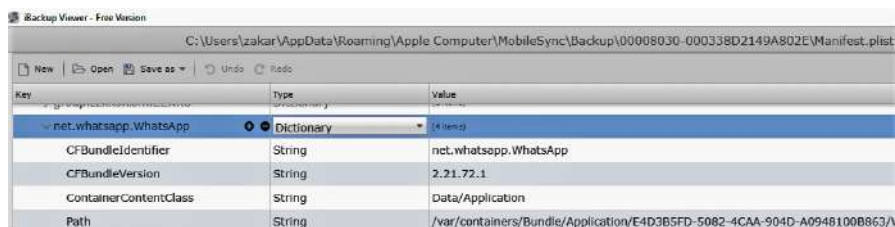


Figure. 16. WhatsApp Version from Manifest.plist file

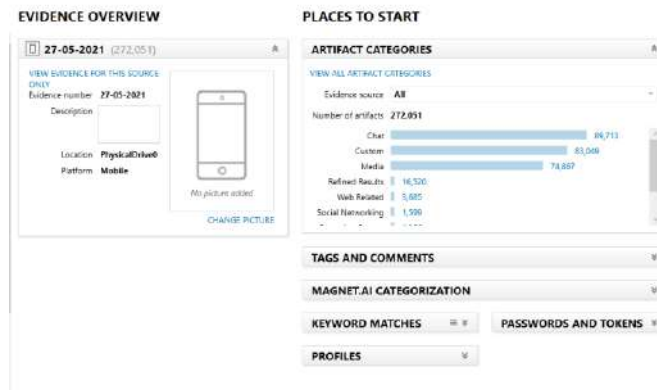
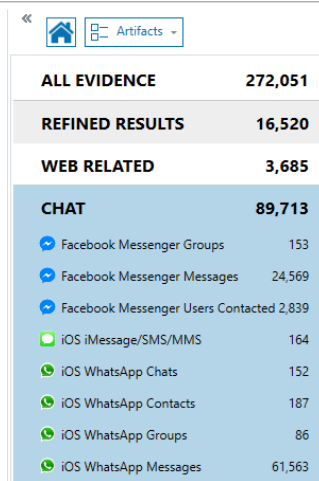


Figure. 17. Magnet AXIOM case dashboard



Figure. 18. Magnet AXIOM Examine Artifacts classification

While the focus of this research was on WA, the artifacts in the study may be used to evaluate the WhatsApp conversations, as demonstrated in Fig. 19. Magnet AXIOM Examine's artifacts module examines the logs of WA conversations, WA contacts, WA groups, and WA messages, as seen in Fig. 20. Fig. 20 depicts the WA chat logs available to the investigator, which indicate the names of individuals and groups, the chat ID, the most recent message sent or received, and the time and date of the most recent communication. Fig. 21 shows the account ID, phone number, complete name, given name, and whether or not the person is a current member of WA by examining the artifacts' WA contacts.



Category	Count
ALL EVIDENCE	272,051
REFINED RESULTS	16,520
WEB RELATED	3,685
CHAT	89,713
Facebook Messenger Groups	153
Facebook Messenger Messages	24,569
Facebook Messenger Users Contacted	2,839
iOS iMessage/SMS/MMS	164
iOS WhatsApp Chats	152
iOS WhatsApp Contacts	187
iOS WhatsApp Groups	86
iOS WhatsApp Messages	61,563

Figure. 19. WhatsApp Chats from the Artifacts view

Individual Chat...	Group Chat Name	Chat ID	Last Message	Last Message Date/Time
Message...		97259...		05/05/2021 6:32:15 PM
Message...		97259...@status	المع...	03/05/2021 9:01:38 PM
Message...		9725...	...	28/04/2021 9:34:12 PM
Message...		97259...		05/05/2021 11:59:48 AM
Message...		97259...@status		
Message...		97256...	...	29/04/2021 10:08:38 AM
+972...		972566...		03/05/2021 9:06:33 AM

Figure. 20. WA chats log

01528000000000000000	+01520000000000000000	00000000000000000000	00000000000000000000	00000000000000000000	00000000000000000000
01520000000000000000	020-0000000000000000	00000000000000000000	00000000000000000000	00000000000000000000	00000000000000000000
01520000000000000000	020-0000000000000000	00000000000000000000	00000000000000000000	00000000000000000000	00000000000000000000
01520000000000000000	02000000000000000000	00000000000000000000	00000000000000000000	00000000000000000000	00000000000000000000
01528000000000000000	020-0000000000000000	00000000000000000000	00000000000000000000	00000000000000000000	00000000000000000000
01528000000000000000	02000000000000000000	00000000000000000000	00000000000000000000	00000000000000000000	00000000000000000000
ID	Phone Number	Full Name	Given Name	email name	Full WhatsApp ID

Figure. 21. WA contacts list

There is a lot of useful information about the user's participation in WA groups that can be gleaned from the artifacts, including the group chat id, the group name, the group's creator id, and the creator's name as illustrated in Fig. 22. As shown in Fig. 23, the WA messages from the artifacts may be used to examine a list of conversations, and by choosing any row of these logs as shown in figure 24, an investigator can access the chat information.

Group Chat ID	Group Name	Creator ID	Creator Name	Admin IDs	Admin Name
97259800000000000000@g.us	...	97259800000000000000	...	97259800000000000000	...
97259800000000000000@g.us	...	97259800000000000000	...	97259800000000000000	...
97259800000000000000@g.us	...	97259800000000000000	...	97259800000000000000	...
97259800000000000000@g.us	...	97259800000000000000	...	97259800000000000000	...
97259800000000000000@g.us	...	97259800000000000000	...	97259800000000000000	...
97259800000000000000@g.us	...	97259800000000000000	...	97259800000000000000	...
97259800000000000000@g.us	...	97259800000000000000	...	97259800000000000000	...

Figure. 22. WA chat groups

Chat...	Sender	Sender Nickname	Receiver	Receiver...	Conversation ID
Individual	97259800000000000000	N...	Local User <...>	...	97259700000000000000@s.whatsapp.net
Individual	Local User <...>	...	97259800000000000000	...	97259800000000000000@s.whatsapp.net
Individual	97259800000000000000	N...	Local User <...>	...	97259800000000000000@s.whatsapp.net
Individual	Local User <...>	...	97259800000000000000	N...	97259700000000000000@s.whatsapp.net
Individual	97259800000000000000	N...	Local User <...>	...	97259700000000000000@s.whatsapp.net
Individual	97259800000000000000	N...	Local User <...>	...	97259800000000000000@s.whatsapp.net
Individual	Local User <...>	...	97259800000000000000	N...	97259700000000000000@s.whatsapp.net

Figure. 23. WA chats list



Figure. 24. WA chats details in the preview pane

Fig. 25 depicts the discovery of WA SQLite databases while utilizing the file system for inquiry and browsing the WA folder. Belkasoft evidence center allows the user to search through the WA folder, as well as export the media files that are sent with friends by the user. However, with SQLite databases, a third-party program is required to access the data.

Artifacts module of Magnet AXIOM Examine was used to evaluate and read existing message lists on WA, as demonstrated in pictures 24 and 25. The interactions in WA were

also examined, as seen in figure 22. Figure 23 shows a list of the WA groups that may be seen in addition to the actual groups themselves. Images, files, and audio messages from the Message\media folder beneath the WA folder were also examined on a file system as part of the transferred media. When looking into the specifics of the chat conversations, it is possible to examine the accompanying media.

Android Analysis

Forensic tools such as Belkasoft evidence center, MOBILedit forensic, and Final mobile forensic tools were used throughout the analysis stage.

4.3.2.1 ADB command-tool backup analysis

Because the obtained device was unrooted, the ADB command-line tool's investigation of the backup file revealed that it included no files or data linked to WA. Figs. 26 and 27 in the Final Mobile Forensic and the backup file on the Belkasoft evidence center both helped to shed light on this.

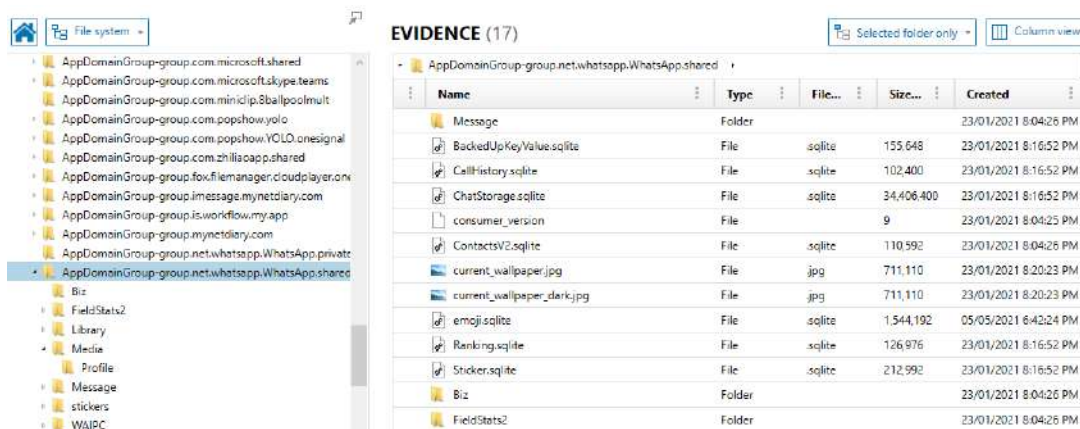


Figure. 25. WA folder in the file system



Figure. 26. ADB command line backup analysis using Belkasoft

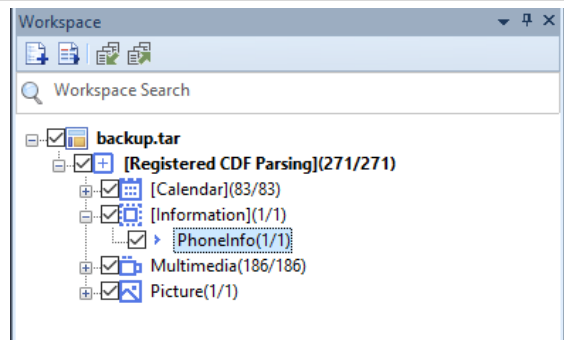


Figure. 27. ADB command-line backup analysis using Final Mobile forensic

4.3.2.4: Analysis using Final mobile forensic

The final mobile forensic was used to analyze the captured picture. Documentation and analysis of all of the digital evidence have been completed.

Fig. 28 shows how the WA account information appears in the final mobile forensic tool. Fig. 29 depicts the evaluation of WA's message lists, while Fig. 30 depicts the reading of existing message information and Fig. 31 depicts the viewing of deleted messages, texts, and attachments.

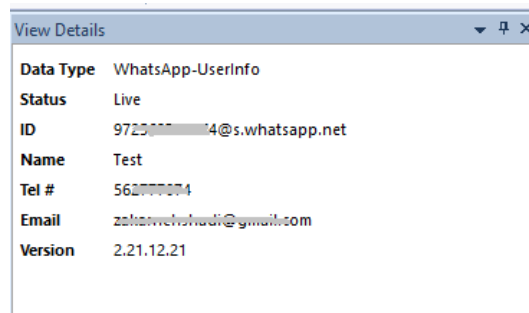


Figure. 28. WA account details in final mobile forensic

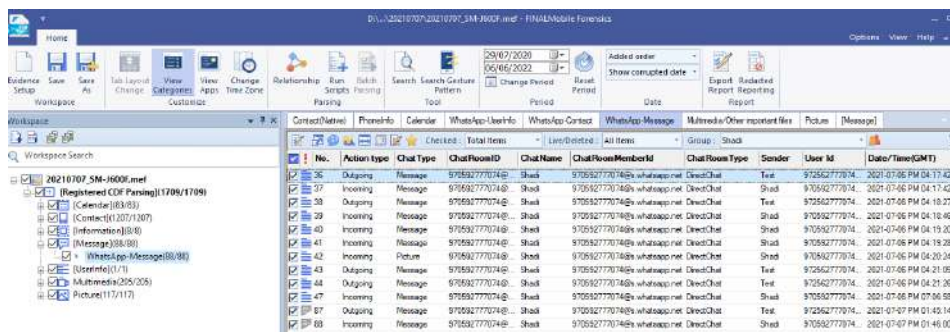


Figure. 29. List of WA messages using Final mobile forensic

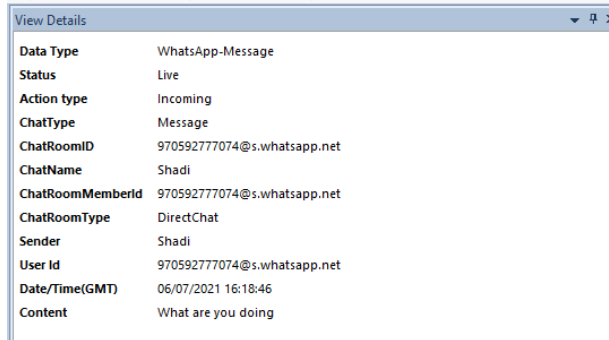


Figure. 30.Details of a live WA message in Final mobile forensic

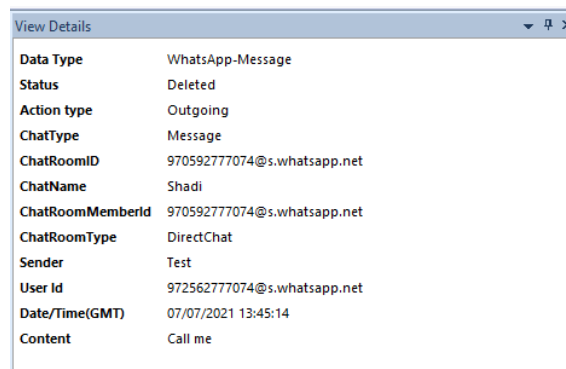


Figure. 31. Details of a deleted WA message in Final mobile forensic

Final mobile forensics may also be used to explore the file system to inspect and analyze the WA folder and its subfolders as shown in Fig. 32, and the WA SQLite database can be examined via an SQLite DB reader as shown in Fig. 33.

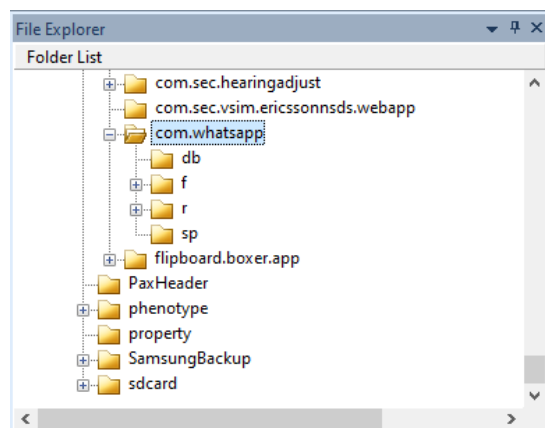


Figure. 32. WA folder and subfolders

No.	TableName	No.	_id	key
1	props			
2	messages			
3	message			
4	chat_list			
5	messages_fts_content	1	1	fts_ready
6	messages_fts_segments	2	3	chat_ready
7	message_fts_segdir	3	4	blank_me_jid_ready
8	message_ftsv2_content	4	5	participant_user_ready
9	message_ftsv2_segments	5	6	broadcast_me_jid_ready
10	message_ftsv2_segdir	6	7	receipt_user_ready
11	message_ftsv2_docsize	7	8	receipt_device_migration_complete
12	message_ftsv2_stat	8	9	status_list_ready
13	message_quotes	9	10	media_message_ready

Figure. 33. WA SQLite DB

4.4 Android Mobile root

To get super user capabilities and complete access to the Android system, the root procedure was carried out.

In addition, the Samsung Galaxy J6 (SM-J600F), which was introduced in 2018 with an Exynos 7870 octa-core CPU and Android 10 with the Knox security feature, is among the devices being investigated. The root attempt was thwarted by the android version and security measures, despite the usage of a variety of tools and methods.

Rooting an Android smartphone requires the following:

- 1- Debugging through USB is enabled in the developer settings, as illustrated in Fig. 34.
- 2- Fig 35 shows how to activate OEM unlock to get access to the bootloader.
- 3- Fig. 36 shows how to put your device into download mode after a hard reset.
- 4- Boot image and custom ROM download.

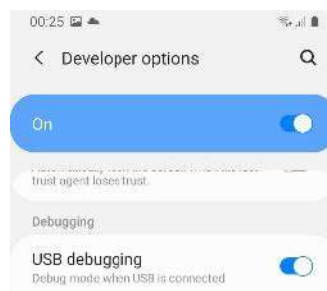


Figure. 34. Enable USB debugging on Android device

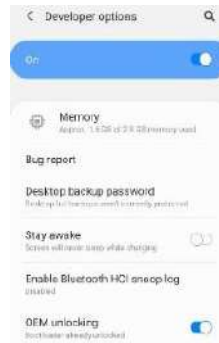


Figure. 35. Enable OEM unlock



Figure. 36. Android download mode.

Using the Odin rooting program, you can get root access to your Android smartphone:

- 1- Using a micro USB cable, connect the phone to the computer.
- 2- Open the Odin program, choose the custom image file, and begin flashing as shown in Fig. 37.



Figure. 37. Flashing custom image using Odin

Using the Magisk and Odin tools to root an Android device:

- 1- Magisk may be installed on an Android smartphone by following the steps outlined in Fig. 38.
- 2- Transfer the AP file from the custom ROM to the phone.
- 3- Use Magisk to apply the patch to the AP file.
- 4- Copy the patched file to the computer and add it to the Odin program, and then use Odin and download mode to flash the patched file to the mobile device.

Using the dr. fone-root program to root the android device as shown in Fig. 39:

- 1- Using a micro USB cable to connect the item to a computer.
- 2- Start the dr. fone-root process and the device will be detected.



Figure. 38. Magisk software for patching image.

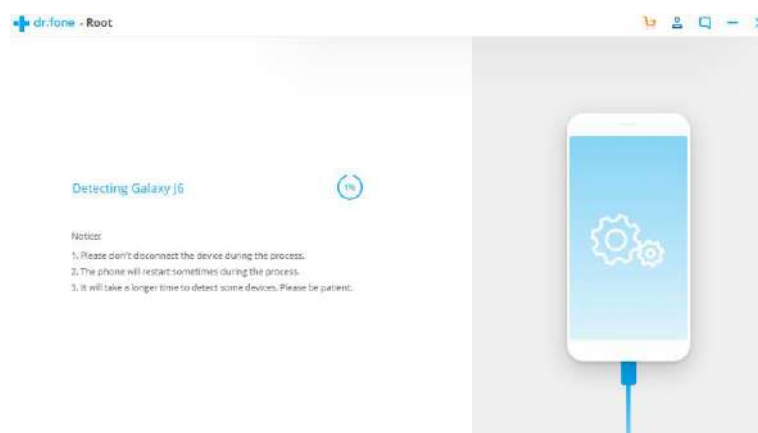


Figure. 39. dr.fone for rooting android devices

5 Results and Discussion

According to the approach, the investigation of WA messages was carried out on iOS and Android mobile devices using a variety of tools and methodologies.

5.1 Examination of the iOS platform

The investigation of WA communications necessitated the employment of a variety of techniques. iBackup viewer, Belkasoft evidence center, Magnet AXIOM analyze, Final mobile forensic, Enigma Recovery, and iBackup viewer were utilized for the inspection and analysis of the backup. In the acquisition phase, several of these tools don't allow for direct connection to the associated devices. Using iTunes backup or a logical backup is possible with one tool, but not with the other. The device's logical backup will not work until it first jailbreaks the device. A cybercrime conducted through the WA application was presumed for the purposes of this research; however, only files and data associated with WA were examined. There was no doubt that the examination process and the method in which the evidence from WA is viewed and presented varies significantly across all of these tools.

5.1.1 Examination of a backup taken by iTunes

The Belkasoft evidence center was used to evaluate and review the WA databases and files. SQLite viewer in Belkasoft may be used to examine and evaluate the database contents, which contain information such as contact information and group members. The databases' contents and structure are shown as tables in the SQLite viewer. In addition to the material that may be accessed from the chat's folder in the file system.

Using the Magnet AXIOM Analyze by looking through the WA folders, files, and database on your computer's hard drive. In addition, the artifacts' vital information for WA may be quickly accessed and categorized for a thorough analysis. Using a UI reminiscent of WA, the Magnet axiom was able to see the contents of the WA database as well as the chat messages. The data from WA required for the inquiry cannot be seen using a Final Mobile forensic. Enigma Recovery and the WA viewer allow you to see the data in the same way you see it in WA.

5.1.2 Examination of a backup taken from the connected iPhone device

Belkasoft evidence center, Magnet AXIOM analysis, Final Mobile Forensic tool, and Enigma Recovery are utilized to back up the linked device. Because the logical backup requires the device to be jailbroken to perform the logical backup, the backup option utilized is the iTunes Backup. When the device is backed up using the iTunes backup option, the results in the examination are the same as when the iTunes software backup is acquired from the local storage by the Belkasoft evidence center. iTunes backup failed on a high-storage device while running Magnet AXIOM on a forensic workstation because the program requires additional hardware. Only minimal data was saved from the linked devices, and this data was missing from the WA files and databases. It was possible to check the WA chat messages as they appear in other WA apps such as text or media messaging by using the Enigma Recovery program.

5.2 Examination of unrooted Android platform

For the investigation of WA communications, several technologies were utilized to collect and analyze data from a Samsung Galaxy J6 running Android 10 and the Knox security feature. ADB command-line tools were used for the acquisition stage, while Belkasoft evidence center and Final mobile forensic were used for the examination of the backup file that resulted. Forensic technologies including Belkasoft evidence center, MOBILedit, and Final mobile forensic were used in a second acquisition procedure.

5.2.1 Examination on a backup taken using ADB Command-line tool

Due to the unavailable storage location for WA on an unrooted device, the ADB command-line tool backup was not beneficial for the inquiry on WA.

5.2.2 Examination on a backup taken using Belkasoft evidence center

An ADB backup option with the ability to back up to shared storage was used to acquire the Android device. The Belkasoft evidence center was used to conduct an investigation, and the investigator discovered that there were no WA-related folders, files, or data.

5.2.3 Examination of a backup taken using MOBILedit forensic

As part of the purchase process, we used ADB logical backup. It was necessary to inspect the WA files and data when the capture was complete, thus the file system was

explored to do so. msgstore.db.crypt14 is the name of the encrypted WA SQLite database files. As a result, no SQLite DB viewer may be used to access the database. The WA folder's subfolders could be seen. Subfolders beneath the WA folder housed the images, videos, and documents that were delivered and received through WA (com.Whatsaspp).

5.2.4 Examination on a backup taken using Final Mobile Forensic

WA was degraded to an earlier, unencrypted version during the purchase process. To read messages and their information, the WA database was encrypted. Status (Removed) is applied to all messages that have been erased, but those that haven't been deleted appear as live. The SQLite database containing the messages may be exported and seen in the SQLite database viewer by browsing the file system and seeing the WA folder and its subfolders. It is also possible to examine and export all subfolders containing media files and documents delivered or received through WA.

5.3 Android mobile Root

It was unable to root the mobile device, even if the operating system was Android 10 with Knox security. Rooting an Android 10 device might be difficult since the ramdisk does not include the root file system. It is difficult to root the system since the root file system is integrated within the operating system. The Knox security feature also prevents any unauthorized image or custom ROM from being flashed or installed on the phone. Since the root cannot be found.

6 Conclusion

WA is the most widely used program for instant messaging, allowing users to share text messages, audio files, video files, and documents, as well as other types of multimedia. Forensic examination of WA on iOS and Android has been the subject of this study. The study uses the NIST digital forensic approach. Final mobile forensics, Belksoft evidence center, MOBILedit, and Magnet AXIOM are just a few of the technologies used throughout the inspection and analysis process. When it came to backing up the confiscated iPhone and the seized Android phone, ADB logical backup was employed. The texts, images, audio files, videos, and contacts of the alleged crimes are examined and studied during this phase of the investigation. An additional tool was

utilized to demonstrate the differences and capabilities of these tools in the examination process and the outcomes of extracting the digital evidence from WA on iOS and Android platforms. Using the NIST approach and the mobile forensic tools, an evidence from WA where collected and analysed including text messages, calls, images, so using these evidences the accused can be brought to court.

A future study may focus on rooting an android version 10 or above devices to extract more data in the acquisition phase. In addition to using different tools to acquire and analyse mobile devices to get more evidences.

References

- [1] E. S. Han and A. goleman, daniel; boyatzis, Richard; Mckee, “Is whatsapp the future of workplace communication?: investigating the use of whatsapp in decision- making episodes,” *J. Chem. Inf. Model.*, vol. 53, no. 9, pp. 1689–1699, 2019.
- [2] R. Umar, I. Riadi, and G. M. Zamroni, “Mobile forensic tools evaluation for digital crime investigation,” *Int. J. Adv. Sci. Eng. Inf. Technol.*, vol. 8, no. 3, pp. 949–955, 2018, doi: 10.18517/ijaseit.8.3.3591.
- [3] Ubaidillah *et al.*, “Analysis whatsapp forensic and visualization in android smartphone with support vector machine (SVM) Method,” *J. Phys. Conf. Ser.*, vol. 1196, no. 1, 2019, doi: 10.1088/1742-6596/1196/1/012064.
- [4] J. Clement, “Most popular global mobile messaging apps 2020,” *Statista*, 2020. <https://www.statista.com/statistics/307143/growth-of-whatsapp-usage-worldwide/> (accessed Apr. 20, 2021).
- [5] I. Abdulai Sawaneh, “Examining the Effects and Challenges of Cybercrime and Cyber Security Within the Cyberspace of Sierra Leone,” *Int. J. Intell. Inf. Syst.*, vol. 7, no. 3, p. 23, 2018, doi: 10.11648/j.ijis.20180703.11.
- [6] FBI’s Internet Crime Complaint Center, “2019 Internet Crime Report,” *2019 Internet Crime Rep.*, pp. 1–28, 2019, [Online]. Available:

https://pdf.ic3.gov/2019_IC3Report.pdf.

- [7] A. Shahbazi, “Technological developments in cyberspace and commission of the crimes in international law and Iran,” *J. Leg. Ethical Regul. Issues*, vol. 22, no. 4, pp. 1–12, 2019.
- [8] PNA, “Law by Decree No. 10 of 2018 on Cybercrime,” no. 10. pp. 1–15, 2018.
- [9] S. AlHidaifi, “Mobile Forensics: Android Platforms and WhatsApp Extraction Tools,” *Int. J. Comput. Appl.*, vol. 179, no. 47, pp. 25–29, 2018, doi: 10.5120/ijca2018917264.
- [10] R. Gyorödi, D. Zmaranda, V. Georgian, and C. Gyorödi, “A Comparative Study between Applications Developed for Android and iOS,” *Int. J. Adv. Comput. Sci. Appl.*, vol. 8, no. 11, 2017, doi: 10.14569/ijacsa.2017.081123.
- [11] F. Aleem, “Layered Architecture used by iOS and its Performance & Portability,” 2019, no. July, pp. 0–19, doi: 10.13140/RG.2.2.22845.20968.
- [12] C. Parth, J. Tamanna, and A. Animesh Kumar, “Comparative analysis of mobile forensic proprietary tools: an application in forensic investigation,” *J. Forensic Sci. Res.*, vol. 6, no. 1, pp. 077–082, 2022, doi: 10.29328/journal.jfsr.1001039.
- [13] D. Afonin, I. Hora, V. Kolesnyk, I. Popovych, and I. Kuchynska, “On the possibilities of using some modern three-dimensional modeling means in forensic examination,” *J. Forensic Sci. Med.*, vol. 8, no. 1, pp. 17–23, 2022, doi: 10.4103/jfsm.jfsm_57_21.
- [14] Rupesh, “iOS Layered Architecture,” 2017. <https://codeingwithios.blogspot.com/2017/09/ios-layered-architecture.html> (accessed May 22, 2021).
- [15] Studytonight, “Android Architecture - Software Stack of Android,” *Studytonight Technologies Pvt. Ltd*, 2020. <https://www.studytonight.com/android/android-architecture#> (accessed Dec. 27, 2020).
- [16] N. Ekanayake, “Android Operating System,” no. July, pp. 1–11, 2018, doi:

10.13140/RG.2.2.20829.72169.

- [17] J. Khan and S. Shahzad, “Android Architecture and Related Security Risks,” *Asian J. Technol. Manag. Res.*, vol. 05, no. December 2015, pp. 2249–892, 2016.
- [18] S. Udenze and B. Oshionebo, “Investigating ‘WhatsApp’ for Collaborative Learning among Undergraduates,” *Etkileşim*, vol. 3, no. 5, pp. 24–50, 2020, doi: 10.32739/etkilesim.2020.5.92.
- [19] H. Shidek, N. Cahyani, and A. A. Wardana, “WhatsApp Chat Visualizer: A Visualization of WhatsApp Messenger’s Artifact Using the Timeline Method,” *Int. J. Inf. Commun. Technol.*, vol. 6, no. 1, p. 1, 2020, doi: 10.21108/ijoint.2020.61.489.
- [20] J. K. Alhassan, B. Abubakar, M. Olalere, M. Abdulhamid, and S. Ahmad, “Forensic Acquisition of Data from a Crypt 12 Encrypted Database of Whatsapp,” *2 nd Int. Eng. Conf.*, no. October, 2017.
- [21] G. L. Jhala KY, “WhatsApp Forensics: Decryption of Encrypted WhatsApp Databases on Non Rooted Android Devices,” *J. Inf. Technol. Softw. Eng.*, vol. 05, no. 02, pp. 2–5, 2015, doi: 10.4172/2165-7866.1000147.

This page intentionally left blank

Design of Maximum Torque Per Ampere Control Method In Squirrel Cage Three-Phase Induction Motor

Regina Chelinia Erianda Putri^{1*}, Feri Yusivar²

¹*Faculty of Science and Technology, Sanata Dharma University,
Yogyakarta, 55281, Indonesia*

²*Faculty of Engineering, University of Indonesia, Depok, 16424, Indonesia*

**Corresponding Author: regina.chelinia@usd.ac.id*

(Received 23-10-2023; Revised 19-01-2024; Accepted 25-04-2024)

Abstract

Improving the performance of three-phase induction motors is currently carried out by various control methods. One of them is controlling a three-phase induction motor using the Maximum Torque Per Ampere (MTPA) method. This paper focuses on the study of modeling specific motor models using the MTPA method. The purpose of the study is to prove that with the squirrel cage motor model, the speed can be increased above its rating. The MTPA method is a method of controlling a three-phase induction motor by controlling the current from the torque speed. Modeling is tested to see the responsiveness of the modeled system. The experimental results were tested using two-speed references and the system showed that MTPA control induction motors can improve the performance of three-phase induction motors. The results from the design show that the MTPA method can increase the performance of three-phase induction motors to reach 84.4%. The results of this study can be used as one way to model induction motors.

Keywords: Induction Motor, Modelling, MTPA

1 Introduction

Developments in the field of transportation in the current era are growing rapidly. However, it is not balanced with waste treatment, making the environment polluted with smoke pollution. According to the results of the study "In the last 100 years the earth has increased in temperature up to 0.18 degrees Celsius" [1].

The transition from fossil fuel energy to electrical energy as energy in the field of transportation requires one component of electric vehicle design, namely the induction motor. Induction motor is the leading technology in many industrial applications, nevertheless, suitable IM designs are proposed even for automotive applications[2]. A



three-phase induction motor is an electronic device that aims to convert electrical energy into mechanical energy. A widely used induction motor is a three-phase induction motor known as an asynchronous motor, called because of the difference in speed from the rotation of the rotor to the rotation speed of the stator.

There are several ways to improve motor capabilities above the rate discussed in previous studies. MTPA Method has several various developments such as the title Direct Quadrature (D-Q) Modeling in the Speed Control System of Three Phase Induction Motors With Field Oriented Control (FOC) Based on P-I Controlled [3] study discusses controlling induction motors with FOC based on PI controllers. Speed Sensorless Control of Parallel Connected Dual Induction Motor Fed by Single Inverter using Direct Torque Control [4] discusses controlling two induction motors with parallel induction motors. Another research titled Comparative Performance of Induction Motor Speed Controller System with Flux Weakening Control discusses the purpose of controlling i_q^* by limiting where there is $|i_q|$ input [5].

The purpose of this study is to prove that with certain motor models, speed can be increased above its rating. The MTPA method is a three-phase induction motor control method by adjusting the reference input of torque current and flux current to control the rotational speed of the induction motor. Recently, the maximum torque per ampere (T/A) scheme has been proposed to minimize the stator current and reduce inverter losses [6]. Neither “minimum loss” nor “maximum torque per ampere” provided optimal motor drive performance and that drive performance was optimal between the two conditions [7]. MTPA is designed to ensure that the current used is the minimum i_d current for development at motor torque, with the total stator flux controlled by the MTPA criterion.

2 Research Method

The system uses models and methods, namely induction motor models, Clark-Park transformation methods, Rotor Field Oriented Control (RFOC), and MTPA modeling.

A. Induction motor model

Induction motor modeling uses the stator voltage vector $(v_s)'$, the stator current vector $(i_s)'$, the stator flux vector $(\psi_s)'$ and the rotor flux vector $(\psi_r)'$. The general equation of the induction motor is as follows.

$$\vec{V}_s' = R_s \vec{i}_s' + \frac{d}{dt} \vec{\psi}_s' + j\omega_e \vec{\psi}_s' \quad (\text{Eq. 1})$$

$$\vec{V}_r' = R_r \vec{i}_r' + \frac{d}{dt} \vec{\psi}_r' + j(\omega_e - \omega_r) \vec{\psi}_r' \quad (\text{Eq. 2})$$

$$\vec{\psi}_s' = L_s \vec{i}_s' + L_m \vec{i}_r' \quad (\text{Eq. 3})$$

$$\vec{\psi}_r' = L_r \vec{i}_r' + L_m \vec{i}_s' \quad (\text{Eq. 4})$$

B. Clark-Park Transformation

The induction motor used is a three-phase induction motor, but modeling is carried out in two phases which aims to simplify calculations and analysis. Transformation from three phases to two phases, the transformations used are Clarke Transformation and Park Transformation. [8]

The Clarke transform is a transformation that transforms a system that is on the (abc) axis into a stationary state frame of reference $(\alpha\beta)$ axis). In the stator frame of reference, $\omega_e = 0$ and then in the cage rotor type, the terminals are briefly connected so that the rotor voltage is $V_r = 0$. The substitution of the equation of stator current and rotor current obtained induction motor model in the $\alpha\beta$ axis becomes,

$$\frac{d}{dt} i_{s\alpha} = \left(-\frac{R_s}{\sigma L_s} - \frac{(1-\sigma)}{\sigma \tau_r} \right) i_{s\alpha} + \frac{L_m}{\sigma L_s L_r \tau_r} \psi_{r\alpha} + \frac{L_m \omega_r}{\sigma L_s L_r} \psi_{r\beta} + \frac{1}{\sigma L_s} V_{s\alpha} \quad (\text{Eq. 5})$$

$$\frac{d}{dt} i_{s\beta} = \left(-\frac{R_s}{\sigma L_s} - \frac{(1-\sigma)}{\sigma \tau_r} \right) i_{s\beta} - \frac{L_m \omega_r}{\sigma L_s L_r} \psi_{r\alpha} + \frac{L_m}{\sigma L_s \tau_r L_r} \psi_{r\beta} + \frac{1}{\sigma L_s} V_{s\beta} \quad (\text{Eq. 6})$$

$$\frac{d}{dt} \psi_{r\alpha} = \frac{R_r}{L_r} L_m i_{s\alpha} - \frac{R_r}{L_r} \psi_{r\alpha} - \omega_r \psi_{r\beta} \quad (\text{Eq. 7})$$

$$\frac{d}{dt} \psi_{r\beta} = \frac{R_r}{L_r} L_m i_{s\beta} + \omega_r \psi_{r\alpha} - \frac{R_r}{L_r} \psi_{r\beta} \quad (\text{Eq. 8})$$

with $\sigma = \frac{L_s L_r - L_m^2}{L_s L_r}$ and $\tau_r = \frac{L_r}{R_r}$

Park transform is a transformation that transforms a two-phase system that is on a stationary frame of reference $(\alpha\beta)$ axis) transformed in a rotating frame of reference (dq) axis). In the rotor frame of reference the location ω_e is put together by the axis of the rotor

causing the magnitude of ω_e is not equal to zero. The stator voltage transformation in equations (1)-(4) will be [9]:

$$\frac{d}{dt} i_{sd} = \left(-\frac{R_s}{\sigma L_s} - \frac{L_m^2}{\sigma L_s L_r \tau_r} \right) i_{sd} + \omega_e i_{sq} + \frac{L_m}{\sigma L_s L_r \tau_r} \psi_{rd} + \frac{L_m}{\sigma L_s L_r} \omega_r \psi_{rq} + \frac{1}{\sigma L_s} V_{sd} \quad (\text{Eq. 9})$$

$$\frac{d}{dt} i_{sq} = -\omega_e i_{sd} + \left(-\frac{R_s}{\sigma L_s} - \frac{L_m^2}{\sigma L_s L_r \tau_r} \right) i_{sq} - \frac{L_m}{\sigma L_s L_r} \omega_r \psi_{rd} + \frac{L_m}{\sigma L_s L_r \tau_r} \psi_{rq} + \frac{1}{\sigma L_s} V_{sq} \quad (\text{Eq. 10})$$

$$\frac{d}{dt} \psi_{rd} = \frac{R_r}{L_r} L_m i_{sd} - \frac{R_r}{L_r} \psi_{rd} + (\omega_e - \omega_r) \psi_{rq} \quad (\text{Eq. 11})$$

$$\frac{d}{dt} \psi_{rq} = \frac{R_r}{L_r} L_m i_{sq} - (\omega_e - \omega_r) \psi_{rd} - \frac{R_r}{L_r} \psi_{rq} \quad (\text{Eq. 12})$$

with, $\sigma = \frac{L_s L_r - L_m^2}{L_s L_r}$ and $\tau_r = \frac{L_r}{R_r}$ and rotor speed equation $\frac{d}{dt} \omega_r = \frac{T_e - T_l}{J}$:

While the mechanical equation of a motor that has a polar p-tide. In this case, electromagnetic torque T_e expressed by,

$$T_e = p \left(\frac{L_m}{L_r} \right) (i_{s\beta} \psi_{r\alpha} - i_{s\alpha} \psi_{r\beta}) \quad (\text{Eq. 13})$$

$$T_e = p \left(\frac{L_m}{L_r} \right) (i_{sq} \psi_{rd} - i_{sd} \psi_{rq}) \quad (\text{Eq. 14})$$

The parameters used are as follows:

R_r = Resistance on the rotor (Ω)	$V_{s\alpha}$ = Stator voltage on α axis (V)
R_s = Resistance on the stator (Ω)	$V_{s\beta}$ = Stator voltage on the β axis (V)
L_m = Magnetic inductance (H)	V_{sd} = Stator voltage on the d-axis (V)
L_s = Magnetic inductance (H)	V_{sq} = Stator voltage on the q-axis (V)
L_r = Magnetic inductance (H)	$\psi_{r\alpha}$ = Flux of α -axis rotor (Wb)
σ = Leakage Coefficient	$\psi_{r\beta}$ = Flux of β -axis rotor (Wb)
$i_{s\alpha}$ = α axis stator current (A)	ψ_{rd} = d-axis rotor flux (Wb)
$i_{s\beta}$ = β axis stator current (A)	ψ_{rq} = q-axis rotor flux (Wb)
i_{sd} = d-axis stator current (A)	ω_r = Rotor velocity (rad/s)
i_{sq} = stator current q axis (A)	ω_e = Rotating field speed (rad/s)
T_e = Electromagnetic torque (Nm)	p = number of poles or poles
T_l = Load torque (Nm)	τ_r = Rotor constant time

C. Rotor Field Oriented Control (RFOC)

The orientation of the FOC (Field Oriented Control) control used has three frames of reference, named the rotor-stator and the air gap. RFOC not require additional processes to separate the interrelationships of variables in the equation. Rotor-oriented FOC (RFOC) can separate (decoupling) flux and torque components so that they can be controlled by d-axis stator current (i_{sd}) and q-axis stator current (i_{sq}) respectively. The separation of the two components U_{sd} and U_{sq} is a linear part of the stator voltage after the decoupling process [10]. V_{cd} and V_{cq} are the non-linear part of the stator voltage after the decoupling process is carried out, as follows,

$$U_{sd} = R_s i_{sd} + L_s \sigma \frac{d}{dt} i_{sd} \quad (\text{Eq. 15})$$

$$U_{sq} = R_s i_{sq} + L_s \sigma \frac{d}{dt} i_{sq} \quad (\text{Eq. 16})$$

$$V_{cd} = -\sigma L_s \omega_e i_{sq} + \frac{L_m}{L_r} \frac{d}{dt} \psi_{rd} \quad (\text{Eq. 17})$$

$$V_{cq} = \sigma L_s \omega_e i_{sd} + \frac{L_m}{L_r} \omega_e \psi_{rd} \quad (\text{Eq. 18})$$

Then the current controller model is modeled as follows:

$$v_{sd}^* = -k_{idp} i_{sd} + k_{idp} i_{sd}^* + k_{idi} x_{sd} - \sigma L_s N \omega_m i_{sq1}^* - \sigma L_s \frac{R_r i_{sq1}^{*2}}{L_r i_{sd2}^*} \quad (\text{Eq. 19})$$

$$v_{sq}^* = -k_{iqp} i_{sq} + k_{iqp} i_{sq}^* + k_{iqi} x_{sq} + \sigma L_s N \omega_m i_{sd1}^* + \sigma L_s \frac{R_r i_{sd1}^* i_{sq1}^{*2}}{L_r i_{sd2}^*} + (1 - \sigma) L_s N \omega_m i_{sd2}^* + \frac{(1 - \sigma) L_s R_r}{L_r} i_{sq1}^* \quad (\text{Eq. 20})$$

$$\text{Where } k_{idp} = \frac{\sigma L_s}{T_d}, k_{idi} = \frac{R_s}{T_d}, k_{iqp} = \frac{\sigma L_s}{T_d}, k_{iqi} = \frac{R_s}{T_d}$$

Further, the first order of the reference current of the slip frequency and decoupling calculation becomes,

$$\frac{d}{dt} i_{sd1}^* = \frac{1}{T_d} i_{sd}^* - \frac{1}{T_d} i_{sd1}^* \quad (\text{Eq. 21})$$

$$\frac{d}{dt} i_{sq1}^* = \frac{1}{T_d} i_{sq}^* - \frac{1}{T_d} i_{sq1}^* \quad (\text{Eq. 22})$$

$$\frac{d}{dt} i_{sd2}^* = \frac{1}{T_2} i_{sd}^* - \frac{1}{T_2} i_{sd2}^* \quad (\text{Eq. 23})$$

D. MTPA Modelling

In fact, for designs produced with high-speed motors, increasing the current ratio limit allows achieving the same rated efficiency but with a lower slot area. This condition is suitable for inverter driven systems and optimized with the Maximum Torque per Ampere method. The maximum torque per ampere condition occurs when a certain torque

speed condition is achieved at the minimum stator current [11]. Normal rate speed electric motor will occur if the motor parameters from the real parameter. The process of the Maximum Torque Per Ampere Method in the MTPA condition process identified for a particular motor torque, the stator current components used are i_d and i_q . MTPA is operated under the condition of each d and q axis flux component in a synchronous reference frame using equations [12][13]. Flow-related signals are used to obtain information about the magnitude of the current that controls the flow. The energy stored in the magnetizing inductance remains constant.

The Maximum Torque Per Ampere method is shown in Fig. 1. The system is tested using Matlab – Simulink – Cmx. The component values of the d and q axes for the flux synchronous reference frame for the MTPA method are given by the equation.

$$\psi_{ds}|_{MTPA} = \frac{L_s}{L_m} \sqrt{\frac{2T_e L_r}{P}} \tag{Eq. 24}$$

$$\psi_{qs}|_{MTPA} = \frac{\sigma L_s}{L_m} \sqrt{\frac{2T_e L_r}{P}} \tag{Eq. 25}$$

The values of the total flux components on the d and q axes in the synchronous reference frame are shown as

$$|\vec{\psi}_s|_{MTPA} = \frac{L_s}{L_m} \sqrt{\frac{2L_r (1 + \sigma^2) T_e}{P}} \tag{Eq. 26}$$

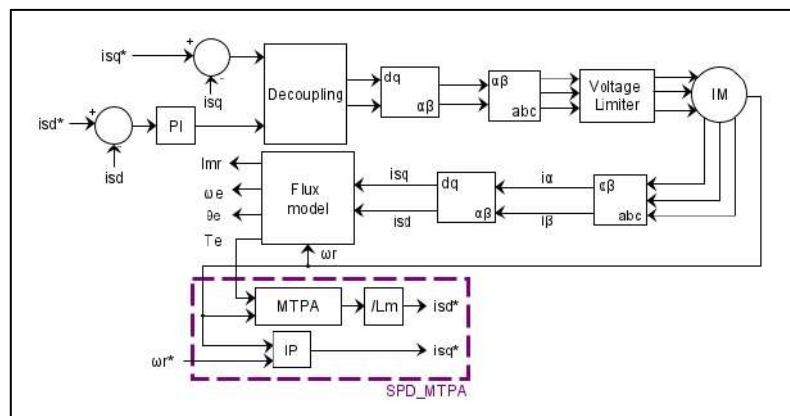


Figure 1 . Block Process Diagram MTPA Method

Then substitute $\omega_{sl} = \frac{R_r i_{sq1}^*}{L_r i_{sd2}^*}$, $v_{sd} = v_{sd}^*$, and $v_{sq} = v_{sq}^*$, $|\psi_s| = \frac{L_s}{L_m} \sqrt{\frac{2L_r(1+\sigma^2)i_{sq}^*}{P}}$ so

$$i_{sd}^* = 1 + \frac{L_s}{L_m^2} \sqrt{\frac{2L_r(1+\sigma^2)i_{sq}^*}{P}}$$

The modeling results that have been linearized into,

$$\begin{aligned} \frac{d}{dt} \Delta i_{sd} = & \left(-\frac{k_{idp} + R_s}{\sigma L_s} - \frac{R_r(1-\sigma)}{\sigma L_r} \right) \Delta i_{sd} + \left(N\omega_{m0} + \frac{R_r i_{sq10}^*}{L_r i_{sd20}^*} \right) \Delta i_{sq} + \left(\frac{L_m R_r}{\sigma L_s L_r^2} \right) \Delta \psi_{rd} + \left(\frac{NL_m \omega_{m0}}{\sigma L_s L_r} \right) \Delta \psi_{rq} + \\ & \left(\frac{k_{idi}}{\sigma L_s} \right) \Delta x_{sd} + \left(\frac{R_r i_{sq0}^*}{L_r i_{sd20}^*} - \frac{2R_r i_{sq10}^*}{L_r i_{sd20}^*} - N\omega_{m0} \right) \Delta i_{sq1}^* + \left(-\frac{R_r i_{sq0}^* i_{sq10}^*}{L_r i_{sd20}^{*2}} + \frac{R_r i_{sq10}^{*2}}{L_r i_{sd20}^{*2}} \right) \Delta i_{sd2}^* + \\ & \left(\frac{1}{2} \frac{k_{idp}}{\sigma L_m^2} \left(\frac{2L_r(1+\sigma^2)i_{sq0}^*}{P} \right)^{-\frac{1}{2}} \right) \Delta i_{sq}^* + \left(N i_{sq0}^* + \frac{NL_m \psi_{rq0}}{\sigma L_s L_r} - N i_{sq10}^* \right) \Delta \omega_m \end{aligned} \quad (Eq. 27)$$

$$\begin{aligned} \frac{d}{dt} \Delta i_{sq} = & \left(-N\omega_{m0} - \frac{R_r i_{sq10}^*}{L_r i_{sd20}^*} \right) \Delta i_{sd} + \left(-\frac{k_{iqp} + R_s}{\sigma L_s} - \frac{R_r(1-\sigma)}{\sigma L_r} \right) \Delta i_{sq} + \left(-\frac{NL_m \omega_{m0}}{\sigma L_s L_r} \right) \Delta \psi_{rd} + \left(\frac{L_m R_r}{\sigma L_s L_r^2} \right) \Delta \psi_{rq} + \\ & \left(\frac{k_{iqi}}{\sigma L_s} \right) \Delta x_{sq} + \left(N\omega_{m0} + \frac{R_r i_{sq10}^*}{L_r i_{sd20}^*} \right) \Delta i_{sd1}^* + \left(-\frac{R_r i_{sd0}^*}{L_r i_{sd20}^*} + \frac{(1-\sigma)R_r}{\sigma L_r} + \frac{R_r i_{sd10}^*}{L_r i_{sd20}^*} \right) \Delta i_{sq1}^* + \\ & \left(\frac{R_r i_{sd0}^* i_{sq10}^*}{L_r i_{sd20}^{*2}} - \frac{R_r i_{sd10}^* i_{sq10}^*}{L_r i_{sd20}^{*2}} + \left(\frac{(1-\sigma)N\omega_{m0}}{\sigma} \right) \right) \Delta i_{sd2}^* + \left(\frac{k_{iqp}}{\sigma L_s} \right) \Delta i_{sq}^* + \left(-N i_{sd0}^* + N i_{sd10}^* - \right. \\ & \left. \frac{NL_m \psi_{rd0}}{\sigma L_s L_r} + \frac{(1-\sigma)N i_{sd20}^*}{\sigma} \right) \Delta \omega_m \end{aligned} \quad (Eq. 28)$$

$$\frac{d}{dt} \Delta \psi_{rd} = \left(\frac{L_m R_r}{L_r} \right) \Delta i_{sd} + \left(-\frac{R_r}{L_r} \right) \Delta \psi_{rd} + \left(\frac{R_r i_{sq10}^*}{L_r i_{sd20}^*} \right) \Delta \psi_{rq} + \left(\frac{R_r \psi_{rq0}}{L_r i_{sd20}^*} \right) \Delta i_{sq1} + \left(-\frac{R_r i_{sq10}^* \psi_{rq0}}{L_r i_{sd20}^{*2}} \right) \Delta i_{sd2}^* \quad (Eq. 29)$$

$$\frac{d}{dt} \Delta \psi_{rq} = \left(\frac{L_m R_r}{L_r} \right) \Delta i_{sq} + \left(\frac{R_r i_{sq10}^*}{L_r i_{sd20}^*} \right) \Delta \psi_{rd} + \left(-\frac{R_r}{L_r} \right) \Delta \psi_{rq} + \left(-\frac{R_r \psi_{rd0}}{L_r i_{sd20}^*} \right) \Delta i_{sq1} + \left(\frac{R_r i_{sq10}^* \psi_{rd0}}{L_r i_{sd20}^{*2}} \right) \Delta i_{sd2}^* \quad (Eq. 30)$$

$$\frac{d}{dt} \Delta \omega_m = \left(-\frac{NL_m \psi_{rq0}}{J L_r} \right) \Delta i_{sd} + \left(\frac{NL_m \psi_{rd0}}{J L_r} \right) \Delta i_{sq} + \left(\frac{NL_m i_{sq0}^*}{J L_r} \right) \Delta \psi_{rd} + \left(-\frac{NL_m i_{sd0}^*}{J L_r} \right) \Delta \psi_{rq} + \left(-\frac{1}{J} \right) \Delta T_L \quad (Eq. 31)$$

$$\frac{d}{dt} \Delta x_{sd} = [-1] \Delta i_{sd} + \left(\frac{1}{2} \frac{L_s}{L_m^2} \left(\frac{2L_r(1+\sigma^2)i_{sq0}^*}{P} \right)^{-\frac{1}{2}} \right) \Delta i_{sq}^* \quad (Eq. 32)$$

$$\frac{d}{dt} \Delta x_{sq} = [-1] \Delta i_{sq} + [1] \Delta i_{sq}^* \quad (Eq. 33)$$

$$\frac{d}{dt} \Delta i_{sd1}^* = \left[-\frac{1}{T_d} \right] \Delta i_{sd1}^* + \left[\frac{1}{T_d} \right] \left(\frac{1}{2} \frac{L_s}{L_m^2} \left(\frac{2L_r(1+\sigma^2)i_{sq0}^*}{P} \right)^{-\frac{1}{2}} \right) \Delta i_{sq}^* \quad (Eq. 34)$$

$$\frac{d}{dt} \Delta i_{sq1}^* = \left[-\frac{1}{T_d} \right] \Delta i_{sq1}^* + \left[\frac{1}{T_d} \right] \Delta i_{sq}^* \quad (Eq. 35)$$

$$\frac{d}{dt} \Delta i_{sd2}^* = \left[-\frac{1}{T_2} \right] \Delta i_{sd2}^* + \left[\frac{1}{T_2} \right] \left(\frac{1}{2} \frac{L_s}{L_m^2} \left(\frac{2L_r(1+\sigma^2)i_{sq0}^*}{P} \right)^{-\frac{1}{2}} \right) \Delta i_{sq}^* \quad (Eq. 36)$$

With the equilibrium point as shown by $\omega_{m0} = 209.4254$, $i_{sd0}^* = 1$, $i_{sq0}^* = 0.23914$

3 Results and Discussions

The induction motor used in this modeling uses an induction motor with specifications, namely a three-phase induction motor, 750 W, 1410 rpm, and 4 poles. The controller parameters used in the simulation process of each method are shown in Table 1-2. [15]

Table 1. Parameters of Induction Motor

Parameter	Symbol	Value
Pole pairs	P	2
Stator Resistance	R_s	2.76 Ω
Rotor Resistance	R_r	2.9 Ω
Stator Inductance	L_s	0.2349 H
Rotor Inductance	L_r	0.2349 H
Mutual Inductance	L_m	0.2279 H

Table 2. Controller Parameters

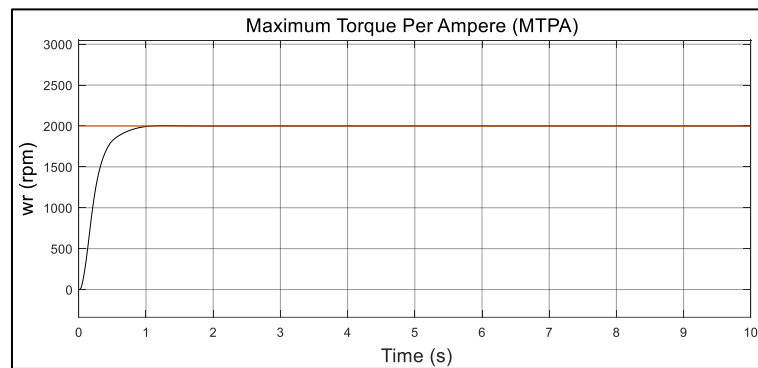
Parameter	Symbol	Value
Kp Speed Controller	Kp	0.9
Ki Speed Controller	Ki	0.2

Modeling test by providing several reference speed inputs at 2000 rpm, 2600 rpm, and 3000 rpm.

a. Testing with 2000 rpm speed reference

The induction motor with the type used with the maximum rate of 1410 rpm experiments increasing the speed by 2000 rpm. The response of the system is shown in Fig. 2. The rise time on system response is 390.146 ms. Overshoot of the response is 0.505%. In simulations the response of the system can follow its reference speed, there are overshoots and the time required to reach a steady state.

The output current for the flux controller current i_{sd} lagging slightly behind the reference current (i_{sd}^*). Output of the system there is an immediate decrease towards the minimum current value. The response of i_{sd} current can follow its reference current (i_{sd}^*) and i_{sq} decrease after the system reaches the reference current speed from the speed

**Figure 2.** MTPA at 2000 rpm

controller (i_{sq}^*). The system is a close loop system by getting error values as input for previous improvements. The response of the system is shown in Fig 3.

b. Testing with 2600 rpm speed reference

The test was carried out by providing a reference of 2600 rpm. The response of the system is shown in Fig 4. The rise time on system response is 442,739 ms. Overshoot of the response is 4.737%. From the overshoot value, the system is safe because the overshoot is still within the tolerance limit of 0 to 10%. The response of the system can follow its reference speed, in simulations, there are overshoots and several oscillations, and the time required to reach a steady state. However, the system can reach a steady-state state.

The current i_{sd} lags behind that of i_{sd}^* , and oscillations occur. The response from the i_{sd} follow the reference current (i_{sd}^*) and can reach its steady state as shown in Fig. 5. The i_{sd} the current controller maintains with maximum current at 3A until the system reaches a speed of 2600 rpm. As for i_{sq} lagging compared to i_{sq}^* . The system follows the

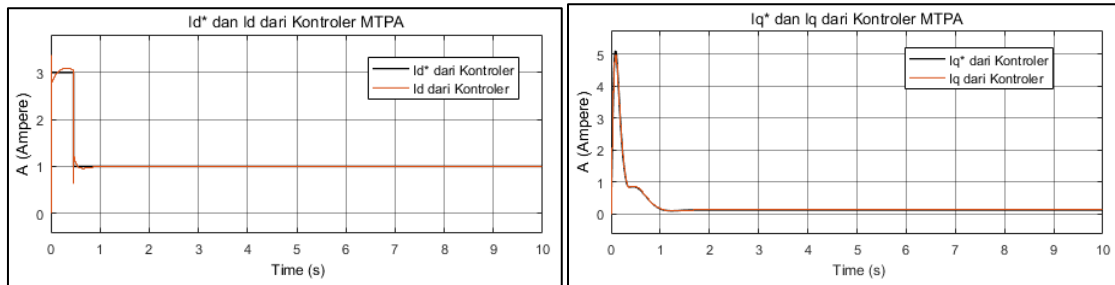


Figure 3. Comparison i_{sq}^* with i_{sq} and i_{sd}^* with i_{sd} MTPA at 2000 rpm

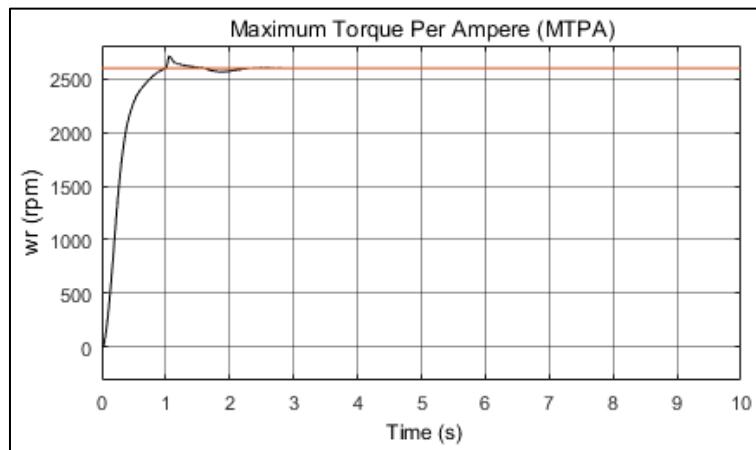


Figure 4. MTPA at 2600 rpm

references and reaches a steady-state state. The reference current undergoes oscillation and then reaches a steady-state state. The output value i_{sq} higher than the current in the previous condition. At a speed of 2600 rpm, the current controller is already at the limit of system saturation.

c. Testing with reference speed 3000 rpm.

The test was carried out by providing a reference of 3000 rpm. The response of the system cannot follow the reference speed, because the desired speed has exceeded the speed limit of the system. The system will only stay in the steady-state position even if it not reach its target speed. The response of the system is shown in Fig 6.

The current controller cannot maintain its current limit so the system failed to reach a steady-state state as shown in Fig. 7. The system continues to oscillate continuously because the system failed to reach the speed target. The desired speed exceeds the capabilities of the system so that the current from the i_{sd} still try to maintain the maximum current to reach its target speed. The condition of i_{sq} is also slightly behind

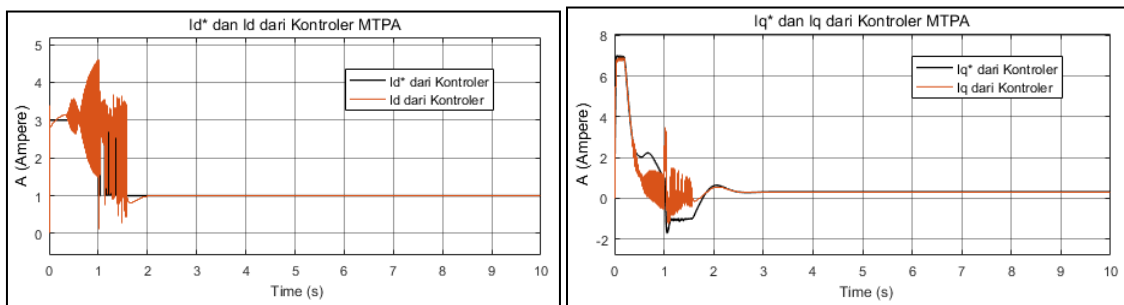


Figure 5. Comparison of i_{sq}^* with i_{sq} and i_{sd}^* with i_{sd} to MTPA i_{sd} at 2600rpm

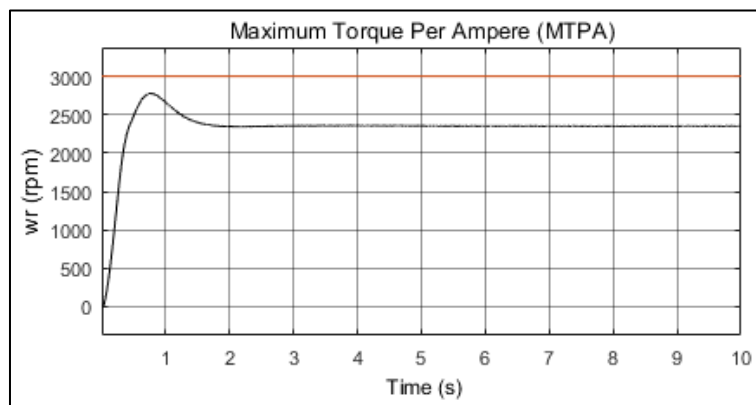


Figure 6. MTPA at 3000 rpm

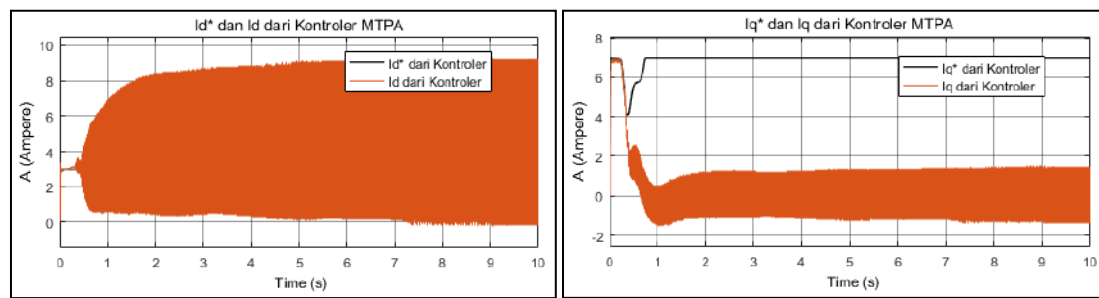


Figure 7. Comparison of i_{sd}^* to MTPA i_{sd} at 3000rpm

compared to i_{sq}^* . At first, the system followed the references, but the system failed to reach a steady-state state. The system failed to reach speed target and exceeded the system's capabilities so that the current from the i_{sq} will stop maintaining its maximum condition. The rate of the induction motor in this model is 1410 rpm. MTPA modeling can increase performance up to 2600 rpm. The modeling method with MTPA can increase performance by 84.4%

4 Conclusions

Studies on modeling with the Maximum Torque Per Ampere (MTPA) Method have been presented. The result of the modeling is that increasing the speed of each different reference input will affect settling time. The higher the speed, the longer it takes for the system to reach a steady-state state. The maximum speed that can be achieved is at a speed of 2600 rpm, so the MTPA method can increase the performance of three-phase induction motors by 84.4%. The above research is limited to the induction motor used is a squirrel cage type three-phase induction motor, and the system uses a speed sensor. The next research direction is to prove the stability of the system by analyzing pole position and movement with variations of K_p , K_i , and K_d and combining the MTPA method with other methods to improve the performance of the induction motor.

Acknowledgments

The writer expresses her thanks to God who always blessed her and to the author's family for every support that writers get. Thank you also to the thesis supervisor who has guided and supported the writer in the process of writing this journal.

References

- [1]. A. Budiarto and O. Judianto, "Design of Eco-Friendly Electric Cars Based on City Car", *Jurnal Inosains Vol. 14 No. 2*, 2009, pp 38-43.
- [2]. M. Popescu, N. Riviere, G. Volpe, M. Villani, G. Fabri, and L. di Leonardo, "A copper rotor induction motor solution for electrical vehicles traction system," in *Proc. IEEE Energy Convers. Congr. Expo*, 2019, pp. 3924–3930.
- [3]. Fauzi R and Khair J. "Direct Quadrature (DQ) Modeling on Three-Phase Induction Motor Speed Control with PI Control-Based Field Oriented Control (FOC)". *ScientiCO: Computer Science and Informatics Journal*, 2018, pp. 25-35
- [4]. H. Setiana, F. Husnayain and F. Yusivar, "Speed Sensorless Control of Dual Induction Motor using Direct Torque Control - Space Vector Modulation," *2019 IEEE 2nd International Conference on Power and Energy Applications (ICPEA)*, Singapore, 2019, pp. 110-114, doi: 10.1109/ICPEA.2019.8818504.
- [5]. Putri. RCE and Feri Yusivar. 2021. "Comparative Performance of Induction Motor Speed Controller System with Flux Weakening Control". *INCITEST 2021 "IOP Conf. Series: Materials Science and Engineering"* Vol. 1158, Iss. 1, (Jun 2021). DOI:10.1088/1757-899X/1158/1/012003
- [6]. O. Wasynczuk, et. al, "A Maximum Torque per Ampere Control Strategy for Induction Motor Drives," *IEEE Transactions on Energy Conversion*, Vol. 13, No. 2, June 1998, pp. 163-169
- [7]. Troy A. Nergaard, Heath E. Kouns, Jih-Sheng Lai, Charles E. Konrad, "Optimal System Efficiency Operation of an Induction Motor Drive," in *Conf. Rec. of IEEE IAS Annual Conference*, Pittsburgh, PA, Oct. 2002, pp. 826 – 831.
- [8]. Harini, Bernadeta Wuri. "The Effect of Motor Parameters on the Induction Motor Speed Sensorless Control System using Luenberger Observer". 2022. *International Journal of Applied Sciences and Smart Technologies*. Volume 4, Issue 1, pages 59-74
- [9]. F. Hamada, F. Husnayain and F. Yusivar, "Speed Sensorless Vector Control of Parallel Connected Induction Motor with Anti-windup Integral-Proportional Speed

-
- Controller," *2019 IEEE 2nd International Conference on Power and Energy Applications (ICPEA)*, Singapore, pp. 89-93, doi: 10.1109/ICPEA.2019.8818527.
- [10]. F. Yusivar and S. Wakao. "Minimum requirements of motor vector control modeling and simulation utilizing CMEX S-function in MATLAB/SIMULINK". in *4th IEEE International Conference on Power Electronics and Drive Systems. IEEE PEDS 2001-Indonesia. (2001). Proceedings (Cat. No.01TH8594)*. pp. 315-321. doi:10.1109/PEDS.2001.975333
- [11]. H. Kouns, J. -S. Lai and C. E. Konrad. " Analysis of a traction induction motor drive operating under maximum efficiency and maximum torque per ampere conditions". *Nineteenth Annual IEEE Applied Power Electronics Conference and Exposition APEC '04*, Anaheim, CA, USA. (2004). pp. 545-551 Vol.1, doi:10.1109/APEC.2004.1295860.
- [12]. P. Naganathan and S. Srinivas, "Maximum Torque Per Ampere Based Direct Torque Control Scheme of IM Drive for Electrical Vehicle Applications", *IEEE 18th International Power Electronics and Motion Control Conference (PEMC)*, Budapest, Hungary, 2018, pp. 256-261, doi: 10.1109/EPEPEMC.2018.8521987.
- [13]. S. Peresada, S. Kovbasa, S. Dymko, and S. Bozhko, "Maximum torque-per-amp tracking control of saturated induction motors," *International Conference on Modern Electrical and Energy Systems (MEES)*, Kremenchuk, Ukraine. (2017). pp. 72-75, doi: 10.1109/MEES.2017.8248955 doi:10.1109/EPEPEMC.2018.8521987
- [14]. Case. M.J, "Induction Motor Reactive Power as a Means of Flux Control", *The Transactions of The SA Institute of Electrical Engineers*. Volume: 84, Issue: 1
- [15]. R. Ridwan, E. Purwanto, H. Oktavianto, M. R. Rusli, and H. Toar, "Three Phase Induction Motor Speed Control Design Using Fuzzy PID Based Indirect Field Oriented Control", *J. Integr.*, 11(2), 146–155, 2019.

This page intentionally left blank

Evaluation of Impact of Biofertilizer and Mulch Types on Growth and Production of Tomato Cultivar Gustavi F1 in Lowland Areas

Raida Kartina^{1*}, Ratih Rahhutami¹, Wika Anrya Darma¹, Sekar Utami Putri¹, Dede Tiara¹, Rianida Taisa¹, Fahri Ali¹

¹ Department of Food Crop Cultivation, Lampung State Polytechnic, Jl. Soekarno Hatta No. 10, Bandar Lampung, Indonesia

*Corresponding Author: raidakartina@polinela.ac.id

(Received 23-10-2023; Revised 19-01-2024; Accepted 25-04-2024)

Abstract

Tomato plants are expected to have an ideal growing environment to optimize their growth and production. Therefore, this study aimed to investigate the effect of various concentrations of biofertilizer, mulch types, and their interactions on growth and production of the Gustavi F1 tomato cultivar. A randomized group design (RGD) arranged factorially was used for the analysis, with the first factor consisting of no mulch (M0), straw mulch (M1), and plastic mulch (M2). The second factor was five biofertilizer concentrations, including 0 ml.l⁻¹ (L0), 5 ml.l⁻¹ (L1), 10 ml.l⁻¹ (L2), 15 ml.l⁻¹ (L3), and 20 ml.l⁻¹ (L4). Data were analyzed using the F test (analysis of variance), and in cases of significant differences, the analysis proceeded with Duncan Multiple Range Test (DMRT) at an α level of 5%. Growth parameters observed in the experiments included plant height at 1 and 3 weeks after planting, while production parameters comprised fruit diameter, the number of fruits per plant, the percentage of fruits experiencing Blossom End-Rot (BER), and fruit weight per plot. The results showed that the use of plastic mulch significantly increased the number of fruits per plant, while the 0 ml.l⁻¹ biofertilizer concentration showed the most effective reduction in the percentage of fruits experiencing BER. Moreover, an interaction between mulch and biofertilizer treatments was observed, particularly in relation to plant height 1 week after planting, the number of fruits per plant, and the percentage of fruits experiencing BER.

Keywords— generative, microbes, ground cover, vegetative

1 Introduction

Tomato is a horticultural commodity with significant economic potential, widely recognized and valued within the community. In Lampung Province, the production of this commodity expresses fluctuations over the period spanning from 2018 to 2022. In

2018, tomato production reached 19,604 tons, followed by 18,669 tons in 2019, 19,096 tons in 2020, 15,934 tons in 2021, and 16,190 tons in 2022 [1].

According to [2], lowland tomato cultivation in this region faces numerous challenges, including high temperatures, low soil fertility, high soil acidity, and pest infestations. The application of biological fertilizers become one of the potential solutions to mitigate these problems. Based on the study of [3], biofertilizer were fertilizers containing a single microorganism or a combination of several microorganisms (consortium) that acted as plant growth promoters, nitrogen fixers, phosphate solvents, and inhibitors of plant disease development. [4] further reported that biofertilizer dose of 4 l.ha⁻¹ significantly affected the number of primary branches and flowers in tomato plants. In addition to biological fertilizers, another strategy to enhance tomato cultivation is the use of mulch.

Mulch, the ground cover material placed around plants, comes in two primary types, including organic and inorganic. According to [5], organic mulch is plant residues such as rice debris, sawdust, corn stalks, and prunings from hedges, leaves, and plant twigs that can improve soil fertility, structure, and water retention capacity. Inorganic mulch, on the other hand, includes all materials derived from rocks, plastics, or other chemicals. [6] showed that providing straw mulch with a thickness of 1.5 cm resulted in a total of 9.00 fruits tan⁻¹, with a fresh weight of 0.62 kg tan⁻¹ in tomato plants. Additionally, [7] reported that black silver plastic mulch outperformed both no mulch and plastic mulch in terms of plant height and total leaf count in red chili plants.

The application of biofertilizer to tomatoes has never been applied and it is hoped the addition of several types of mulch will affect the effectiveness of the microorganism consortium in biofertilizer. Based on research by [8], the use of straw as mulch in the short term, although only able to increase the consortia of certain soil microorganisms, is still able to increase the production of unstable C and N components and accelerate the C and N cycle in cultivated land. This study aims to assess the effect of diverse concentrations of biological fertilizers, mulch types, and their interaction on growth and production of tomato plants.

2 Material and Methods

The study was conducted from September to December 2022 in the experimental garden of Lampung State Polytechnic. Various tools were used for the experiment, including hoes, meters, measuring cups, seedling containers, hand sprayers, knapsack sprayers, bamboo stakes, buckets, digital scales, and a hallway. The materials used were Gustavi F1 cultivar tomato seeds, Liquid Organic Biofertilizer (LOB) produced by PT Great Giant Pineapple, containing *Bacillus sp.*, *Meyerozyma sp.*, and *Saccharomyces sp.* which facilitated phosphate dissolution and production of plant growth hormones (IAA/Auxin, Gibberalin, Kinetin, and Zeatin), plastic mulch, straw mulch, chemical insecticides, NPK Mutiara fertilizer, seedling plastic, subsoil, cow dung organic fertilizer, and raffia rope.

The study began with the sowing of tomato seeds, which were nurtured for 7 days after sowing (DAS) in seedling containers. Subsequently, the seedlings were transplanted into 1x1 m beds using plastic mulch and kept for 14 days. Two weeks after planting (WAP), the seedlings were transferred to the field, spaced at 60 x 50 cm on previously prepared soil enriched with 20 tons.ha⁻¹ of cow dung organic fertilizer and 5 kg.ha⁻¹ of dolomite. Maintenance comprised three applications of NPK Mutiara fertilizer, with the first applied 4 days after planting (DAP) at a dose of 5 g.plant⁻¹, and the second and third applications given at 18 DAP and 39 DAP, respectively, at 20 g.plant⁻¹. Furthermore, regular chemical insecticide spraying was carried out in the experiment. Hilling, bud pruning, and weeding were performed as part of routine plant care, with plant staking conducted at 14 DAP. Biofertilizer was applied 4 times, precisely at 1, 2, 3, and 4 weeks after planting, with a predetermined concentration. Mulch was installed after soil preparation by using mulch types corresponding to each treatment within the experimental plots. Additionally, harvesting occurred regularly between 7 to 11 weeks after planting.

The parameters observed in this study included plant height at 1 and 3 weeks after planting, fruit diameter, number of fruits per plant, the percentage of fruits experiencing Blossom End-Rot (BER), and fruit weight per plot. Plant height measurements were taken at 1 and 3 weeks after planting, while fruit diameter, the number of fruits per plant, the

percentage of fruits experiencing BER, and fruit weight per plot were recorded at each harvest and subsequently averaged.

A randomized group design (RGD) arranged factorially was used for the experiment, with the first factor comprising no mulch (M0), straw mulch (M1), and plastic mulch (M2). The second factor was five concentrations of biofertilizer, including 0 ml.l⁻¹ (L0), 5 ml.l⁻¹ (L1), 10 ml.l⁻¹ (L2) 15 ml.l⁻¹ (L3), and 20 ml.l⁻¹ (L4). This resulted in a total combination of 15 treatment levels, each of which was replicated three times, yielding 45 experimental units. Each experimental unit consisted of six plant samples, resulting in a total of 270 plant samples analyzed. Data collected from these samples were subjected to analysis using the F test (analysis of variance). In cases where significant differences were observed, further analysis was conducted using Duncan Multiple Range Test (DMRT) at an α level of. DMRT is used to compare all pairs of treatments and for treatments that are used more than two [9]

3 Results and Discussions

The use of diverse mulch types in this study expressed a significant impact solely on the total number of tomato fruits. Meanwhile, the application of various concentrations of biological fertilizers only had a substantial effect on the percentage of fruits experiencing BER. The interaction between these two treatments yielded a significant effect on plant height at 1 week after planting, the number of tomato fruits, and the number of fruits affected by BER. Detailed results of DMRT concerning impact of mulch and biological fertilizer on plant height, fruit diameter, number of fruits per plant, percentage of fruits experiencing BER, and fruit weight per plot in tomato plants could be found in Table 1. Furthermore, the interaction between mulch and biological fertilizer in relation to growth of plant height 1 week after planting, the number of fruits per plant, and the percentage of fruits experiencing BER could be observed in Table 2.

The isolated impact in Table 1 of applying various mulch types yielded no significant effects on the plant height, fruit diameter, the percentage of fruits experiencing BER, and fruit weight per plot. This result was consistent with [10] who showed that the application of organic mulch had no substantial effect on various parameters, including plant height, leaf count, leaf length and width, flowering time, and fruit weight in tomato

plants. Furthermore, [11] reported that the use of straw mulch, plastic mulch, and no mulch had no significant impact on stalk weight and the total flower count in chili plants. This could be attributed to the incomplete decomposition of the organic mulch used, specifically rice straw, rendering the nutrients less accessible to plants. Moreover, the variable air temperature conditions in the planting location, particularly in Lampung, contributed to this effect.

[12] reported that the effectiveness of black and silver plastic mulch in vegetable crops was more pronounced when the surrounding temperature was relatively low. When the air temperature method optimal conditions, plastic mulch might not have yielded significant effects. Table 1 can be seen that the isolated application of various biofertilizer concentrations failed to have a significant influence on plant height, fruit diameter, fruit number, and fruit weight per plot. These results were consistent with [13], showing that the application of biofertilizer up to 20 ml.l⁻¹ did not affect growth and production of tomatoes. This might have been attributed to the higher concentration of applied biofertilizer, leading to increased microbial competition. According to [14], this competition among microbes for nutrients could result in suboptimal microbial performance.

The use of plastic mulch significantly increased the number of tomato fruits. Tomato plants, which used mulch showed a greater fruit yield compared to those without mulch. The result was consistent with the study by [15], showing that the application of black and silver plastic led to a higher number of fruits in tomato plants. This effect could be attributed to the capacity of mulch to reduce soil water evaporation, thereby maintaining adequate water availability for tomato plants. Mulch played a crucial role in mitigating soil temperature fluctuations and preserving soil moisture. The consistent water supply provided by mulch allowed tomato plants to achieve higher fruit production. The use of plastic mulch does not pollute the soil in the long term because waste from plastic mulch will be managed in waste management site.

The application of biofertilizer had a significant impact on increasing the percentage of fruits experiencing BER (Table 1). The addition of biological fertilizer to the soil is thought to increase the availability of nitrogen (N) and phosphorus (P) nutrients for the plants. Apart from that, the increase in N and P suspected that at the time of the research,

NPK fertilizer was applied at a dose of 5 grams/plant which is applied 3 times during the planting period. BER in tomato fruit was commonly linked to abiotic factors and calcium (Ca) deficiency. This observation was consistent with the results from [16], who reported a lower incidence of BER disorder in plants receiving a calcium fertilizer dose of 10 kg ha⁻¹ compared to those receiving 0 and 5 kg ha⁻¹ doses. Furthermore, an imbalance between Ca and other elements such as N, P, and K in tomato fruits could lead to BER [17].

Table 1. Effect of mulch and biofertilizer on plant height, fruit diameter, number of fruits per plant, percentage of fruits with BER, and fruit weight per plot of tomato plants

Treatment	Plant height 1 WAP (cm)	Plant height 3 WAP (cm)	Number of fruits per plant	Percentage of fruit with BER	Fruit diameter (cm)	Fruit weight/plot (gram)
Mulch						
No Mulch	20.21	125.80	22.97 b	10.63	4.45	6168.95
Straw	21.99	120.38	26.87 b	11.46	4.52	9907.98
Plastic	23.92	121.64	32.5 a	9.09	4.51	7976.46
Biofertilizer Concentration						
0 ml	22.54	117.35	27.98	6.83 b	4.48	5392.37
5 ml	20.81	117.52	23.81	12.21 a	4.40	12044.69
10 ml	20.57	141.80	29.50	13.06 a	4.69	8901.99
15 ml	21.23	115.37	28.91	9.40 ab	4.44	7052.98
20 ml	25.05	121.00	27.02	10.45 ab	4.45	6696.96
Interaction	*	tn	*	*	tn	tn

Notes: Numbers followed by the same letter in the same column indicate results that are not significantly different based on DMRT at $\alpha = 5\%$, tn = no significant effect, * = significant effect.

The combined application of mulch and biofertilizer treatments had a significant effect on plant height 1 week after planting, the number of fruits, and the percentage of fruits experiencing BER. The use of plastic mulch without biofertilizer resulted in the most robust plant height growth compared to the use of plastic mulch with a 20 ml.l⁻¹ biofertilizer (Table 2). This suggested that the application of biofertilizer alongside mulch at the initial stages of planting might not have optimized plant growth.

Table 2. Interaction between mulch and biofertilizer on growth of tomato plant height at 1 week after planting, the number of fruits per plant, and the percentage of fruits experiencing BER

Treatment	Plant height at 1 WAP	Number of fruits per plant	Percentage of fruit with BER
M0P0	17.62 ef	28.00 bcde	8.81cdef
M0P1	16.44 ef	11.94 f	8.91cdef
M0P2	25.67 abcd	33.44 abc	8.54cdef
M0P3	25.14 abcd	21.89 def	6.97def
M0P4	16.17 ef	19.56 ef	19.90 a
M1P0	19.28 def	29.39 bcde	9.47 bcdef
M1P1	16.50 ef	19.44 ef	16.90 ab
M1P2	23.14 bcde	27.61 bcde	14.53 abcd
M1P3	22.47 cde	33.50 abc	10.73 bcde
M1P4	28.58 abc	24.39 cde	5.66 ef
M2P0	30.72 a	26.56 bcde	2.22 f
M2P1	29.47 ab	40.06 a	10.82 bcde
M2P2	12.92 f	27.44 bcde	16.11 abc
M2P3	16.08 ef	31.33 abcd	10.51 bcde
M2P4	30.39 a	37.11 ab	5.78 ef

Notes: Numbers followed by the same letter in the same column indicate results that are not significantly different based on DMRT at $\alpha = 5\%$, tn = no significant effect, * = significant effect, M0 = without mulch, M1 = straw mulch, M2 = silver plastic mulch, P0 = without biofertilizer, P1 = 5ml.l⁻¹, P2 = 10ml.l⁻¹, P3 = 15ml.l⁻¹, P4 = 20ml.l⁻¹.

The black portion of PHP mulch was positioned facing downward, making direct contact with the soil. This configuration has a significant impact on increasing soil moisture and creating a favorable microclimate. Simultaneously, the provision of NPK fertilizer during transplanting played a crucial role in initiating nutrient absorption essential for early-stage plant growth.

The silver part of mulch, situated above the ground, functioned by indicating sunlight that reached the surface of mulch [18]. This showed sunlight provided plants with increased light and influenced the temperature above the ground, resulting in higher temperatures. Therefore, any rain or irrigation water collected on mulch surface dried more rapidly [19]. This feature proved particularly advantageous in reducing the percentage of fruits affected by BER. Based on the data obtained, the use of black and silver plastic mulch appeared more effective in reducing the percentage of BER-affected fruits. Table 2 showed that the lowest percentage of fruits experiencing BER occurred when black and silver plastic were used without biofertilizer application.

Creating a favorable microenvironment enhanced nutrient availability for plant absorption, increased cation exchange capacity, and improved soil porosity, collectively supporting the survival of soil microbes. For instance, biofertilizers contained aerobic bacteria such as *Pseudomonas sp.* and *Bacillus sp.*, commonly found in biofertilizer. These aerobic bacteria expanded in oxygen-rich environments, optimizing the mineralization process [20].

The mineralization process signified the final stage of organic matter decomposition, converting it into mineral plant nutrients in relatively modest quantities. Soil organic matter serving as a nitrogen source, was subjected to a transformation known as ammonification, where microbes converted it into amino acids and subsequently into ammonium. This process might not have significantly benefited plant growth, as observed in the plant height at 1 week after planting (Table 3). In treatments with plastic mulch and no biofertilizer (M2P0), plant height expressed superior growth compared to those with 20ml.l⁻¹ biofertilizer application (M2P4).

The mineralization process and the efficacy of biofertilizer were believed to become optimal after several weeks of observation. In Table 2, it was evident that the combination of plastic mulch with 20 ml.l⁻¹ biofertilizer yielded a higher number of fruits when

compared to other treatment combinations. Biofertilizer contributed to increased phosphorus (P) availability in the soil. [21] stated that when phosphorus was adequately available in the root zone, it facilitated the absorption of other essential nutrients, such as potassium (K). Phosphorus was instrumental in the fertilization process, while potassium enhanced fruit quality, ultimately influencing the harvest.

4 Conclusions

In conclusion, it was observed that plastic mulch became the most effective, yielding the highest tomato fruit count compared to other alternatives. The concentration of 0 ml.l⁻¹ LOB proved to be the most effective in mitigating the occurrence of BER-affected fruits. The interaction between mulch types and LOB concentrations manifested significant effects exclusively in terms of plant height 1 week after planting, the number of fruits, and the percentage of fruits experiencing BER. An optimal combination for achieving the highest fruit yield per plant in tomato cultivation comprised the use of black and silver plastic mulch in conjunction with a 5 ml.l⁻¹ LOB concentration.

Acknowledgements

The authors are grateful to all those who contributed to the successful execution of this study. The authors extend their gratitude to the Lampung State Polytechnic for providing the necessary funding for the publication of this article.

References

- [1] Badan Pusat Statistik, Produksi Tanaman Sayuran 2023, Available: <https://www.bps.go.id/indicator/55/61/1/produksi-tanaman-sayuran.html>, 2023.
- [2] S. Sabahannur and L. Herawati, Pertumbuhan dan produksi tanaman tomat (*Lycopersicum esculentum* Mill.) pada berbagai jarak tanam dan pemangkasan, *Jurnal Agrotek*, vol. 1, no. 2, pp. 32-42, 2017.
- [3] R. Kumar, N. Kumawat, and Y.K. Sahu, Role of biofertilizers in agriculture, *Popular Kheti*. vol. 5, no. 4, pp. 63-66, 2017.

-
- [4] P. Sanjaya, N. Kurnia, K. Hendarto, and F. Yelli, Pengaruh pupuk kandang dan pupuk hayati pada pertumbuhan dan produksi tanaman tomat (*Lycopersicum esculentum* Mill.), *Jurnal Agrotek Tropika*, vol. 9, no. 1, pp. 171-176, 2021.
- [5] D.R.R. Damaiyanti, N. Aini, and Koesriharti, Kajian penggunaan macam mulsa organik pada pertumbuhan dan hasil tanaman cabai besar (*Capsicum annum* L.), *Jurnal Produksi Tanaman*, vol. 1, no. 2, pp. 25-32, 2013.
- [6] D. Anggorowati, R. Sulistyono, and N. Herlina. Respon tanaman tomat (*Lycopersicum esculentum* Mill.) pada berbagai tingkat ketebalan mulsa jerami padi. *Jurnal Produksi Tanaman*, vol. 4, pp. 378-384, 2016.
- [7] G.D. Trenaldi, Y. Sepriani, D.H. Adam, and I.A.P. Septyani, Respon penggunaan plastik hitam perak terhadap pertumbuhan tanaman cabai merah (*Capsicum annum* L.) di Perkebunan Afdeling 2 Kecamatan Bilah Barat Kabupaten Labuhan Batu, *Jurnal Education and Development*, vol. 10, no. 3, pp. 14-18, 2022
- [8] B. Liu *et al.*, "Straw mulch improves soil carbon and nitrogen cycle by mediating microbial community structure and function in the maize field," *Front. Microbiol.*, vol. 14, 2023, doi: 10.3389/fmicb.2023.1217966.
- [9] A. . Matjik and I. . Sumertajaya, *Perancangan Percobaan I*. 2006.
- [10] H. Yulianingrum, E. Suprptomomo, and P. Setyanto, Pengaruh pemberian mulsa jerami padi terhadap kelimpahan gulma dan pertumbuhan tanaman tomat (*Solanum lycopersicum*) di lahan tadah hujan. Prosiding Konser Karya Ilmiah. Universitas Kristen Satya Wacana, Salatiga. 4 Agustus 2016, 2016.
- [11] S. Ardhona, K. Hendarto, A. Karyanto, and Y.C. Ginting, Pengaruh pemberian dua jenis mulsa dan tanpa mulsa terhadap karakteristik pertumbuhan dan produksi tanaman cabai merah (*capsicum annum* L.) pada dataran rendah, *Jurnal Agrotek Tropika*, vol.1, no. 2, pp. 153-158, 2013.
- [12] R. Rukmana, *Budidaya Kubis Bunga dan Broccoli*, Kanisius, Yogyakarta, 1995.
- [13] A.R. Ziladi, K. Hendarto, Y.C. Ginting, and A. Karyanto, Pengaruh jenis pupuk organik dan aplikasi pupuk hayati terhadap pertumbuhan dan produksi tanaman tomat (*Solanum lycopersicum* Mill.) di Desa Sukabanjar Kecamatan Gedong Tataan, *Jurnal Agrotek Tropika*, vol. 9, no. 1, pp. 145-151, 2021.

-
- [14] R.D.M. Simanungkalit, A.S. Didi, S. Rasti, S. Diah, and H. Wiwik, Pupuk Organik dan Pupuk Hayati, Balai Besar Penelitian dan Pengembangan Sumberdaya Lahan Pertanian, Jawa Barat, 2006.
- [15] R. Fadel, R. Yusuf, and A. Syakur, Pertumbuhan dan hasil tanaman tomat (*Lycopersicum esculentum* mill.) pada pemberian berbagai jenis mulsa, *Jurnal Agrotekbis*, vol. 5, no. 2, pp. 152 – 160, 2017.
- [16] C. Rachmah, M. Nawawi, and Koesriharti, Pengaruh aplikasi pupuk kalsium (CaCO_3) dan gibereline pada pertumbuhan, hasil, dan kualitas buah pada tanaman tomat (*Lycopersicum esculentum* Mill.), *Jurnal Produksi Tanaman*, vol. 5, no. 3, pp. 515-520, 2017.
- [17] L.C.Ho and P. Adams, Nutrient uptake and distribution in relation to crop quality, *Acta Hort*, 396: 33-44, 1995.
- [18] M. Muslim and R. Soelistyono, “The Effect Of Silver Black Plastic Mulch With Various Form And High Of Seedbed On Growth Of Cauliflower (*Brassica oleracea* var. *Botrytis* L.),” *PLANTROPICA J. Agric. Sci.* 2017, vol. 2, no. 2, pp. 85–90, 2017.
- [19] M. Setyowati, T. Sarwanidas, and Maimunsyah, “The Effect Of Types Mulch And Doses Of NPK Fertilizer On The Growth And Results Melon Plants (*Cucumis melo* L.),” *J. Agrotek Lestari*, vol. 2, no. 2, pp. 37–46, 2016.
- [20] E. Marista, S. Khotimah, and R. Linda, “Bakteri Pelarut Fosfat Hasil Isolasi dari Tiga Jenis Tanah Rizosfer Tanaman Pisang Nipah (*Musa paradisiaca* var. *nipah*) di Kota Singkawang,” *Protobiont*, vol. 2, no. 2, pp. 93–101, 2013.
- [21] Koesriharti and D. R. Meylia, “Pengaruh Pemberian Pupuk Fosfor dan Sumber Kalium Yang berbeda Terhadap Pertumbuhan dan Hasil Tanaman Tomat (*Lycopersicum esculentum* Mill.) effect of phosphorus fertilizer and potassium different source on the growth and yield of tomato plants (*Lycoper*,” *J. Produksi Tanam.*, vol. 6, no. 8, pp. 1934–1941, 2018.

This page intentionally left blank

Response of Shoots from Porang Leaf Bulbs to Cytokinins and IAA in Shoot Multiplication In Vitro

Lisa Erfa^{1, *}, Desi Maulida¹, Rahmadyah Hamiranti¹, Ferziana¹,
Yuriansyah¹, Betari Safitri¹, Yeni¹

¹*Department of Food Plant Cultivation Lampung State Polytechnic, Jln
Soekarno Hatta Rajabasa Bandar Lampung. Indonesia*

**Corresponding Author: lisaerfa@polinela.ac.id*

(Received 16-11-2023; Revised 13-02-2024; Accepted 29-02-2024)

Abstract

The growth regulators in media have the potential to significantly influence the process of in vitro plant regeneration. The response of explants in forming shoots also depends on the type and the combination of growth regulators. This research aimed to identify the most optimal type and concentration of cytokinin for the multiplication of in vitro porang shoots. Additionally, it determined whether the addition of cytokinins should be accompanied by auxin/IAA for porang shoot multiplication. To achieve these objectives, a completely randomized design with six replications was employed, followed by a 5% LSD. The tested treatments consisted of various combinations of growth regulators. Several observations were recorded, including the speed of explants forming prospective shoots/shoots (days), the age of the explants forming prospective shoots/shoots, the number of prospective shoots and shoots produced per explant, and shoot height (cm). The results showed that 1) Tdz 2 and IAA 0.5 mg.l-1 formed the highest shoots candidates and shoots in porang multiplication in vitro, and 2) the addition of BAP and Tdz 2 mg.l-1 should be combined with IAA 0.5 mg.l-1, while BAP and Tdz 3 mg.l-1 did not require IAA.

Keywords: BAP, IAA, multiplication, porang, thidiazuron

1 Introduction

Porang (*Amorphophallus muelleri* Blume), also recognized as iles-iles, is one of the three varieties of tubers cultivated for commercial purposes, improving significant economic value [1]. According to [2], the tuber has a high selling price due to its main compound, glucomannan [3], functioning as a cholesterol-lowering agent [4], anti-diabetic [5], anti-colorectal cancer [6], and anti-inflammatory [7].



According to [8], the propagation of porang plants can be accomplished generatively or vegetatively. Furthermore, the seeds are not always available [9] and planting with corms or bulbils takes a long time due to dormancy in the bulbs. To support the availability of seedlings, the propagation is obtained using tissue culture methods since it can produce uniform plantlets in large quantities within a relatively short time and free from diseases [10].

The response of plant tissues/parts cultured in vitro shoot formation depends on the type of media [11]. As stated by [12] the response depends on the combination of growth regulators, including auxin [13], cytokinin [14], and the genotype (type and cultivar) of the plant [15]. Several research [16-18] stated that the highest number of shoots produced in porang multiplication was achieved using MS media with the addition of BAP without auxin. According to [19] showed that there was an interaction between IAA and kinetin (Kin) in shoot multiplication and the best combination was obtained with 0 mg.l⁻¹ IAA and 2 mg.l⁻¹ Kin. The research conducted by [20] on *Prunus duicis* Mill. (Almond) showed that thidiazuron (Tdz) was more effective than the other cytokinins. Application of Tdz at a concentration of 1 mg.l⁻¹ significantly increased shoot proliferation. According to [21] on Rhododendron plants, the frequency of shoot regeneration and the number per explant increase with the concentration of Tdz. Therefore, this research aimed to determine the effect of cytokinin types (with or without combination with IAA) and their concentrations in promoting axillary shoot growth, particularly in the shoot multiplication stage.

2 Material and Methods

This research was conducted between May and October 2022 at the Tissue Culture Laboratory of Lampung State Polytechnic. The materials used consisted of propagules obtained from the previous year's initiation, along with Murashige and Skoog [22] basal media. This was supplemented with vitamins (thiamine-HCl, pyridoxine-HCl, nicotinic acid), and myo-inositol, as well as growth cytokinin (BAP, Kin, and Tdz), and auxin (IAA). Additionally, HCl and NaOH, agar, sugar, rubber, plastic, and aluminum foil were employed. The tools also used encompassed an

autoclave, laminar air flow cabinet, hand sprayer, and dissection equipment (forceps, scalpel, petri dish).

The experiment was conducted using a completely randomized design (CRD). The treatments tested were BAP 2 mg.l-1 + 0 mg.l-1 IAA (P1), BAP 2 mg.l-1 + 0.5 mg.l-1 IAA (P2), BAP 3 mg.l-1 + 0 mg.l-1 IAA (P3), BAP 3 mg.l-1 + 0.5 mg.l-1 IAA (P4), Kin 2 mg.l-1 + 0 mg.l-1 IAA (P5), Kin 2 mg.l-1 + 0.5 mg.l-1 IAA (P6), Kin 3 mg.l-1 + 0 mg.l-1 IAA (P7), Kin 3 mg.l-1 + 0.5 mg.l-1 IAA (P8), Tdz 2 mg.l-1 + 0 mg.l-1 IAA (P9), Tdz 2 mg.l-1 + 0.5 mg.l-1 IAA (P10), Tdz 3 mg.l-1 + 0 mg.l-1 IAA (P11), and Tdz 3 mg.l-1 + 0.5 mg.l-1 IAA (P12). The data were subjected to analysis of variance, and differences between treatments were tested using the LSD test at the 5% level.

This research started by preparing the treatment media and the chemical materials of Murashige and Skoog basal media were prepared as stock solutions. The media were prepared by pipetting each stock solution and adding the growth regulators according to the treatments. Subsequently, 30 g.l-1 of sugar and distilled water were added, and the pH was adjusted to 5.7 by adding HCl 1 N or NaOH 1 N. The media were sterilized at a temperature of 121°C for 20 minutes, then incubated for 3-5 days. Apart from the treatment media, MS0 media (media without growth regulators) were also prepared to grow to shoot candidates into shoots used as explants. The planted explants were maintained in a room with a temperature of 25°C - 27°C, with 16 and 8 hours of light and darkness. The observations were made on the following variables 1) the speed of explant forming shoot candidates/shoots (days), 2) the age of explants forming shoot candidates/shoots, 3) the number of shoot candidates produced per explant, and 4) shoot height (cm).

3 Results and Discussions

The shoot candidates were grown into shoots by subculturing the propagules on Murashige and Skoog media until proliferation occurred, which were used as explants in the multiplication stage (Fig. 1).

Shoot proliferation for the explants occurred 3-5 weeks after subculturing. The shoots, which had reached a size of 1 cm, were isolated and planted on the treatment

media. Generally, the explants showed a response in multiplication with a speed of forming shoot candidates/shoots ranging from 10 to 20 days after being subcultured on the treatment media. Meanwhile, the number of shoots on the explants ranged from 1-2 shoots per explant with a shoot height of 0.6-0.8 cm, as shown in Table 1.

The analysis of variance showed that the treatment of cytokinin with or without auxin significantly influenced the number of shoot candidates produced on the explants. According to [23], shoot meristem formation requires an increase in cytokinin and auxin levels. Furthermore, cytokinin and auxin are needed for cell division and play a role in meristem formation and activity. Cytokinin also plays a crucial role in shoot organogenesis when the ratio to auxin increases.

Explants planted on treatment media showed different rates of forming shoot candidates. The LSD test at a 5% significance level showed that explants cultured on media with the addition of BAP 2 IAA 0,5 mg.l-1, BAP 3 IAA 0 mg.l-1, Tdz 2 IAA 0,5 mg.l-1, and Tdz 3 IAA 0 mg.l-1+ exhibited the fastest growth response in shoot candidate and took 10-10.2 days (Table 2). Meanwhile, explants cultured on media with the addition of BAP 3 IAA 0.5 mg.l-1, Kin 2 IAA 0.5 mg.l-1, and Kin 3 IAA 0.5 mg.l-1 showed the slowest growth response in shoot candidate and formation, taking 19.7-20.2 days. The LSD test at a 5% significance level showed that the explants cultured on media with the addition of Tdz 2 IAA 0.5 mg.l-1 (P10) produced the highest number of shoot candidates and shoots (31.33), followed by the treatment of BAP 3 IAA 0 mg.l-1 (P3) at 22.00 (Table 2). The lowest number of shoot candidates and shoots were obtained from the explants cultured on media with the addition of Kin 3 IAA 0.5 mg.l-1 (P8) at 6.33 (Fig. 2).



Propagules of shoot candidates



Proliferation of shoots on propagules



Porang shoot explants

Figure 1. The stage of preparing shoot explants for multiplication



Tdz 2 IAA 0.5 mg.l⁻¹ (P10)



BAP 3 IAA 0 m g.l⁻¹ (P3)



Kin 3 IAA 0.5 (P8)

Figure 2. Growth of prospective shoots and shoots on explants cultured on treatment media

The research [16-18] on porang showed that the use of a single cytokinin can increase the number of formed shoots. Furthermore, [19,24] stated that the combination of cytokinin with low auxin can improve the percentage of shoot formation and multiplication. According to [25], the response of plants to the use of specific types and concentrations of auxin and cytokinin in organ regeneration is species-specific, depending on the genotype of the cultured plant. [26] stated that the use of Tdz combined with IAA has been widely reported to promote shoot regeneration in many plant species. The combination of these two growth regulators with a lower concentration of IAA plays a crucial role in morphogenesis, such as inducing and proliferating axillary shoots.

Table 1. Average age of explants forming shoot candidates/shoots, number of shoots, and shoot height (cm)

Treatment	Speed of Forming Candidates and Shoots (days)	Explants Shoot and	Number of Shoots	Shoot Height (cm)
P1 (BAP 2 + IAA 0 mg.l-1)	15		1	0.6
P2 (BAP 2 + IAA 0.5 mg.l-1)	10		1	0.7
P3 (BAP 3 + IAA 0 mg.l-1)	10		1.2	0.8
P4 (BAP 3 + IAA 0.5 mg.l-1)	20		1	0.6
P5 (Kin 2 + IAA 0 mg.l-1)	14.7		1	0.7
P6 (Kin 2 + IAA 0.5 mg.l-1)	19.7		1	0.7
P7 (Kin 3 + IAA 0 mg.l-1)	15		1	0.7
P8 (Kin 3 + IAA 0.5 mg.l-1)	20.2		1	0.8

P9 (Tdz 2 + IAA 0 mg.l ⁻¹)	13.2	1	0.8
P10 (Tdz 2 + IAA 0.5 mg.l ⁻¹)	10	1	0.7
P11 (Tdz 3 + IAA 0 mg.l ⁻¹)	10.2	0.8	0.6
P12 (Tdz 3 + IAA 0.5 mg.l ⁻¹)	11	1	0.7

Table 2. LSD test at the 5% significance level for the variable of the speed of explant forming shoot candidates and shoots, as well as the number of shoot candidates and shoots formed on the explants

No.	Treatment	Average Speed of Explants to Form Shoot Candidates & Shoots (days)	Average of the Number of Shoot Candidates and Shoots
1.	P1 (BAP 2 + IAA 0 mg.l ⁻¹)	15.0 C	13.33 E
2.	P2 (BAP 2 + IAA 0.5 mg.l ⁻¹)	10.0 A	20.00 B C
3.	P3 (BAP 3 + IAA 0 mg.l ⁻¹)	10.0 A	22.00 B
4.	P4 (BAP 3 + IAA 0.5 mg.l ⁻¹)	20.0 D	12.50 E
5.	P5 (Kin 2 + IAA 0 mg.l ⁻¹)	14.7 C	11.00 E
6.	P6 (Kin 2 + IAA 0.5 mg.l ⁻¹)	19.7 D	14.00 D E
7.	P7 (Kin 3 + IAA 0 mg.l ⁻¹)	15.0 C	17.67 C D
8.	P8 (Kin 3 + IAA 0.5 mg.l ⁻¹)	20.2 D	6.33 F
9.	P9 (Tdz 2 + IAA 0 mg.l ⁻¹)	13.2 B C	10.33 E
10.	P10 (Tdz 2 + IAA 0.5 mg.l ⁻¹)	10.0 A	31.33 A
11.	P11 (Tdz 3 + IAA 0 mg.l ⁻¹)	10.2 A	18.50 C
12.	P12 (Tdz 3 + IAA 0.5 mg.l ⁻¹)	11.0 A B	12.00 E

Even though the use of a single cytokinin was the primary factor for inducing and proliferating shoots, this research showed that the addition of both auxin and cytokinin to the shoot induction media resulted in a higher number of shoots. The explants showed a faster ability to form shoots compared to the treatment with a single cytokinin.

The effectiveness of Tdz as cytokinin in shoot induction and multiplication may be due to its ability to stimulate endogenous cytokinin biosynthesis, which will alter the metabolism of endogenous cytokinins. The compound is also highly resistant to degradation by cytokinin oxidase enzymes in plants. Therefore, Tdz exhibits strong cytokinin-like activity that surpasses other commonly used adenine types such as benzylaminopurine or Kin [27].

IAA as auxin also affected on number of shoots. This may due of its activity on cell division and cell differentiation that makes shoots proliferation higher. [28] stated

that effectivity on cell division of IAA is more powerful than another auxin such as NAA and IBA.

Based on the results, the response of porang shoot explants to growth regulators in forming shoot candidates and shoots is best observed with Tdz (Tdz 2 IAA 0.5 mg.l⁻¹), which outperforms BAP and Kin. This was consistent with [21] in Sutsukui Azalea (*Rhododendron indicum*), where Tdz optimally induced shoots compared to BA and Kin. It also aligned with [20] that Tdz was more effective than the other cytokinins in enhancing shoot proliferation. According to [29], the use of Tdz in *Gymnocladus assamicus* resulted in higher shoot induction and proliferation compared to BA.

4 Conclusions

Based on the research on the effects of cytokinin and IAA treatments in media, the following conclusions were drawn:

1. The application of Tdz 2 + IAA 0.5 mg.l⁻¹ resulted in the highest formation of shoot candidates and shoots in *in vitro* multiplication of porang shoots.
2. The addition of BAP and Tdz 2 mg.l⁻¹ should be combined with IAA 0.5 mg.l⁻¹, while BAP and Tdz 3 mg.l⁻¹ did not require IAA.

Acknowledgements

The authors would like to acknowledge the Lampung State Polytechnic, Indonesia, for its financial support.

References

- [1] E. Pranita, (2021). 7 Cara Menanam Porang dari Tanah hingga Panen agar Hasil Berkualitas. Putri, G.S. (Ed.). <https://www.kompas.com/sains/read/2021/04/15/170100423/7-cara-menanam-porang-dari-tanah-hingga-panen-agar-hasil-berkualitas>. [1 November 2022]
- [2] Y. Meo, H. Tanto, and D. Novita, Pengaruh Pemberian Tepung Porang (*Amorphophallus muelleri* Blume) Terhadap Kadar Ureum pada Tikus (*Rattus novergicus*) Strain Wistar DM Tipe 2. *Nursing News*, 2(2):665–677, 2017.

-
- [3] C. U. Wirawati, and D. E. Nirmagustina, Supplementation of Konjac (*Amorphophallus oncophyllus*) Glucomannan Hydrolisate in Synbiotic Product. *Jurnal Penelitian Pertanian Terapan*, 22(1), pp.37–44, 2022.
- [4] M. Zhang, S. Lin, Z. Wencui, P. Xiaoxia, L. Fuqiang, W. Yanping, B. Yajing, Z. Hengbi, and Z. Yifa, Cholesteryl-Modification of a Glucomannan from *Bletilla striata* and Its Hydrogel Properties. *Molecule*, 1(9), pp.9089–9100, 2014.
- [5] CH. P. Kumar, T. Lokesh, M. Gobinath, B. Kumar, and D. Saravanan, Anti-Diabetic and Anti-Hyperlipidemic Activities of Glucomannan Isolated from *Araucaria cunninghamii* Seeds. *Journal of Chemical and Pharmaceutical Sciences*, 6(3), pp.204–209, 2013.
- [6] Pranita, E. (2021). Perbedaan Porang, Iles-iles, Suweg, dan Walur, dari Ciri hingga Manfaatnya. Dewi, B.K. (Ed.). <https://www.kompas.com/sains/read/2021/04/21/163000623/perbedaan-porang-iles-iles-suweg-dan-walur-dari-ciri-hingga-manfaatnya?page=all>. [1 November 2022]
- [7] Q. Zheng, L. Wenfeng, L. Shan, Z. Heng, Y. Hui, L. Min, and Z. Yan, Effects of Ultrasonic Treatment on the Molecular Weight and Anti-Inflamantory Activity of Oxidized Konjac Glucomannan. *Journal of Food*, 17(1), pp.1–10, 2019.
- [8] Sumarwoto. Iles-iles (*Amorphophallus muelleri* Blume), deskripsi dan sifat-sifat lainnya. *Biodiversitas*, 6(3), pp.185–190, 2015.
- [9] M. M. Aziz, R. Evie, and S. R. Yuni, Induksi Kalus Umbi Iles-Iles (*Amorphophallus muelleri*) dengan Kombinasi Konsentrasi 2,4-D dan BAP Secara In Vitro. *LenteraBio*, 3(2), pp.109–114, 2014.
- [10] E. Sulistiani, and S. A. Yani, Produksi Bibit Tanaman dengan Menggunakan Teknik Kultur Jaringan. SEAMEO BIOTROP. Southeast Asian Regional Centre for Tropical Biology. Bogor. 147 Hal, 2012.
- [11] Widiyanto, S. Mikropropagasi dalam Sains dan Bioteknologi Tumbuhan. Makalah Pidato Ilmiah Guru Besar Institut Teknologi Bandung. Bandung, 2011.
- [12] K. M. Tabori, J. D. Anszki, J. A. Teixeira da Silva, S. M. Bulley, and I. Hudak, The role of cytokinins in shoot organogenesis in apple. *Plant Cell, Tissue and Organ Culture*, 101(3), pp.251–267, 2010.

- [13] E. Firoozabady, and Y. Moy, Regeneration of pineapple plants via somatic embryogenesis and organogenesis. *In Vitro Cell Dev. Biol. Plant*, 40, pp. 67–74, 2004.
- [14] S. Sripaoraya, R. Marchant, J. B. Power, and M. R. Davey, Plant regeneration via somatic embryogenesis and organogenesis of commercial pineapple (*Ananas comosus* L.)'. *In Vitro CellDev. Biol. Plant*, 39, pp. 450–454, 2003.
- [15] L. W. Gunawan, Teknik Kultur Jaringan Tumbuhan. Bogor: IPB Press, 1992.
- [16] R. Wardana, Jumiaturun and E. Rosdiana, Multipikasi Tanaman Iles – Iles (*Amorphophallus Mulleri* Blume) Secara In Vitro Sebagai Upaya Peningkatan Produksi Pangan Lokal. Seminar Nasional Hasil Penelitian (hlm. 353–357). 08 Februari 2018. Jember: Polije, 2018.
- [17] D. Suheriyanto, Romaidi, and R. S. Resmisari, Pengembangan Bibit Unggul Porang (*Amorphophallus Oncophilus*) melalui Teknik Kultur In Vitro untuk Mendukung Ketahanan Pangan Nasional. *El-Hayah*, 3(1), pp.16–23, 2012.
- [18] Ferziana, L. Erfa, D. Maulida, R. M. Sari, and F. Yuniardi, In vitro regeneration of porang (*Amorphophallus muelleri* Blume) at several concentrations of BAP (benzyl amino purine). International Conference on Agriculture and Applied Science (hlm. 76-83). 19 November 2021. Lampung: Polinela.
- [19] K. Zakiyah, Multiplikasi Tunas Porang (*Amorphophallus muelleri* Blume) Dengan Penambahan IAA (Indole Acetic Acid) Dan Kinetin Secara In vitro (Skripsi). Fakultas Sains dan Teknologi. UIN Maulana Malik Ibrahim. Malang, 2021.
- [20] S. Kodad, R. Melhaoui, C. Hano, M. Addi, N. Sahib, A. Elamrani, M. Abid, and A. Mihamou, Effect of culture media and plant growth regulators on shoot proliferation and rooting of internode explants from Moroccan native almond (*Prunus dulcis* Mill.) genotypes. *Hindawi International Journal of Agronomy*, pp.1–10, 2021.
- [21] S. Rahimi, R. Naderib, S. A. Ghaemaghani, S. Kalatejari, and B. Farham, Study on effects of different Plant Growth Regulators types in shoot regeneration and node formation of Sutsuki Azalea (*Rhododendron indicum*): a commercially important bonsai. *Procedia Engineering*, 59, pp.240–246, 2013.

- [22] T. Murashige, and F. Skoog, A revised medium for rapid growth and bioassays with tobacco tissue cultures. *Physiologia Plantarum*, 15, pp.473–497, 1962.
- [23] K. Hill, and G. E. Schaller, Enhancing Plant Regeneration in Tissue culture. *Plant Signal Behav*, 8(10), pp.1–5, 2013.
- [24] M. Imelda, A. Wulansari, and Y. S. Poerba, (2008). Regenerasi Tunas dari Kultur Tangkai Daun Iles-iles (*Amorphophallus muelleri* Blume). *Biodiversitas*, 9(3), pp.173–176, 2008.
- [25] Y. Yusnita, E. Danial, D. Hapsoro, In Vitro Shoot Regeneration of Indonesian Bananas (*Musa* spp.) cv. Ambon Kuning and Raja Bulu, Plantlet Acclimatization and Field Performance. *Agrivita*, 37, pp.51–58, 2015.
- [26] B. Guo, B. H. Abbasi, A. Zeb, L. L. Xu, and Y. H. Wei, Thidiazuron: A multi-dimensional plant growth regulator. *African Journal of Biotechnology*, 10(45), pp. 8984–9000, 2011.
- [27] Z. D. Dalila, J. Hafisah, Z. Rokiah, K. Rodziah, and M. N. Madihah, Thidiazuron Induces High Frequency Direct Somatic Embryogenesis Growth from Cotyledon Culture of *Eurycoma longifolia*. *Sains Malaysiana*, 44(7), pp.913–920, 2015.
- [28] D. Hapsoro, and Yusnita. 2018. *Kultur Jaringan “Teori dan Praktik”*. Andi. Yogyakarta. 167 hlm.
- [29] S. Gupta, A. A. Mao, and S. Sarm, Effects of Thidiazuron (TDZ) on Direct Shoot Organogenesis of *Gymnocladus assamicus*: A Threatened and Critically Endangered Species from Northeast India. *The National Academy of Sciences*, 43, pp.85–91, 2019.

This page intentionally left blank

Implementation of Scrum in the manufacture of non-invasive blood sugar detection devices using Photoplethysmography signals

Rafly Arief Kanza¹, Erita Cicilia Febrianti¹, Izza Nur Afifah¹,
Rifqi Affan¹, Arna Fariza^{1*}, Hestiasari Rante¹

¹ *Departement Informatics and Computer Engineering, Politeknik
Elektronika Negeri Surabaya, 60111, Indonesia*

**Corresponding Author: arna@pens.ac.id*

(Received 16-11-2023; Revised 13-02-2024; Accepted 29-02-2024)

Abstract

This study presents the effective integration of Scrum methodology in the production process of non-invasive blood sugar testing devices using Photoplethysmography (PPG) signals. During three months, a team consisting of a product owner, Scrum master, and developer team successfully utilized Scrum's agile structure to manage the challenges of PPG signal processing, hardware integration, and software development. The repeated sprint cycles enabled swift adjustment to new obstacles and stakeholder input, guaranteeing both effectiveness and agility in the development process. The dynamic approach facilitated both the punctual delivery of complex medical equipment and the cultivation of a culture focused on ongoing enhancement, establishing a model for the future use of agile approaches in healthcare technology. The successful implementation highlights the effectiveness of Scrum in managing the complexities of medical device development. It provides a model for improving non-invasive blood sugar detection devices and establishes agile methodologies as a key driver of innovation in healthcare technology.

Keywords: scrum, ppg, blood sugar, medical, non-invasive

1 Introduction

The healthcare technology industry is currently undergoing a significant transformation, with a growing emphasis on non-invasive methods for monitoring and treating chronic illnesses [1]. In line with this shift, the application of Scrum methodology in the production of medical devices, particularly non-invasive blood sugar testing devices, holds substantial promise [2]. Traditional approaches to product development in

the medical sector have often been rigid and time-consuming, hindering the swift integration of new technologies. Scrum offers a more flexible and iterative approach, allowing for quicker adaptation to evolving requirements and technological advancements. By adopting Scrum, teams can enhance collaboration, streamline processes, and expedite the development of innovative healthcare solutions. This research aims to explore the implementation of Scrum in the development and production process of non-invasive blood sugar testing devices, leveraging its benefits to accelerate progress and deliver effective solutions to patients and healthcare providers [3].

Through the utilization of Scrum in the development process, the technological obstacles associated with incorporating PPG signals could be minimized while guaranteeing an agile and adaptable approach to the ever-changing field of medical device technologies. Scrum is one of the agile practices, its an incremental approach and iterative nature is used to manage complex work, these practices can be applied in development of complex software products with frequently changing business requirements. This is proven in the development of blood sugar detection devices without intrusive methods, the complex nature of developing this product requires a collaborative and adaptable approach that Scrum possess. The framework essential for attaining these objectives is provided by Scrum's cross-functional teams, short development sprints, and regular stakeholder engagements [4]. This research provides a comprehensive background for grasping the pivotal role Scrum methodology plays in shaping the future landscape of healthcare technology, specifically in the realm of developing non-invasive blood sugar testing devices utilizing photoplethysmography (PPG) signals. By elucidating the challenges associated with traditional product development approaches in the medical sector and highlighting the increasing demand for non-intrusive solutions in diabetes care, this study underscores the urgency and relevance of adopting agile methodologies like Scrum. Through detailed analysis and case studies, this research illuminates how Scrum's iterative and collaborative framework empowers teams to efficiently navigate complex development processes, accelerate innovation, and ultimately drive the advancement of cutting-edge healthcare technologies.

2 Material and Methods

In this study, the Scrum methodology is being utilized for the development of our application. Scrum is a nimble framework designed to aid people, companies, or teams in accomplishing their goals by providing flexible solutions to intricate challenges. The explanation of the Scrum framework is described in Fig. 1.

Various methods, approaches, and tactics can be utilized within the framework. Scrum can either include or replace existing approaches. Scrum allows for the evaluation of the comparative effectiveness of current management, environment, and work procedures, hence enabling possibilities for improvements. Scrum is based on the principles of scientific proof and lean thinking. Empiricism asserts that knowledge is obtained by direct experience and the act of making choices according to observed occurrences. Lean thinking eliminates inefficiencies and prioritizes the key features. Scrum utilizes a process that involves repeating and gradually improving methods to increase the ability to forecast outcomes and control potential hazards. Scrum forms teams consisting of persons who have the necessary skills and knowledge to complete the tasks at hand. It also promotes the sharing or acquisition of extra competencies as needed. Scrum includes four organized sessions for examination and adjustment inside a broader event known as the Sprint. The success of these occurrences can be due to their effective

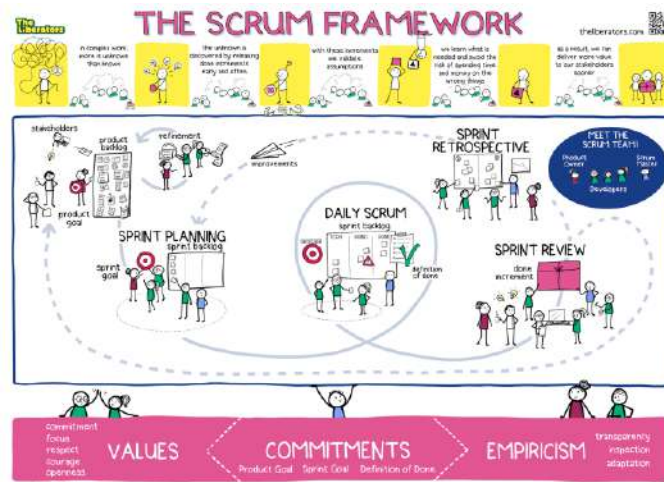


Figure 1. The scrum framework [5].

utilization of the scientific Scrum principles of openness, assessment, and adaptation [9], [10].

A. Scrum Team Composition

The composition of the Scrum Team for this research consists of three essential roles: the Product owner, Scrum master, and developer team as shown in Fig. 2. The product owner is responsible primarily on managing product backlog, establishing priorities, and ensuring that the product meets the expectations of stakeholders. The Scrum master oversees the Scrum process, eliminates obstacles, and guarantees compliance with Scrum principles. The developer teams consist of proficient experts with varied experiences, encompassing biomedical engineering, software development, and quality assurance.

B. Scrum Artifacts

The artifacts in Scrum works as a means to enhance the clarity of information on the development of a product, while also ensuring that the progress of each role can be quantified. Therefore, it strengthens the principles of empiricism and its values for both the team and their stakeholders [7], [11].

The initial component of Scrum is the product backlog. The product backlog is a vital component that comprises of a prioritized inventory for the necessary enhancements

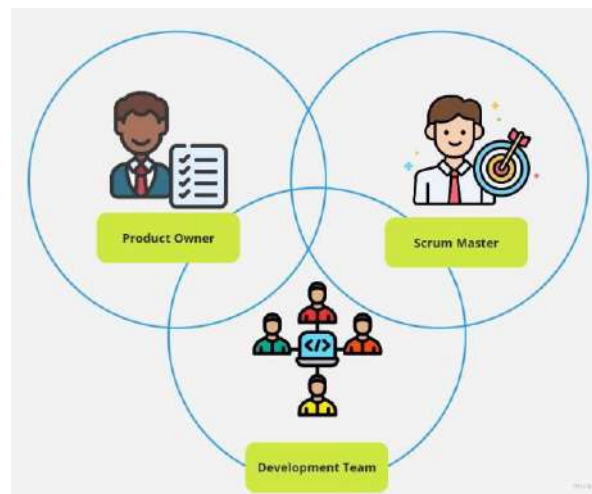


Figure 2. Scrum team composition.

for the product. Therefore, it serves as the origin of the tasks that must be carry out by the Scrum Team [7]. The product owner is responsible for establishing and overseeing the order in which tasks are completed. During the initial week, the product owner engages in collaboration with stakeholders to create a thorough product backlog. The backlog comprises of user account about PPG signal processing techniques, sensor integration, hardware design, software development, user interface, and regulatory compliance. The process of prioritization relies on input from stakeholders and the assessment of the value it brings to the organization.

The second component of Scrum is the sprint backlog. The sprint backlog is a strategic plan devised by the development team to systematically divide each desired targets into a series of activities, incorporating a design element and employing just-in-time planning to accomplish the necessary objectives. The Sprint Backlog should be consistently updated during the Sprint since it serves to evaluate the progress made during the daily scrum.

The third component of Scrum is referred as the increment. The increment is to a series of definite steps that must be taken to accomplish the product goal, ensuring that the final product is of high quality and has the ability to be shipped[12]. Each increment is an additional amount gained by the team, surpassing the previous increment. Multiple increments can be made during the sprint to ensure the cohesive functioning of all increments [7]. The project timeframe is segmented into six consecutive two-week sprints. During the initial two weeks, the team carries out Sprint 0, which primarily involves establishing the project, determining the Definition of Done (DoD), and enhancing the initial product backlog. The following sprints are allocated to certain features and functionality specified in the prioritized product backlog. Sprint planning meetings are conducted at the start of every sprint to choose tasks and establish sprint objectives.

The increment performs as a formal declaration that defines the criteria for measuring the needed product quality. It aims to foster transparency among team members by synchronizing their shared knowledge of accomplished tasks [7].

C. Scrum Tools

As we embark on the development journey of non-invasive blood sugar testing devices using PPG signals within a challenging three-month timeframe, our team harnesses a variety of methods to optimize task management and collaboration. Two essential tools in our arsenal are Miro board and Notion, each offering unique capabilities to support our Scrum-based development process.

Miro board, available at miro.com, serves as a dynamic digital whiteboard tailored for collaborative work. Its rapid, cost-free, and user-friendly interface provides an expansive surface adaptable to diverse domains, including research, design, planning, teaching, and agile operations management. Through Miro, our team engages in collaborative brainstorming, sprint planning, and visualizing workflow dependencies, fostering efficiency and alignment throughout the development cycle [13].

Complementing Miro, Notion (notion.so) emerges as a cutting-edge platform for team collaboration. Notion's customizable markdowns and diverse templates, such as kanban boards, tasks, wikis, and databases, empower our team to organize information, manage tasks, and track project progress seamlessly. Its versatility extends to note-taking, knowledge organization, and data management, further enhancing our ability to navigate the complexities of device development within tight time constraints.

Aligned with our commitment to delivering high-quality, regulatory-compliant, and user-centric products, we adopt Scrum methodology as the cornerstone of our development approach. Scrum's iterative and collaborative framework ensures timely delivery of our non-invasive blood sugar testing devices while upholding rigorous standards of quality and regulatory compliance. By integrating Scrum with Miro and Notion, our team capitalizes on agile practices and digital tools to drive innovation and achieve our development objectives effectively

3 Results and Discussions

In this research experiment, we followed the Agile Scrum framework to execute all events and create the final product. In addition, we generated documentation and designs that illustrate how we used the Agile Scrum process to develop the application.

A. Results

Following assigning Scrum roles to individuals involved in the product's development, the product owner coordinates with stakeholders to collect and define the product's requirements. These requirements are then converted into product backlog items. These items go through a prioritization procedure before being divided into several sprints for efficient completion.

Fig. 3 depicts the story of user activities within the application, illustrating tasks from user/patient, doctor, and admin. Establishing the product goal early in Scrum events is crucial to ensure that the product achieves significant commercial value. This statement is crucial for properly directing the development process. Fig. 4 depicts the product goal, displaying it as a long-term objective and emphasizing its importance in the area of business strategy.

The relationship between the product goal and the narrative story is essential for ensuring coherence and alignment throughout the development process. The narrative story provides context and specificity to the product goal by illustrating how users interact with the application and the specific tasks and functionalities they engage with to achieve desired outcomes. Conversely, the product goal sets the overarching direction and

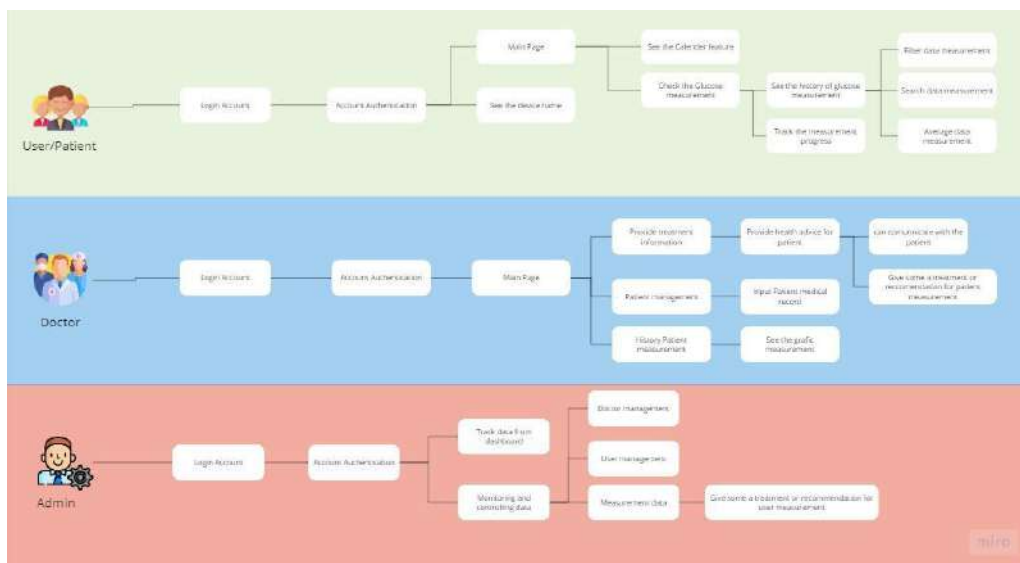


Figure 3. Narratives

purpose for the development effort, guiding the translation of user needs and requirements into actionable tasks and features within the application.

Table 1 illustrates how the narrative stories is transformed into a list of user stories. The table supports the creation of product backlog items based on simplified and summarized user needs. It makes the development team's job easier by allowing them to focus on product tasks within each sprint.

A non-invasive blood sugar detection device using Photoplethysmography (PPG) signals was developed for painless blood sampling, particularly for diabetes patients who are concerned about wound healing time. This device helps with remote blood sugar monitoring, making it easier for medical professionals to monitor patients and enabling specific actions for high or low blood sugar levels.

Figure 4. Product goal

Table 1. List of user Stories

User Story
USER
As a user, I want the application to be able to log in so I can access other features.
As a user, I want the device name and password so that I can log in and access the application.
As a user, I would like to see a "Hello Device Name" display after logging in so that I can see the connected device information.
As a user, I want to see the day and date feature on the main page so I can know what time it is.
As a user, I want to be able to see today's glucose measurement results so I can monitor my blood sugar.
As a user, I want to see a calendar feature to select a date so I can view previous data.
As a user, I want to see the history of glucose measurements in mg/dl so I can track my progress.
As a user, I want a data search feature based on date so that I can search for specific data.

As a user, I want to average glucose measurements over 1 week so I can see short-term trends.
ADMIN
As an admin, I want to log in as admin and do pin authentication so I can access admin data.
As an admin, I want to see the data collected today or on a certain date so I can manage the data.
As an admin, I want to see health suggestions (discovery feature) so that I can provide health recommendations.
DOCTOR
As a doctor, I want to log in as a doctor and do PIN authentication so I can access patient data.
As a doctor, I want to see patient history and collect data on certain dates and times so that I can provide appropriate treatment.
As a doctor, I want to input patient information so that I can complete the patient's medical record.
As a doctor, I want to see the average results of patient glucose measurements in a certain period so that I can carry out a more in-depth analysis.
As a doctor, I want to have access to a graph of the patient's glucose measurement results so that I can better visualize the data.
As a doctor, I want to be able to provide health advice to patients based on the results of their glucose measurements so that I can help them manage their condition.
As a doctor, I want to see overall patient intake data so I can make better decisions in patient care.
As a doctor, I want to see the patient's contact information so I can communicate with them.

The sprint backlog consists of user stories structured as product backlog items as illustrated in Fig. 5. Each sprint is focused on a specific goal aligned with the ongoing item under development. Each sprint has a duration of one week, and addresses an equal amount of items. This approach ensures a systematic and balanced progression of tasks over time.

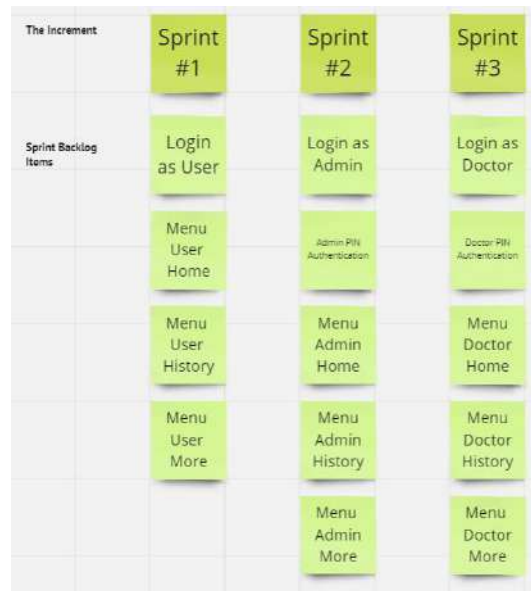


Figure 5. Product backlog items and sprints

Then, the user stories are transformed into a functional ToDo list. This conversion is accomplished utilizing a website application called Notion. The ToDo list demonstrates a practical method for transforming abstract user stories into tasks that can be managed effectively. It is useful for organizing and tracking the progress of product development. Furthermore, it also enhances transparency by clearly outlining the tasks given to each member of the development team, simplifying the handling of individual contributions and overall project development. Figure 6 depicts the transformation of user stories into a functional ToDo list.

Analyzing Fig. 6 in detail, we can observe the arrangement of tasks within the sprint backlog for the first sprint. These tasks are divided into three stages: “to do”, “doing”, and “done”. The tasks include authentication features, profile features, and PPG system. Each of these tasks requires specific work to be completed by the development team. The items already completed are sign-in and sign-up. The current priority is on finalizing the authentication process. The remaining tasks to be completed are the development of log-out and profile features.

Fig. 7 illustrates The Definition of Done in Scrum, which explains the criteria used to determine whether the product improvements are ready for release. This definition functions as a checklist of conditions that must be fulfilled for every task to be considered

finished within the Scrum framework. For example, declaration of an increment as complete will fulfil the “Done” condition. All members of the development team need to understand the criteria to maintain uniformity of understanding in the “Done” condition.

The sprint, as an integral component of Scrum, demonstrates to be an effective framework for facilitating collaboration within a team especially when supported by suitable guidance and a well-structured timetable. A sprint calendar is required for arranging various Scrum events including sprint planning, daily meetings, sprint reviews,

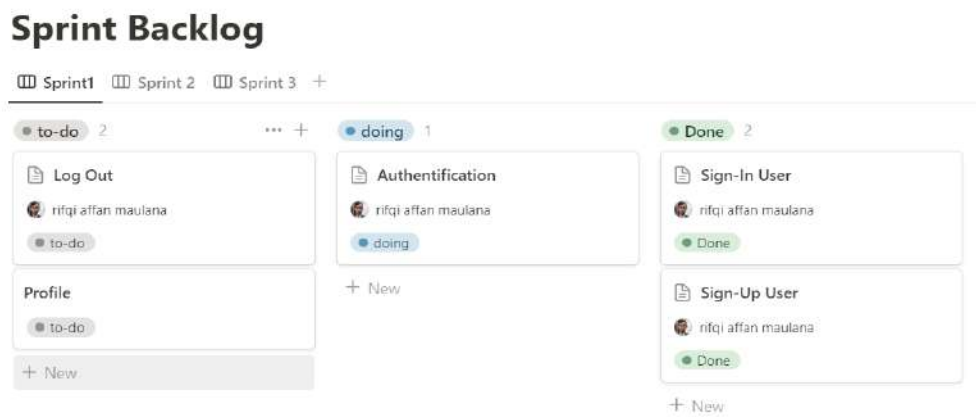


Figure 6. Product backlog on notion

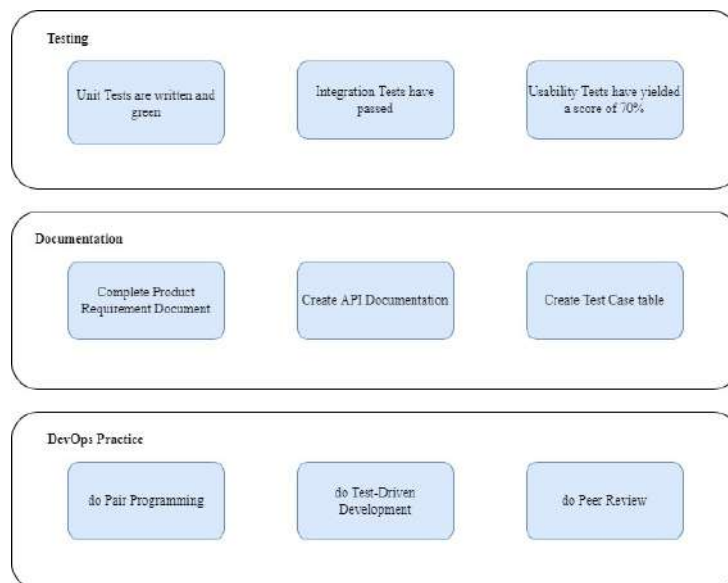


Figure 7. Definition of done (DoD)

and sprint retrospectives. The primary purpose of implementing a sprint calendar is to keep the team on track and to be used as a reminder for important Scrum activities. It also helps to prevent time waste during sprint planning and development by providing a clear and organized overview of the activities to be completed.

A sprint calendar shown in Fig. 8 illustrates the scheduling and execution of Scrum events by the team. Over numerous sprints, the development team has successfully met the timelines. As an example, on October 2, 2023, the team initiated the sprint with a sprint planning session. The following day was dedicated to routine daily scrum meetings, which were held to ensure constant communication, monitor the development progress of the application, and handle any challenges faced by the team during the development of a non-invasive blood sugar detection device using Photoplethysmography (PPG) signals. This daily interaction is crucial for keeping the entire team aligned and informed. Following this routine, on October 9, 2023, the team conducted a sprint review and a sprint retrospective. Then on October 10, 2023, the team evaluated on the finished sprint and planned improvements. Then the team continues the tasks as presented on the sprint calendar provided as shown in Fig. 8.

Sprint planning is a pivotal meeting in the Scrum framework where the team deliberates on the sprint objective, the production timetable, and tasks allocated to the team for the duration of the sprint. All Scrum team members are required to attend this crucial Scrum event. The Scrum Master's responsibility extends beyond assuring attendance; they are also accountable for ensuring that each team member comprehends their designated duties and tasks.

Fig. 9 depicts the unique duties allocated to each scrum roles particularly during the sprint planning phase. The product owner has the responsibility of showcasing the product backlog, providing detailed explanations of backlog items, responding to inquiries, resolving issues, defining acceptance criteria, and prioritizing backlog items. Scrum

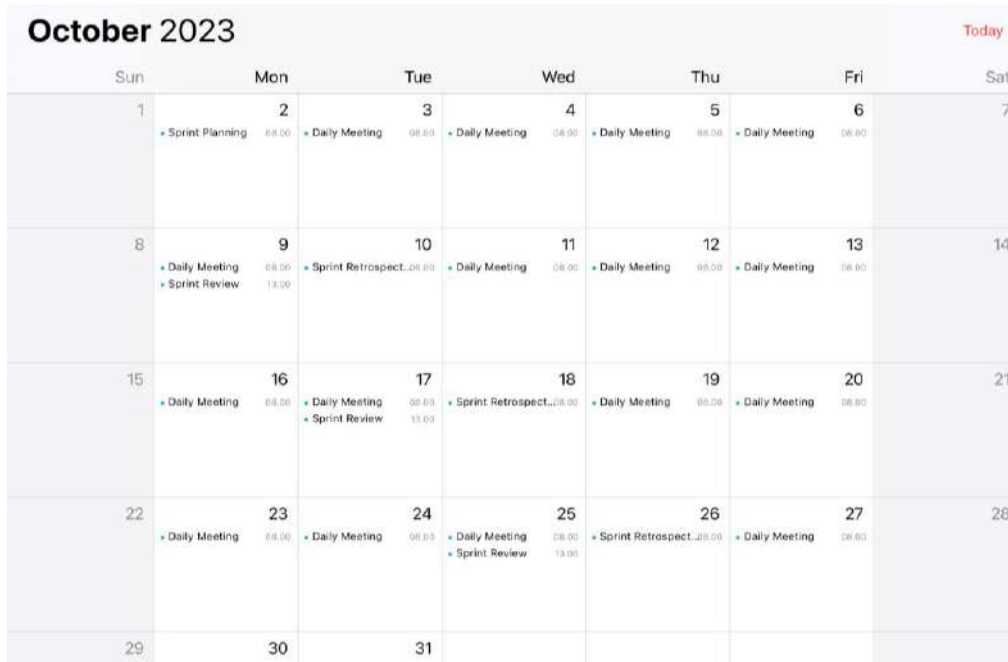


Figure 8. Sprint calendar

master include overseeing meetings, leading team discussions, resolving obstacles, managing time, and assisting the product owner. Meanwhile, the development team is tasked with evaluating the amount of work required, breaking down the items in the backlog, resolving any dependencies, choosing which items to work on during the sprint, and making a commitment to achieving the sprint goals.

The development of a non-invasive blood sugar detection device employing Photoplethysmography (PPG) signals incorporates Scrum as the software development framework, with specific Scrum roles tailored for the device's purpose. The Scrum framework encompasses several key roles, namely the product owner, scrum master, development team, and two stakeholders, as depicted in Fig. 10. Mrs. Hesti and Mrs. Arna are individuals who have a vested interest in the application. The stakeholders are



Figure 9. Sprint planning

collaborating with Erita, who is the product owner of the application. Erita will engage with the team to oversee the advancement of the development and manage the product backlog. Additionally, she represents the desires of stakeholders in relation to the product backlog. Subsequently, Izza ought to assume the role of the scrum master. Izza is responsible for overseeing the functioning of the scrum team and ensuring that the team remains free from disagreements or barriers. She is not involved in product development. The last aspect to consider is the development team. The composition of our development team consists of Rifqi, who serves as both the UI/UX designer and developer, and Rafly, who fulfills the roles of a backend engineer and DevOps engineer. They possess a high level of expertise.

The team of developers engages in a daily scrum meeting lasting 15 minutes [7]. In this study, there were two development teams consisting of Rifqi, who served as the UI/UX designer and developer, and Rafly, who fulfilled the roles of a backend engineer

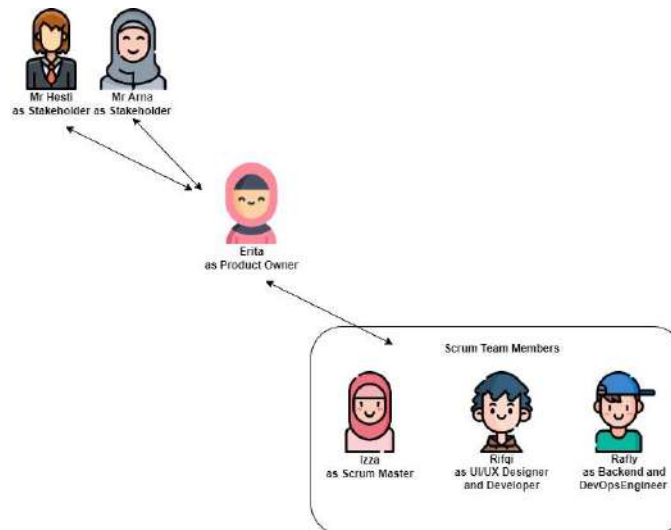


Figure 10. Scrum roles

and DevOps engineer. The four development teams provided updates on their activities from the previous day, identified any obstacles hindering their progress, and outlined their current tasks.

Fig. 11 illustrates a daily meeting that took place on December 4th, 2023. This figure serves as documentation since it presents a comprehensive breakdown of the reports discussed at the meeting. Rifqi informed that she successfully finalized the design of the registration page, and accomplished the implementation of One-Time Password (OTP) and Short Message Service (SMS) connectivity. Rafly developed a service specifically for new users and also established an Application Programming Interface (API) for new users in the "What did you work on yesterday?" report section. After seeing the report section titled "What issues are impeding progress?", the four members of the developer team did not face any difficulties during their daily meetings. The upcoming tasks for today, as mentioned in the last report titled "What are you working on today?", are as follows: Rifqi will be responsible for designing the profile page and integrating the API and SMS provider. On the other hand, Rafly will focus on creating a sign-up page view. Additionally, Rifqi will also handle the integration of the API and SMS provider. The daily scrum activities provide insights into the performance of the developer team and the achievement of the project's sprint goals. During the sprint review, the scrum team showcases their work to stakeholders and engages in discussions regarding the progress

made towards achieving the product goal [7]. If the duration of the sprint is one month, the maximum duration for the sprint review is four hours.

Fig. 12 illustrates the sprint review actions that took place during sprint 1. A Scrum team is showcasing the system design of an application that utilizes Photoplethysmography (PPG) signals to detect blood sugar levels in a non-invasive manner. Our team conducts sprint reviews remotely using the Zoom platform.

Daily Meeting 04/12/2023		
	Rifqi as UI/UX Designer and Developer	Rofly as Backend and DevOps Engineer
What did on your work yesterday?	High fidelity registration is carried out.	New user data API is done
What issues are blocking you?	i have no issues are blocking me	i have no issues are blocking me
What are you working on today?	I will create high fidelity of history's page	Integrate API and SMS Provider

Figure 11. Sample of daily meeting activity by development team

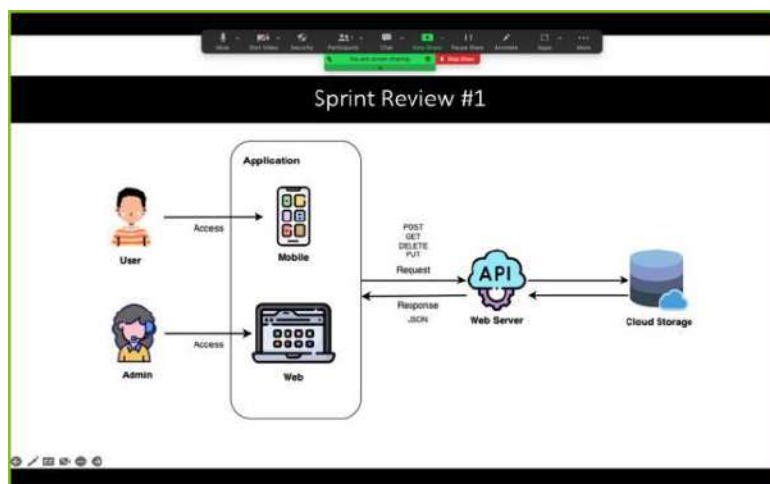


Figure 12. Development team's exemplary sprint review activity

The sprint retrospective involves analyzing the performance of a certain sprint, identifying any encountered problems, and devising solutions to address those problems [8] The objective of the sprint retrospective is to gain insights from the performance of the previous sprint and utilize that knowledge in the subsequent sprint. The length of the retrospective sprint is governed by the length of the sprint itself. For instance, if a sprint lasts for one month, the maximum duration of the retrospective sprint is three hours.

Fig. 13 illustrates the retrospective sprint employed in this investigation. Every member of the development team reviews the sprints that have been finished. Rifqi expressed a positive assessment of the successful sprint. In contrast to Rifqi, Rafly demonstrated the ability to discern between personal problems and the task at hand by providing comments.

B. Discussions

Based on the findings, there are several benefits to adopting the Scrum framework for the development of an application for non-invasive blood sugar testing device employing Photoplethysmography (PPG) signals in its current form, as indicated in Table 2.



Figure 13. Sample of Sprint Retrospective Activity by Development Team

Table 2. The benefits of implementing agile scrum methodology into the development of the application

Case	Benefit
Estimation of Tasks	The task plan is more detailed for team members during the sprint (1-2 weeks).
Product Monitoring	To effectively track the progress of product execution, we create a "to-do list"
Changes in Business Processes	It is highly adaptable to changes required to support the business side. After the final sprint, the development team receives input in the form of new sprint tasks.
Feedback from Users	The user can contribute to the product's development by testing and providing feedback. Aside from that, the requirements of the users and stakeholders must be aligned during the final sprint discussion.
Transparency in the Project	During the sprint review, each member of the development team shows off their work from the sprint. As a result, they can all learn about the product's development progress.

Comparing the benefits of adopting the Scrum framework with other project management methodologies can provide insights into why Scrum may be the preferred choice for developing a mobile application for a non-invasive blood sugar detection device using PPG signals. Let's compare Scrum with the traditional Waterfall model and the Kanban method:

Task Estimation:

Scrum: In Scrum, task estimation is done collaboratively by the team during sprint planning sessions. The tasks are broken down into smaller, manageable units, allowing for a more detailed plan within short timeframes (1-2 weeks).

Waterfall: In the Waterfall model, task estimation is typically done upfront during the planning phase. However, this estimation may be less detailed and flexible compared to Scrum, as the entire project is planned in advance.

Kanban: Kanban also allows for task estimation, but it doesn't follow strict timeboxed iterations like Scrum. Instead, tasks are pulled from a backlog as capacity allows, and estimation may vary based on workflow dynamics.

Product Monitoring:

Scrum: Scrum emphasizes transparency and accountability through sprint planning and daily stand-up meetings. Progress is tracked using a "to-do list" or a Kanban board, providing visibility into the status of tasks.

Waterfall: In the Waterfall model, product monitoring may be less dynamic, as progress is evaluated at predefined stages (e.g., requirements, design, implementation). Changes may be challenging to accommodate once the project is underway.

Kanban: Kanban provides real-time visibility into workflow status, but it may not have the structured sprint planning and review events found in Scrum.

Changes in Business Processes:

Scrum: Scrum is highly adaptable to changes, as new requirements can be accommodated in subsequent sprints. The iterative nature of Scrum allows for flexibility in responding to evolving business needs.

Waterfall: The Waterfall model is less flexible in accommodating changes once the project is underway. Changes may require significant rework and impact project timelines and budgets.

Kanban: Kanban allows for incremental improvements, but major changes may require adjustments to the workflow and may not be as structured as in Scrum.

Feedback from Users:

Scrum: Scrum encourages frequent feedback from users through sprint reviews and demos. User input is integral to the development process, ensuring that the product meets user needs.

Waterfall: User feedback may be limited until the end of the project when the final product is delivered. Changes based on user feedback may be costly and time-consuming to implement.

Kanban: Kanban allows for feedback throughout the development process but may not have dedicated events for user review and feedback like Scrum.

Transparency in the Project:

Scrum: Scrum promotes transparency through its ceremonies, such as sprint planning, daily stand-ups, and sprint reviews. This fosters open communication and collaboration within the team.

Waterfall: Transparency may vary in Waterfall, as progress is evaluated at predefined stages, and there may be less visibility into ongoing work between stages.

Kanban: Kanban provides transparency through its visual board, but it may not have the structured events for team collaboration found in Scrum.

Overall, while each methodology has its strengths, the iterative and collaborative nature of Scrum, along with its emphasis on adaptability and user feedback, may make it more suitable for the dynamic and evolving nature of software development projects, such as creating a mobile application for a non-invasive blood sugar detection device.

Table 2 reveals that implementing agile scrum as a product management approach in this study offers five advantages for handling the software development life cycle with greater efficiency and effectiveness. These benefits include detailed task estimation, user involvement in product development through feedback and reviews, and increased transparency within the development team, which can help minimize miscommunication. In addition, Scrum's timeline and sprint planning facilitate the monitoring of productivity in software development, enabling accurate determination of time costs.

In addition, the developers use daily meeting to share information about their work, ensuring that all team members are informed about the progress of developing the mobile application for the non-invasive blood sugar detection device using Photoplethysmography (PPG) signals. Following the sprint, a sprint retrospective is conducted to assess the performance of individual developers and determine the results of the ongoing product development.

The agile scrum approach can be implemented in the creation of mobile application for the non-invasive blood sugar detection device using Photoplethysmography (PPG) signals. This choice was made based on adherence to the Scrum values, execution of the Scrum events in real-life scenarios, and formation of the team according to the Scrum instructions. The degree of execution of all of the prescribed actions outlined in the guide as a measure of the effective deployment of the Agile Scrum

methodology in the development of software applications. By utilizing thoroughly documented Scrum, we can streamline progress tracking, assume a guiding role in system development, provide a historical record, and evaluate the adoption of Scrum throughout the development process.

C. Application Implementations

The following are the results of the application implementation from login to application results. Fig. 14 is one of the results of the application implementation, namely the results of the user application

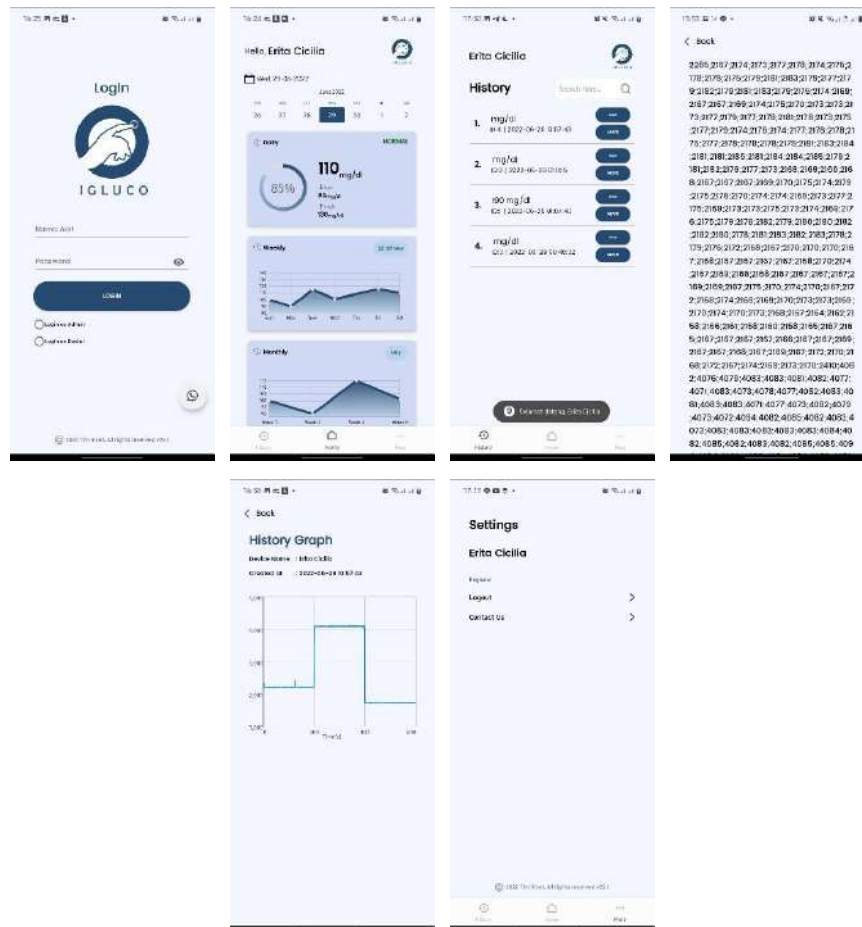


Figure 14. The result of the user application

4 Conclusions

In conclusion, the integration of Scrum methodology in the manufacture of non-invasive blood sugar detection devices utilizing PPG signals has yielded significant benefits within the confined three-month timeframe. The iterative and collaborative nature of Scrum allowed our cross-functional team, comprised of the Product Owner, Scrum Master, and Developer Team, to navigate the intricacies of PPG signal processing, hardware integration, and software development with agility. The sprint cycles facilitated quick adaptations, enabling the team to stay responsive to emerging challenges and stakeholder feedback. This dynamic approach not only ensured the timely delivery of a sophisticated medical device but also fostered a culture of continuous improvement, setting a precedent for future endeavors in the realm of healthcare technology.

Looking forward, the successful implementation of Scrum underscores its efficacy in managing the complexities inherent in medical device development. The balance between flexibility and structure afforded by Scrum proved instrumental in not only meeting technological benchmarks but also aligning the final product with the practical needs of healthcare professionals and end-users. The lessons learned from this experience not only contribute to the advancement of non-invasive blood sugar detection devices but also serve as a testament to the adaptability and efficiency that agile methodologies, particularly Scrum, bring to the forefront of innovative medical technology development.

References

- [1] A. I. Stoumpos, F. Kitsios, and M. A. Talias, "Digital Transformation in Healthcare: Technology Acceptance and Its Applications," *Int J Environ Res Public Health*, vol. 20, no. 4, p. 3407, Feb. 2023, doi: 10.3390/ijerph20043407.
- [2] S. Flessa and C. Huebner, "Innovations in Health Care—A Conceptual Framework," *Int J Environ Res Public Health*, vol. 18, no. 19, p. 10026, Sep. 2021, doi: 10.3390/ijerph181910026.
- [3] M. Ghamari, "A review on wearable photoplethysmography sensors and their potential future applications in health care," *Int J Biosens Bioelectron*, vol. 4, no. 4, 2018, doi: 10.15406/ijbsbe.2018.04.00125.

-
- [4] S. Alsaqqa, S. Sawalha, and H. Abdel-Nabi, “Agile Software Development: Methodologies and Trends,” *International Journal of Interactive Mobile Technologies (iJIM)*, vol. 14, no. 11, p. 246, Jul. 2020, doi: 10.3991/ijim.v14i11.13269.
- [5] “The Scrum framework, illustrated. Scrum.org. (n.d.). .”
- [6] N. W. Hidayah, R. R. Sasmita, M. K. Mayangsari, O. G. W. Kusuma, H. Rante, and A. Fariza, “Invitin Project: Scrum Framework Implementation in a Software Development Project Management,” *INTEK: Jurnal Penelitian*, vol. 9, no. 1, p. 58, Apr. 2022, doi: 10.31963/intek.v9i1.3332.
- [7] “The Scrum Guide,” in *Software in 30 Days*, Wiley, 2012, pp. 133–152. doi: 10.1002/9781119203278.app2.
- [8] R. A. S and M. Shalahuddin, *Rekayasa Perangkat Lunak Terstruktur dan Berorientasi Objek*. 2015.
- [9] F. Hayat, A. U. Rehman, K. S. Arif, K. Wahab, and M. Abbas, “The Influence of Agile Methodology (Scrum) on Software Project Management,” in *2019 20th IEEE/ACIS International Conference on Software Engineering, Artificial Intelligence, Networking and Parallel/Distributed Computing (SNPD)*, IEEE, Jul. 2019, pp. 145–149. doi: 10.1109/SNPD.2019.8935813.
- [10] H. Hutrianto and A. Putra, “Implementasi Scrum Model Dalam Pengembagnan Aplikasi Pelaporan Sampah Sebagai Wujud Smart Cleaning,” *JUPI (Jurnal Ilmiah Penelitian dan Pembelajaran Informatika)*, vol. 5, no. 1, p. 9, Jun. 2020, doi: 10.29100/jipi.v5i1.1552.
- [11] N. Ramadan and S. Megahed, “Requirements Engineering in Scrum Framework,” *Int J Comput Appl*, vol. 149, no. 8, pp. 24–29, Sep. 2016, doi: 10.5120/ijca2016911530.
- [12] K. S. Rubin, *Essential Scrum*. Pearson Publisher, 2012.
- [13] J. E. C. Skubik-Peplaski, S. Shisley, and W. Cook, “Agile Learning and Teaching with Miro Boards,” *Proc. 2021 Pedagog. Agil. Teach. Learn. Approaches Appl*, pp. 1–6, 2022.

This page intentionally left blank

Characteristics of Straight Trapezoidal Cross-Sectional Fins under Unsteady Conditions

Michael Seen^{1*}, Doddy Purwadianto¹, Gilang Argya Dyaksa¹,
Heryoga Winarbawa¹, Rines¹, Stefan Mardikus¹, Wibowo
Kusbandono¹, YB. Lukiyanto¹

¹*Department of Mechanical Engineering, Faculty of Science and
Technology, Sanata Dharma University,
Yogyakarta, Indonesia*

**Corresponding Author: michaelseen@dosen.usd.ac.id*

(Received 15-01-2024; Revised 07-03-2024; Accepted 30-04-2024)

Abstract

The aim of this research is to understand the characteristics of fins with a trapezoidal cross-section. The shape of the fin's cross-section is one of the influential factors affecting fin characteristics. In the design of fins, it is crucial to comprehend the characteristics of the fin as they relate to temperature distribution, heat transfer rate, and the efficiency of the fin. The research was conducted using numerical computation with an explicit finite difference method. Variations were made in the length of side 3 of the trapezium to 0 m, 0.02 m, and 0.04 m. The research results indicate that increasing the width of the fin enhances the temperature distribution, flow rate, and efficiency achievable by the fin. Significant improvement occurred when varying the side length from 0 m to 0.02 m, whereas subsequent variations did not considerably alter the efficiency. The highest efficiency achieved was 0.90 when the length of side 3 was 4 cm at the 300 seconds.

Keywords: Fin characteristics, finite difference method, unsteady state

1 Introduction

A working machine generates heat. If this generated heat is not dissipated, it can decrease the performance of the machine and even cause damage [1]. One way to reduce heat in a machine is by using fins. Fins serve to increase the rate of heat transfer from an object to the surrounding fluid. The heat transfer rate in fins is influenced by several

factors such as the temperature difference between the fin surface and the fluid, the material of the fin, the geometry, and the cross-sectional area of the fin.[2–4]

In unsteady-state conditions, the temperature distribution in fins is influenced by the density (ρ), specific heat capacity (c), thermal conductivity (k), and thermal diffusivity (α) of the material composing the fin. Meanwhile, in steady-state conditions, only thermal conductivity significantly affects the temperature distribution. The convective heat transfer coefficient (h) is influenced by the properties of the fluid around the fin, fluid flow velocity, as well as the surface temperature of the fin and the temperature of the flowing fluid around it [5]. Moreover, higher fluid flow velocities result in larger values of the convective heat transfer coefficient (h). Temperature differences also play a role in determining these fluid properties. [6–9]

In its application, various forms of fins are utilized, and numerous studies on fins have been conducted employing different shapes such as capsule, cylinder, square, and triangle. Each fin shape possesses its distinct characteristics. The variation in fin geometry affects the fin's cross-sectional area, influencing temperature distribution and the rate of heat transfer from the fin [10–13]. In this study, temperature distribution calculations were obtained through numerical simulations using the explicit finite difference method. Understanding the temperature distribution and heat flow rate allows the efficiency of the fin to be computed. Efficiency, as one of the characteristics of a fin, is crucial to determine when designing a fin. Fin efficiency is the ratio between the actual heat released by the fin and the heat released if the entire fin surface had the same temperature as the fin base. This research aims to understand the characteristics of a trapezoidal cross-sectional fin under unsteady conditions, including (a) temperature distribution, (b) the rate of heat flow that the fin can release, and (c) fin efficiency.

2 Material and Methods

This research was conducted using computational methods employing an explicit finite difference approach. The fin was divided into 21 small elements known as control volumes. Each control volume has an equal distance of Δx , except for the control volumes located at the base and tip of the fin, which have a distance of $0.5\Delta x$. The fin has a trapezoidal cross-section with a varied length of side 3, as shown in Fig. 1.

The fin material is iron with a density of $\rho = 7870 \text{ kg/m}^3$, thermal conductivity $k = 80.2 \text{ W/m}^\circ\text{C}$, and specific heat capacity $c = 447 \text{ J/kg}^\circ\text{C}$. Iron is one of the natural materials widely used in alloys, for example in steel. Despite having lower strength compared to steel, iron has higher conductivity. The fin has an overall length of 0.05 m, a height of 0.02 m, and a distance between control volumes $\Delta x = 0.0025 \text{ m}$. Side lengths 1 and 2 are 0.025 m and 0.015 m, respectively, while side length 3 is varied as 0 m, 0.02 m, and 0.04 m. The base temperature of the fin is considered constant at $T_b = 100^\circ\text{C}$, and the surrounding fluid temperature is $T_f = 30^\circ\text{C}$. The convective heat transfer coefficient is assumed constant at $h = 50 \text{ W/m}^2\text{C}$.

The temperature distribution in each control volume is calculated using numerical equations derived from the principle of energy balance. There are three equations used to calculate the temperature distribution in the control volumes: at the base of the fin, between the base and the tip of the fin, and at the tip of the fin.

The temperature at the base control volume of the fin is maintained at T_b and remains unchanged over time, which can be expressed by equation (1).

$$T_i^{n+1} = T_1^{n+1} = T(0, t) = T_b \tag{1}$$

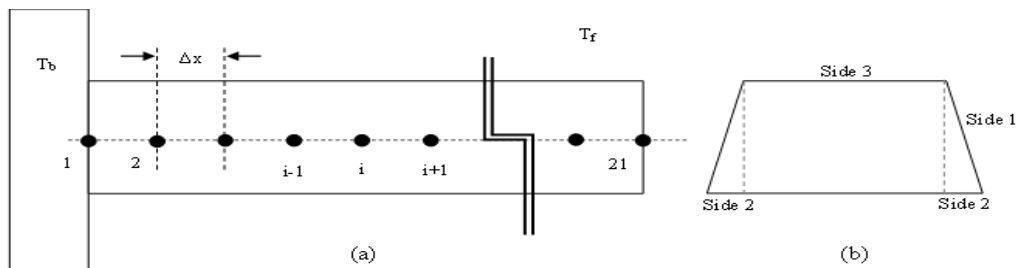


Figure 1. Straight fin with a trapezoidal cross-section, (a) side view, (b) front view

The temperature in the control volume between the base and the tip of the fin can be determined using equation (2). The temperature in the control volume at the tip of the fin is expressed by equation (3).

$$T_i = \frac{k \times \Delta x}{\rho \times c \times \Delta x^2} (T_{i-1}^n - T_i^n + T_{i+1}^n - T_i^n) + \left(\frac{h \times \Delta x}{k} \times \frac{A_{s,i}}{A_p} \times (T_f - T_i^n) + T_i^n \right) \tag{2}$$

$$T_i^{n+1} = \frac{k \times \Delta t}{0,5 \times \rho \times c \times \Delta x^2} \left((T_{i-1}^n - T_i) + \left(\frac{h \times \Delta x}{k} (T_f - T_i^n) \right) + \left(\frac{h \times \Delta x}{k} \times \frac{A_{s,i}}{A_p} (T_f - T_i^n) \right) \right) + T_i^n \quad (3)$$

In unsteady-state conditions, the actual heat transfer rate ($q_{fin,actual}$), the maximum heat transfer rate ($q_{fin,ideal}$), and the heat transfer rate without fins (q_{nofin}) can be calculated successively using equations (4), (5), and (6).

$$q_{fin,actual}^{n+1} = h \sum_{i=1}^m A_s (T_i^{n+1} - T_f) \quad (4)$$

$$q_{fin,ideal}^{n+1} = h A_s (T_b - T_f) \quad (5)$$

$$q_{nofin}^{n+1} = h A_b (T_b - T_f) \quad (6)$$

The efficiency of the fin, which is the ratio between the actual heat released by the fin and the maximum heat that the fin can release, is calculated using equation (7).

$$\eta^{n+1} = \frac{q_{fin,actual}^{n+1}}{q_{fin,ideal}^{n+1}} \quad (7)$$

In equations (1)-(7):

T_i^{n+1} : The temperature at the i position, in the $n+1$ iteration ($^{\circ}\text{C}$)

T_i^n : The temperature at the i position, in the n iteration ($^{\circ}\text{C}$)

T_{i-1}^n : The temperature at the $i-1$ position, in the n iteration ($^{\circ}\text{C}$)

T_{i+1}^n : The temperature at the $i+1$ position, in the n iteration ($^{\circ}\text{C}$)

T_f : Fluid temperature around the fin ($^{\circ}\text{C}$)

Δt : Time step, from the n to the $n+1$ iteration (s)

Δx : Distance between control volumes (m)

$A_{s,i}$: Area of the surface of the control volume at the i position touching the fluids around the fin (m^2)

A_p : Area of the cross section of the fin (m^2)

ρ : The density of the fin material (kg/m^3)

c : Specific heat of the fin material ($\text{J}/\text{kg}^{\circ}\text{C}$)

k : Thermal conductivity ($\text{W}/\text{m}^{\circ}\text{C}$)

h : Convection heat transfer coefficient ($\text{W}/\text{m}^2\text{°C}$)

3 Results and Discussions

The results of temperature distribution, heat transfer rate, and fin efficiency can be observed in Fig. 2. In unsteady-state conditions, the temperature distribution continues to change over time. In this study, because T_b is maintained at a constant temperature of 100°C , higher than the surrounding fluid, the temperature at each control volume will continue to increase until reaching a steady state throughout the control volumes. In Fig. 2, the temperature distribution is examined at the 300 seconds by comparing the temperature of each control volume for various fin cross-sectional width variations or lengths of side 3. Heat transfer rates and efficiency are evaluated at each time unit for various fin cross-sectional width variations.

In Fig. 2(a), it is evident that increasing the length of side 3 of the trapezium enhances the temperature distribution within the fin. Heat from the base of the fin is transferred more rapidly and extensively towards the fin's end, specifically at control volume 21. The difference in temperature distribution between variations of side 3 at 2 cm and 4 cm is smaller compared to having a length of 0 cm or no side 3. At the 300 seconds, nearing a steady state, the temperature at the end of the fin for the 4 cm variation reaches 89.3°C , the 2 cm variation reaches 88.2°C , and the 0 cm variation reaches 84.5°C . Fig. 2(b) demonstrates that over time, the heat transfer rate increases until reaching a certain point before leveling off. The heat transfer rate is proportional to the rise in temperature at each control volume. The substantial difference between the fin's temperature and the surrounding fluid amplifies the heat transfer rate. The 4 cm variation exhibits the highest heat transfer rate at 300 seconds, measuring 28.6 W, followed by the 2 cm variation at 20.9 W, and finally, the 0 cm variation at 12.9 W. Fig. 3, displays the efficiency of the three fin variations. The fin efficiency increases proportionally with the larger temperature difference between the fin's control volume and the surrounding fluid.

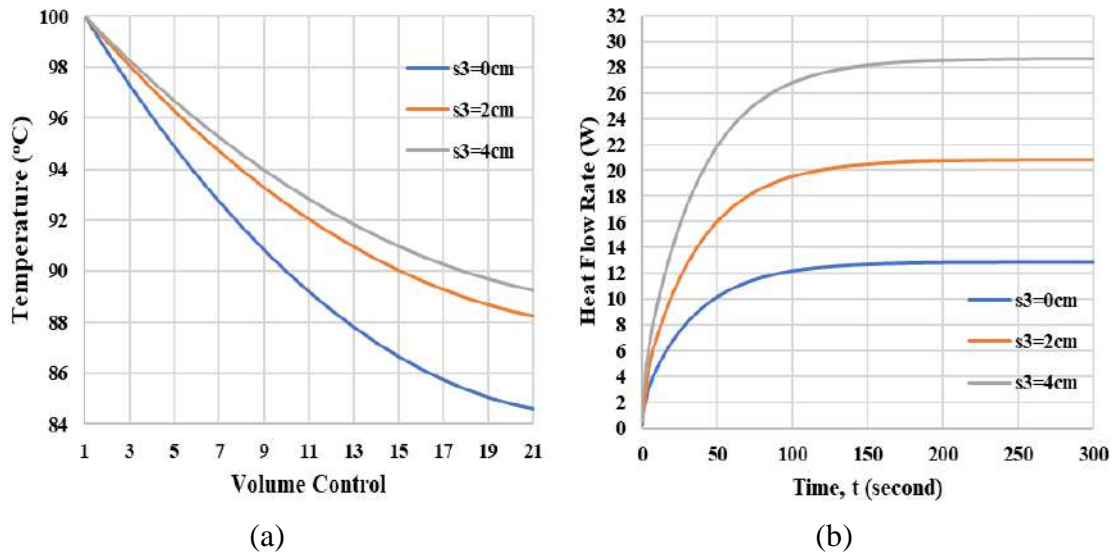


Figure 2. (a) Temperature distribution, $t = 300$ seconds, (b) Heat transfer rate

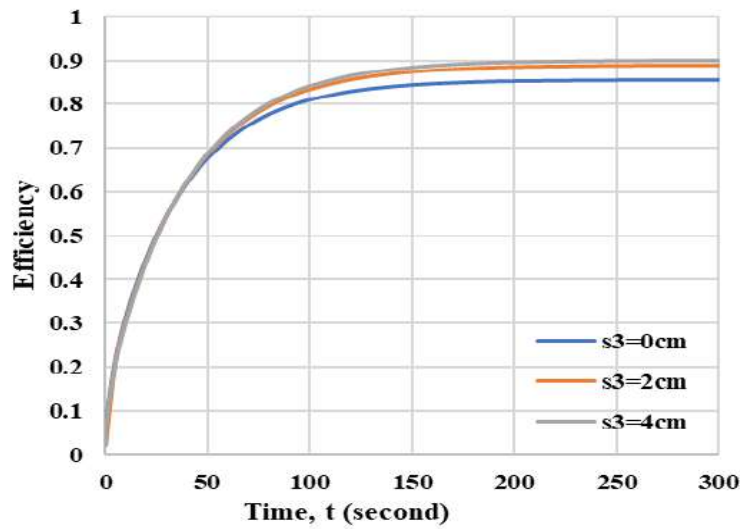


Figure 3. Fin efficiency

The 4 cm and 2 cm variations have closely similar efficiency graphs, indicating that increasing the length of side 3 beyond 2 cm doesn't yield a significant improvement in efficiency compared to having no side 3, or the 0 cm variation. The highest efficiency achievable by the trapezoidal fin with a 4 cm side 3 is 0.90, which is not significantly different from the 2 cm variation, reaching a maximum efficiency of 0.89, while the 0 cm variation or without side 3 attains a maximum efficiency of 0.85.

4 Conclusions

From the research findings, it can be concluded that the width variation in trapezoidal-shaped fins influences the fin's characteristics. Increasing the fin width enhances the temperature distribution, heat transfer rate, and efficiency achievable by the fin. Significant improvements occur when transitioning from a side length variation of 0 cm to 2 cm, while subsequent variations show little change in efficiency. The highest achievable efficiency is 0.90 at a side length variation of 4 cm at the 300 seconds.

Acknowledgements

This research was conducted at Sanata Dharma University. The authors thank Sanata Dharma University for supporting this research.

References

- [1] F. Lumbanbatu, "Analisis pipa-pipa radiator yang memakai pendingin air beralih ke coolant pada mobil Toyota Avanza," *Focus Teknik Mesin UPMI*, vol. 1, no. 1, pp. 12-20, 2020.
- [2] K. Ginting, P.K. Purwadi, and S. Mungkasi, "Efficiency and effectiveness of a fin having capsule-shaped cross section dependent on the one-dimensional position," Proceedings of the 1st International Conference on Science and Technology for an Internet of Things, 20 October 2018, Yogyakarta, Indonesia.
- [3] P. K. Purwadi and M. Seen, "Efficiency and effectiveness of a fin having the capsule-shaped cross section in the unsteady state," *AIP Conference Proceedings*, vol. 2202, art. 020092, 2019.
- [4] P. K. Purwadi, B. Setyahandana, and R. B. P. Harsilo, "Obtaining the efficiency and effectiveness of fin in unsteady state conditions using explicit finite difference method," *International Journal of Applied Sciences and Smart Technologies*, vol. 3, no. 1, pp. 111-124, 2021.
- [5] P. S. Prabowo and S. Mardikus, "Heat Transfer Characteristic on Wing Pairs Vortex Generator using 3D Simulation of Computational Fluid Dynamic,"

- International Journal of Applied Sciences and Smart Technologies*, vol. 3, no. 2, pp. 215-224, 2021.
- [6] P. K. Purwadi and B. Y. Pratama, "Efficiency and effectiveness of a truncated cone-shaped fin consisting of two different materials in the steady-state," *AIP Conference Proceedings*, vol.2202, art. 020091, 2019.
- [7] T. D. Nugroho and P. K. Purwadi, "Fins effectiveness and efficiency with position function of rhombus sectional area in unsteady condition," *AIP Conference Proceedings*, vol. 1788, art. 030034,2017.
- [8] P. K. Purwadi and M. Seen, "The efficiency and effectiveness of fins made from two different materials in unsteady-state," *Journal of Physics: Conference Series*, vol. 1511, no. 1, 2020.
- [9] P. K. Purwadi, B. Setyahandana, and M. Seen, "Efficiency and effectiveness of a fin having the ellipse cross section in the unsteady state condition", *AIP Conference Proceedings*, vol.2364, art. 030001, 2021.
- [10] A. W. Vidjabhakti, P. K. Purwadi, and S. Mungkasi, "Efficiency and Effectiveness of a Fin Having Pentagonal Cross Section Dependent on the One-Dimensional Position," Proceedings of the 1st International Conference on Science and Technology for an Internet of Things, 20 October 2018, Yogyakarta, Indonesia.
- [11] P.K. Purwadi, Y. Angga, and S. Mungkasi, "Efficiency and Effectiveness of a Rotation-Shaped Fin Having the Cross-Section Area Dependent on the One-Dimensional Position," Proceedings of the 2nd International Conference of Science and Technology for the Internet of Things, ICSTI 2019, September 3rd 2019, Yogyakarta, Indonesia.
- [12] P. K. Purwadi, "Mekanika Efisiensi Sirip Berbentuk Silinder," *Mekanika: Majalah Ilmiah Mekanika*, vol. 9, no. 1, pp. 231-237, 2010.
- [13] P. K. Purwadi, "Efisiensi dan Efektivitas Sirip Longitudinal dengan Profil Siku Empat Keadaan Tak Tunak Kasus 2D," Seminar Nasional Aplikasi Sains dan Teknologi, IST Akprind, Yogyakarta, 2008.

Clustering and Trend Analysis of Priority Commodities in The Archipelago Capital Region (IKN) Using A Data Mining Approach

Pandu Pangestu¹, Syamsul Maarip¹, Yuldan Nur Addinsyah¹,
Vega Purwayoga^{1*},

¹*Department of Informatics, Faculty of Engineering, Siliwangi University,
Tasikmalaya, West Java, Indonesia*

**Corresponding Author: vega.purwayoga@unsil.ac.id*

(Received 20-12-2023; Revised 19-05-2024; Accepted 21-05-2024)

Abstract

The process of moving the capital requires careful preparation. One thing that needs to be considered is food security in IKN. This research provides recommendations for the main food commodities in IKN by applying data mining. We collect food productivity data available on the official website for East Kalimantan province. These data are processed and grouped into two groups, namely horticulture and livestock products using the K-Means method. After grouping, we predict the increase in productivity of each group using the ARIMA method. This research produces output in the form of grouping commodities into horticulture and livestock products. Productivity results for each type of commodity are displayed from 2016 to 2020 based on data on the official East Kalimantan Province website. Based on this data, predictions are made using the ARIMA method to predict productivity results from 2021 to 2025. Commodities with total productivity are grouped into high-priority commodities. Grouping the amount of productivity is carried out using the clustering method by comparing the amount of productivity for each commodity and producing commodities that are low priority, middle priority, priority and top priority based on the highest to lowest productivity numbers. The cluster quality for grouping horticultural commodities is 99.1%, while the cluster quality for grouping livestock commodities is 87.5%. Hasil prediksi terbaik yaitu ketika memprediksi produksi salak dan slaughter cattle dengan model ARIMA (0, 1, 0) dan ARIMA (2, 2, 2).

Keywords: ARIMA, Clustering, Holticultural Commodities, K-Means, Livestock Commodities

1 Introduction

Food security is a key issue in fulfilling community welfare because it will determine economic, social and political stability in a country [1]. Food security is a challenge for Indonesia considering that Indonesia is an archipelagic and agricultural



country. Food security must include factors of availability, distribution and consumption. One way of sustainable development is paying attention to aspects of food security [2]-[3]. Indonesia, as the fourth largest country in the world and a country with a tropical season, certainly has the advantage of diversity in agricultural and livestock products. On the other hand, this can also be a challenge because the limited availability of agricultural and livestock products must be able to meet the increasing needs of society [4].

The migration process and especially the relocation of the capital from Jakarta to East Kalimantan can affect the food needs of the affected areas [5]. There are many factors that will change a region's food needs. Land that was previously agricultural land was replaced with factories or buildings [6]. This transfer of agricultural land can reduce the productivity of agricultural products. Because agricultural output decreases, people's food needs will change. Therefore, food management is needed to regulate agricultural and livestock products so that they are sufficient for the community, especially the new capital area. If it is not managed well, the worst impact will be a food crisis. The food crisis occurs because food commodities are not managed well [7]. Several studies related to grouping priority commodities have been carried out by several researchers. The research [8] has grouped plantation crops using K-Means which has produced several regional groups according to their productivity levels. Other research was conducted by [4] using K-Means to identify commodities with high to low production. According to [9] research, the performance of K-Means for grouping agricultural commodities produces good cluster quality.

Several studies assess that K-Means has good performance, especially in grouping priority commodities in a region. K-Means can be used to group data, but K-Means is not an algorithm that can predict the productivity of a commodity. With the current development of data technology, prediction systems have become very important to prevent problems that will occur in the future, such as food crises. The prediction system can be used as the right solution to overcome the food crisis problem [10]. The results of the predictions can be used as a recommendation for selecting which commodities are considered important [11]. One prediction algorithm with good performance is Autoregressive Integrated Moving Average (ARIMA). The ARIMA algorithm is suitable for determining patterns and trends in data over a certain period of time [12]. This research

not only carries out groupings as in previous research, but also carries out a prediction process using ARIMA to determine the need for livestock commodities and horticultural commodities in the future.

2 Research Methods

Study Area and Research Data

The study area in this research is data on livestock commodities and horticultural commodities in East Kalimantan [9]. East Kalimantan is a province that is planned to become (IKN), thus allowing the need for livestock and horticultural commodities to increase [13]. The data obtained contains horticultural and livestock production data from 2016 to 2020. This research has several stages which are presented in Fig. 1.

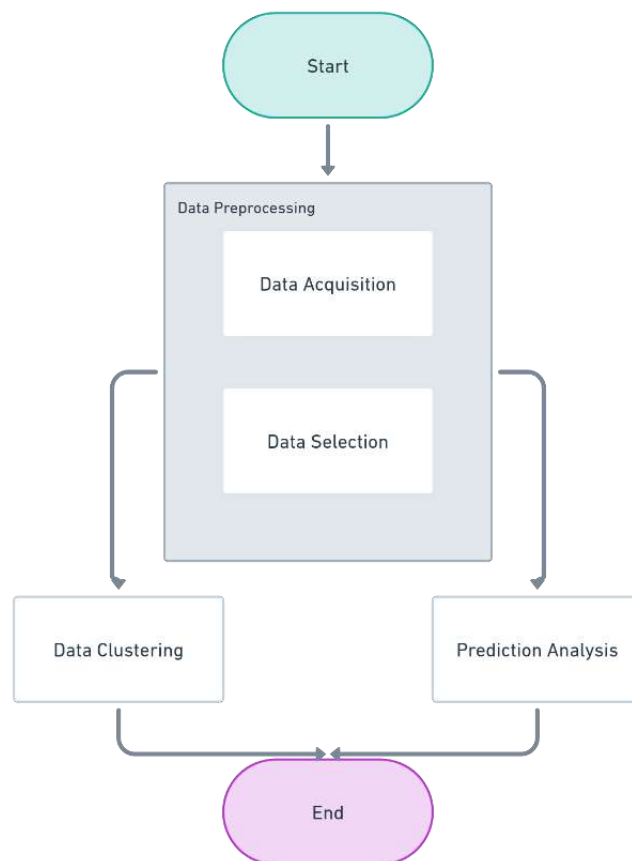


Figure 1. Research Stages

Data Preprocessing

Data preprocessing is carried out in the data analysis process to improve the quality of the data set [14]. Good data analysis results influence the quality of the data [15]. Data preprocessing is one of the main processes in data analysis so it needs to be done. Data preprocessing in this research, namely data collection and data selection [16].

Clustering of Priority Commodities for IKN Regions

Clustering is the process of grouping data to find out whether data belongs to a certain group based on the closeness of the value of an object to other objects [17][18]. This research uses the K-Means algorithm to clusterize priority commodities in the IKN area. K-Means is a popular clustering algorithm which performs well for grouping data [19]. K-Means uses Euclidean distance to measure the closeness of values between objects. The Euclidean distance method has been presented in formula 1.

$$dist(i, j) = \sqrt{(x_{i1} - x_{j1})^2 + \dots + (x_{in} - x_{jn})^2} \quad (1)$$

Where, x = object, $i = (x_{i1}, x_{i2}, \dots, x_{in})$, $j = (x_{j1}, x_{j2}, \dots, x_{jn})$ is two-dimensional object data.

Trend Analysis of Priority Commodity Predictions for IKN Regions

The prediction process is carried out using ARIMA. ARIMA is an algorithm that is reliable in predicting time series data in short periods of time [20]. The prediction process is carried out by utilizing past data to calculate values that will occur in the future.

3 Results and Discussions

Data Preprocessing

In data preprocessing, what is carried out is the data acquisition process obtained from data.kaltimprov.go.id. After the data acquisition process, the data obtained is selected based on the attributes of livestock commodities, horticultural commodities and the amount of production each year. The selected data will be analyzed using clustering

methods and trend analysis. This research uses the R programming language. The results of acquisition and pre-processing of livestock and horticultural commodities data are presented in Table 1 and Table 2.

Table 1. Livestock data preprocessing results

Number	Livestock Commodities	Production Amount (Tons)
1	Slaughter Cattle	7310
2	Dairy Cattle	140,76
3	Goat	520,38
4	Sheep	0,15
5	Pig	1835,96
...
14	Duck Egg Manila	237,82
15	Manila Duck	28,59
16	Quail Egg	68,47
17	Quail	6,65
18	Pigeons	1,38

Table 2. Horticultural data preprocessing results

Number	Horticultural Commodities	Production Amount (Tons)
1	Mango	4310
2	Orange	12692
3	Papaya	15113
4	Banana	95149
5	Pineapple	21948
...
22	Onion	267
23	Chili	9079
24	Mustard	7694
25	Spring onion	319
26	Cauliflower	207

Clustering of Priority Commodities for IKN Regions

The clustering process is carried out using the K-Means algorithm with the help of the cluster library in R programming language [21]. Before the clustering process is carried out, the data is converted into a standard scale using StandardScaler [22]. The use of StandardScaler aims to increase grouping accuracy. The clustering and categorization of livestock commodities can be seen in Table 3. Meanwhile, the clustering and categorization of horticultural commodities can be seen in Table 4. Quality testing of grouping results was carried out using the total within-cluster sum of square measures method. The cluster quality for grouping horticultural commodities is 99.1%, while the cluster quality for grouping livestock commodities is 87.5%.

Based on cluster quality calculations, the clustering results for livestock commodity data are classified as good. Table 3 shows that the data is grouped into 4 clusters. Cluster 0 consists of eleven commodities, cluster 1 consists of one commodity, cluster 2 consists of three commodities, and cluster 3 also consists of three commodities. Based on the average commodity value of each cluster, cluster members are converted into 4 categories, namely low priority, middle priority, priority, and top priority. A visualization of the livestock commodities category is presented in Fig. 2.

Table 3. Result Clustering Livestock Commodities

Cluster	Livestock Commodities	Category
0	Dairy cattle, Goat, Sheep, Buffalo, Horse, Duck, Duck egg manila, Manila duck, Quail egg, Quail, Pigeons	Low priority
1	Broiler	Top priority
2	Slaughter cattle, Rabbit, Laying hans	Middle priority
3	Pig, Organic chicken, Duck egg	Priority

Based on Fig. 2, many commodities are included in the low priority category. Low priority means that the amount of production in that category is still low. The cluster quality results for horticultural commodities show good results, namely 87.5%, but are lower than the cluster results for livestock commodities. Cluster results for horticultural commodities can be seen in Table 4.

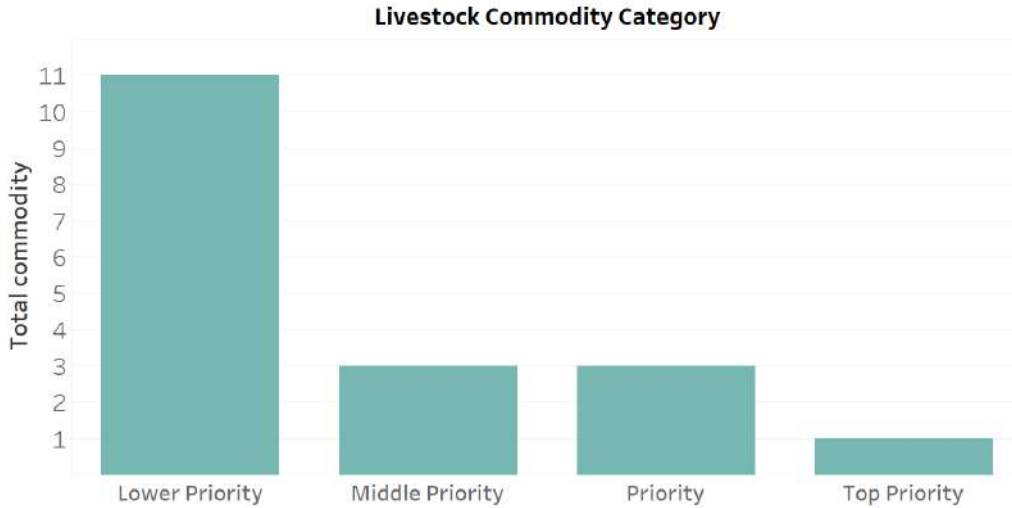


Figure 2. Distribution of livestock data categorization results

Table 4. Result Clustering Horticultural Commodities

Cluster	Horticultural Commodities	Category
0	Mango, Mangosteen, Melon, Avocado, Starfruit, Guava, Rose Apple, Sapodillah, Soursop, Passion fruit, breadfruit, Melinjo, Onion, Spring onion, Cauliflower	Low priority
1	Banana	Top priority
2	Pineapple, Sneakfruit	Priority
3	Orange, Papaya, Durian, Duku, Jackfruit, Rambutan, Chili, Mustard	Middle riority

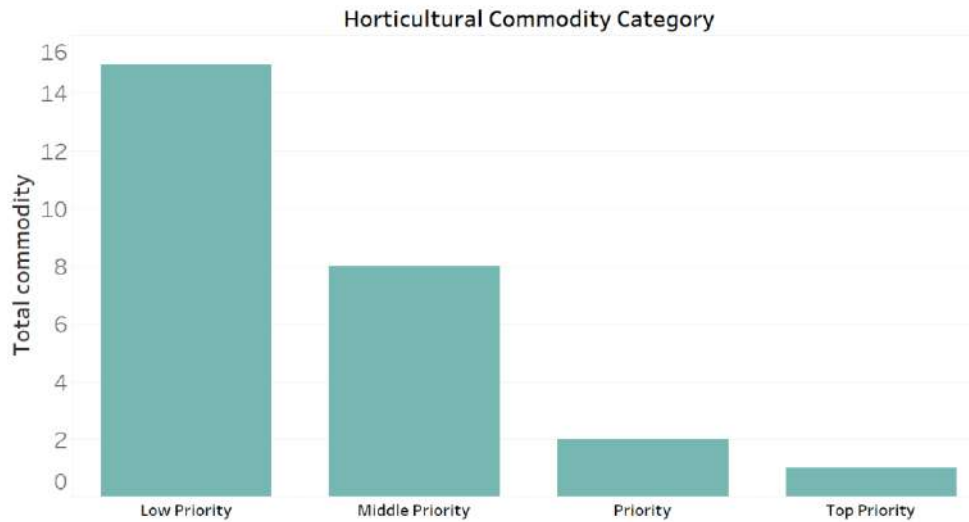


Figure 3. Distribution of horticultural data categorization results

As presented in Table 4, cluster 0 consists of fifteen commodities, cluster 1 consists of one commodity, cluster 2 consists of two commodities, and cluster 3 consists of eight commodities. A visualization of commodities in a category is presented in Figure 3. Based on Fig. 3, the number of commodities classified as low priority dominates compared to other categories. In top priority there is only one commodity, namely bananas. This shows that only bananas have very high productivity.

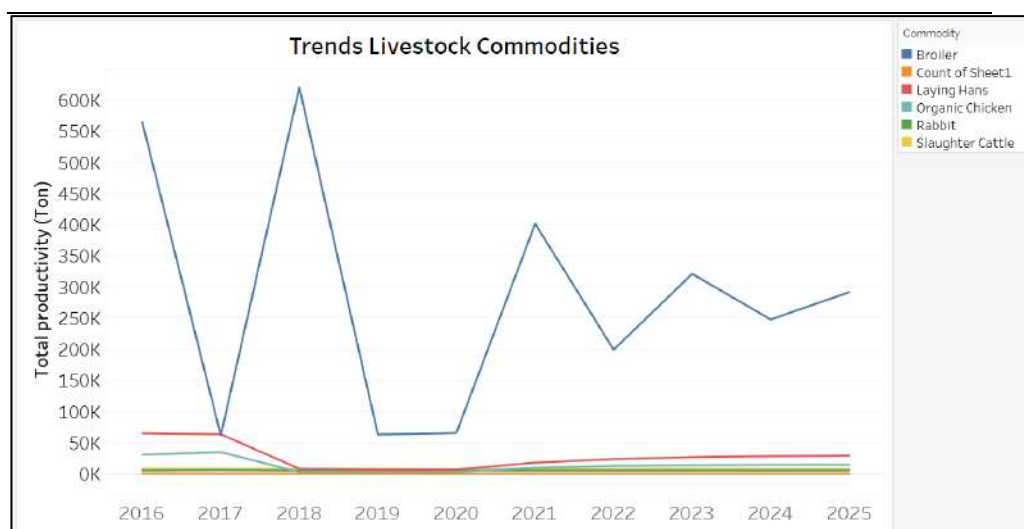
Trend Analysis of Priority Commodity Predictions for IKN Regions

The ARIMA method is applied to livestock and horticultural data using the `tseries` and `forecast` library. The steps involve training a model using historical data to make data predictions for subsequent years. The prediction results for livestock and horticultural commodities using them are presented in Tables 5 and 6. Predicted trends in production quantities for each commodity are presented in Fig. 4 and Fig. 5.

A visualization of livestock commodity trends can be seen in Fig. 4. The data used to make predictions is from 2016 to 2020. Prediction accuracy assessment is carried out by looking at the Mean Absolute Percentage Error (MAPE) value. The best MAPE is produced when predicting Slaughter Cattle production, namely 21% with the ARIMA model (0, 1, 0).

Table 5. Result Clustering Livestock Commodities

Number	Livestock Commodities	Total production in 2016	Total production in 2025
1	Slaughter Cattle	65369,34	291752,1
2	Dairy Cattle	7310	8000,88
3	Goat	6911,08	29077,89
4	Sheep	5202,76	5270,04
5	Pig	1468,12	871,35
...
14	Duck Egg Manila	237,82	146,23
15	Manila Duck	28,59	24,52
16	Quail Egg	68,47	42,17
17	Quail	64,15	58,21
18	Pigeons	1,38	1,27

**Figure 4.** Livestock data productivity trends**Table 6.** Horticultural commodities predictions

Number	Livestock Commodities	Total production in 2020	Total production in 2025
1	Mango	95149	78776,45
2	Orange	21948	22592,55

3	Papaya	19850	88508,54
4	Banana	12692	16195,48
5	Pineapple	15113	17836,33
...
22	Onion	1158	12965,3
23	Chili	519	487,98
24	Mustard	463	389,27
25	Spring onion	3683	36473,13
26	Cauliflower	207	136,12

A visualization of horticultural commodity trends can be seen in Fig. 5. The data used to make predictions is from 2016 to 2020. Each horticultural commodity is predicted using ARIMA to determine the production level of each commodity. The best ARIMA model was produced when predicting snake fruit production, namely 20%. The best ARIMA model is (2, 2, 2).

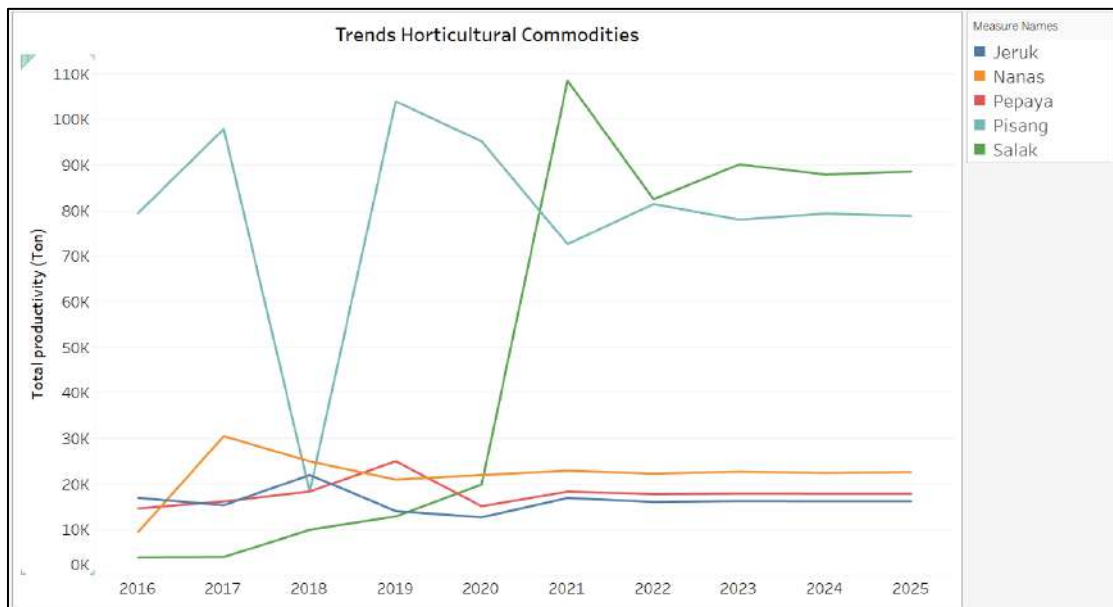


Figure 5. Horticulture data productivity trends

4 Conclusions

This research has succeeded in grouping horticultural commodities and livestock products using the K-Means method with good quality. Not only does this research carry out groupings, it also predicts the productivity of each commodity by applying the ARIMA method. The best ARIMA model quality for predicting horticultural commodities and livestock commodities is ARIMA (2, 2, 2) and ARIMA (0, 1, 0). The MAPE value of the ARIMA model cannot be said to be ideal, because the MAPE value is still $\geq 20\%$. The ideal MAPE value is $\leq 20\%$ [19].

Thus, this research makes an important contribution to decision making regarding food policy in the IKN Region. The resulting priority commodity recommendations can become a basis for optimizing food production and achieving food independence in the region. The use of the K-Means and ARIMA methods in predictions also provides reliability in projecting productivity results for the future. It is hoped that future research will pay attention to aspects of public consumption in the IKN area for certain commodities. When the production level of a commodity is low, but demand is high, the commodity must be developed. The production development process can be carried out by expanding the land for a horticultural commodity using a land suitability analysis approach.

References

- [1] R. Harini, I. Sukri, R. D. Ariani, E. P. I. Faroh, H. Nadia, and U. Kafafa, "The Study of Food Security in the Special Region of Yogyakarta, Indonesia," *Forum Geografi*, vol. 35, no. 2, Feb. 2022, doi: 10.23917/forgeo.v35i2.15855.
- [2] A. Garbero and L. Jäckering, "The potential of agricultural programs for improving food security: A multi-country perspective," *Glob Food Sec*, vol. 29, p. 100529, Jun. 2021, doi: 10.1016/j.gfs.2021.100529.
- [3] T. T. Tora, D. T. Degaga, and A. U. Utallo, "Drought vulnerability perceptions and food security status of rural lowland communities: An insight from Southwest Ethiopia," *Current Research in Environmental Sustainability*, vol. 3, p. 100073, 2021, doi: 10.1016/j.crsust.2021.100073.

- [4] N. Endey, I. Kadek, S. Arsana, A. Y. Katili, A. Sahabi, and M. A. Talalu, "Analisis Daya Saing Komoditi Unggulan Gorontalo Dalam Mendukung Ibu Kota Negara Baru Republik Indonesia," vol. 3, [Online]. Available: <http://journal.unismuh.ac.id/index.php/equilibrium>
- [5] A. Zezza, C. Carletto, B. Davis, and P. Winters, "Assessing the impact of migration on food and nutrition security," *Food Policy*, vol. 36, no. 1, pp. 1–6, Feb. 2011, doi: 10.1016/j.foodpol.2010.11.005.
- [6] S. Min, L. Hou, W. Hermann, J. Huang, and Y. Mu, "The impact of migration on the food consumption and nutrition of left-behind family members: Evidence from a minority mountainous region of southwestern China," *J Integr Agric*, vol. 18, no. 8, pp. 1780–1792, Aug. 2019, doi: 10.1016/S2095-3119(19)62588-8.
- [7] A. Parven *et al.*, "Impacts of disaster and land-use change on food security and adaptation: Evidence from the delta community in Bangladesh," *International Journal of Disaster Risk Reduction*, vol. 78, p. 103119, Aug. 2022, doi: 10.1016/j.ijdrr.2022.103119.
- [8] A. A. Simangunsong, I. Gunawan, Z. M. Nasution, and G. Artikel, "Pengelompokan Hasil Produksi Tanaman Perkebunan Berdasarkan Provinsi Menggunakan Metode K-Means Clustering Production of Plantation Crops by Province Using the K-Means Method Article Info ABSTRAK," *JOMLAI: Journal of Machine Learning and Artificial Intelligence*, vol. 1, no. 4, pp. 2828–9099, 2022, doi: 10.55123/jomlai.v1i4.1661.
- [9] L. M. Harahap, W. Fuadi, L. Rosnita, E. Darnila, and R. Meiyanti, "Klastering Sayuran Unggulan Menggunakan Algoritma K-Means," *Jurnal Teknik Informatika dan Sistem Informasi*, vol. 8, no. 3, Dec. 2022, doi: 10.28932/jutisi.v8i3.5277.
- [10] S. Nosratabadi, S. Ardabili, Z. Lakner, C. Mako, and A. Mosavi, "Prediction of Food Production Using Machine Learning Algorithms of Multilayer Perceptron and ANFIS," *Agriculture*, vol. 11, no. 5, p. 408, May 2021, doi: 10.3390/agriculture11050408.
- [11] R. Nugroho, A. Polina, and Y. Mahendra, "Tourism Site Recommender System Using Item-Based Collaborative Filtering Approach," *International Journal of*

-
- Applied Sciences and Smart Technologies*, vol. 2, no. 2, pp. 119–126, Dec. 2020, doi: 10.24071/ijasst.v2i2.2987.
- [12] J. Fattah, L. Ezzine, Z. Aman, H. El Moussami, and A. Lachhab, “Forecasting of demand using ARIMA model,” *International Journal of Engineering Business Management*, vol. 10, p. 184797901880867, Jan. 2018, doi: 10.1177/1847979018808673.
- [13] A. H. Salsabila and N. Nurwati, “Deforestasi dan Migrasi Penduduk ke Ibu Kota Baru Kalimantan Timur: Peran Sinergis Pemerintah Dan Masyarakat,” *Prosiding Penelitian dan Pengabdian kepada Masyarakat*, vol. 7, no. 1, p. 27, Jul. 2020, doi: 10.24198/jppm.v7i1.28259.
- [14] K. K. Al-jabery, T. Obafemi-Ajayi, G. R. Olbricht, and D. C. Wunsch II, “Data preprocessing,” in *Computational Learning Approaches to Data Analytics in Biomedical Applications*, Elsevier, 2020, pp. 7–27. doi: 10.1016/B978-0-12-814482-4.00002-4.
- [15] V. Purwayoga and I. S. Sitanggang, “Clustering Potential Area of Fusarium Oxysporum As A Disease of Garlic,” in *IOP Conference Series: Earth and Environmental Science*, Institute of Physics Publishing, Jul. 2020. doi: 10.1088/1755-1315/528/1/012040.
- [16] V. Purwayoga, “Modified skyline query to measure priority region for personal protective equipment recipient of COVID-19 health workers,” *Jurnal Teknologi dan Sistem Komputer*, vol. 9, no. 3, pp. 167–173, Jul. 2021, doi: 10.14710/jtsiskom.2021.14003.
- [17] V. Purwayoga, “Optimasi Jumlah Cluster pada Algoritme K-Means untuk Evaluasi Kinerja Dosen,” *Jurnal Informatika Universitas Pamulang*, vol. 6, no. 1, p. 118, Mar. 2021, doi: 10.32493/informatika.v6i1.9522.
- [18] E. H. S. Atmaja, “Implementation of k-Medoids Clustering Algorithm to Cluster Crime Patterns in Yogyakarta,” *International Journal of Applied Sciences and Smart Technologies*, vol. 1, no. 1, pp. 33–44, Jun. 2019, doi: 10.24071/ijasst.v1i1.1859.

- [19] H. Jurnal, S. Budi, and H. Sakur, “Jurnal Informatika dan Teknologi Komputer Perbandingan Distance Measures Pada K-Means Cluster Dan Topsis Dengan Korelasi Pearson Dan Spearman,” *Maret*, vol. 3, no. 1, pp. 74–81, 2023.
- [20] L. N. Kasanah, “Aplikasi Autoregressive Integrated Moving Average (ARIMA) untuk Meramalkan Jumlah Demam Berdarah Dengue (DBD) di Puskesmas Mulyorejo,” *Jurnal Biometrika dan Kependudukan*, vol. 5, no. 2, p. 177, Sep. 2017, doi: 10.20473/jbk.v5i2.2016.177-189.
- [21] S. D. Sudrazat, H. Purba, E. Wijaksono, W. Pranowo, and M. I. Hibatullah, “Prediksi Kecepatan Gelombang S Dengan Machine Learning Pada Sumur ‘S-1’, Cekungan Sumatera Tengah, Indonesia,” *Lembaran publikasi minyak dan gas bumi*, vol. 54, no. 1, pp. 29–35, Apr. 2020, doi: 10.29017/LPMGB.54.1.502.
- [22] N. D. Arianti, E. Saputra, and A. Sitorus, “An automatic generation of pre-processing strategy combined with machine learning multivariate analysis for NIR spectral data,” *J Agric Food Res*, vol. 13, p. 100625, Sep. 2023, doi: 10.1016/j.jafr.2023.100625.

Sentiment Analysis on Tweets about Waste Problem in Yogyakarta using SVM

Robertus Adi Nugroho^{1,*}, Sri Hartati Wijono¹,
Kartono Pinaryanto¹, Ridowati Gunawan¹, F.X. Sinungharjo²

¹*Faculty of Science and Technology, Sanata Dharma University,
Yogyakarta, Indonesia*

²*Faculty of Literature, Sanata Dharma University, Yogyakarta, Indonesia*

**Corresponding Author: robertus.adi@usd.ac.id*

(Received 26-10-2023; Revised 26-05-2024; Accepted 30-05-2024)

Abstract

Yogyakarta Province is facing a waste management problem. The closure of the only Integrated Waste Treatment Plant in Piyungan, Yogyakarta, has a huge impact in society life. Much waste generated from industries and houses cannot be handled appropriately until final disposal. This problem can be solved through government policies. Its effectiveness can be seen from the public response on social media. Sentiment analysis on social media, especially X, can be efficiently conducted using Support Vector Machines (SVM). Data is directly obtained from X, and text processing is performed on it. The accuracy rate of sentiment analysis using SVM on the topic of garbage in Yogyakarta is quite good at 87%. This accuracy is obtained using parameter $C = 1$ in SVM and $k = 10$ in K-Fold Cross Validation. By using these C and k values, 40% of the data is identified as positive sentiment and 60% as negative sentiment.

Keywords: Garbage, Sentiment Analysis, Support Vector Machine, Yogyakarta

1 Introduction

The world's waste problem requires serious attention. This is also the case in Yogyakarta, a province in Indonesia. Yogyakarta faces waste management problems that are quite troubling to the community. The closure of the only Integrated Waste Treatment Plant in Piyungan, Yogyakarta, has hampered the waste management process in the community. The closure of the Integrated Waste Treatment Plant in Piyungan was urged by the local community, who had been disturbed by the waste pollution caused by the Integrated Waste Treatment Plant [1]. The waste management problem in Yogyakarta can



be solved through local government policies. However, the steps taken by the government have not been effective in solving the waste problem.

Currently, social media such as Facebook, X, and Instagram are places often used by the public to give opinions or discuss a problem happening in society. The more social media users who talk about an issue causes the emergence of a trending topic that can attract the attention of parties with an interest in the issue. This can be an early warning system for parties with an interest in the issue that becomes the trending topic. If the trending topic is the waste management problem in Yogyakarta, then public opinion about it can be a warning for the local government in Yogyakarta. Hopefully, the government can immediately take steps to solve the problem.

The development of science in the field of Machine Learning, especially on Natural Language Processing, can help analyze the sentiment of opinions that develop on social media. Some research about it has been done successfully. Diekson et al. [2] conducted a sentiment analysis of Traveloka user satisfaction with the services provided by Traveloka to its users. The study used three classification methods including: Support Vector Model (SVM), Logistic Regression, and Naïve Bayes. User satisfaction data used is taken from Twitter. Pavitha et al. [3] conducted research on a movie recommendation system which involved a sentiment analysis process on movie reviews. Sentiment analysis uses two machine learning algorithms, namely Naïve Bayes and Support Vector Machine (SVM). Wang and Zhao [4] used Support Vector Machine to predict investor sentiment towards news about stock prices. The prediction results are used by users to decide the right investment. Borg and Boldt [5] investigated sentiment analysis of Customer Support at the Swedish Telecom company. The data used in this study are emails sent to the company's Customer Support. The sentiment analysis process uses Vader for the labeling process and SVM for the classification process. Jaya Hidayat et al. [6] conducted research on public sentiment towards development on Rinca Island, Indonesia. Data is taken from Twitter. The classification algorithms used in this study are SVM and Logistic Regression. Isnani et al. [7] tried to analyze user sentiment towards the TikTok application. The criticism and response data analyzed were taken from the Google Play Store. The classification algorithm used to analyze the sentiment is SVM. Styawati et al. [8] have an interest in the phenomenon of using online transportation such as Gojek and

Grab. Some users give positive opinions and some give negative opinions. Styawati et al. tried to do sentiment analysis on the responses of these online transportation users on the Google Play Store using SVM. Chen and Zhang [9] conducted research on text sentiment analysis using CNN (Convolutional Neural Networks) and SVM. Chen and Zhang tried to improve the accuracy of sentiment analysis by combining CNN and SVM. Taufik et al. [10] used the Support Vector Machine (SVM) approach to analyze the sentiment towards public figures on Twitter. Saputri et al. [11] researched the classification of Borobudur Temple tourist sentiment on the TripAdvisor site using SVM and K-Nearest Neighbor (KNN).

From these studies, it can be seen that the use of machine learning approach was appropriate to be applied in sentiment analysis, especially in classification process. The reliability of machine learning in performing classification is not only in sentiment analysis but also in other cases. Yadav et al. [12] tried to classify traffic sign images that appear in a video using SVM. The classification results would be used to generate sounds that match the traffic sign. Then the sound would be used to remind the driver. Kumalasanti [13] also used SVM to classify a person's handwriting with his personality. Therefore, this research tried to conduct sentiment analysis for the topic of waste management in Yogyakarta using machine learning approach so that the polarization of public opinion on waste management can be known. The algorithm that was used in this research was Support Vector Machine (SVM).

2 Material and Methods

The purpose of sentiment analysis of a document or sentence is to determine the polarity of the document or sentence. The three types of polarity are positive, negative, or neutral [14]. According to [15], sentiment analysis methods are categorized into three types, namely:

- a) Lexicon Based Method
- b) Machine learning Based Method
- c) Hybrid Method

The lexicon-based method uses a word sentiment dictionary to determine the sentiment of a document or sentence. Machine learning methods use datasets with sentiment to determine the sentiment of new sentences or documents. The hybrid method will combine the two methods above.

Support Vector Machine (SVM) is one of the popular algorithms in machine learning. Based on the research conducted by Diekson et al. [2], Pavitha et al. [3], Wang and Zhao [4], Borg and Boldt [5], Jaya Hidayat et al. [6], Isnan et al. [7], Styawati et al. [8], Chen and Zhang [9], Taufik et al. [10], and Saputri et al. [11], the use of SVM algorithm in performing sentiment analysis gave good results. In fact, when compared to several other algorithms, the use of SVM gave better results. From the research conducted by Diekson et al. [2], based on F1 score evaluation, SVM gave better results than Logistic Regression and Naïve Bayes in classifying user satisfaction about Traveloka services. Pavitha et al. [3] concluded the accuracy score of SVM is better than Naïve Bayes in classifying movie reviews. Then, Wang and Zhao [4] successfully predict the investor sentiment from the news. The accuracy reached 59%. Borg and Boldt [5] showed us that SVM could predict the sentiment of customer email successfully with the mean F1 score of 0.688. Jaya Hidayat et al. [6] used SVM and Logistic Regression to analyse the sentiment of citizen's opinion about Rinca Island development. The result was good, the accuracy rate of SVM was about 86% and Logistic Regression was about 75%. Isnan et al. [7] and Styawati [8] gave the same conclusion that the accuracy of the sentiment analysis by using SVM was above 80%. Chen and Zhang [9] got the result that using CNN combined with SVM could improve the accuracy of the sentiment classification. Taufik et al. [10] tried to use SVM in classifying the sentiment to the public figure. They got the accuracy was about 80%. Saputri et al. [11] compared SVM and KNN in classifying the sentiment of tourist opinion about Borobudur Temple in TripAdvisor. They got the result that SVM gave a better accuracy than KNN. From these researches, the use of SVM to analyze sentiment is very appropriate. Therefore, in this research, SVM was used to analyze sentiment of public opinion in X about waste problem in Yogyakarta.

Next, we will explain the steps for sentiment analysis regarding the waste problem in Yogyakarta. In the first stage, this research collected data from X and saved it into a CSV file. The second stage is preprocessing the raw data. The process is carried out to

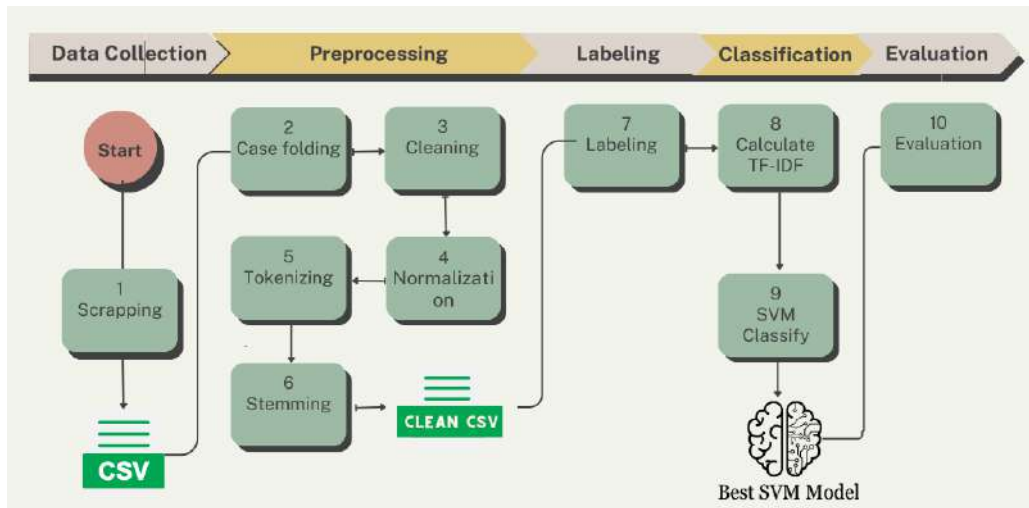


Figure 1. Process diagram of this research

clean the data of unnecessary characters. After the data is clean, the next step is labeling positive or negative sentiment. The fourth stage is the classification process using the Support Vector Machine (SVM) method. After the classification process, the best SVM model will be obtained. The best SVM model is used for the evaluation process. This step is shown in the Fig 1.

2.1. Data Collection

The data used is a collection of Indonesian language reviews on X social media that discuss the topic of waste. The hashtags used are *sampah*, *sampahyogya*, *sampahpiyungan*, *bakarsampahyogya*. Data was gathered by web scraping with the *tweepy*¹ library from Python. The data collection period spanned from September 2023 to October 2023. The web scraping yielded 1211 tweets. The tweet results were selected by removing duplicate and irrelevant tweets. This selection process produces 1000 tweets, which are used for the next step. The web scraping results contain tweet data, user data, URL address, retrieval time, and other data. The data used is only tweet data for further processing.

¹ tweepy.org

2.2. Data Preprocessing

This step aims to remove unnecessary characters that would affect the classification process. The first step is case folding, namely making all the letters lowercase. Next is to remove unnecessary characters such as @, #, \$, ?, !, and others. Apart from that, unnecessary tagging was also removed. The only characters used are letters, so other than that, they will not be used. This process is carried out using the *re* library from Python.

The next step is the normalization, which is conducted to correct incorrect spellings of words. Another goal is to restore original words from abbreviations or slang words commonly used in tweets. This process requires checking Kamus Besar Bahasa Indonesia² (KBBI) and the Alay dictionary³. After the tweet does not contain abbreviations and slang words, the following process is tokenizing the tweet using the *nlTK* library from Python. The results of this stage are in the form of a list of tokens.

The final preprocessing step is the lemmatization or stemming process, namely removing affixes to get the stem word. The stemming process is conducted using the Sastrawi library⁴.

We do not carry out a stopword removal process because it can lose meaning. For example, "Dia tidak suka membuang sampah" (He does not like throwing rubbish). The sentence's sentiment will change if the word "tidak" (not) becomes a stopword.

2.3. Labeling

Labeling was done manually by two annotators. One of the annotators is a linguist. Linguists train other annotators to determine the polarity of tweets. Every tweet annotated by one annotator will be double-checked by a linguist so that there is no bias in determining the polarity of the tweet.

2.4. Classification

Before classification, term frequency (TF) and index document frequency (IDF) are calculated. TF-IDF weight evaluates how important a word is in a sentence. Term

² <https://kbbi.kemdikbud.go.id/Beranda>

³ <https://github.com/fendiirfan/Kamus-Alay>

⁴ <https://github.com/sastrawi/sastrawi>

Frequency (TF) is the opposite of IDF (eq. 1); the higher the frequency of occurrence of a term in a document, the higher the weight of the term itself. IDF is the opposite of TF; the higher the frequency of occurrence of a term, the lower the weight of the term itself. TF-IDF calculation is done using Python program code.

$$IDF(t) = \log \frac{N}{df(t)} \quad (1)$$

IDF(t) = IDF of the word t

N = total sentence

df = number of documents containing the word t

The method used for the sentiment-based X classification process uses SVM. SVM attempts to identify the best hyperplane to separate large data into two optimal classes. For example, if we want to divide two-dimensional space, we need a one-dimensional hyperplane, namely a line. SVM will classify data using a hyperplane that maximizes the boundaries between classes in the training data. First of all, SVM tries to divide the data into two dimensions. If the data classes formed cannot divide the data linearly, the algorithm will change the margin until the hyperplane can separate the data into its classes linearly. Margin is the distance between the hyperplane and each class's closest member (support vector). The following (eq. 2) is the hyperplane calculation formula:

$$f(x) = w \cdot x + b \quad (2)$$

w = the chosen hyperplane parameter

x = data input x

b = the hyperplane parameter that was selected

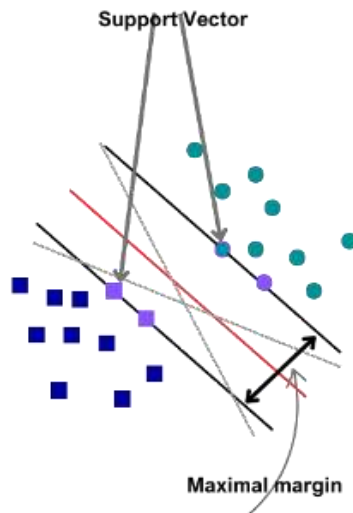


Figure 2. Support Vector Machine

SVM tries to maximize the margin in order to find the right hyperplane to divide classes and minimize classification errors (see Fig 2). So, the two interests contradict each other. If we increase the margin, we will obtain a higher misclassification rate; if we decrease the margin, we will get a lower misclassification rate. Parameter C is the answer to control between maximizing margin and minimizing error. In this research, experiments were conducted to find the C value that best suited our data [16].

SVM increased in size when used for classification with many classes, and SVM was theoretically developed to solve classification problems with two classes. This research uses linear kernels for SVM classification. Program implementation uses the Sklearn library from Python.

2.5. Evaluation

This research evaluates a sentiment analysis system using recall, precision, F1 and accuracy. Recall, precision, F1, and accuracy are used to assess the accuracy of the results. Where recall (True Positive Rate) (eq.3) is the proportion of true positive data identified versus all true positive data. Precision (Positive Predictive Value) (eq.4) is the proportion of correct identifications of all identified positive findings. F1 score (eq. 6) is the sum of precision and recall. Accuracy (eq.5) is the correct identifications (positive and negative)

ratio to the total data. Evaluation was conducted on separated data using k fold cross-validation. Testing with different k values will produce an SVM model. This research will evaluate this SVM model.

$$recall = \frac{TP}{TP + FN} \quad (3)$$

$$precision = \frac{TP}{TP + FP} \quad (4)$$

$$accuracy = \frac{TP + TN}{TP + TN + FP + FN} \quad (5)$$

$$F1 = 2 * \frac{precision + recall}{precision * recall} \quad (6)$$

3 Results and Discussions

Several experiments have been conducted on the sentiment analysis approach proposed in this research. Experiments were conducted for several types of C to determine the most optimal C parameter values in SVM. Experiments were conducted on data that was divided using k-fold cross-validation for each type of C.

From several experiments with a combination of parameters C and k, the best combination will be obtained in carrying out sentiment analysis from the prepared tweet data set. Some of the C values used include C=1, C=10, and C=100. At the same time, the value of k in k-Fold Cross Validation includes k = 2, 3, 4, 5, 6, 7, 8, 9, and 10.

In the first experiment, parameter C is set to 1. Table 1 shows that the best accuracy is 87%. It is got when the k-value equals 10.

Table 1. Experiment Result with C=1

k	Accuracy	Precision	Recall	F1 Score
2	77.60%	77%	78%	77%
3	81.98%	82%	82%	82%
4	80.40%	80%	80%	80%
5	84.50%	85%	84%	84%

6	82.23%	84%	83%	83%
7	83.21%	83%	83%	83%
8	86.40%	87%	86%	86%
9	84.68%	85%	85%	85%
10	87.00%	88%	87%	87%

Table 2. Experiment Result with C=10

K	Accuracy	Precision	Recall	F1 Score
2	77.80%	78%	78%	78%
3	81.98%	82%	82%	82%
4	81.60%	83%	82%	81%
5	84.50%	85%	84%	84%
6	85.02%	85%	85%	85%
7	82.51%	83%	83%	82%
8	86.40%	86%	86%	86%
9	84.68%	85%	85%	85%
10	86.00%	86%	86%	86%

In the second experiment, parameter C is set to 10. Table 2 show that the best accuracy occurs when k-value is 8, which is 86.40%. In the third experiment, parameter C is set to 100. As shown in Table 3, the best accuracy is 86.40%. It occurs when the k-value equals to 8.

Table 3. Experiment Result with C=100

K	Accuracy	Precision	Recall	F1 Score
2	77.80%	78%	78%	78%
3	81.98%	82%	82%	82%
4	81.60%	83%	82%	81%
5	84.50%	85%	84%	84%
6	85.02%	85%	85%	85%
7	82.51%	83%	82%	82%
8	86.40%	86%	86%	86%
9	84.68%	85%	85%	85%
10	86%	86%	86%	86%

From those experiments, it can be seen that C parameters influence the accuracy of the sentiment analysis result, although it is not significant. Moreover, in C=10 and C=100, the experiment result shows no differences for all evaluation aspects, such as accuracy, precision, recall, and F1 score. It means that C parameters could not improve the prediction results anymore. (see Figs 3 and 4).

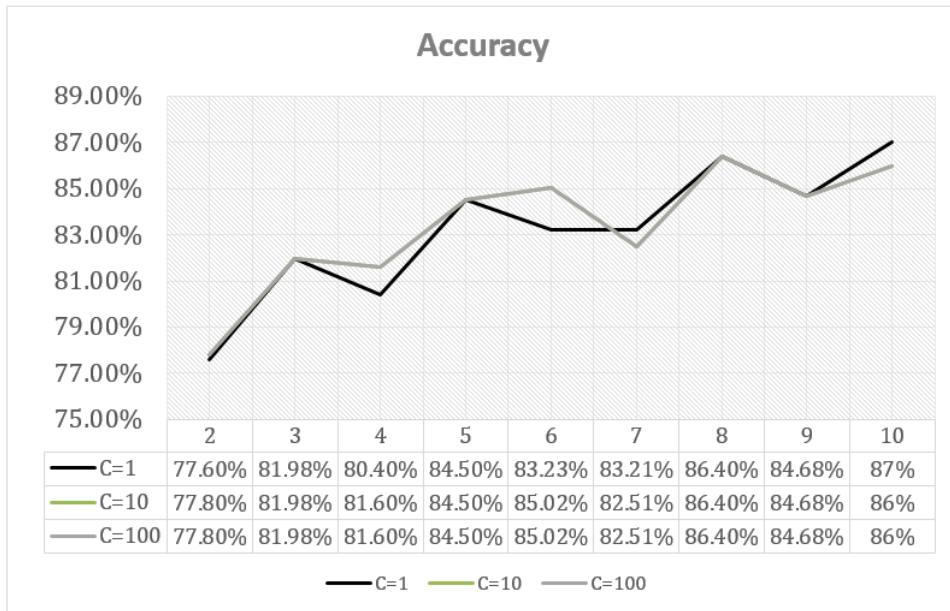


Figure 3. Accuracy comparison

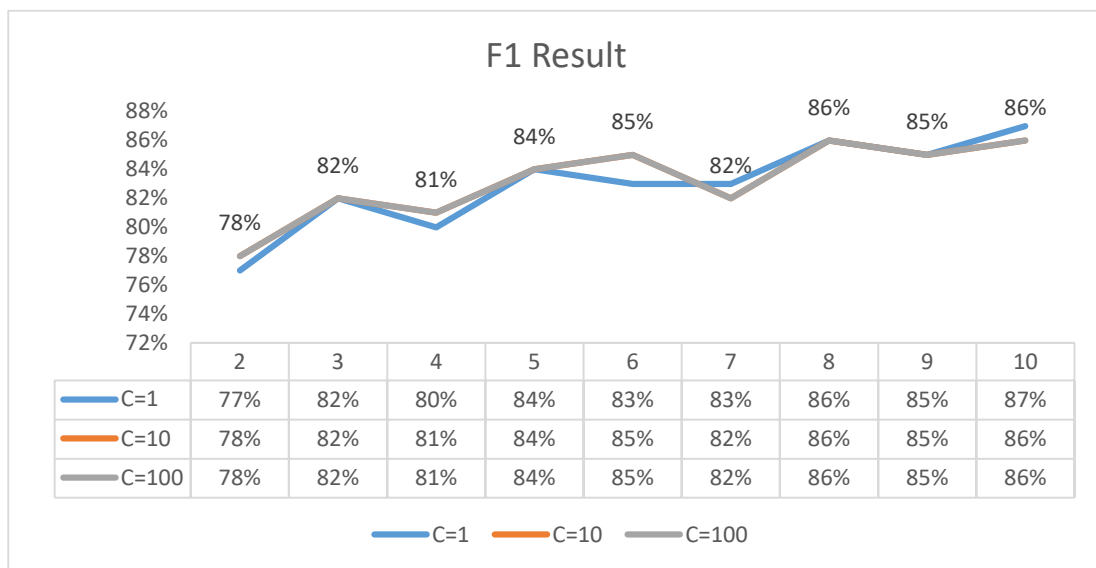


Figure 4. F1 comparison

As seen in figure 3 and figure 4, the best sentiment analysis result is obtained using $C=1$ and $k=10$. By this configuration, the proposed method could predict 397 tweets as positive and 603 tweets as negative tweets. It means that the sentiment of the X data about waste management in Yogyakarta is 40% positive and 60% negative.

From these results it can be seen that as many as 60% of tweets from data taken from X regarding waste management in Yogyakarta are categorized as tweets with negative sentiment. This information can illustrate that the handling of waste in Yogyakarta has not fully received positive appreciation from the public. The majority of people still give negative sentiments. The government can utilize this information to follow up by evaluating policies on waste management in Yogyakarta.

4 Conclusions

From the experiments that have been carried out, it can be concluded that the sentiment analysis approach using SVM can be applied to analyze sentiment regarding waste management in Yogyakarta province. Using parameters $C = 1$ and $k = 10$ is the best combination for sentiment analysis, which can produce an accuracy of 87%. From the configuration values of C and k , it is found that X data about waste management in Yogyakarta province has 40% positive sentiment and 60% negative sentiment.

Acknowledgements

This research was funded by LPPM Sanata Dharma University in the framework of a Research Assignment with the theme Universal Apostolic Preferences (UAP).

References

- [1] M. Fakhrudin, "Yogyakarta Darurat Sampah," *Republika*, May 13, 2022. [Online]. Available: <https://news.republika.co.id/berita/rbq3q8318/yogyakarta-darurat-sampah>
- [2] Z. A. Diekson, M. R. B. Prakoso, M. S. Q. Putra, M. S. A. F. Syaputra, S. Achmad, and R. Sutoyo, "Sentiment Analysis for Customer Review: Case Study of

-
- Traveloka,” *Procedia Computer Science*, vol. 216, pp. 682–690, 2023, doi: 10.1016/j.procs.2022.12.184.
- [3] N. Pavitha *et al.*, “Movie Recommendation and Sentiment Analysis Using Machine Learning,” *Global Transitions Proceedings*, vol. 3, no. 1, pp. 279–284, Jun. 2022, doi: 10.1016/j.gltp.2022.03.012.
- [4] D. Wang and Y. Zhao, “Using News to Predict Investor Sentiment: Based on SVM Model,” *Procedia Computer Science*, vol. 174, pp. 191–199, 2020, doi: 10.1016/j.procs.2020.06.074.
- [5] A. Borg and M. Boldt, “Using VADER Sentiment and SVM for Predicting Customer Response Sentiment,” *Expert Systems with Applications*, vol. 162, p. 113746, Dec. 2020, doi: 10.1016/j.eswa.2020.113746.
- [6] T. H. Jaya Hidayat, Y. Ruldeviyani, A. R. Aditama, G. R. Madya, A. W. Nugraha, and M. W. Adisaputra, “Sentiment Analysis of Twitter Data Related to Rinca Island Development Using Doc2Vec and SVM and Logistic Regression as Classifier,” *Procedia Computer Science*, vol. 197, pp. 660–667, 2022, doi: 10.1016/j.procs.2021.12.187.
- [7] M. Isnan, G. N. Elwirehardja, and B. Pardamean, “Sentiment Analysis for TikTok Review Using VADER Sentiment and SVM Model,” *Procedia Computer Science*, vol. 227, pp. 168–175, 2023, doi: 10.1016/j.procs.2023.10.514.
- [8] S. Styawati, A. Nurkholis, A. A. Aldino, S. Samsugi, E. Suryati, and R. P. Cahyono, “Sentiment Analysis on Online Transportation Reviews Using Word2Vec Text Embedding Model Feature Extraction and Support Vector Machine (SVM) Algorithm,” in *2021 International Seminar on Machine Learning, Optimization, and Data Science (ISMODE)*, Jakarta, Indonesia: IEEE, Jan. 2022, pp. 163–167. doi: 10.1109/ISMODE53584.2022.9742906.
- [9] Y. Chen and Z. Zhang, “Research on Text Sentiment Analysis Based on CNNs and SVM,” in *2018 13th IEEE Conference on Industrial Electronics and Applications (ICIEA)*, Wuhan: IEEE, May 2018, pp. 2731–2734. doi: 10.1109/ICIEA.2018.8398173.

- [10] I. Taufik and S. A. Pamungkas, “Analisis Sentimen Terhadap Tokoh Publik Menggunakan Algoritma Support Vector Machine (SVM),” *Jurnal Logika*, vol. 8, no. 1, 2018.
- [11] R. P. Saputri, W. S. Winahju, and K. Fithriasari, “Klasifikasi Sentimen Wisatawan Candi Borobudur pada Situs TripAdvisor Menggunakan Support Vector Machine dan K-Nearest Neighbor,” *Jurnal Sains dan Seni Institut Teknologi Sepuluh November*, vol. 8, no. 2, 2019, doi: 10.12962/j23373520.v8i2.44391.
- [12] S. Yadav, A. Patwa, S. Rane, and C. Narvekar, “Indian Traffic Signboard Recognition and Driver Alert System Using Machine Learning,” *Int.J.Appl.Sci.Smart Technol.*, vol. 1, no. 1, pp. 1–10, Jun. 2019, doi: 10.24071/ijasst.v1i1.1843.
- [13] R. A. Kumalasanti, “Design of Someone’s Character Identification Based on Handwriting Patterns Using Support Vector Machine,” *Int.J.Appl.Sci.Smart Technol.*, vol. 4, no. 2, pp. 233–240, Dec. 2022, doi: 10.24071/ijasst.v4i2.5417.
- [14] B. Pang and L. Lee, “Opinion Mining and Sentiment Analysis,” *Found. Trends Inf. Retr.*, vol. 2, no. 1–2, pp. 1–135, Jan. 2008, doi: 10.1561/15000000011.
- [15] M. Rathan, V. R. Hulipalled, P. Murugeswari, and H. M. Sushmitha, “Every Post Matters: A Survey on Applications of Sentiment Analysis in Social Media,” *2017 International Conference On Smart Technologies For Smart Nation (SmartTechCon)*, pp. 709–714, 2017.
- [16] C. Campbell and Y. Ying, *Learning with Support Vector Machines*, vol. 5. 2011. doi: 10.2200/S00324ED1V01Y201102AIM010.

Image Detection Analysis for Javanese Character Using YOLOv9 Models

Hari Suparwito^{1*}

¹*Faculty of Science and Technology, University of Sanata Dharma,
Yogyakarta 55281, Indonesia*

**Corresponding author: shirsj@jesuits.net*

(Received 05-06-2024; Revised 19-06-2024; Accepted 20-06-2024)

Abstract

The Javanese script needs to be digitized to improve access and usage, especially among younger generations. Digitizing Javanese characters is crucial for preserving Javanese culture and traditions in the long term. This study aims to detect and recognize Javanese characters using the YOLOv9 algorithm model, known for its ability to detect various object types, including Latin and non-Latin scripts. The dataset used consists of 85 images of complete Javanese script arranged in a 4x5 grid of different characters. The dataset was divided into a training dataset (75 images) and a validation dataset (10 images). All data pre-processing was done using Roboflow tools. Two experiments were conducted, varying the weights of the YOLOv9 algorithm model: YOLOv9-c and YOLOv9-c-converted. The research results showed that the YOLOv9-c model outperformed YOLOv9-c-converted, achieving a confidence level of over 80% and an mAP value of 0.95 in recognizing Javanese script images. In other words, the YOLOv9 algorithm model succeeded in detecting and recognizing Javanese scripts well.

Keywords: Deep learning, Image detection, Javanese character, Roboflow, YOLOv9

1 Introduction

The Javanese script, an ancient writing system utilized in Indonesia, particularly on the island of Java, holds immense cultural significance. It manifests itself in an array of written forms, including literature, documents, and inscriptions. Consequently, the digitization of the Javanese script becomes imperative, as it enables broader accessibility and utilization by the wider community, notably the younger generation [1]. The importance of digitizing the Javanese script is twofold: firstly, it aids in the preservation and transmission of Javanese cultural identity to future generations. Secondly, it has the potential to enhance public awareness and appreciation for Javanese culture, thereby stimulating efforts to safeguard Indonesia's cultural heritage. Ultimately, the

digitalization of Javanese characters plays a critical role in ensuring the continuation and long-term viability of Javanese culture and traditions. Consequently, it becomes evident that the digitalization of the Javanese script contributes significantly to the preservation of Javanese culture and traditions [2].

With the increasing availability of digital images, there is a growing demand for efficient and accurate methods to detect Javanese script in these images. Traditional approaches to detect Javanese script involve the use of feature extraction and classification techniques such as convolutional neural network (CNN) and support vector machine (SVM) [3]. Previous studies have employed various methods and algorithms to detect Javanese script images. Katili et al. [4] proposed a novel character recognition workflow that combines Local Binary Pattern (LBP) and Information Gain. The LBP method is used to determine the texture or shape characteristics of an image. The feature selection algorithm utilizes Information Gain, while the classification method employs SVM, k-NN, and Naïve Bayes. This study demonstrates that the information gain method can improve accuracy by 2%. Additionally, the study compares SVM classification to k-NN and Naive Bayes classification methods, revealing that SVM classification yields the highest accuracy results (87.86%) with a ten-fold cross-validation and a 64x64 cell size. Another study utilizes the YOLOv5 model in conjunction with the U-Net model to assist in identifying the location of Javanese characters in an input document image [5]. Experimental results show that YOLOv5 model performs well in character location detection, with a loss rate of approximately 0.05. Similarly, the U-Net model achieves an accuracy range of 75% to 90% in predicting character regions. Although YOLOv5 model may not be able to perfectly detect all Javanese characters, using the U-Net model can enhance the detection rates by 1.2% [6]. The Linear Binary Pattern (LBP) feature extraction technique is also employed to process the dataset, aiding in the local characterization and description of image texture for the analysis and detection of Javanese scripts [2]. In this study, a pre-processing step is conducted using $r = 4$ and a thresholding method with $d = 0.3$. Subsequently, the K-Nearest Neighbour algorithm is used for further research. The results obtained from ten Javanese script word datasets indicate an average accuracy rate of 90.5%. The highest accuracy achieved was 100%, while the lowest accuracy was 50%.

In this study, the YOLOv9 algorithm model is selected due to its real-time object detection capabilities, which do not require explicit feature extraction or classification. The YOLOv9 algorithm model has been successfully used for various object detection tasks, including Latin and non-Latin scripts [7]. Its ability to handle variations in font style and image quality makes it well-suited for detecting Javanese script. Therefore, the YOLOv9 algorithm model will be employed in this study to detect Javanese script. To assess image detection, the shape of the Javanese script image will be altered. Typically, the Javanese script image is organized in a 4x5 matrix format, which will be utilized in the training and validation datasets. For testing purposes, different image formats such as 4x5 and 2x10 character image matrices, as well as single images, will be used. Detecting Javanese script is expected to contribute to the advancement of image detection applications in various fields, particularly in language learning and the transliteration of regional languages with special characters into Latin characters.

2 Material and Methods

2.1 Data acquisition

The data utilized in this study was acquired from the publicly available Kaggle dataset [8]. This dataset comprises 85 images, each encompassing 20 Javanese character images. It is divided into two subsets: the training dataset, consisting of 75 images, and the validation dataset, comprising 10 images. The 85 data images are formed in 4x5 arrangement of Javanese word images as shown in Fig. 1. All pre-processing tasks were undertaken by Roboflow tools.



Figure 1. 4x5 arrangements of Javanese character images [9]

Conventionally, these 20 characters are systematically arranged in a 4x5 matrix. This research encompasses a collection of 85 images, wherein each image features a 4x5 matrix showcasing 20 Javanese characters. Subsequently, a data labelling procedure is implemented to assign a unique character label to each of the aforementioned characters, resulting in 20 distinctive character labels present within a solitary image. To put it differently, a single image comprises 20 script image labels.

2.2 YOLO model

The You Only Look Once (YOLO) algorithm model is widely recognized in the field of computer vision for its real-time processing capabilities and significant impact on object detection. Initially released in 2016 as YOLOv1, this algorithm introduced a single neural network that efficiently predicted bounding boxes and class probabilities from complete images in a single pass. This approach greatly accelerated the object detection process, distinguishing itself from traditional methods that employed multiple stages for detection [10].

Fig. 2 describes the CNN architecture used in YOLO (You Only Look Once). It consists of three key components: Convolutional Layers, Max Pooling Layers, and Fully Connected Layers. The Convolutional Layers extract features from the input image, reducing spatial dimensions and increasing the number of channels. ReLU activation functions introduce non-linearity. Max Pooling Layers are used to down-sample the

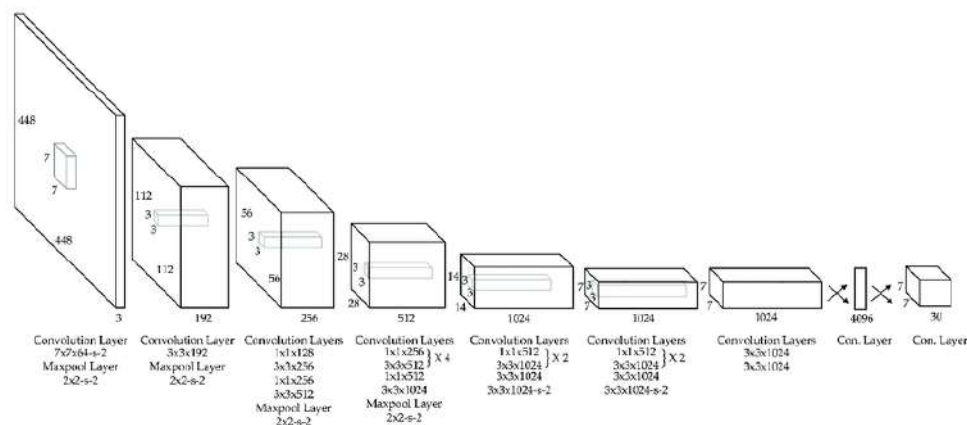


Figure 2. The basic CNN algorithm that is in YOLO model architecture [11]

feature maps, further reducing spatial dimensions and decreasing the number of parameters in the network. The final stage of the network is made up of Fully Connected Layers, which predict class probabilities and bounding box coordinates. These layers make predictions based on the features extracted by the convolutional and pooling layers.

The network uses a combination of techniques such as batch normalization and dropout to regularize the model and prevent overfitting. The CNN architecture is designed to be efficient and fast, allowing it to process images in real-time. The network is trained using a combination of techniques such as data augmentation and transfer learning to improve its performance on object detection tasks.

As of the most recent version, YOLOv9 model, the YOLO series continues to be a leading force in the field of object detection research, consistently pushing the boundaries of real-time detection tasks in terms of speed, accuracy, and efficiency. The progression of YOLO from its origin to the present day exemplifies the ongoing advancements in deep learning and computer vision, fundamentally shaping the manner in which we comprehend and engage with visual data across diverse applications.

2.3 Methods

The following diagram (Fig. 3) illustrates the process carried out in the study of detection and recognition of Javanese script using the YOLOv9 algorithm model. This study commenced by acquiring data in the form of images containing Javanese scripts. To facilitate data collection, we utilized a publicly available Kaggle dataset. For data pre-processing, the Roboflow tools were employed, specifically for labelling and segregating the data into training and validation datasets. Subsequently, the YOLOv9

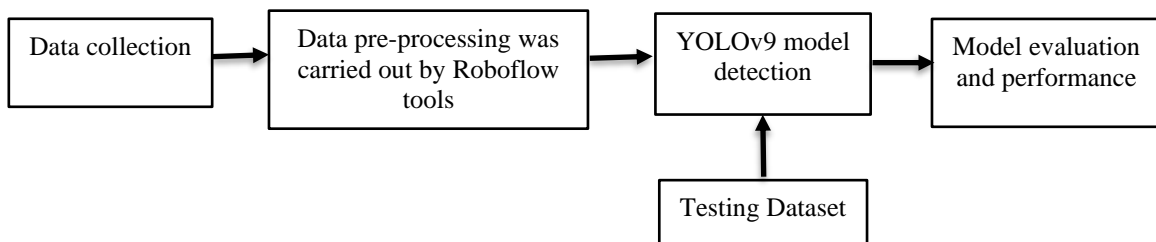


Figure 3. The steps in Javanese script images detection analysis using YOLOv9

algorithm was utilized for modelling. The resulting model was then assessed using the validation dataset. The final step involved employing a distinct set of testing dataset, which differed from both the training and validation dataset, to evaluate the model's capability to accurately detect and identify Javanese script objects. Notably, the testing dataset incorporated diverse variations of Javanese script that were not present in the training and validation datasets.

2.4 Experiments

Two experiments were conducted to compare the utilization of learning rate and weight parameters in YOLOv9 model, aiming to investigate their impact on the model's performance. The learning rate function, a crucial hyperparameter in deep learning, governs the extent to which the model adjusts its weights during the training process. It determines the step size for each iteration of the optimization algorithm, enabling the model to converge towards the minimum loss function. Given that the learning rate function can influence the weights, this study examines its effect on the weight parameter, evaluating the outcome using mean Average Precision (mAP) on images tested with the training model. Therefore, this study would compare the performance of 2 weight parameters of YOLOv9, namely YOLOv9-c and YOLOv9-c-converted. The remaining parameters, including activation function, dropout, and epochs, adhere to the default settings of the YOLOv9 algorithm. Table 1. showed the YOLOv9 parameters used in the experiments.

Table 1. YOLOv9 parameters used in experiments

Parameters	Experiment 1	Experiment 2
Weight	YOLOv9 – c	YOLOv9 – c – converted
Epoch		100
Dropout		0.5
Optimizer		Adam
Batch size		8
Learning rate		0.001

The YOLOv9 model is trained using 75 Javanese script images, followed by validation with ten additional images. In order to optimize the results, the model is trained for 100 epochs, utilizing a batch size of 8 and learning rates of 0.001. By analyzing the changes in learning rate and corresponding mAP results, it becomes possible to determine which parameters yield the highest accuracy.

3 Results and Discussions

After training the model, we proceeded to evaluate its performance using the validation set. The model's accuracy in detecting Javanese characters was assessed using metrics such as F1-score and mAP (mean Average Precision). Two distinct weight variations provided by YOLOv9, namely YOLOv9-c and YOLOv9-c-converted, were employed in this study. Table 2 presents the mAP values and F1-scores obtained from these two weight configurations. However, it is important to note that the observed differences in both metrics are not statistically significant. The results of the model evaluation are presented in the following table.

Table 2. The mAP and F1-confidence results

Weight parameters	mAP50	mAP50-95	F1 score
YOLOv9-c	0.95	0.72	0.943
YOLOv9-c-converted	0.92	0.71	0.932

The graph presented in Fig.4 displays the F1-score and Confusion Matrix results for all Javanese characters at varying confidence levels. Only the most optimal results are presented in this analysis. The F1-confidence score in YOLO (You Only Look Once) model is a measure of a model's accuracy that considers both precision and recall. It is the harmonic mean of precision and recall, providing a balance between the two. The F1-confidence score is plotted against different confidence thresholds in the F1 Confidence Curve, which helps in determining the optimal confidence threshold for making predictions. A higher F1 score indicates better performance, and the confidence threshold at which the F1 score is maximized is often considered the optimal threshold. Fig. 4 showed that for all classes (20 classes) the higher value is 0.89 at 0.552. This means that with a confidence value of 0.55, a good average precision value will be obtained for all

classes (for all characters). However, it can also be seen that for each class, the F1 value and the confidence value are different for each script. If we focus on the confidence value of 0.55, it can be seen that the characters "ba", "sa", and "la" give the three lowest F1 values compared to other characters. Next, we also computed the confusion matrix for each character in the Javanese script.

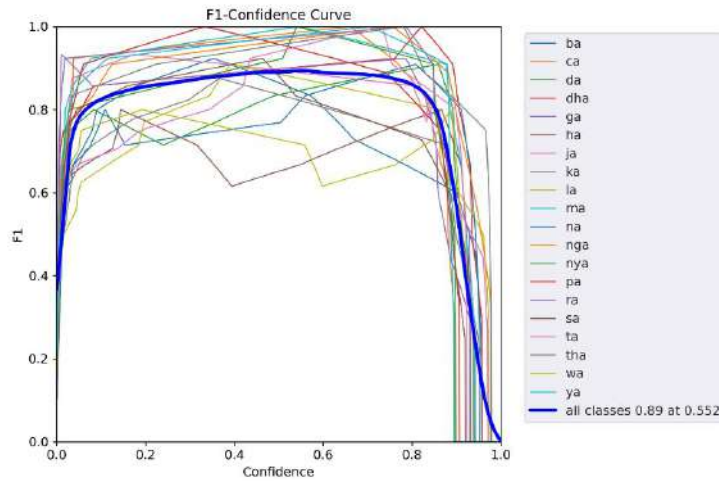


Figure 4. F1-confidence graph for each Javanese character and all classes using the best training model

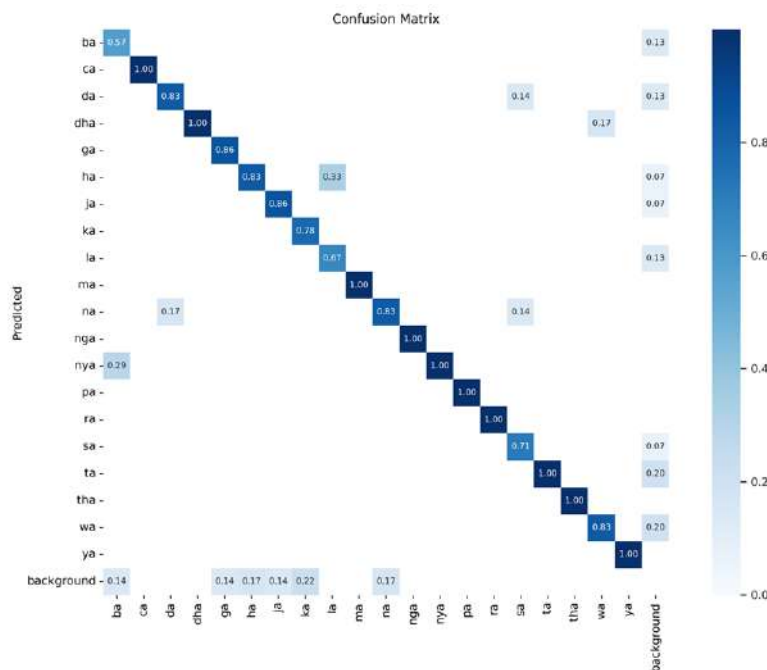


Figure 5. The Confusion Matrix for each Javanese character

A confusion matrix's diagonal values represent the number of instances in which the predicted label matches the true label. In other words, they display correctly classified instances. The higher the diagonal values, the better the model's performance at correctly identifying classes. Fig. 5 shows that the three lowest diagonal values are "ba," "la," and "sa," with values of 0.57, 0.67, and 0.71, respectively. This means that the model is less capable of predicting that three Javanese scripts. Otherwise, the model can accurately predict other Javanese scripts with a value greater than 0.8. The character "ba" received a low score of 0.57 in confusion matrix table because the shape of the character "ba" is similar to the shape of the character "nya". Similarly, the character "sa", in the confusion matrix table is equated with the characters "na" and "da" because of the similarity of the shape of each character

To successfully apply the trained YOLOv9 model for Javanese character recognition, we utilized the model to detect and recognize Javanese characters in various image formats, including a 4x5 matrix, a 2x10 matrix, and two individual images. The subsequent images display the obtained outcomes.

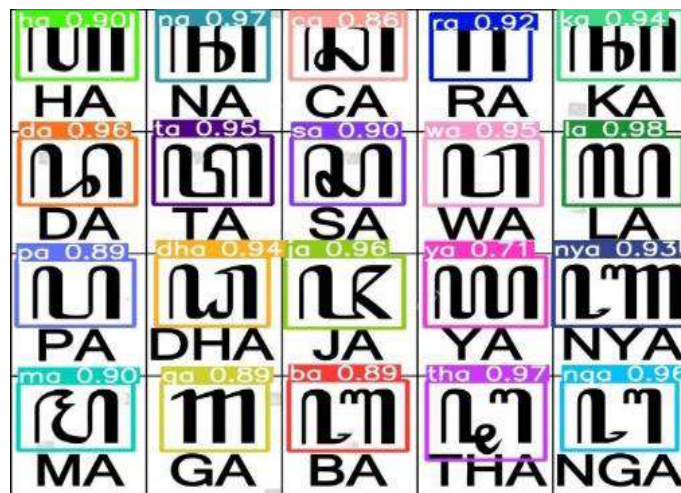


Figure 6. The detection model was implemented on the Javanese script arranged in 4x5 matrix

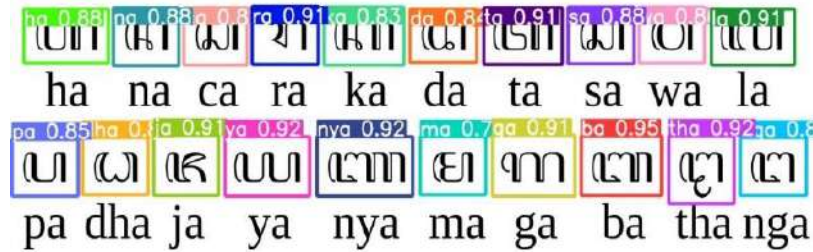


Figure 7. The detection model was implemented on the Javanese script arranged in 2x10 matrix



Figure 8. The detection model was implemented to the two Javanese scripts in the two single forms

We assessed the performance of the Javanese character reading model by comparing the recognized text with the ground truth text. In the first image (Fig. 6), the model achieved a good confidence level. However, only one character provided the lowest level i.e., "ya" obtained a confidence level at 0.71 while the highest confidence level was achieved for the character "la" at 0.98. The model seems to have difficulty predicting the image "ya" because it is similar to some other characters, such as "pa", "ba", and "ga" even though the format of the printed image is a 4x5 matrix similar to the printed image in training dataset. Additionally, in the second image (Fig.7), where the images were arranged in a 2x10 format, the confidence levels ranged between 0.8 and 0.95. For the third test, we examined two single form images (Fig.8). The character "ta" had a confidence value of 0.96, whereas the character "sa" had a value of 0.71. If we look at the confusion matrix result, it showed that the character "sa" got a fairly low result of 0.71 and this result seems affecting the prediction of the testing data in the single image. It can be seen here that the YOLOv9 model less capable to identified the Javanese characters that are in the similar shapes. The superior performance can be attributed to the fact that the training data images arranged in a 4x5 matrix yielded better average results compared to other arrangements.

4 Conclusions

The YOLOv9 algorithm model was used to detect Javanese script. Two studies were carried out to compare the effect of weight parameters on YOLOv9. The algorithm's ability to recognise Javanese characters was tested by comparing the recognised text to the ground truth text. Confidence levels ranged between 0.8 and 0.95 obtained when photos were grouped in a 2x10 matrix. Another trial with single form photos yielded a confidence value of 0.96 for "ta" and 0.71 for "sa". Image's data testing in a 4x5 matrix generated generally better results than alternative formats. In future studies, addressing the variability among Javanese scripts and the opportunity to use handwriting format remains an open and active research topic. Moreover, this study could be used as the development of the machine learning algorithm by implementing the model in different local character languages.

Acknowledgements

We express our gratitude to the Department of Informatics at University of Sanata Dharma for granting us permission to utilize their workstation facilities and the Artificial Intelligence Laboratory for the purpose of conducting this study.

References

- [1] D. Iskandar, S. Hidayat, U. Jamaludin, and S. M. Leksono, "Javanese script digitalization and its utilization as learning media: an etnopedagogical approach," *International Journal of Mathematics and Sciences Education*, vol. 1, no. 1, 2023, pp. 21–30.
- [2] A. Susanto, I. U. W. Mulyono, C. A. Sari, E. H. Rachmawanto, and R. R. Ali, "Javanese character recognition based on k-nearest neighbor and linear binary pattern features," *Kinetik: Game Technology, Information System, Computer Network, Computing, Electronics, and Control*, 2022, pp. 309–316.
- [3] F. T. Anggraeny, Y. V. Via, and R. Mumpuni, "Image preprocessing analysis in handwritten Javanese character recognition," *Bulletin of Electrical Engineering and Informatics*, vol. 12, no. 2, 2023, pp. 860–867.

-
- [4] I. F. Katili, M. A. Soeleman, and R. A. Pramunendar, "Character Recognition of Handwriting of Javanese Character Image using Information Gain Based on the Comparison of Classification Method," *Jurnal RESTI (Rekayasa Sistem dan Teknologi Informasi)*, vol. 7, no. 1, 2023, pp. 193–200.
- [5] M. A. Rasyidi, T. Bariyah, Y. I. Riskajaya, and A. D. Septyani, "Classification of handwritten Javanese script using random forest algorithm," *Bulletin of Electrical Engineering and Informatics*, vol. 10, no. 3, 2021, pp. 1308–1315.
- [6] A. Prasetiadi, J. Saputra, I. Kresna, and I. Ramadhanti, "YOLOv5 and U-Net-based Character Detection for Nusantara Script," *Jurnal Online Informatika*, vol. 8, no. 2, 2023, pp. 232–241.
- [7] J. Redmon and A. Farhadi, "Yolov3: An incremental improvement," *arXiv preprint arXiv:1804.02767*, 2018.
- [8] H. Sugiharto, "Aksara Jawa YOLO v5 Dataset." [Online]. Available: <https://www.kaggle.com/datasets/hermansugiharto/aksara-jawa-yolo-v5-dataset>. [Accessed: May 04, 2024]
- [9] A. Budi, "Hanacaraka dan Makna Bijak di Balikny." [Online]. Available: <https://www.goodnewsfromindonesia.id/2017/01/23/hanacaraka-dan-makna-bijak-di-baliknya>. [Accessed: May 15, 2024]
- [10] M. Hussain, "YOLO-v1 to YOLO-v8, the rise of YOLO and its complementary nature toward digital manufacturing and industrial defect detection," *Machines*, vol. 11, no. 7, 2023, p. 677.
- [11] C. Koylu, C. Zhao, and W. Shao, "Deep neural networks and kernel density estimation for detecting human activity patterns from geo-tagged images: A case study of birdwatching on flickr," *ISPRS Int J Geoinf*, vol. 8, no. 1, 2019, p. 45.

AUTHOR GUIDELINES

Author guidelines are available at the journal website:
<http://e-journal.usd.ac.id/index.php/IJASST/about/submissions#authorGuidelines>

This page intentionally left blank